

LUND UNIVERSITY

Computational Methods in Conceptual Structural Design

Alic, Vedad

2018

Document Version:
Publisher's PDF, also known as Version of record

Link to publication

Citation for published version (APA):
Alic, V. (2018). *Computational Methods in Conceptual Structural Design*. [Doctoral Thesis (compilation), Faculty of Engineering, LTH]. Lund University. Faculty of Engineering (LTH), Division of Structural Mechanics.

Total number of authors:
1

General rights
Unless other specific re-use rights are stated the following general rights apply:
Copyright and moral rights for the publications made accessible in the public portal are retained by the authors and/or other copyright owners and it is a condition of accessing publications that users recognise and abide by the legal requirements associated with these rights.
• Users may download and print one copy of any publication from the public portal for the purpose of private study or research.
• You may not further distribute the material or use it for any profit-making activity or commercial gain
• You may freely distribute the URL identifying the publication in the public portal

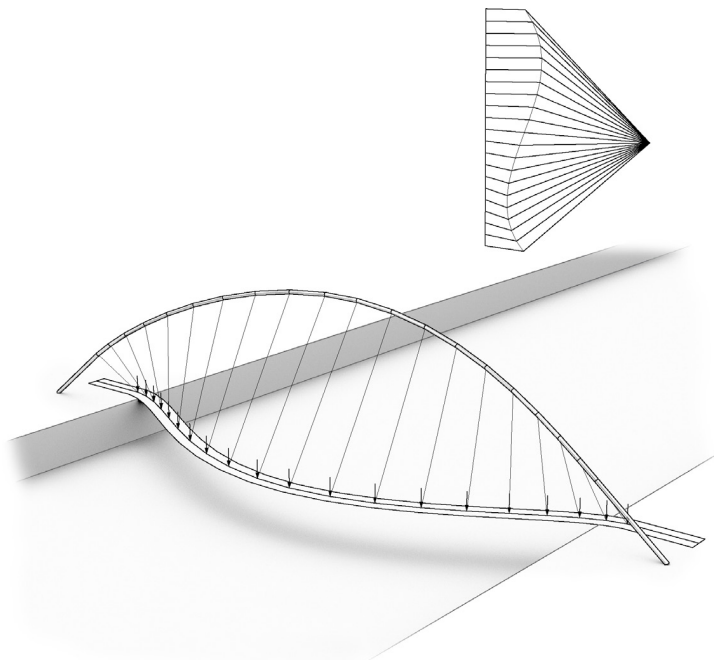
Read more about Creative commons licenses: https://creativecommons.org/licenses/

Take down policy
If you believe that this document breaches copyright please contact us providing details, and we will remove access to the work immediately and investigate your claim.

LUND UNIVERSITY

PO Box 117
221 00 Lund
+46 46-222 00 00

LUND UNIVERSITY



COMPUTATIONAL METHODS IN CONCEPTUAL STRUCTURAL DESIGN

VEDAD ALIC

Structural Mechanics

Doctoral Thesis

DEPARTMENT OF CONSTRUCTION SCIENCES
DIVISION OF STRUCTURAL MECHANICS

ISRN LUTVDG/TVSM--18/1030--SE (1-175) | ISSN 0281-6679
ISBN 978-91-7753-790-8 (print) | ISBN 978-91-7753-791-5 (pdf)
DOCTORAL THESIS

COMPUTATIONAL METHODS IN CONCEPTUAL STRUCTURAL DESIGN

VEDAD ALIC

Copyright © Vedad Alic 2018.
Printed by V-husets tryckeri LTH, Lund, Sweden, October 2018 *(Pl)*.

For information, address:
Division of Structural Mechanics,
Faculty of Engineering LTH, Lund University, Box 118, SE-221 00 Lund, Sweden.
Homepage: www.byggmek.lth.se

Acknowledgements

The work presented in this thesis was carried out at the Division of Structural Mechanics, Faculty of Engineering at Lund University, Sweden. During the work, Prof. Kent Persson acted as my main supervisor, and Profs. Karl-Gunnar Olsson and Erik Serrano as my co-supervisors. The financial support was provided by the Swedish strategic research programme eSSENCE and the Swedish Research Council FORMAS. The support is gratefully acknowledged. I would like to thank my supervisors, Prof. Kent Persson, Prof. Karl-Gunnar Olsson and Prof. Erik Serrano, without whose support the work would not have been possible. Thanks for the worthwhile research related discussions, numerous proof-reads, and continued encouragement and guidance.

I owe my gratitude to the staff of Construction Sciences, including all of the ”Pers-”, for the friendly discussions, and a pleasant work environment. Furthermore, I would like to thank those who I have been fortunate to share an office with, Henrik Danielsson, Daniel Åkesson, Alex Spetz and Anders Sjöström, thanks for some fun banter, ping-pong, nice music, and a friendly atmosphere. I would like to extend some extra thanks to Daniel Åkesson for discussions of our shared research area. I am grateful for the help from Dr. Jonas Lindemann regarding programming and software development and some research related discussions. Thanks to Bo Zadig for helping with the design of some graphics for the thesis. Thanks to Håkan Hansson for practical office matters and to Artur Grabowski for keeping the computers running.

Finally, I would like to thank my family and friends for their endless support and encouragement, and for keeping me occupied with other things out of office.

Lund, October 2018
Vedad Alic

Abstract

Conceptual design is the first phase in the design process in which all the requirements and design objectives are synthesized into conceptual alternatives. In practice today, major decisions regarding the buildings function, massing, and overall form are usually made during the first phase. Considering structural performance requirements during conceptual design enhances interdisciplinary interaction, and creates a visual link between form and numeric performance evaluations, reducing work on poorly performing solutions. To include structural performance in conceptual design requires, amongst other things, the availability of tools such as simulation software, suitable for conceptual studies.

The aim of the research is to develop new efficient methods and procedures for supporting an interactive and iterative design process that includes engineering aspects. By integrating engineering knowledge and physical aspects in the developed tools, a more efficient and better-adapted design process can be obtained. Supporting an interactive and iterative design process requires new interaction models and numerical approaches in the tools used.

The research is limited to three different areas. The first area is related to conceptual studies for reducing ground borne wave propagations in an urban scale. A tool is developed for simulating forms with masses placed on top of soil in an urban scale and studying the resulting effect that the forms have on the propagating waves. The tool uses the finite element method and studies the vibration reduction effects in the frequency domain. Paper A presents the tool and draws some conclusions related to the levels of vibration reduction for various patterns, showing that some patterns are effective in mitigating the incoming vibrations. The approach in the tool makes it possible to obtain results in minutes, allowing the user to generate many alternative proposals quickly, and act as an aid in brainstorming sessions.

Papers B and C focus on a recent extension of the finite element method, isogeometric analysis, that is the subject of the second area. The implementation of isogeometric analysis with membrane elements for form finding of efficient shapes for shells is presented. The dynamic relaxation method is used for finding the static solutions. The method is employed directly on design geometry, which is described by non-uniform rational b-splines (NURBS), without the need for any further discretization. Paper B investigates various selections of mass and damping for the dynamic relaxation method with NURBS based membrane elements. The resulting methods are implemented in two plug-ins for the computer aided design applications Rhinoceros 3D and Grasshopper 3D, of which the former is presented in Paper C. The method describes form found geometries well with very few elements and can be used to explore different efficient shapes for shells very rapidly and directly in design software, and is thus suited for design explorations.

The third area is about graphic statics – an old method which is again gaining popularity due to progress in CAD and computational methods. The strength of the method is in an intuitive

and graphical representation of form and the internal forces of static equilibrium, which are presented in two diagrams – the form diagram, and the force diagram. The current research efforts in graphic statics aim to apply the method as a design tool rather than to use it for analysis. A second aim is to investigate the benefits of computer based graphic statics. Paper D presents a root finding approach for computing a form diagram based on manipulations of a force diagram. Paper E presents an algebraic method for computing form diagrams based on force diagrams. Paper F presents an application of graphic statics for automatically generating initial strut-and-tie patterns.

Populärvetenskaplig sammanfattning

I byggprocessen handskas arkitekter och ingenjörer med komplexa frågor. Formgivandet av en ny byggnad brukar börja med att uppdraget ges till en grupp bestående av bl.a. ingenjörer och arkitekter. En formgivningsprocess inleds där gruppen sorterar och bygger upp kunskap om uppgiftens olika frågeställningar. De tidiga skedena i en formgivningsprocess utförs vanligtvis av arkitekter som koncentrerar sig på byggnadens funktion, rum, rumssamband, och övergripande form. Betraktandet av tekniska aspekter som bärande system, klimatskal, och akustiska egenskaper brukar senareläggas vilket kan leda till svårigheter när olika blir inblandade i processen vilket kan resultera i byggnader som inte når upp till sin fulla potential. I denna avhandling presenteras metoder och verktyg riktade till ingenjörer som är involverade i tidiga skeden av formgivningsprocessen. Verktygen stödjer ett kreativt och interaktiv arbete med att formge funktionella och effektiva lastbärande strukturer.

Arbetet har avgränsats till tre olika områden. Det första har handlat om att studera möjligheten att reducera vibrationer vid en känslig anläggning genom att placera byggnader mellan anläggningen och intilliggande tungt trafikerade vägar. För att möjliggöra studien har ett skissverktyg utvecklats som ger insikt kring byggnaders form och placering och deras effekt på vibrationers fortplantning i marken. Genom ett enkelt skissverktyg underlättas möjligheterna till att studera byggnadernas effekt på vibrationers fortplantning i samband med stadsplaneringsprocessen.

I det andra området söks effektiva former för skalstrukturer med stora spännvidder genom kombinationen av en ny beräkningsmetod med befintliga beräkningstekniker. Den nya beräkningsmetoden gör det möjlig att utföra en simulering direkt på en geometri som är ritad i ett ritprogram. Tidigare metoder har inneburit ett tidskrävande arbete med att konvertera arkitektens ritningar till en beräkningsmodell. Genom att reducera detta tidskrävande steg kan ingenjörer istället fokusera på utformning och analys. Ingenjörens återkoppling till arkitekten kan ske i ett interaktivt samtal, vilket kan ibland leda till byggnader där strukturella och arkitektoniska intentioner är sammankopplade.

I det tredje området har en över 100 år gammal och på sin tid flitigt använd metod för strukturanalys - grafisk statik studerats. Metodens styrka ligger i en tydlig och intuitiv presentation av formen och de inre och yttre krafter som verkar på strukturen. Metoden har återigen börjat studeras och användas, men nu handlar frågorna om vilka fördelar det finns med att digitalisera metoden, samt hur den kan användas som ett designverktyg och inte enbart för analys. Därmed möjliggörs ett sökande efter former med goda mekaniska egenskaper.

Contents

I Introduction and overview **xiii**

1 Introduction **1**
- 1.1 Aims and objectives . . . 4
- 1.2 Scope . . . 5
  - 1.2.1 Forms for vibration reduction . . . 6
  - 1.2.2 Isogeometric analysis . . . 6
  - 1.2.3 Graphic statics . . . 7
- 1.3 Disposition . . . 8

2 Summary of appended papers **9**
- 2.1 Appended papers . . . 9
- 2.2 Developed demonstrator programs . . . 12
- 2.3 Other publications by the author . . . 12

3 The design process **15**
- 3.1 Architectural and structural design . . . 15
  - 3.1.1 Architectural design process . . . 15
  - 3.1.2 Structural design process . . . 16
  - 3.1.3 Collaboration and Communication . . . 16
  - 3.1.4 Considering structural performance . . . 17
- 3.2 Computational design . . . 18
  - 3.2.1 Design space exploration . . . 19
  - 3.2.2 Structural design space exploration . . . 20
- 3.3 Conclusions and present research . . . 21

4 Tools for conceptual structural design **23**
- 4.1 Rapid feedback tools . . . 23
- 4.2 CAD and CAE . . . 25
- 4.3 Form finding . . . 27
- 4.4 Graphical methods . . . 30
- 4.5 Structural optimization . . . 31

5 Finding forms for vibration reduction **33**
- 5.1 Background . . . 33
  - 5.1.1 Present research . . . 33

5.2 Theory . . . 34
5.2.1 Elasticity . . . 34
5.2.2 The finite element method . . . 36
5.2.3 Structural dynamics . . . 38
5.3 Developed model and form finding examples . . . 40
5.3.1 Earlier studies . . . 40
5.3.2 Computational model . . . 41
5.3.3 Examples . . . 45
5.4 Summary . . . 46

6 Finding form with IGA **47**
6.1 Background . . . 47
6.1.1 Present research . . . 47
6.2 Theory . . . 48
6.2.1 Geometric preliminaries . . . 49
6.2.2 NURBS based isogeometric analysis . . . 51
6.2.3 Kirchhoff-Love shell and membrane theory . . . 53
6.2.4 Dynamic relaxation . . . 60
6.3 Form finding examples . . . 61
6.3.1 Plug-ins . . . 61
6.3.2 Simple example . . . 63
6.3.3 Multi-patch examples . . . 65
6.4 Summary . . . 65

7 Design exploration using graphic statics **69**
7.1 Literature review . . . 69
7.1.1 Background . . . 71
7.1.2 Graphic statics using Bow's notation . . . 71
7.1.3 Renewed interest in graphic statics . . . 73
7.1.4 Computer based graphic statics . . . 74
7.1.5 Present research . . . 75
7.2 Theory . . . 75
7.2.1 Graph theory and reciprocal diagrams . . . 75
7.2.2 The force density method . . . 77
7.2.3 Pin-jointed structures . . . 78
7.2.4 Lower bound theorem of plasticity . . . 79
7.3 Developed framework and applications . . . 79
7.3.1 Need for both approaches . . . 81
7.3.2 Developed graphic statics framework and Rhino plug-in . . . 81
7.3.3 Automatic generation of strut-and-tie patterns . . . 82
7.4 Summary . . . 82

8 Conclusions **85**
8.1 Main contributions . . . 85

8.2 Further research 86

References **89**

II Appended publications **99**

Paper A
Form Finding for Ground Vibration Reduction in an Urban Scale.
Vedad Alic and Kent Persson.
Proceedings of IASS-SLTE Symposium 2014: Shells, Membranes and Spatial Structures: Footprints.

Paper B
Form Finding with Dynamic Relaxation and Isogeometric Membrane Elements.
Vedad Alic and Kent Persson.
Published in: Computer Methods in Applied Mechanics and Engineering.
http://dx.doi.org/10.1016/j.cma.2015.12.009

Paper C
Using isogoemetric elements and dynamic relaxation as a form finding technique.
Vedad Alic and Kent Persson.
Proceedings of IASS 2015 Amsterdam Symposium: Future Visions.

Paper D
Bi-directional algebraic graphic statics.
Vedad Alic and Daniel Åkesson.
Published in: Computer-Aided Design.
http://dx.doi.org/10.1016/j.cad.2017.08.003

Paper E
Design explorations based on force diagrams.
Vedad Alic and Kent Persson.
In review: International Journal of Space Structures

Paper F
Generating initial reinforcement layouts using graphic statics.
Vedad Alic and Kent Persson.
Proceedings of IASS 2018 Boston Symposium: Creativity in structural design.

Part I

Introduction and overview

1 Introduction

In the early phases of the building design process requirements and design objectives are synthesized into conceptual alternatives. In practice today, major decisions regarding the buildings geometry, massing and overall form are usually made during the early phases. In most buildings and facilities there are physics and engineering related demands that must be addressed, such as efficient load-bearing systems, energy efficient climate shelters, acoustic comfort, maximum level of vibrations for laboratory equipment, etc. By developing the design process in the early stages and exploring alternatives for such demands already in conceptual design, better performing and more intriguing buildings can be constructed. The opposite also holds, if only the engineering aspects are focused upon, functional design requirements may not be fulfilled. Considering engineering related demands in conceptual design requires close collaboration and communication between architects and engineers in different fields. It is then required that tools such as simulation software, suitable for conceptual studies are available to support this communication.

In the early phases of a complex design process it is common to use a couple of driving ideas or rules to help reason about and re-frame the specific design questions. Considering mechanical phenomena in the design can lead to holistic and integrated structural and architectural designs. To illustrate this, an example related to a state-of-the-art research facility located near a new town development area, but also near some roads with dense traffic, is used, see Fig. 1.1a. The research facility is sensitive to vibrations, and considerable effort was put into investigating whether vibrations caused by external sources would be a concern. To mitigate vibrations there are some traditional measures, such as digging trenches or stiffening the substrate. These measures rely on modifying physical parameters that are part of the governing differential equation that describes wave propagation in solids, as for instance stiffness, mass, damping or geometry. Another idea came up during the discussions in that the facility was situated close to the new buildings. The thought came of placing the buildings closer to the facility, and letting them serve as vibration reduction measures by being located between the vibration sources and the facility. By being in the vicinity and also by being shaped by the requirements of facility, the other buildings could take part in the science/research going on at the facility. Fig. 1.1 illustrates the concept.

By placing out patterns of heavy masses, or buildings, on the soil surface between the external

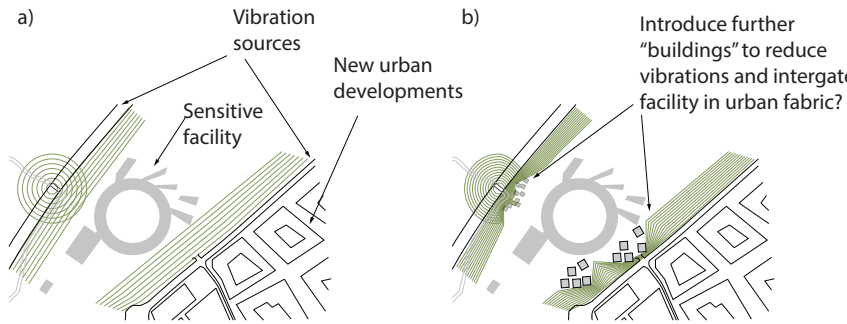


Figure 1.1: Could the area surrounding the facility be shaped to reduce vibrations from external sources?

sources and the facility, vibration reduction was achieved. A solution that is cost effective and maintenance free, and as one that is more appropriate in an urban situation than more traditional methods such as trenches or other barriers. At this stage of the design the range of possible solutions is vast. The masses might be buildings, parts of buildings, sculptures, soil, or other objects. As such, it is of interest to investigate if it is a possible method of vibration mitigation, and which configurations are most efficient in order to select a strategy that is suitable when considered together with other aspects that are important for urban plans.

To include the vibration reduction strategy as one of the ideas of the architectural design required several things. First, studies to figure out if masses are favorable for vibration reduction were performed, investigating which parameters characterize the phenomena. These studies were performed in two-dimensional (2D) analysis, concluding that heavy masses could work, however, the total mass needed to be rather large. Several sketches were made on how masses or buildings could be included on the site, Fig. 1.2.

A factor in direct relation to the architectural design is how these masses are shaped and or-

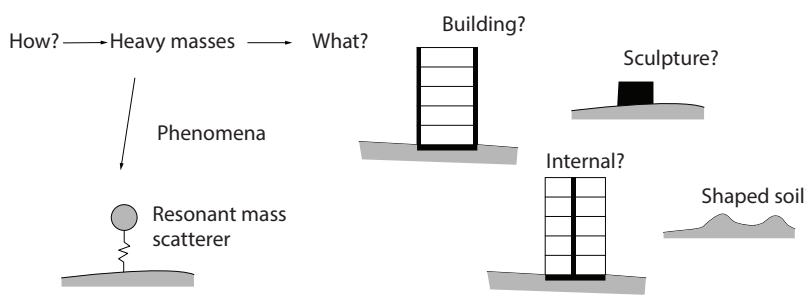


Figure 1.2: How would it be made part of the built environment?

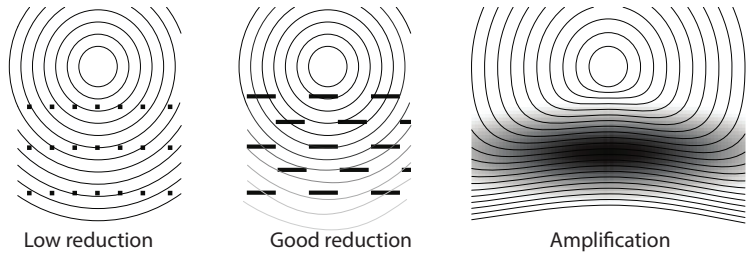


Figure 1.3: Which shapes would work? How do they relate to the research facility?

ganized. To address this, required collaboration between the architect and structural engineer, since the urban plan needs to fulfill architectural requirements while including a strategy for vibration reduction. In order to support the collaboration and communication a new tool was required, which could facilitate the exploration of different plans and how well these could work for vibration reduction. The developed tool can give numerical feedback quickly on whether a certain spatial organization of masses is suitable for vibration mitigation or not, the tool and further details are presented in Paper A. The organization of masses with respect to vibration reduction could then be included while developing the urban plan.

Using the tool, several different examples were tried out. Some gave a marked reduction in vibrations, some made no practical difference and some resulted in undesirable results with increased vibrations (amplification). Fig. 1.3 shows examples illustrating some aspects that were found to be important when placing out masses. The left example shows small solids uniformly spaced, they have little effect on the propagating vibrations. The middle example shows lines of solids, arranged such that there is no straight path from the source to the other side, they have favorable vibration reduction. The right example shows solids of different mass placed over the whole area, their organization leads to increased vibrations. Finally, a design proposal based on the studies with the tool was found which could work well together with other aspects for the urban plan. Buildings placed along lines perpendicular to the waves between the source and the facility which also block any straight paths were seen as efficient, similar to the middle example in Fig. 1.3. The design of these could also be incorporated with the tangential extensions on the circumference of the round facility, thus connecting to the building form.

The main research question in the thesis is: How can better adapted computational methods, concepts, strategies and visualizations of results inform and support design decisions?

The design example in the introduction shows how, in a collaborative setting with engineers and architects it is possible to explore alternative structural systems and phenomena through simulation and visualization early in the design process. This can lead to a more creative and informed collaborative design process. In order to include physical phenomena and patterns, and integrate them in the overall concept, and in order to present and communicate to mem-

bers of the design team without structural knowledge engineers have different tools available, such as, sketching, hand computations, computer tools and so on. Modeling tools for conceptual studies must encourage creativity and be capable of interactively modifying the model in a sketch-like fashion once it has been created. This is a fundamental aspect in any design activity, where the designers are constantly going forward and backwards, re-elaborating over some particular aspect of the model, its general layout, or even coming back to a previous solution that had been temporarily abandoned Several alternatives are explored and used to further specify and reformulate the design goals.

1.1 AIMS AND OBJECTIVES

The main aim of the research is:

- to develop computational methods and strategies suitable for explorations of structural design spaces that can be used for improving informed decision making in conceptual design of structures.

In the long term, the research will result in new developed methods and tools that improve the conceptual design process and collaboration between architects, engineers, etc. This enables reduced environmental and construction cost, creates inherent safety in the structures and makes integration of the functional and technical goals possible. Another result by including structural considerations early is that engineers, designers and architects will have a greater awareness and understanding of how engineering and physical aspects affect the design process and how these are expressed in structures.

The objectives in the thesis are:

- Performing literature studies of methods and tools suitable for conceptual structural design. Possible directions for the research are identified.
- Development of numerical methods that meet the objectives stated in the literature review.
- Implementation of computer based frameworks based on the numerical methods.
- Implementation of demonstration programs.

The work is limited to computer based tools. The collaborative aspects are reflected upon in relation to communicating and presenting structural phenomena. An important aspect in the thesis is the relationship between structure and form.

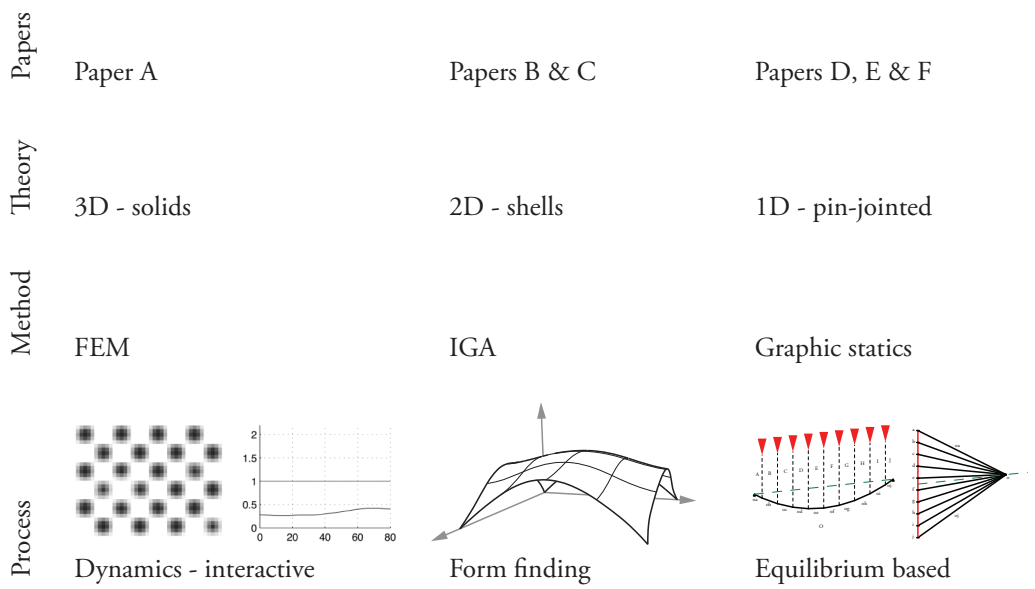


Figure 1.4: The contributions of the thesis.

1.2 SCOPE

Structural mechanics is a well developed area with many theories and numerical methods available for design and analysis. The available techniques offer different insights, and are based on mathematical analysis and three types of laws - the equations of motion, the constitutive equations, and the kinematic equations. The techniques vary in suitability depending on the project requirements. The research presented in the thesis includes three different theories of structural mechanics. Paper A utilizes the theory of solid structures, which is a general three-dimensional theory. Papers B and C deal with shells, parametrized in two dimensions. Papers D, E and F deal with pin-jointed structures, which are represented by one-dimensional lines. Each is studied together with an appropriate computational method: finite element analysis (FEA), isogeometric analysis (IGA), and graphic statics respectively. Each deals with a design process. The first allows for free exploration of mass distribution. The second restricts the forms to a sub-set that is mechanically suitable for shells with a dominant design load (usually the self-weight). The third offers different types of design processes — interactive or optimization based. Fig. 1.4 contains a table summarizing the thesis scope.

1.2.1 Forms for vibration reduction

Most tools for conceptual structural design deal with considerations of static problems. The phenomena that are studied within structural mechanics are vast and the phenomena considered by design tools could therefore be broadened. The first research question is related to the design example in the introduction:

- How can the effect of mass distribution on vibration reduction be computed and visualized for rapid feedback in an ongoing design dialogue?

One of the tools presented in the thesis is related to conceptual studies of ground-borne wave propagations in an urban scale. The tool is based on FEA and can be used to study the effect of placing forms with masses on top of soil as well as the resulting effect that the forms have on the propagating waves, see Fig 1.4. Such computations require powerful computers and are normally very time consuming. However, the approach used in the developed tool makes it possible to obtain results in minutes, allowing the user to reflect over the results and generate many alternative proposals quickly and act as an aid in brain-storming sessions. In a broader sense, this type of tool could be used as an aid in studying the effects of vibration from road and rail traffic, as well as structure-soil-structure interactions, in the ever increasing density of cities. The research is published in Paper A. The objectives set out to answer the research question were:

- Perform 2D parametric studies in order to identify important parameters.
- Develop an interactive tool for studying organizations of masses on the ground surface.
- Perform studies of different organizations, investigating which patterns are suitable for urban plans.

1.2.2 Isogeometric analysis

The second part of the research presented in the thesis is related to a recent extension of FEA, IGA, see Fig. 1.4. IGA allows for performing FEA directly on a Computer Aided Design (CAD) geometry.

The design of efficient shell structures requires a combined architectural and structural approach. Efficient shell structures primarily carry the dominant load in membrane action by being shaped correctly. The design used to be performed by physical form finding methods. These fell out of favor when computers got powerful enough, since computers simplified parts of the design process, by streamlining modifications and improving measurements. Using computers made form finding more intuitive, faster and more accurate, thereby allowing for a better exploration of the design space of efficient shell structures. The resulting shape is highly

dependent on the initial conditions, and often several iterations are required to achieve a desired design, making CAD software an important tool thanks to the provided interactivity. Recently a new development of FEA allows for analysis directly using Non-Uniform Rational B-Splines (NURBS), which are a common technique for representing geometry in commercial CAD software. CAD software (Rhinoceros) are also today commonly used for the form finding of shell structures. The geometry in Rhinoceros is based on NURBS, and using NURBS for the form finding might be of benefit, which leads to the research question:

- How can the same formulation for the numerical structural analysis and geometric representation be used to improve the workflow in an early design phase of shell structures?

The approach taken here, is that the integration of the form finding of shell structures using hanging methods directly into CAD software with CAD geometry can further streamline the design process of shells.

The research is published in Papers B and C. The objectives for this part were:

- Develop and implement the hanging model based form finding using NURBS based membrane elements and the dynamic relaxation approach.
- Implement demonstrator tools using the developed method.
- Compare the numerical performance of the developed method using NURBS based FEA to classical FEA.
- Investigate the advantages of using the same mathematical formulation for CAD and FEA.

1.2.3 Graphic statics

The design of discrete 1-dimensional members which carry loads only in axial tension or compression has been supported by a vast array of methods. One of the first methods for analysis of pin-jointed structures was graphic statics. The methods of graphic statics were very popular in the 19th and beginning of the 20th centuries. The methods employed graphical ways of analyzing structures. What is remarkable is that most textbooks on graphic statics presented it as a method for performing analysis, but its intuitive approach lead to several well-known engineers using the method as a design tool. The current research on graphic statics focuses on generalization and on modernizing it by using computational methods and linear algebra, as well as researching on how the method can be used for design.

Traditionally in structural mechanics we make use of the theory of elasticity in order to get a unique solution in statically indeterminate cases, however, with graphic statics we only use

the equations of equilibrium. Further we work in two dimensions, and only with pin-jointed structures – tension and compression. For these limitations, graphic statics offers a graphical presentation of the relationship between the form and the forces, through the form diagram, which represents the geometry and lines of action of the forces, and the force diagram, which represents the magnitude of the forces and the nodal equilibrium of each node of the form diagram. The force diagram also includes the global equilibrium, such that any manipulations of a force diagram guarantee that the resulting form and force diagrams are still in equilibrium.

For pin-jointed structures the shape is a determining factor for the force distribution, and geometric methods allow us to intuitively manipulate both the form and the forces. Computer based graphic statics is thus a promising research area for exploring form based on direct manipulations of forces. The research question for this part is:

- How can graphic statics methodology change how pin-jointed structures are explored through force diagram manipulations?

The research is published in Papers D, E and F. The objectives were the following:

- Formulate a bi-directional graphic statics framework.
- Implement a graphic statics demonstrator tool.
- Test the method trough different examples and applications.
- Use the method for strut-and-tie modeling.

1.3 DISPOSITION

The thesis consists of two parts. The first part is an overview of the work, divided in 8 chapters. The second part consists of 6 appended papers that have been produced during this research.

The first part is organized as follows: Chapter 1 introduces the thesis. In chapter 2 a summary of the appended papers and developed demonstrator programs is provided. Chapter 3 briefly presents the architectural and structural design processes as well as design space exploration. Chapter 4 concerns existing tools for conceptual structural design. Chapter 5 presents research related to conceptual studies of ground-borne wave propagation in an urban scale, and a mitigation strategy. Chapter 6 is about form finding for shells under self-with using isogeometric membrane elements. Chapter 7 introduces the research related to graphic statics. Chapter 8 concludes the thesis.

2 Summary of appended papers

2.1 APPENDED PAPERS

Paper A
Form Finding for Ground Vibration Reduction in an Urban Scale.
Vedad Alic and Kent Persson.
Published as a reviewed paper in: Proceedings of IASS-SLTE Symposium 2014: Shells, Membranes and Spatial Structures: Footprints.

Paper A investigates the search of forms in an urban scale that are effective in reducing vibration propagation from external sources, such as highways, high-speed railroads and industrial plants. It describes the implementation of a MATLAB tool for sketching different masses and investigating their affects on vibration reduction.

Contributions by Vedad Alic
Vedad Alic was the main author of the paper, carried out all the simulations, performed the FE modeling in ABAQUS and the subsequent model reductions in MATLAB as well as developed the tool for sketching different arrangements of masses and drawing of conclusions.

Paper B
Form Finding with Dynamic Relaxation and Isogeometric Membrane Elements.
Vedad Alic and Kent Persson.
Published in: Computer Methods in Applied Mechanics and Engineering.
http://dx.doi.org/10.1016/j.cma.2015.12.009

A method for form finding with dynamic relaxation and Non-Uniform Rational B-Splines (NURBS) based isogeometric membrane elements has been implemented and studied regarding the influence of the discretization and element shape on the form finding. The procedure allows for rapid form finding since NURBS describe the curved geometry well and it is shown that the form-finding can be performed using a coarse mesh. However, to minimize the bending strain energy a fine mesh is needed. Using smaller elements is more advantageous than increasing the degree of the basis functions, keeping the number of integration points few

and converging at a lesser number of iterations. Using isogeometric analysis (IGA) simplifies further studies since the form-found shape can be exactly represented with a shell element formulation. The method is suitable to be used in computer aided design environments such as Rhinoceros 3D during design stages, where the form finding can be evaluated together with other studies in a design context.

Contributions by Vedad Alic
Vedad Alic was the main author of the paper, planned the research, implemented the methods, carried out the investigations and wrote the paper.

Paper C
Using isogoemetric elements and dynamic relaxation as a form finding technique.
Vedad Alic and Kent Persson.
Published as a reviewed paper in: Proceedings of IASS 2015 Amsterdam Symposium: Future Visions.

The use of NURBS based isogeometric analysis for form finding and further design of form found structures is presented in this paper. The form finding is performed with non-linear isogoemetric membrane elements together with dynamic relaxation. The method has previously been tested on simple geometries in a computational environment, and is here further integrated in a CAD program, Rhinoceros 3D where the method is evaluated for complex geometries in a design scenario. The form found shape is further studied and it is shown how the membrane and bending utilization can be plotted on the shape by making refinements to the mesh without affecting the geometry. Finally the form finding is employed on some complex geometries to show the possibilities of using coarse NURBS meshes for form finding.

Contributions by Vedad Alic
Part of the implementation of the Rhinoceros 3D plug-in presented in the paper was performed by a Master's dissertation student [1], together with the aid and supervision of Vedad Alic. Vedad Alic was the main author of the paper, and wrote pats of the plug-in.

Paper D
Bi-directional algebraic graphic statics.
Vedad Alic and Daniel Åkesson.
Published in: Computer-Aided Design.
http://dx.doi.org/10.1016/j.cad.2017.08.003

A pre-existing algebraic graphic statics method is extended to allow for interactive manipulations of the force diagram, from which an updated form diagram is determined. Newton's method is used to solve a set of non-linear equations, and the required Jacobian matrix is derived. Additional geometric constraints on the form diagram are introduced, and methods for improving the robustness of the method are presented. We discuss the implementation of the method as a back-end to an interactive application, and demonstrate the usability of the method in several examples where the qualities of directly manipulating the force diagram are

emphasized.

Contributions by Vedad Alic
The authors co-wrote, developed and implemented the methods for the first draft of the paper. Vedad Alic did two additional revisions of the paper, where further investigations and writing was carried out.

Paper E
Design explorations based on force diagrams.
Vedad Alic and Kent Persson.
In review: International Journal of Space Structures

A method for generation and exploration of forms based on force diagrams and graphic statics is presented. Algebraic equations are formulated to compute the form diagram from a given force diagram. The construction of the connectivity and incidence matrices from the force and the algebraic equations for computing the form diagram are presented. Finally, methods for including linear equality constraints are presented. An approach for constructing crossing-free drawings for force (and form) diagrams is presented. We present a method for making topological refinements to the force diagram. The usability of the method is demonstrated in several examples that allow for explorations of forms based on manipulations of the force diagram.

Contributions by Vedad Alic
Vedad Alic was the main author of the paper, developed and implemented the methods, carried out the investigations and wrote the paper.

Paper F
Generating initial reinforcement layouts using graphic statics.
Vedad Alic and Kent Persson.
Published as a reviewed paper in: Proceedings of IASS 2018 Boston Symposium: Creativity in structural design.

A key step to the strut-and-tie method is the selection of an appropriate truss model, due to the static indeterminacy of reinforced concrete there are often several suitable models possible. A method for automatically generating a suitable truss model by using graphic statics is presented. Optimal layouts are found by minimizing the total load path. A formulation of constraints suitable for generating an initial strut-and-tie model confined to an arbitrary polygon with holes is also presented. The performance by using derivative based and derivative free solvers is compared. The method is applied to several examples and the results are compared to existing methods from literature as well as to the principal stress patterns based on finite element analysis. All of the presented examples yield good results and the optimal layouts found can be used as a starting point for further design with the strut-and-tie method.

Contributions by Vedad Alic
Vedad Alic was the main author of the paper, developed the idea, implemented the methods,

carried out the investigations and wrote the paper.

2.2 DEVELOPED DEMONSTRATOR PROGRAMS

During the work several tools have been developed to try out the methods: A tool for exploring optimal position of masses, a form finding plug-in for Rhinoceros 3D and a plug-in for the visual programming environment Grasshopper 3D. Additionally, a framework for bi-directional graphic statics has been developed.

Placing masses To explore different shapes of masses and their effect on mitigating soil wave propagations a tool was developed for sketching shapes of masses on top of soil. Developed by the author.

Isogemetric Analysis toolbox An Isogeometric Analysis toolbox for CALFEM for MATLAB was developed by the author during the research in Papers B and C. It is available on-line [2].

Rhinoceros 3D plug-in A Rhinoceros 3D [3] plug-in was developed for form finding of efficient shapes for shell structures. Developed by the author and by a Master's dissertation student [1].

Grasshopper 3D plug-in The Grasshopper 3D [4] plug-in uses the same back end as the Rhinoceros 3D plug-in. Developed by the author.

Graphic statics framework The algorithms are implemented using MATLAB, Python and C++ and have been used for the research in Papers D–F. A GUI in Rhino has been written using .NET and is connected to the backend by message passing. The algorithms are currently being added to the COMPAS_AGS package, as an open source extension, COMPAS_BI_AGS, available in a separate branch at [5]. The COMPAS framework is an open-source, Python-based framework for computational research and collaboration in architecture, engineering and digital fabrication. COMPAS_AGS is a COMPAS package for Computational Graphic Statics and implements [6, 7] and Paper D.

2.3 OTHER PUBLICATIONS BY THE AUTHOR

Licentiate dissertation: *Numerical Methods for Conceptual Structural Design.*
Vedad Alic.

Licentiate Dissertation, Report TVSM-3075, Lund University, 2016

Conference papers:
On the Implementation of Isogeometric Analysis for thin shells.
Puria Safari Hesari, Sara Almstedt, Fredirk Larsson, Mats Ander, Vedad Alic and Rasti Bartek.
(2017) 30th Nordic Seminar on Computational Mechanics – NSCM30.

Bi-directional Algebraic Graphic Statics - On Force Diagram Constraints.
Vedad Alic, Daniel Åkesson and Kent Persson.
(2017) Proceedings of IASS Symposium 2017: Interfaces: architecture.engineering.science.

NURBS based form finding of efficient shapes for shells.
Vedad Alic and Kent Persson.
(2016) 29th Nordic Seminar on Computational Mechanics – NSCM29

Isogeometric elements in the dynamic relaxation method.
Vedad Alic and Kent Persson.
(2014) 27th Nordic Seminar on Computational Mechanics – NSCM27

Vibration reduction in soil by addition of surface masses.
Vedad Alic and Kent Persson.
(2013) 26th Nordic Seminar on Computational Mechanics – NSCM26

Conference abstracts with oral presentation:
Form finding with T-splines and Dynamic Relaxation.
Vedad Alic and Kent Persson.
(2015) III International Conference on Isogeometric Analysis.

Simulating hanging models with Isogeometric Analysis.
Vedad Alic and Kent Persson.
(2015) 3rd Symposium on Structures in Architecture 2015.

Interactive computational modelling in early-stage architectural design.
Daniel Åkesson and Vedad Alic.
(2014) 2nd Symposium on Structures in Architecture 2014.

Vibration reduction in soil.
Vedad Alic and Kent Persson.
(2013) 1st Symposium on Structures in Architecture 2013.

3 The design process

This chapter briefly presents the architectural and structural design processes, their differences and some aspects about collaboration and communication. Further design space exploration and structural design space exploration are also presented.

3.1 ARCHITECTURAL AND STRUCTURAL DESIGN

3.1.1 Architectural design process

The early phases of a building design process are characterized by an ambiguity of design constraints and requirements and a creative work where several alternative variations of a design based on the initial requirements are quickly generated [8]. The process is often creative and iterative. The amount of design freedom and impact of design decisions is very high in the early phase, which is considered the most important phase [9, 10]. According to [9] it has been estimated that about 75% of the final product cost is accounted for by design decisions.

There are not always objective criteria for evaluation in architectural design and problems rarely have a well defined criteria for termination - one can always further improve the design [11]. It is common in architectural design to make the problem more specific while it is being solved, goals are iteratively redefined based on the previous and current design proposals. The distinction between routine and creative design can be made by how well- or ill-defined the design problems are [11]. For well-defined design problems (routine design) it is possible to follow a known procedure in order to arrive at a design proposal [12, 13].

Schön describes a part of the iterative design process as *reflection-in-action* [14]. A designer often makes representations to be constructed by others. The making process is complex with more variables and design paths that can be represented or explored in a design process. "*Because of this complexity, the designer's moves tend to produce consequences other than those intended. When this happens, the designer may take account of the unintended changes he has made in the situation and reformulate design goals and outcomes. He shapes the situation, in accordance with his initial appreciation of it, the situation 'talks back,' and he responds to the situation's back-talk.*

In a good process of design, this conversation with the situation is reflective. In answer to the situation's back-talk, the designer reflects-in-action on the construction of the problem, the strategies of action, or the model of the phenomena, which have been implicit in his moves." - Donald Shön, The reflective practitioner, 1983 [14].

To help make sense of the design situation the architect makes use of his *repertoire*, gathered from past experience and study of examples, images, understandings and actions [14].

Experienced architects tend to develop a variety of conceptual design propositions before going into depth on a select few, sometimes referred to as *breadth first, depth next* [11]. This allows for a broad search of a design space before identifying candidates for further study and detailed development. According to Akin, [11], architects tend to apply creative design strategies even for routine design problems, while engineers tend to stick to a few (or the initial) problem definition.

3.1.2 Structural design process

Mike Schlaich [15] describes the structural engineering process to consist of sound scientific and theoretical knowledge combined with creativity. He divides the daily work of the engineer into four steps: conceiving, modelling, dimensioning and detailing. The conceiving step is the most important, where the overall structural concept and important details are developed and it is argued that a structure is developed from a given context (topograhpical, technical, political, cultural...). Errors and difficulties that arise later in the project are often due to poor decisions in the conceptual design [15]. It is further described that the design process is never straight forward, solutions are often reached in an iterative and slightly chaotic manner. Schlaich's views are that the engineer bears cultural and social resposibility for his structures and and that he is a partner of the architect and not a stress analyst [15]. The views that the engineer should be part of the initial design are shared by other engineers [16, 17].

Engineers need to justify decisions based on calculations and structural theory. A building which cannot be proven sound should not be built, leading to design processes where often the early stages are neglected in favour of investing time into the later more rational and analytic parts of the engineering design process. Creative structural design includes subjective choices - "*It appears to be forgotten that for every engineering task there are a practically unlimited number of solutions and that, because of this, it is never possible to make a choice according to purely functional considerations. Of necessity, it must be hit upon subjectively.*" - Jörg Schlaich [18].

3.1.3 Collaboration and Communication

"*Collaboration can only be fruitful and the overall quality of the building satisfactory, if each partner understands the language of the other*" - Jörg Schlaich, On the conceptual design of structures, 1996 [17].

The earlier stages are usually performed by the architecture team alone, without the expertise of the engineers. Some of the main design decision by the architecture team affect the performance aspects of the building, such as related to structure, acoustics, and energy [19]. Engineers are often omitted from the stage where they have the greatest opportunity to influence the structural performance [20]. However, this is not always the case. Schlaich and his office likes to be included early, and attempt to provide several conceptual structural designs which they think work with the overall concept. If none of the designs are satisfactory new ones will be suggested until one is agreed upon together with the architects [18].

Balmond [21] is another engineer involved early in design projects. In [21] he describes how he together with Rem Koolhaas designs a villa with the desire to make it 'fly'. Mechanical concepts are used throughout the design process to help reach this goal, both in the overall shape but also in the detailing. Throughout the process, simple sketches are used to share and communicate ideas - sketches and drawings become an important means of communication.

3.1.4 Considering structural performance

There are several reasons for why it is important to include structural performance considerations early on in the conceptual design stage. Form and member topology are the two most important aspects of structural performance [22], they are generally already determined during conceptual design. Another important factor for structural performance is the boundary conditions. If the effects of form, member topology and boundary conditions on the building as a structure have not been considered it can lead to wasteful and poorly performing solutions resulting in that structural engineers need to make poor design work. If the form of the building is innovative, it can be difficult to realise with a conventional structural system, and a challenging task for the structural engineers to understand the structural behaviour. Results can be wasteful, expensive, and maintenance-intensive, and it can ultimately lead to poor design and even collapse, see for example [22, 23].

If the structural design, however, is considered from the beginning of the project, the work load on the structural engineering team is reduced. Structures whose conceptual design is well thought out early in the project, with ideas of load paths and overall structural behaviour included from the start are often easier to deal with in the detailed design and analysis stages [15]. Moreover, the range of solutions is much larger as only a few constraints have been set, and there are opportunities for better performing solutions, and on occasion, solutions whose quantifiable aspects are integrated into the design.

Well performing structures require less use of material, lead to savings in cost, consume fewer resources, are more sustainable, safer, are more durable and easier to build [22].

Consideration of form early on in a design process makes it more likely that the architectural intentions of the project will be realized, since the risk of requiring changes to the design due to structural considerations in later stages are reduced. Early structural considerations can lead to

an increased architectural variety. It can also lead to buildings where the aesthetic, functional and technical considerations are in harmony.

In conclusion, considering only parts of the design requirements during conceptual design limits the success of the whole design process and the final proposal. Enlarging the set of requirements assessed at an early stage, enhances interdisciplinary interaction, and creates designs whose performance aspects have greater chances of success. To include engineering related aspects in early-stage design requires close collaboration and communication between architects and experts in different fields of engineering, as well as the availability of tools, such as simulation software suitable for conceptual studies and design.

3.2 COMPUTATIONAL DESIGN

The use of computer tools has become widespread in engineering and in architecture. Software tools for making design decisions have been developed, however, most of the software available today are applicable to detailed design phases [9, 10]. Poor choices made in the conceptual design phase are difficult to compensate for in the detailed design phase, yet there have been very few computer-tools developed for the conceptual design phase. Partly since the amount of design specific information available in the early phases of a design is limited [9], and early stage design often includes rapid changes in design direction. These factors make it difficult to use computer based tools which often require precise information that is time-consuming to input into the computer, and the solution methods used are slow and not suitable for interactive manipulations.

The current availability of computational tools reflect and strengthen the separation of design from structural behaviour [22]. Architectural tools are focusing on geometry, independent of performance, whereas structural tools are focusing on analysis of an already established geometry.

However, the time available to create a design proposal is getting increasingly shorter due to increased financial pressure while projects are in general increasing in complexity. In the later design stages computers help produce results faster and manage the complexity better. Developing computer tools for the early design process can help in making better, more informed decisions that include more aspects in the early design, and streamline the later stages of detailed design process. The use of computational tools also has the advantage of being able to store, re-use and share the generated design knowledge, and potentially apply it to other projects.

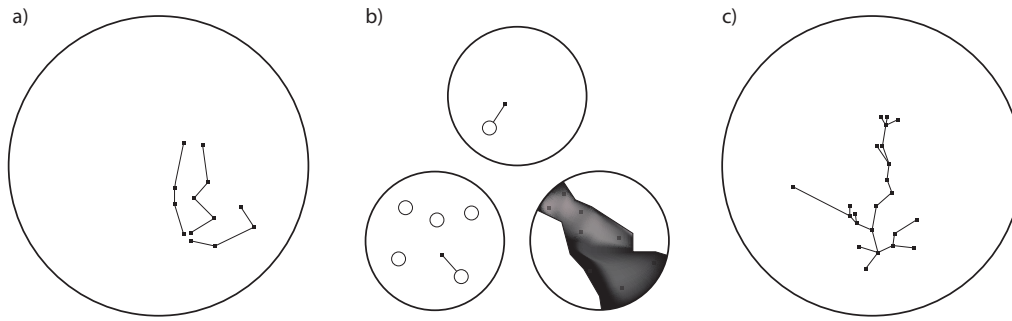


Figure 3.1: Design space traversals: (a) parametric studies (b) optimization (c) interactive exploration.

3.2.1 Design space exploration

Design space exploration is the task of exploring many design alternatives before deciding on a final solution. This task rests on the idea that the computer can usefully portray design as the procedure of exploring alternatives [24]. Akin's terminology of *breadth first, depth next* [11] sounds like exploration, whether Akin's work translates to the digital medium is discussed in [24]. Design differs from problem solving in that the goals are not fixed from the start [25]. This requires the representation of many designs from a network called a design space, which is explored by traversing paths in the network. Fig. 3.1 depicts some common types of traversals of a design space.

Design space exploration rests on three premises [24], first that it is a model that support observed designer workflows, second that designers benefit from tools that amplify abilities to search for designs, represent goals and problem spaces, and the third relates to the availability of representations and algorithms suitable for design exploration. Each of these is an area of research. In [24] an overview of each is given, here, some parts related to the thesis are briefly recounted.

Features of design representations suitable for design exploration contain the following properties: they are partial and intentional representations of an object; carry both strong and weak representational qualia; and must support alterations to the object represented [24]. Design spaces are vast, and an random initial design is unlikely to be acceptable, thus it is important that suitable designs are attainable with reasonable effort during exploration.

Further, strategies for amplifying human cognitive abilities are described, these include [24]:

- Representational prowess – representations of objects should be just enough to enable exploring without overburdening with specifics. For instance, solid modeling allows for abstract boolean operations without requiring considerations of what the solid consists

of.

- Codification – designers prefer to use past successful moves in new designs. By encoding parts of a design using rules it can be adapted to other settings and some design decisions may be postponed to later stages. This includes scripting, parametric modeling and rule based generative systems. The methods developed in Papers B–E support use with parametric modeling.
- Explicit design space – an explicit design space contains alternative solutions to the problem at hand and can be an accessible way of making new discoveries in the implicit space. Alternatives are also important in that only some of them may be able to represent some of the design criteria. Paper E includes an example by using self-organizing maps which organize high-dimensional data by providing an orderly mapping to a low-dimensional grid and provide an overview of the possible designs in a design space. Another common approach in engineering is to perform parametric studies.
- Implication – further designs on a design path can only be reached from the current state, thus what can be inferred from the design representation is important. An example of this is creating renderings from a model which enables different views, lightning conditions and material selections.
- Speed – the design paths explored and decisions taken should be with reasonable effort. If designs can be computed quickly, the speed will be governed by the ability to make choices which further the design. The methods in Papers B–E can compute designs quickly, and provide different means of visualization in order to support decision making.
- Backup – most CAD systems include an undo command, which significantly reduces the costs of recovery from mistakes.
- Recall – extends the idea of back to further distances or time. This can even include precedents from other designers, one method of including this can for instance be through search engines.
- Replay – using a precedent in a new context. The most common method in CAD systems is trough copy and paste, or to copy and apply path, i.e. apply design rules to a new context.

3.2.2 Structural design space exploration

Mueller discusses different means of computing structural design space [22]. Two categories of conceptual structural design tools are identified; feedback tools and guidance tools. Feedback tools use existing analysis and verification methods but rely on real-time or near real-time structural analysis integrated into design tools in a user guided interactive experience. The

aim is to provide rapid feedback about the structural performance in order to aid in exploring different structural solutions for the design. Guidance tools use optimization techniques in order to suggest new design alternatives based on structural performance.

Olsson discusses the term *structure and quality* in [26]. Several concepts from structural mechanics are discussed regarding their qualitative and abstract values - equilibrium, stiffness, mechanisms, etc. are used to reason about the relationships between matter, space, structure and loads. These give limited and alternative views on how a sketch might be interpreted as a structure, which is in line with features of design representations discussed in [24].

Research of conceptual structural design tools is an emerging field where researchers have taken several different directions, the literature review in the following chapter and [22, 27] give a brief overview. Although there has been some research done, there is a need for development of methods and tools to be used in conceptual structural design.

3.3 CONCLUSIONS AND PRESENT RESEARCH

During the last decades, there has been an extraordinary development of computer-based tools intended for presenting or communicating the results of architectural projects. However, the tools primarily focus on the geometric aspects of the design. The literature review in this chapter covered the architectural and structural design process, and the computational design strategy of design space exploration. Including engineering aspects and supporting collaboration in early design space exploration requires suitable tools. In the following chapters a summary of representations and algorithms suitable for design space explorations where structural considerations are included will be presented.

4 Tools for conceptual structural design

In this chapter, computer based tools for conceptual structural design are discussed. Implementations of the formal design space strategies described in the previous chapter are here presented in tools that are available and used for structural design. It covers rapid feedback tools, computer aided design and computer aided engineering, conceptual representations of structures, introduces graphic statics. Additionally, an overview of form finding and structural optimization is covered.

4.1 RAPID FEEDBACK TOOLS

Rapid feedback tools rely on that results can be produced very quickly. In terms of design space exploration the key is not only to compute results quickly, but that it leads to quick unfolding of paths in the design space [24].

Several rapid feedback tools based on the finite element method have been developed at the Division of Structural Mechanics, Lund University. These are ForcePAD [28], ObjectiveFrame [29], and Sketch a Frame [30]. Finite element based rapid feedback tools are adapted to conceptual design by removing time consuming aspects such as precise geometry, material specification, and meshing. The approach doesn't necessarily provide results of high accuracy, but gives insight and allows for qualitative studies of structural behavior.

The key idea behind ForcePAD is that it employs metaphors similar to those of image editing applications. In the application one paints a structure where the stiffness of different parts is controlled by the gray scale, where white is no stiffness, and black is maximal stiffness. The method allows for quick sketching of structures and to make changes to them.

ObjectiveFrame provides real time deformation feedback of loads applied to frame structures, as an idea to imitate the learning of structures trough physical models. There has been some recent development of ObjectiveFrame by use of the Leap Motion controller, which allows the user to interact with structural models by using their hands to apply forces, see Fig. 4.2.

Sketch a Frame is a tablet computer application for conceptual design of trusses and frames,

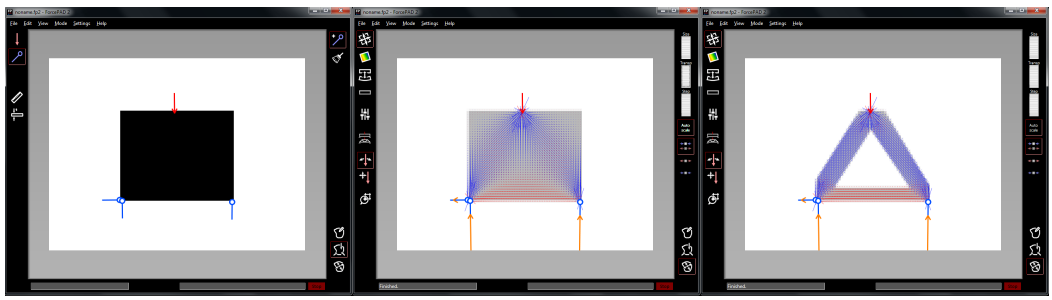


Figure 4.1: The GUI of ForcePAD showing a simply supported block: (left) Physics mode, (middle) Action mode showing the principal stresses, blue is compression and red is tension, (right) Action mode with modified structure, where low stress parts are removed, resulting in a truss.

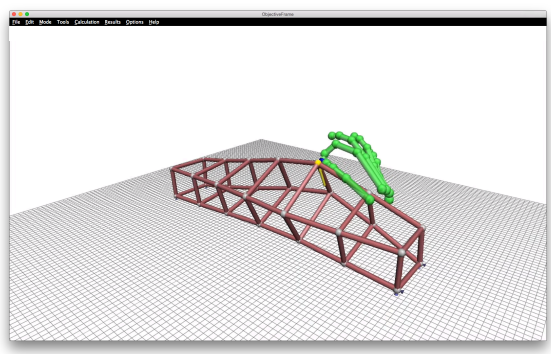


Figure 4.2: The GUI of ObjectiveFrame, showing a deformed model and the hand input.

developed for use on the iPad. It allows the user to directly manipulate structures and loads trough a multi-touch interface. Providing real time feedback it allows for exploration of form, see Fig. 4.3 for an example. The tool also has the capability to show normalized static redundancy factors, allowing the user to identify members that can be removed from a statically indeterminate structure.

Other academic and commercial applications of real time numerical tools have also been developed, such as the Model-Alive feature of SAP2000 [31], Force Effect [32], PointSkecth2D [33], and Dr. Frame 3D.

Recently, a number of tools have been developed with the intention to include structural considerations into Computer Aided Design (CAD) software. Their approach is to integrate structural analysis modules into CAD software and allow for a smooth work-flow, allowing the user to make changes to a design and immediately perform an analysis. Through iterations, it

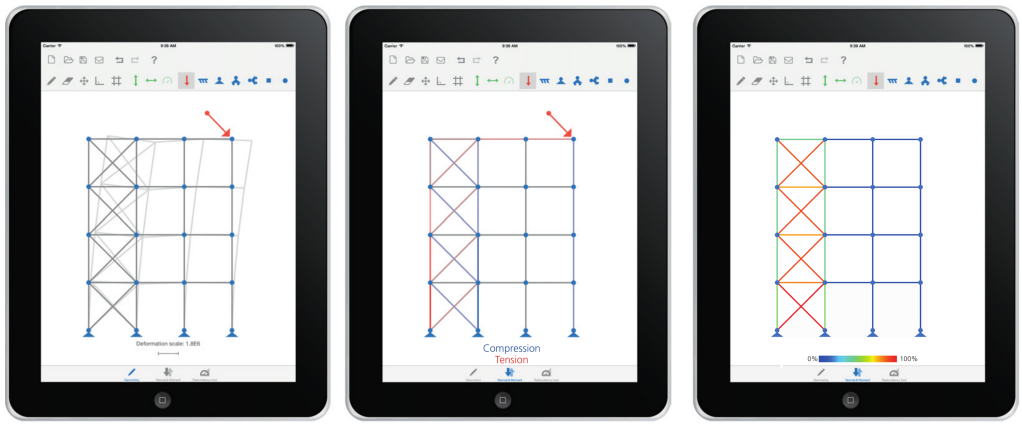


Figure 4.3: The GUI of Sketch a Frame, showing (left to right) deformation, normal forces, and normalized static redundancy factors.

becomes apparent how design changes affect the performance. The tools can make analysis directly for the available geometry in the main software, however, additional discretizations of the geometry is necessary after changes in the geometry, before the numerical analysis is performed. It is not always possible to automate the discretization, and the design geometry can have many details that are unnecessary in the analysis and may make it time consuming. The tools are often limited to a single CAD application, or a combination of a CAD and FEA-program.

Some popular examples of such tools are Geometry Gym for Rhinoceros (Mirtschin, 2011), Karamba [34] for Rhinoceros, Kangaroo Physics [35] for Rhinoceros and Robot [36] for Revit. Karamba provides the ability to set up structural models in the visual programming environment (also called parametric environment) Grasshopper for Rhino. Geometry Gym also interacts with Grasshopper and connects the parametric models to popular BIM or structural analysis software.

The tool developed during the research presented in Paper A belongs to the class of rapid feedback tools. It uses the same metaphors as ForcePAD.

4.2 CAD AND CAE

CAD tools are used for developing designs, drafting, documentation, and communication of for instance a proposed design or construction documents. One of the first computer tools in the area of CAD was Sketchpad 1963 [37]. The ancestor to CAD pioneered the way of human-computer interaction, graphics user interfaces and computer graphics. In the beginning commercial CAD tools were used for documentation of designs by use of 2D drafting,

and have since been developed to capable 3D software. CAD tools used in the built environment are categorized as follows:

- Drafting tools: 2D drafting, 3D drafting
- Building information modelling (BIM)
- Design computation

It was simple to introduce 2D drafting into existing design processes as it continued the practice of representing buildings as multiple 2D drawings [38]. Some believe that it delayed the use of 3D tools even though they were available [38].

The foundations of BIM were established in the 80s [38]. BIM represents a design as an assembly of objects. BIM workflow forces one to define or use pre-defined objects before the overall form. The object approach limits itself to later stages since it requires detailed information which is missing in the conceptual design. BIM is often criticized for being easy to create the obvious (using common objects) but difficult when one needs to deviate and create design innovations. BIM has good support for collaboration, multiple disciplines can work in a common model.

If drafting and BIM are the first two eras of building related CAD then design computation is the third (although their developments overlap each other). According to [38] some objectives of design computation are to overcome limitations of BIM (the ability to define own objects and inter-object behaviors) and to move away from manual modeling. In design computation the designer is no longer directly modeling the building: instead time is spent developing a graph or script whose execution generates the model. An apparently minor edit to the graph or script could have a large effect on the generated building, enabling the exploration of a vast array of alternatives. Recently the visual programming environment Grasshopper [4] for the CAD program Rhinoceros [3] is such a tool that has become very popular, see Fig. 4.4. In Grasshopper the user creates parametric models by connecting consecutive components (creating a graph) which operate on geometry in Rhino. A similar tool to Grasshopper is Autodesk Dynamo [39].

Apart from the mentioned three general categories there are other CAD tools available. Solid modelers are common as design tools in other industries, but are a rare occurrence in building design, but have occasionally been used, e.g. solid modeling in Digital Project originally developed by Gehry Technologies. General graphics suites e.g. Maya have been used as conceptual sculpting tools at some architectural studios (e.g. Zaha Hadid Architects) since they are well suited for free form modeling.

CAD tools are well developed and successfully used in early design stages to explore geometric alternatives. However, they are often limited to geometric considerations and do not consider structure or other performance based aspects of buildings.

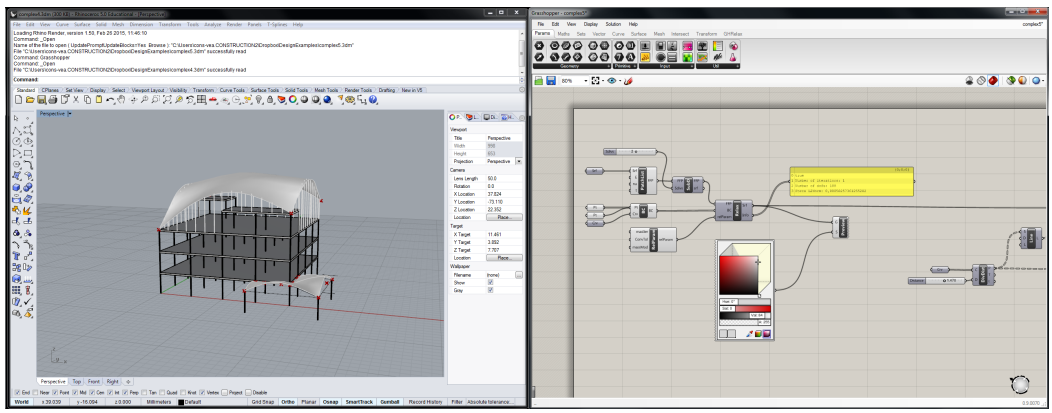


Figure 4.4: The GUI of Rhinoceros V.5 (left) and Grasshopper V.0.9 (right).

Software tools that support engineering tasks are termed CAE, the term is broad and includes software for FEA, computational fluid dynamics (CFD), multi-body dynamics (MBD) and optimization.

Finite element programs offer capabilities to perform detailed analysis of a structure, including stresses and displacements, but also non-linear effects such as plasticity, fracture, and buckling. Although being very powerful and able to handle complex geometries, finite element programs require the definition of a pre-set geometry, selected materials, application of forces and defined support conditions in order to provide a solution. The amount of detailed information required for a typical finite element program limits their use in conceptual design. Further, traditional FEA tools produce results with very high precision, however, in conceptual simulations only qualitative results are necessary. Attempts have been made to adapt the FEA to conceptual structural design, some of these are part of the literature review in the following section.

4.3 FORM FINDING

There have been several definitions of classical form finding, one is [40] "*form finding is a forward process in which parameters are explicitly/directly controlled to find an 'optimal' geometry of a structure which is in static equilibrium with a design loading.*". Some recent definitions of form finding are much broader, [41] "*finding an appropriate architectural and structural shape*", allowing for additional constraints and performance criteria. In [42], the different types of definitions are separated into classical and modern form finding.

Regardless of which definition is used, it is known that geometry has a key role on structural performance related goals in buildings. Geometry is also important for other performance related aspects, such as energy, whose relationship to geometry has in the last decade seen an

increase in studies [43].

Classical form finding methods are used to find efficient shapes for arches, shells and membranes under certain loads, such as the self-weight or pre-stress. The methods are a type of optimization, but do not rely on general mathematical optimization techniques, but rather on finding states of equilibrium for a prescribed load or stress. The methods can be divided into two types. The first is related to pre-stressed structures, whose shapes are analogous to minimal surfaces. The second is related to the hanging chain and its inverse.

Pre-stressed structures carry applied loads trough tension and are stiffened by the pre-stressing. These can be cable nets or fabric membranes. These structures are some of the most efficient in terms of dead-load to span ratio. The aim of the form finding for pre-stressed structures is to find a shape that is in equilibrium for the prescribed pre-stress. One approach to do this physically is to use soap films which almost assume the shapes of minimal surfaces, see Fig. 4.5, bounded by rigid steel wires. Frei Otto [44] at the Institute for Lightweight Structures (IL) was one of the early adopters of such methods. The shapes from soap film experiments are related to isotropic pre-stress states, however, for fabrics the material properties in the directions of the warp and weft can vary, and it is possible to prescribe an anisotropic pre-stress.

The idea of the hanging chain and its inverse is well known. As the hanging chain cannot take any bending stresses the resultant shape will be in pure tension, which is generally a much more efficient use of material than in bending. A physical form finding model with hanging chains is shown in Fig. 4.5. Inverting the shape creates an arch in pure compression. The method can be extended to membranes which are physically form-found using hanging cloths, which when inverted give the shape of a vault in compression (for simple geometries). For shapes that are more complex the process of finding shapes by use of hanging cloths becomes difficult due to wrinkling from in-plane compressive forces. Heinz Isler [45] pioneered the use of cloths for form finding both as conceptual models and for precise measurements. Using these techniques in physical models required knowledge about the cloths anisotropic properties, the cutting pattern, as well as good structural intuition and patience. Generally, care must be taken when designing compressive structures, such as vaults and arches since buckling may occur.

There is a wide range of numerical methods for form finding, most of which were initially developed for the form finding of pre-stressed structures. For the form finding of pre-stressed structures, pre-stress is prescribed to an initial form which deforms until it settles in an equilibrium state. During the process only geometric stiffness is accounted for, which causes singularities in the tangential mesh direction (nodes are allowed to move freely on the surface). In form finding of hanging models with membrane elements, another type of singularity arises in the surface normal direction, since the elements only provide stiffness in the surface directions. This can for very fine meshes lead to mesh dependent, artificial wrinkling patterns. Different approaches for dealing with the mentioned singularities have been studied and can be divided into three different types [42]:

- *Dynamic methods* solve for the static equilibrium by the use of a fictitious dynamic sim-

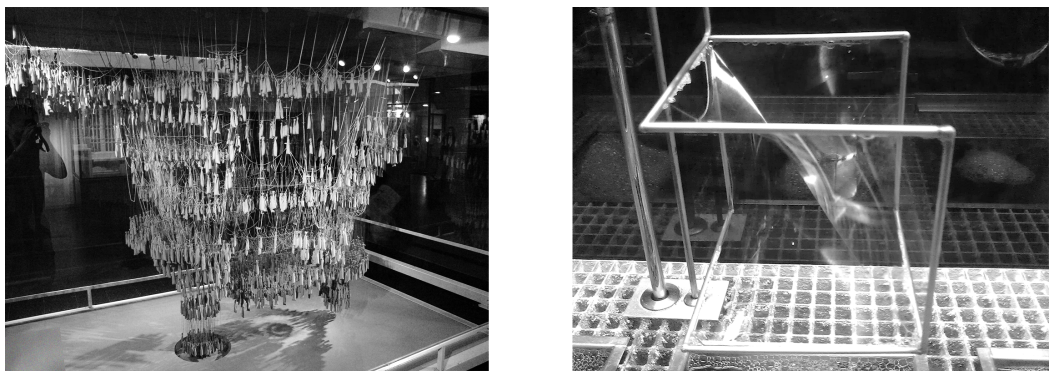


Figure 4.5: Hanging model and soap film model, from Wikimedia Commons.

ulation. The addition of inertia avoids the difficulties of the singular stiffness matrices. A popular method in this category is dynamic relaxation [46,47]. For the pre-stress type of singularity fictitious forces tangent to the surface may be needed.

- *Geometric stiffness methods*, such as the force density method [48], used for the form finding of cable nets. The cable force is replaced by a force density, which is the ratio of cable force to cable element length. The replacement makes the equations of equilibrium linear.

- *Stiffness matrix methods* rely on adding penalty stiffness to the stiffness matrix to prevent or control singularities. See, for instance [49, 50].

Form finding usually requires several iterations, where the designer alternates between specifying mechanical requirements and performing form finding and evaluating the shapes with respect to other design criteria. If it is necessary, changes are made to some mechanical conditions (boundary, initial geometry, material parameters) until a form that fulfils the design requirements is found. Mechanical considerations and design aspects are closely connected and require good communiction between FEA and CAD tools. There are many tools developed which simplify this connection. The tools exist both as standalone tools, such as CADenary [51], one of the first tools for interactively exploring hanging models, and, as plug-ins to CAD software: Kangaroo [35], Karamba [34], SmartForm [52], Rhinomembrane [53], RhinoVault [54].

All of the developed methods and tools that have been covered in the literature review require the discretization of some initial geometry into finite elements. Because of the discretization, it is difficult to continue changing the geometry of a model after the form finding process, since common CAD tools have poor support for FEA type of geometries. Often the employed elements in the FE simulation are flat and lead to faceted geometries, while shells and membranes are curved and smooth, see Fig. 4.6.

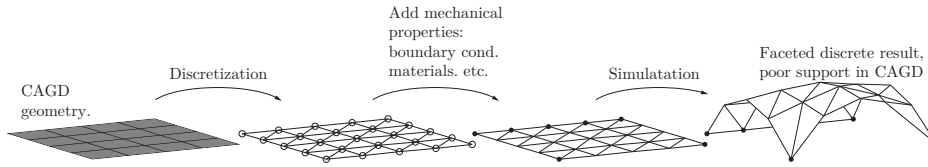


Figure 4.6: Traditional work-flow for form finding, starting with a CAD geometry and ending with a FE-solution with discrete geometry.

Papers B and C present a form finding framework based on NURBS based membrane elements solved with dynamic relaxation, which can be used directly in CAD software.

4.4 GRAPHICAL METHODS

Graphical methods present the geometric relationships between a structural configuration and its internal distribution of stresses. In the 19th century graphical methods were devised to analyze trusses, offering an alternative way to solving the equilibrium equations by hand. They lost in popularity when calculators and modern computers became available. They are again increasing in popularity and research due to advances in CAD and computational methods.

The recent developments do not aim to compete with structural analysis methods, instead, the aim is to provide means for exploring structures in static equilibrium, for early conceptual design. The methods can be automated in modern CAD environments and are no longer limited to two-dimensions. With the use of algebra the relationships between geometry and internal forces and the manipulation of the relationships can be made clear and precise, removing old limitations such as requiring the structures to be statically determinate and not requiring tedious iterative procedural drawing by hand to reach specific geometric configurations that fulfill assumptions on loads and geometry (for instance having a self-weight and a geometric configuration that goes trough some select points).

The most common version of graphic statics is based on the construction of two reciprocal diagrams: the form diagram representing the actual geometry of the structure, and the force diagram that represents the internal forces through vectors. Changes in the geometry are reflected in the force diagram, providing a visual relationship between the two. Similarly, changes in the force diagram are reflected in the form diagram. Because forces are graphically represented using vectors, no numerical analysis is required to calculate the forces.

Papers D–E formulate a framework for force driven design using graphic statics. The framework enables interactive manipulations of graphic statics diagrams that are straightforward to integrate into CAD software.

4.5 STRUCTURAL OPTIMIZATION

Exploring a design space and searching for well performing solutions is a process well suited for optimization techniques. In structural design, optimization combines techniques from CAD, non-linear mathematical programming, and computational mechanics [55]. The methods optimize some objective function f (for instance the weight, stiffness, or strain energy) with respect to some design variables $\mathbf{x}$. Normally constraints and variable bounds on $\mathbf{x}$ need to be satisfied as well.

There are three common types of structural optimization: size optimization, shape optimization and topology optimization. Optimization tools are able to change the geometry to better suit the objective, and can act as guidance tools by suggesting geometry changes.

For shape optimization problems the state of the art approach is to describe the geometry and design variables using NURBS patches. This is done to avoid mesh distortion which is common if the coordinates of the finite element nodes are used as design variables directly [55]. Further, by using NURBS patches there is an advantage that the number of design variables are reduced.

For truss structures the most common optimization approaches are topology optimization, both using a continuum [56] and using the ground structure approach [55]. Both have been studied for the automatic generation of strut-and-tie models (STM), see [57] and [58] respectively. Paper F uses structural optimization to find optimal strut-and-tie networks in arbitrary polygonal regions. The objective function is formulated using graphic statics.

Traditional optimization has the limitation that it converges to one optimal solution, this is not well suited for conceptual design where the designer wants to generate multiple solutions and where some goals can be of a qualitative type. To generate multiple alternatives usually requires a change of the initial conditions, which can result in that the optimization algorithm converges to different local optimum. An alternative is to use heuristic optimisation methods, such as genetic algorithms, can generate multiple well performing designs. These can be better suited from other design objectives which are either still not discovered as important by the designer, or are difficult do describe in an objective function [59] (i.e. non-performance oriented objectives). Mueller [22] has proposed methods for allowing the user to interact with an optimization algorithm, [60], being able to generate several design proposals with good performance but not necessarily the optimal, which are instead selected out of other aspects. See for instance the online tool structureFIT [61].

5 Finding forms for vibration reduction

5.1 BACKGROUND

Most existing tools for conceptual structural computations focus on problems related to statics. However, on some occasions it is important to consider dynamic effects in the conceptual design phase. As our cities continue to grow and get denser, noise and vibration pollution will be important to consider. In the prototype tool presented here a method proposes how to place masses or buildings to reduce vibrations nearby a high-tech facility which is sensitive to vibrations.

In [22] computational structural design tools are grouped in to two groups, feedback tools and guidance tools. Since the questions asked in the stage of the urban planning process are very broad and imprecise, a guidance based tool (which typically requires a well-defined objective function and design variables) was not developed, and focus was on developing a rapid feedback tool, since it offered a freer exploration and could be used as support in a collaborative setting.

5.1.1 Present research

MAX IV, a synchrotron light source, is a national laboratory in Lund, which is operated jointly by the Swedish Research Council (VR) and Lund University. The facility is located northeast of Lund, at the outskirt of a new area, Lund North-East, roughly 100 meters southeast of the highway E22, see Fig. 5.1 (a).

The instruments that are operating on nano-level scale at MAX-IV are sensitive to vibrations, where a vertical displacement requirement of 20–30 nm RMS during one second for frequencies above 5 Hz and below 100 Hz has been set in order to ensure good quality of the measurements. With the facility located closely to the highway, vibration reduction measures have been taken to ensure good operation of the facility. The measures include stabilization of the soil underneath the facility to a depth of 4 m (stiffening), and the shaping of the ground topography around the facility in a way that will reduce vibrations, see [62, 63]. Other more conventional methods for vibration reduction have also been studied, such as open and in-

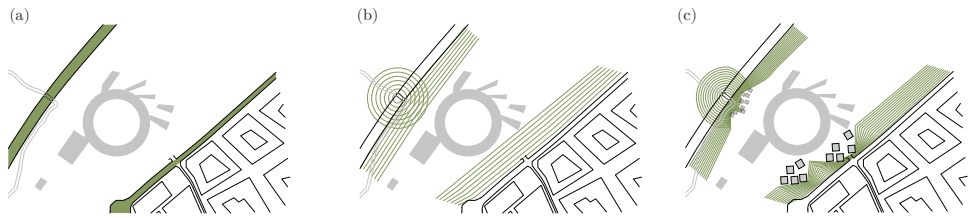


Figure 5.1: Research idea: (a) roads close to facility (b) vibrations from roads (c) reduced by masses of buildings placed in patterns.

filled trenches [64].

Placing out patterns of heavy masses or buildings on the soil surface between the external sources and the facility, see Fig. 5.1c, could be a cost effective and maintenance free solution, and as one that is more appropriate in an urban situation than more traditional methods such as trenches. As such, it is of interest to find out if it is a possible method of vibration mitigation, and, if this was the case, which configurations are most effective. In order to achieve the objectives, a form finding tool was developed where heavy elastic bodies could be added on top of the soil surface between the vibration source and facility. The tool was developed using the finite element method and in order to achieve quick unfolding of paths in the design space a reduction method was devised to improve the computational cost of the method. The heavy elastic bodies added on the soil surface are here on referred to as masses.

The following sections present the theory and application for the development of the exploration tool used in the introductory example of the thesis and in Paper A.

5.2 THEORY

5.2.1 Elasticity

In the derivations operators beginning with capitals are related to material coordinates, and those beginning with lower case relate to spatial coordinates. For instance

$$\mathrm{Div}(\mathbf{A}) = \frac{\partial A_{ij}}{\partial X^j}\mathbf{e}_i; \qquad \mathrm{div}(\mathbf{A}) = \frac{\partial A_{ij}}{\partial x^j}\mathbf{e}_i \tag{5.1}$$

where X^j are material coordinates and x^j are spatial and $\mathbf{e}_i$ are unit basis vectors pointing in the axes of a Cartesian reference frame. Summation of repeated indices is implied. Roman indices range from 1 to 3, and Greek indices range from 1 to 2.

Strong form of elasticity

The structural mechanics theory used throughout the thesis begins with the equation of motion (EOM). Cauchy's first EOM can be derived from the balance of linear momentum [65]. In the local form along with the necessary boundary conditions in the spatial description, Cauchy's EOM is [65]

$$\left.\begin{aligned} \operatorname{div}(\boldsymbol{\sigma}) + \mathbf{b} &= \rho\ddot{\mathbf{u}} \\ \mathbf{u} = \bar{\mathbf{u}} \quad &\text{on} \quad \partial v_u \\ \mathbf{t} = \boldsymbol{\sigma}\mathbf{n} = \bar{\mathbf{t}} \quad &\text{on} \quad \partial v_\sigma \end{aligned}\right\} \tag{5.2}$$

where $\boldsymbol{\sigma}$ is the Cauchy stress tensor, $\mathbf{b}$ is the current body force per unit current volume and $\rho\ddot{\mathbf{u}}$ is the inertia force per unit current volume. The displacements $\mathbf{u} = \mathbf{u}(\mathbf{x}, t)$ are prescribed on ∂v_u and the traction $\mathbf{t} = \mathbf{t}(\mathbf{x}, t, \mathbf{n})$ is prescribed on ∂v_σ. The boundary to the body v is the surface $\partial v = \partial v_u \cup \partial v_\sigma$. $\mathbf{n}$ is the unit outward normal to the surface. The prescribed displacements and tractions must be supplied for $t = 0$. Additionally, since this is an initial value problem the initial conditions need to be prescribed [65]. The local form is assumed to hold in every point of the body and for all times.

Weak form and virtual work

To obtain the principle of virtual work in the spatial description we multiply Cauchy's first equation of motion with an arbitrary vector valued weight function $\mathbf{v} = \mathbf{v}(\mathbf{x})$ and integrate over the volume v. After some manipulations and the application of the divergence theorem we first obtain the weak form of Eq. (5.2)

$$f(\mathbf{u}, \mathbf{v}) = \int_v [\boldsymbol{\sigma} : \operatorname{grad}(\mathbf{v}) - (\mathbf{b} - \rho\ddot{\mathbf{u}}) \cdot \mathbf{v}] \mathrm{d}v - \int_{\partial v} \boldsymbol{\sigma}\mathbf{v} \cdot \mathbf{n} \mathrm{d}s = 0 \tag{5.3}$$

where $\mathbf{v}$ vanishes over the part of the surface where $\mathbf{u}$ is prescribed. The weak form needs to be supplied with the essential boundary conditions at $t = 0$, as well as the initial conditions.

If the weight functions $\mathbf{v}$ are considered to be the virtual displacements $\delta\mathbf{u}$ then the weak form leads to the principle of virtual work in spatial description

$$f(\mathbf{u}, \delta\mathbf{u}) = \int_v [\boldsymbol{\sigma} : \operatorname{grad}(\delta\mathbf{u}) - (\mathbf{b} - \rho\ddot{\mathbf{u}}) \cdot \delta\mathbf{u}] \mathrm{d}v - \int_{\partial v_\sigma} \bar{\mathbf{t}} \cdot \delta\mathbf{u} \mathrm{d}s = 0 \tag{5.4}$$

which can be separated into the internal and external virtual work

$$\delta W_{\text{int}}(\mathbf{u}, \delta\mathbf{u}) = \int_v \boldsymbol{\sigma} : \operatorname{grad}(\delta\mathbf{u}) \mathrm{d}v \tag{5.5}$$

$$\delta W_{\text{ext}}(\mathbf{u}, \delta\mathbf{u}) = \int_v \mathbf{b} \cdot \delta\mathbf{u} \mathrm{d}v + \int_{\partial v_\sigma} \bar{\mathbf{t}} \cdot \delta\mathbf{u} \mathrm{d}s \tag{5.6}$$

where the inertia terms have been neglected and the equilibrium condition is $\delta W_{\text{int}} - \delta W_{\text{ext}} = 0$, valid for any virtual displacements $\delta\mathbf{u}$.

The equations are written in material coordinates using pull-back operations [65], and the internal virtual work is now written as

$$\delta W_{\text{int}}(\mathbf{u}, \delta\mathbf{u}) = \int_V \mathbf{P} : \text{Grad}(\delta\mathbf{u}) \text{d}V = \int_V \mathbf{S} : (\delta\mathbf{E}) \text{d}V \tag{5.7}$$

where $\mathbf{P}$ is the first Piola-Kirchhoff stress tensor and $\mathbf{S}$ is the second Piola-Kirchhoff stress tensor. $\mathbf{E}$ is the Green-Lagrange strain tensor, and its variation is $\delta\mathbf{E}$. The external virtual work in material coordinates is

$$\delta W_{\text{ext}}(\mathbf{u}, \delta\mathbf{u}) = \int_V \mathbf{B} \cdot \delta\mathbf{u} \text{d}V + \int_{\partial V_\sigma} \bar{\mathbf{T}} \cdot \delta\mathbf{u} \text{d}S \tag{5.8}$$

where $\mathbf{B}$ is the body force per unit reference volume and which is related to $\mathbf{b}$ trough $\mathbf{b} = J^{-1}\mathbf{B}$ (and the volume change $\text{d}v = J\text{d}V$), and $\bar{\mathbf{T}}\text{d}S = \bar{\mathbf{t}}\text{d}s$. J is the determinant of the deformation gradient $\mathbf{F}$. Lastly the integral for the inertia terms is related by $\rho_0 \text{d}V = \rho \text{d}v$.

Linear elasticity

In Paper A the assumptions of linear elasticity and small displacements are employed, i.e. the displacements are assumed to be infinitesimally small, and a linear elastic material law is used. Under these assumptions the equilibrium of a body can be established in the undeformed configuration and the equation of virtual work is simplified to

$$\delta W = \int_V [\boldsymbol{\sigma} : (\delta\boldsymbol{\epsilon}) - (\mathbf{b} - \rho\ddot{\mathbf{u}}) \cdot \delta\mathbf{u}] \text{d}V - \int_{\partial V_\sigma} \bar{\mathbf{t}} \cdot \delta\mathbf{u} \text{d}S = 0 \tag{5.9}$$

where $\delta\boldsymbol{\epsilon}$ is the variation of the engineering strain, and $\boldsymbol{\sigma}$ is the engineering stress [66].

5.2.2 The finite element method

The finite element method is based on dividing a region governed by physical phenomena into a set of smaller regions, or finite elements. Approximations of the primary unknown are assumed over the elements. Even though the physical phenomena may vary in a highly non-linear fashion over the whole region the simpler linear or quadratic approximation may hold over the element, provided the element is small enough. The approximations are some kind of interpolation over the element where it is assumed that the values are known at some certain *nodal* points, which are usually located at the boundary of each element.

For a problem where the displacement field is to be approximated, we have e.g. $\mathbf{u} = \Sigma_{i=1}^{n} N_i \hat{\mathbf{u}}_i$ where $\mathbf{u}$ is the discretized displacement field, N_i is the i:th basis function, which is typically non-zero over a sub-set of elements, and $\hat{\mathbf{u}}_i$ is the nodal displacement vector of the i:th node.

To apply the finite element method to Eq. (5.9), Galerkin's method is adopted, whereby the virtual displacements are discretized using the same basis functions. Using Voigt notation and arranging the basis functions and nodal displacement vectors (and virtual) into $[3\ x\ n]$ and $[n\ x1\ ]$ matrices respectively, i.e.

$$\mathbf{N} = [N_1\mathbf{I} \ldots N_i\mathbf{I} \ldots N_{n/3}\mathbf{I}]\,; \qquad \hat{\mathbf{u}} = \left[\mathbf{u}_1^{\mathrm{T}} \ldots \mathbf{u}_i^{\mathrm{T}} \ldots \mathbf{u}_{n/3}^{\mathrm{T}}\right]^{\mathrm{T}} \tag{5.10}$$

where n is the number of degrees of freedom and $\mathbf{I}$ is a $[3\ x\ 3]$ identity matrix. The discretizations can be written as

$$\mathbf{u} = \mathbf{N}\hat{\mathbf{u}}; \qquad \mathbf{u} = \mathbf{N}\delta\hat{\mathbf{u}} \tag{5.11}$$

and accordingly for the strains

$$\boldsymbol{\epsilon} = \mathbf{B}\hat{\mathbf{u}}; \qquad \delta\boldsymbol{\epsilon} = \mathbf{B}\delta\hat{\mathbf{u}} \tag{5.12}$$

where $\mathbf{B}$ contains derivatives of the basis functions, i.e. for the engineering strain

$$\mathbf{B} = \begin{bmatrix} \frac{\partial}{\partial x} & 0 & 0 & 0 & \frac{\partial}{\partial x} & \frac{\partial}{\partial y} \\ 0 & \frac{\partial}{\partial y} & 0 & \frac{\partial}{\partial x} & 0 & \frac{\partial}{\partial z} \\ 0 & 0 & \frac{\partial}{\partial z} & \frac{\partial}{\partial y} & \frac{\partial}{\partial z} & 0 \end{bmatrix}^{\mathrm{T}} \mathbf{N}. \tag{5.13}$$

The linear elastic material law is

$$\boldsymbol{\sigma} = \mathbf{D}\boldsymbol{\epsilon}. \tag{5.14}$$

Inserting Eqs. (5.11, 5.12, 5.14) into Eq. (5.9) we get

$$\delta\hat{\mathbf{u}}^{\mathrm{T}}\left(\int_V \mathbf{B}^{\mathrm{T}}\mathbf{D}\mathbf{B}\mathrm{d}V\hat{\mathbf{u}} + \int_V \rho\mathbf{N}^{\mathrm{T}}\mathbf{N}\mathrm{d}V\ddot{\hat{\mathbf{u}}}\right) = \delta\hat{\mathbf{u}}^{\mathrm{T}}\left(\int_V \mathbf{N}^{\mathrm{T}}\mathbf{b}\mathrm{d}V + \int_{\partial V_\sigma} \mathbf{N}^{\mathrm{T}}\mathbf{t}\mathrm{d}S\right). \tag{5.15}$$

The equation should hold for arbitrary $\delta\hat{\mathbf{u}}$, which leads a set of linear equations, and after dropping the hats we get

$$\mathbf{K}\mathbf{u} + \mathbf{M}\ddot{\mathbf{u}} = \mathbf{f} \tag{5.16}$$

where

$$\mathbf{K} = \int_V \mathbf{B}^{\mathrm{T}}\mathbf{D}\mathbf{B}\mathrm{d}V; \qquad \mathbf{M} = \int_V \rho\mathbf{N}^{\mathrm{T}}\mathbf{N}\mathrm{d}V; \qquad \mathbf{f} = \int_V \mathbf{N}^{\mathrm{T}}\mathbf{b}\mathrm{d}V + \int_{\partial V_\sigma} \mathbf{N}^{\mathrm{T}}\mathbf{t}\mathrm{d}S.$$

The finite element method is numerically stable, meaning that errors from input and intermediate calculations do not grow and cause inaccuracies which make the results meaningless. To minimize the errors from the approximations (or increase precision) a finer mesh with smaller elements or elements with a higher order of basis functions (e.g. going from linear to quadratic elements) may be used, at the expense of computational cost.

5.2.3 Structural dynamics

The EOM for a multi degree of freedom (MDOF) system can from Eq. (5.9) be formulated by use of the FE-method, and with the addition of damping it is given by

$$\mathbf{M}\ddot{\mathbf{u}} + \mathbf{C}\dot{\mathbf{u}} + \mathbf{K}\mathbf{u} = \mathbf{f} \qquad \forall t \in (0, T) \tag{5.17}$$

with $\mathbf{u}(t = 0) = \mathbf{u}_0$ and $\dot{\mathbf{u}}(t = 0) = \dot{\mathbf{u}}_0$, where $\mathbf{M}$ is the mass matrix, $\mathbf{C}$ is the damping matrix, $\mathbf{K}$ is the stiffness matrix, $\mathbf{u}$ is the nodal displacements vector and $\mathbf{f}$ is the force vector. In Paper A, the steady-state vibrations of a soil-mass system are studied, and the following subsection will briefly go trough the corresponding theory.

Steady-state dynamics

Assuming steady-state harmonic behavior with common time factor $e^{i\omega t}$, the equation of motion for a discretized MDOF system can be written using complex arithmetic

$$\mathbf{M}\ddot{\bar{\mathbf{u}}} + \mathbf{C}\dot{\bar{\mathbf{u}}} + \mathbf{K}\bar{\mathbf{u}} = \bar{\mathbf{f}} = \mathbf{f}_0 e^{\mathrm{i}\omega t} \tag{5.18}$$

with the steady-state solution on the form

$$\bar{\mathbf{u}}(t) = \bar{\mathbf{U}} e^{\mathrm{i}\omega t} \tag{5.19}$$

where the overbar denotes a vector in the complex plane. The complex response is

$$\bar{\mathbf{u}} = \mathbf{u}_{\Re} + \mathbf{u}_{\Im} \tag{5.20}$$

where it is understood that the actual steady-state motion is given by either the real or imaginary part depending on the nature of the excitation (i.e. cos or sin respectively). By inserting Eq. (5.19) into Eq. (5.18) and omitting the common time factor we get

$$(-\omega^2\mathbf{M} + \mathrm{i}\omega\mathbf{C} + \mathbf{K})\bar{\mathbf{U}} = \mathbf{f}_0 \tag{5.21}$$

or

$$\mathbf{D}(\omega)\bar{\mathbf{U}} = \mathbf{f}_0 \tag{5.22}$$

where $\mathbf{D}(\omega)$ is the dynamic stiffness matrix, dependent on the angular frequency ω

$$\mathbf{D}(\omega) = -\omega^2\mathbf{M} + \mathrm{i}\omega\mathbf{C} + \mathbf{K} \tag{5.23}$$

which may be used to calculate the complex amplitude $\bar{\mathbf{U}}$, which in turn can be used to determine the amplitude and phase of the steady-state response. The damping can be introduced by, for instance, computing the damping matrix by use of Rayleigh damping or by computing a structural damping matrix by use of a loss factor, [67]. Note that in the next section the overbar and uppercase are dropped and the complex amplitude is simply referred to as $\mathbf{u}$. For more information the reader is referred to [67].

Dynamic model reduction with damping

Model reduction methods within engineering are used to lessen computational costs of an analysis. One of the most common reduction method is referred to as Guyan reduction. A set of active *master* coordinates, and a set of dependent *slave* coordinates which may be reduced are chosen. The matrices are then re-ordered and partitioned into separate parts relating to the master and slave degrees of freedom (dofs). If no forces are applied to the slave dofs and the damping is neglectable the equation of motion for the system can be written as (with subscripts m and s for master and slave dofs, no summations on repeated indices are implied in this subsection)

$$\begin{bmatrix} \mathbf{M}_{mm} & \mathbf{M}_{ms} \\ \mathbf{M}_{sm} & \mathbf{M}_{ss} \end{bmatrix} \begin{Bmatrix} \ddot{\mathbf{u}}_m \\ \ddot{\mathbf{u}}_s \end{Bmatrix} + \begin{bmatrix} \mathbf{K}_{mm} & \mathbf{K}_{ms} \\ \mathbf{K}_{sm} & \mathbf{K}_{ss} \end{bmatrix} \begin{Bmatrix} \mathbf{u}_m \\ \mathbf{u}_s \end{Bmatrix} = \begin{Bmatrix} \mathbf{f}_m \\ 0 \end{Bmatrix} \tag{5.24}$$

by neglecting the inertia terms in Equation 5.24 the transformation matrix $\mathbf{T}$ may be written as

$$\begin{Bmatrix} \mathbf{u}_m \\ \mathbf{u}_s \end{Bmatrix} = \begin{bmatrix} \mathbf{I} \\ -\mathbf{K}_{ss}^{-1}\mathbf{K}_{sm} \end{bmatrix} \mathbf{u}_m = \mathbf{T}\mathbf{u}_m \tag{5.25}$$

the reduced mass and stiffness matrices can then be given as

$$\begin{aligned} \mathbf{K}_r &= \mathbf{T}^{\mathrm{T}}\mathbf{K}\mathbf{T} \\ \mathbf{M}_r &= \mathbf{T}^{\mathrm{T}}\mathbf{M}\mathbf{T}. \end{aligned} \tag{5.26}$$

The method is exact at frequency zero and approximate at all other frequencies as the inertia terms have been neglected. Guyan reduction may be extended to Dynamic reduction at steady-state harmonic conditions, by using the dynamic stiffness matrix one gets the transformation matrix

$$\begin{Bmatrix} \mathbf{u}_m \\ \mathbf{u}_s \end{Bmatrix} = \begin{bmatrix} \mathbf{I} \\ -\mathbf{D}_{ss}^{-1}\mathbf{D}_{sm} \end{bmatrix} \mathbf{u}_m = \mathbf{T}\mathbf{u}_m \tag{5.27}$$

which can be used in Eq. (5.26) to obtain the reduced system matrices, where $\mathbf{C}_r$ follows in the same procedure. As no error is introduced in the transformation matrix this method is exact at frequency ω but the resulting reduced system matrices $\mathbf{M}_r$, $\mathbf{C}_r$ and $\mathbf{K}_r$ are complex [68]. The reduced system matrices produced by these methods are no longer sparse and require a significant reduction of dofs in order to be of computational benefit.

Multi-level sub-structuring

Sub-structuring methods solve a boundary value problem (BVP) by dividing it up in smaller BVPs in sub-domains. The methods work well for parallel computing, as the problems on the sub-domains are independent of each other and can be solved independently. The continuity of the solution over the sub-domains is ensured by representing the values of the neighboring interfaces (where the sub-domain boundaries meet) by the same unknowns. Finite element

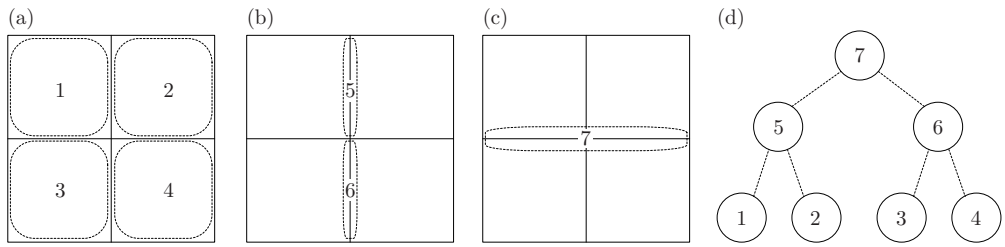


Figure 5.2: (a) bottom level sub-structures and internal dofs. (b) higher level sub-structures and interface dofs for the bottom level sub-structures (dashed area). (c) highest level sub-structure with interface dofs between sub-structures 5 and 6. (d) sub-structure tree.

analysis with models of large size typically require hours to solve for each time-step or frequency, making parallel calculations invaluable for minimizing the calculation time.

To illustrate a method of sub-structuring Fig. 5.2 is showing a domain divided into four sub-domains. Each domain has a set of internal dofs (cf. Fig. 5.2a), and interface dofs (cf. Fig. 5.2b) which are used to connect it to the next sub-structure level, which again has sets of internal and interface dofs used to connect it to the final level seen in Fig. 5.2c.

In Paper A multi-level sub-structuring method has been used to reduce the computational cost and time of the dynamic reduction, where the dynamic reduction has been applied to each sub-structure. The leaf sub-structures consist of a master and a slave set. The parents consist of a master, a slave, and an interface set. A child's set of master dofs consists of the parents master and interface sets. The reduction is applied by traversing the sub-structure tree using a depth-first search since the child nodes must be reduced prior to assembling the parent sub-structures, see Fig. 5.2d. Only the the interface and master dofs are kept after the reduction. Once all of the child nodes are reduced they are used to assemble the parent sub-structure, and the process is then performed on the higher sub-structure level. The reduction ends at the root of the tree, where only the master dofs are kept.

5.3 DEVELOPED MODEL AND FORM FINDING EXAMPLES

5.3.1 Earlier studies

Mixed-use zoning has once again become popular due to benefits such as reduced distances between housing, workplaces and retail, more compact development, and a more lively urban fabric. As the office sleeps the living room is awake meaning the mixed used zone has more potential as an active place. This research was based on an earlier Architectural thesis performed

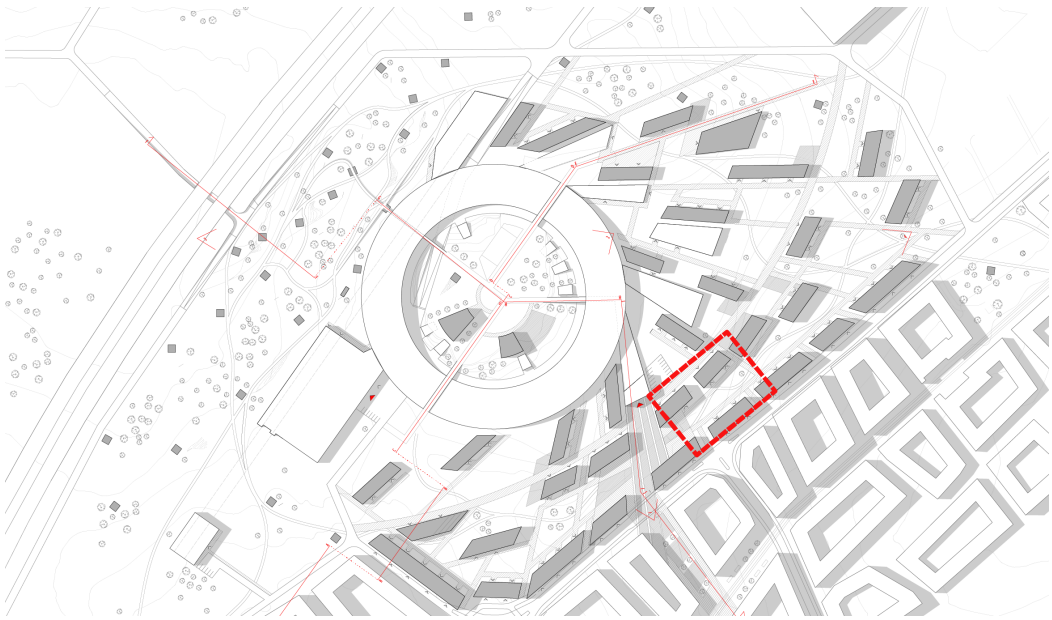


Figure 5.3: Plan from architectural master's thesis, 80 by 60 meter part that was used in Fig. 5.8 marked in red, [69].

at Chalmers University of Technology, at the Department of Architecture [69]. In that thesis, the area around the new research facility MAX IV, was studied and a proposal was made with the ambition to incorporate MAX IV closer into the city of Lund. Building a bit on the mixed-use zoning idea the citizens of Lund living nearby MAX IV would be exposed to a pool of knowledge, but the question to answer was in what way could MAX IV benefit from the proximity? One idea during the Architectural thesis was that placing the buildings in specific patterns could potentially reduce the incoming vibrations from surrounding traffic.

In the architectural an urban design was proposed, see Fig. 5.3, from solutions that worked well in a digital Ripple Tank Simulator, as well as, physical experiments with scale models using JELL-O as soil and placing out masses on top mimicking buildings. The research presented here was done later to provide a conceptual tool which simulates the wave propagation phenomena. From the conceptual tool vibration reduction by placing different patterns of masses on the ground was investigated.

5.3.2 Computational model

A full 3D model was created with the aim to study the vibration reduction effects of masses. Pre-processing was conducted in *ABAQUS* from which the global system matrices $\mathbf{K}$, $\mathbf{C}$, and $\mathbf{M}$ were extracted and exported into *MATLAB* where a dynamic model reduction was performed in order to reduce the number of dofs and speed up the analysis. The dynamic reduction was

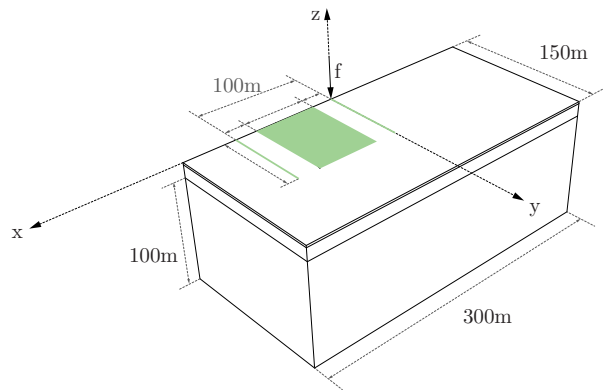


Figure 5.4: 3D model with the retained dofs in the reduced model marked in green.

computationally intensive, requiring excessive amounts of memory on the full 3D model. This was instead solved by dividing the model into sub-structures and performing the reduction in several iterations, see the following section or Section 5.2.3.

Sub-structuring and dynamic reduction of soil model

Fig. 5.4 shows the final dimensions of the model and the master dofs from the soil model which were retained after reduction of the system. In the figure, the green area and the two green lines parallel to the $y-$axis at $x = 0$ m and $x = 100$ m on the soil surface show the areas of the retained dofs. The line at $x = 100$ m was used for evaluations and a unit load was applied vertically at the origin. The green area was used for adding mass. The added mass was modeled as elastic bodies on top of the soil surface, with dimensions $2 \times 2 \times 2\,\mathrm{m}^3$. In the following, the added elastic bodies are referred to as masses.

Since the reduced system matrices from the dynamic reduction method are frequency dependent a reduced system was constructed for each frequency that was solved for in the steady-state analysis. As the largest displacements were in the 5–30 Hz range and the number of frequencies had to be kept low due to long computational time, the frequencies studied ranged from 5–29 Hz with steps of 2 Hz.

Since the whole model had 2 620 860 complex dofs, performing a dynamic reduction directly proved to be computationally difficult. The structure was then divided into 25 sub-structures by simply slicing the model into pieces from the top view as indicated by Fig. 5.5 (a). The top view was used because it offered simplicity to the sub-structuring script. In addition, the bedrock elements were much longer in z-direction and using the top-view meant that the number of nodes in all three directions of the sub-structure would be fairly even providing a favorable ratio between internal and interface dofs. Each sub-structure contained about 100

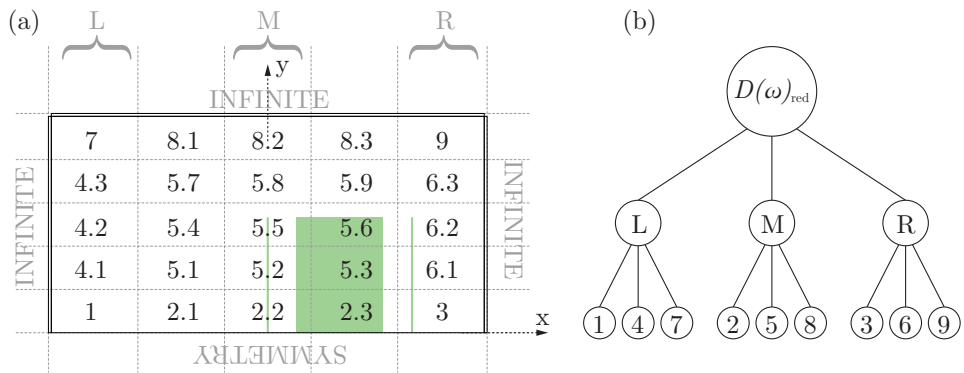


Figure 5.5: (a) Top view of model with sub-structures (b) Sub-structure assembly order.

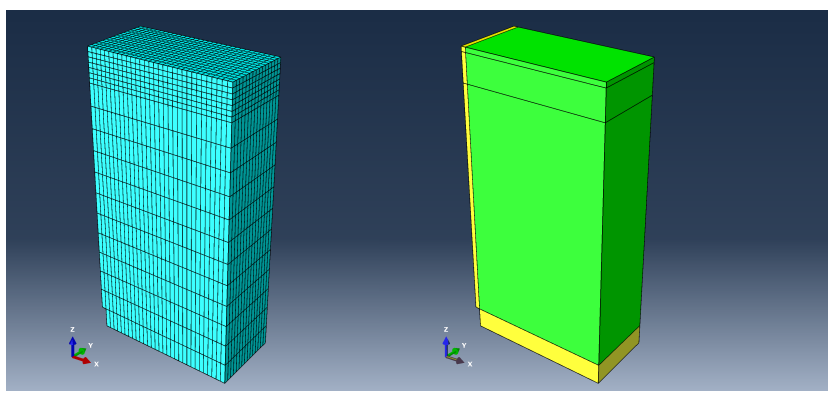


Figure 5.6: (left) Mesh of sub-structure 1 (right) Material layers of sub-structure 1, non-reflecting boundaries are marked in yellow [70].

000 dofs. Out of the 25 sub-structures only nine unique instances were identified, as indicated by the first digit in Fig. 5.5. Only nine of the sub-structures were thus needed to build the final model. Fig. 5.6 shows the mesh and layers of sub-structure 1.

For each sub-structure the dofs to be retained (consisting of the green parts in Fig. 5.4, and of interfaces between substructures) and to be reduced were identified. In the first sub-structuring step shown in the bottom of Fig. 5.5b, the interior dofs were reduced in all nine sub-structures. In step two the *Left*, *Middle* and *Right* parts consisting of (1–4.1–4.2–4.3–7), (2.2–5.2–5.5–5.8–8.2) and (3–6.1–6.2–6.3–9), respectively were assembled to three separate structures. A new set of dofs could be identified to be retained and to be reduced at the next sub-structure level. Finally, in the third step the *Left*, 3 of the *Middle*, and *Right* parts were assembled and a third reduction was to form the final reduced matrix $\mathbf{D}(\omega)_{\text{red}}$ for each frequency, leaving only the dofs related to the green parts in Fig. 5.4.

The final reduced system then contained the dofs at the marked area in Fig. 5.4, the load dofs

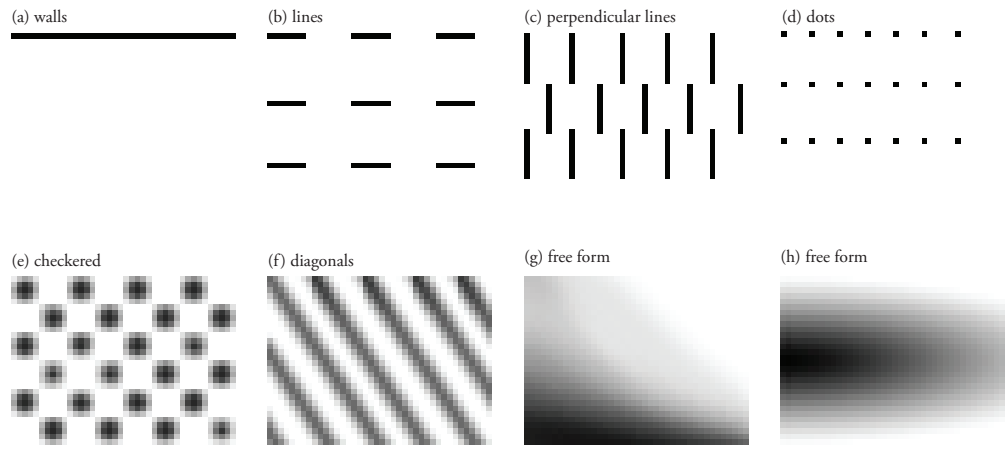


Figure 5.7: Different types of patterns used in 3D simulations.

and the evaluation dofs. Initially it was planned to use the whole soil area between the load and evaluation point for placement of masses. However, since the reduced soil system consisted of full and complex matrices it was important to keep down the number of dofs as much as possible. The final reduced soil model consisted of 11 646 dofs, taking up about 2.5 GB of memory per matrix. To further reduce the memory usage only the dynamic matrices $\mathbf{D}(\omega)$ were stored. The reduced model usually took between 10–20 minutes to run, depending on the amount of masses assembled on top.

Patterns

Different organizations of masses were finally assembled on the green area, see Fig. 5.4, and a frequency sweep analysis in steady-state was performed, ranging from 5 to 29 Hz with 2 Hz steps and unit loading applied at the origin. The results were evaluated in terms of the root mean square value (RMS) of the vertical displacement magnitudes, along the green line at a distance of 100 m from the load. For the material parameters and details, see Paper A.

The reduced model consisted of an area to place masses that was between $x \in [20 : 80]$, $y \in [0 : 80]$. With a mesh size of two by two meters, the total number of possible positions for placing a mass was $30 \times 40 = 1200$. A function was written to read grey-scale images of 30×40 pixels, where each pixel was a possible position for a mass and the value of the pixel was used for the mass density, white meant no density (no mass assembled at the position) and black meant the largest density, $\rho = 8271\,\mathrm{kg/m^3}$ unless otherwise stated. The same type of 20-node quadratic brick elements *C3D20R* were used for the elastic bodies to model the masses, as for the soil. No material damping was applied to the masses, and Young's modulus was set to $\mathrm{E} = 215\,\mathrm{MPa}$, and Poission's ratio $\nu = 0.48$, which was the same as the properties

for the upper soil layer.

The model allowed for any configuration of masses to be investigated. Fig. 5.7 shows some examples of the different types of patterns. The patterns that were studied were classified into the following types:

Walls were made of a line, or a set of lines that were parallel to the y-axis, that is perpendicular to the main wave-propagation direction from the source to the evaluation points, like a barrier.

Lines were similar to the walls, but did not span the whole distance along the y-axis, and if there were more rows of them they were allowed to be shifted in relation to each other.

Perpendicular lines were lines that were ordered to go in the main direction of the wave propagation.

Dots and checkered patterns were tried out both with individual masses (dots) placed in an ordered fashion, and also with larger sets of masses ordered in a checkered pattern.

Diagonals with many masses of varying density were tested.

Free form patterns were painted out in some different manners to see if anything out of the ordinary might happen.

Buildings. Some organizations of masses that were more in the scale of buildings were also tried out, for all of these the Young's modulus was set to $\mathrm{E} = 30\,\mathrm{GPa}$. Some parts of the buildings of the architectural thesis proposal were also tried as patterns.

5.3.3 Examples

Some results of using the tool are shown in Paper A. The tool is able to identify several important effects. Masses applied continuously over the whole area can lead to both reduction as well as amplification compared to having no masses. Amplification was obtained due to lensing as shown in Fig. 5.7h, or acting as wave guides, Fig. 5.7f, however, all patterns with discrete masses show reductions in vibrations; Small masses applied with large spacing are ineffective, Fig. 5.7d; Straight open paths from the load to the evaluation point lead to little reduction, Fig. 5.7b; Density variation for the different masses has a larger effect on vibration reductions than their position. The results concluded here are shown in Paper A.

In Figs. 5.8 and 5.9 simulations with a part of the building plan from the architectural thesis, are shown. A few different parts of the urban plan were studied, but the 3D steady-state model was too small to study the whole plan at once. No parts of those that were tried showed an increase in RMS of vertical displacement magnitude.

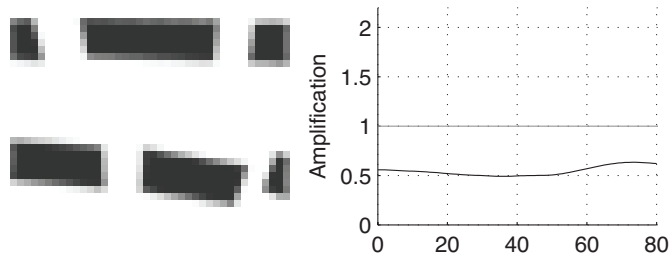


Figure 5.8: Part of pattern from Architectural Thesis, see Fig. 5.3.

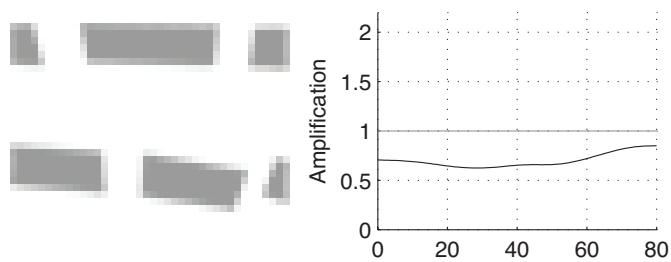


Figure 5.9: Part of pattern from Architectural Thesis, lower density.

5.4 SUMMARY

The contributions of this part of the research are:

- The research described the general phenomena of resonant mass scatterers, and showed the effects on the specific site using 2D numerical studies.
- An exploration tool for studying the organization of masses was developed.
- An approach for efficient computations related to models used in the 3D tool was developed.
- The vibration reduction effects of different patterns of masses on soil were shown.

The reduction method used to reduce the number of dofs in the tool presented in Paper A made it possible to explore different alternatives quickly and find the most effective patterns, but also patterns that may even amplify the vibrations in the soil. In the paper, this was applied to the site of the new synchrotron research facility, MAX IV. However, tools such as this could be valuable in the planning of our urban environments, which are getting more populated and dense. Being able to get rapid predictions of vibrations in planned areas could allow for cities with reduced noise and vibration problems.

6 Finding form with IGA

6.1 BACKGROUND

Shells are efficient structures. They can resist bending, but in order to be efficient they should carry load primarily by in plane membrane stress (normal and shear stress in the tangent directions to the shell surface). If the dominant load of the shell is the self-weight then a shell which is given shape by a form finding process will carry that load efficiently. Other loads, such as, asymmetric snow and wind are then resisted through the shells bending capacity. If the shell is designed to be very efficient for carrying the dead load then it can become sensitive to imperfections and buckling, since thin shells have little bending resistance.

Modern thin concrete shells began to appear in the 1920s. Torroja and Nervi designed very expressive shell structures. Heinz Isler and Félix Candela pioneered the use of physical hanging models under gravity load for generating efficient forms for shell structures. In Fig. 6.1 a few examples of thin concrete shells and other related structures are shown.

Concrete shells are seldom built today, instead it is more common to use cable nets, textile membranes or steel grids. The structural difference of nets and membranes from shells is that they are form-active systems without flexural stiffness and change their shape to carry the applied load. Shells are form-passive and do not adjust their shape to the loading conditions. Membranes and nets can be stiffened by pre-stress and for a high degree of stiffening must be anticlastic (saddle-like) with a negative Gaussian curvature. A challenge shell structures face today is that building the form work is expensive, however new fabrication techniques such as 3d printing or pneumatic form works could improve on this.

6.1.1 Present research

A recent development of finite element analysis is isogeometric analysis [71], where basis functions from CAD (e.g. b-splines, NURBS, subdivision surfaces) are used instead of the standard Lagrange polynomial basis functions for the finite element approximations.



Figure 6.1: Top left: Munich Olympic stadium (F. Otto). Top right: Concrete dome (H. Isler), image from Chriusha, Wikimedia Commons. Bottom left: L'Oceanogràfic (Félix Candela). Bottom right: Mannheim Multihalle (F. Otto/B. Happold).

In the research presented here, dynamic relaxation based form finding with NURBS based membrane elements was investigated. There are several potential advantages to this. Using the same geometry for both FEA and CAD simplifies iterative processes, since there is no need to discretize the NURBS geometry. It allows for form finding directly in the CAD software and in the architectural context. CAD programs are in general better at treating complex geometries and modifying them, compared to FE programs. The initial geometries used for the form finding procedure can at times be rather complex. NURBS patches are already successfully used for structural shape optimization. NURBS are particularly well suited for curved geometries. Recently, other authors have studied similar approaches, see [72, 73].

6.2 THEORY

The theory presented in this chapter aims to provide a more detailed description of the element implementation used in Papers B and C. It covers some topics of CAD, Isogeometric Analysis (IGA), Kirchhoff-Love shell and membrane theory, all of which have been used in the present research.

6.2.1 Geometric preliminaries

In the appended Papers B and C use is made of NURBS based IGA. In order to explain IGA the necessary B-spline and NURBS theory which is commonly used in CAD is briefly presented. For further reading, see for instance [74–76].

B-splines

Basis splines (B-splines) are non-interpolating, piecewise polynomial curves. A B-spline curve $\mathbf{C}(\xi)$ is defined by its polynomial degree p, a knot vector $\Xi = \left\{\xi_1, \xi_2, \ldots, \xi_{n+p+1}\right\}$, and a set of n control points $\mathbf{B}_i = (x_i, y_i, z_i)$. The knot vector contains non decreasing values and divides the parametric space into intervals known as knot spans, the first and last values in the knot vector are repeated $p + 1$ times. If an internal knot is repeated r times it is said to have a multiplicity of r. The curve is computed by a summation of the B-spline basis functions multiplied by the control points

$$\mathbf{C}(\xi) = \sum_{i=1}^{n} N_{i,p}(\xi)\mathbf{B}_i \tag{6.1}$$

where the i:th basis function $N_{i,p}$ is constructed recursively, using the Cox-de Boor formula [77, 78], for $p = 0$

$$N_{i,0}(\xi) = \begin{cases} 1 & \text{if } \xi_i \leq \xi < \xi_{i+1} \\ 0 & \text{otherwise.} \end{cases} \tag{6.2}$$

For $p = 1, 2, 3, \ldots$, recursively

$$N_{i,p}(\xi) = \frac{\xi - \xi_i}{\xi_{i+p} - \xi_i} N_{i,p-1}(\xi) + \frac{\xi_{i+p+1} - \xi}{\xi_{i+p+1} - \xi_i} N_{i+1,p-1}(\xi) \tag{6.3}$$

for which implementations can be found in [75]. The continuity of the basis functions at a repeated knot is C^{p-r}, meaning that it is $p-r$ times continuously differentiable. All derivatives exist in the interior of a knot span. Each control point, $\mathbf{B}_i$, has an associated basis function which is non-zero in $p + 1$ knot spans in the half open interval $\left[\xi_i, \xi_{i+p+1}\right)$, which is known as local support. The local support of the B-spline basis makes them highly intuitive and predictable for geometrical modeling. The basis functions are only interpolatory at the ends of the knot vector, and at knots with multiplicity $r = p$, leading to C^0 continuity, for an example, see the knot at $\xi = 4$ in Fig. 6.2, where a quadratic B-spline basis with the knot vector $\Xi = \{0, 0, 0, 1, 2, 3, 4, 4, 5, 5, 5\}$ is shown. The division of the parameter space into knot-intervals is indicated by the dashed vertical lines, and the multiplicity of the knots is shown with the dots below the basis functions. The curve on the right in Fig. 6.2 is generated using the basis functions and the 8 control points $\mathbf{B}_i$, the dashed lines between the control points form the control point polygon. The knot positions in the physical space are indicated with circles.

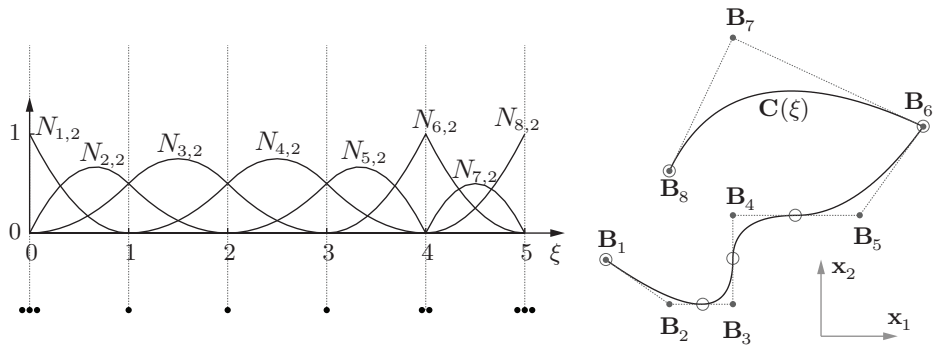


Figure 6.2: Basis functions for a quadratic B-spline and a curve generated with the basis functions.

In general, the number of knots does not coincide with the number of control points or basis functions. The denominators in the quotients in Eq. (6.3) can become zero, but the quotients are in those cases defined as zero [75]. The control polygon is tangent to the endpoints of a B-spline curve.

A B-spline surface is defined using the tensor product approach, where another set of univariate basis functions $M_{j,q}(\eta)$ of degree q, with the knot vector $\mathbf{H} = \left\{\eta_1, \eta_2, \ldots, \eta_{m+q+1}\right\}$, with m control points in the second direction and the control point net $\mathbf{B}_{i,j}$ is used

$$\mathbf{S}(\xi, \eta) = \sum_{i=1}^{n} \sum_{j=1}^{m} N_{i,p}(\xi) M_{j,q}(\eta) \mathbf{B}_{i,j} \tag{6.4}$$

and by adding a third direction one can in a similar fashion generate B-spline solids. B-spline surfaces and solids constructed by the tensor product approach are also referred to as patches. In Fig. 6.3 a bi-quadratic B-spline surface and its parametric space are shown, with $\xi, \eta \in [0, 1]$. The control point net is visible with dashed lines, containing the 9 control points $\mathbf{B}_{i,j}$ with $i, j = 1, 2, 3$. The point (ξ_0, η_0) in parametric space is mapped to $\mathbf{S}(\xi_0, \eta_0)$ in three-dimensional Euclidean space.

Non-Uniform Rational B-Splines

A B-spline curve is extended to a NURBS by adding a weight to each control point

$$\mathbf{C}(\xi) = \frac{\sum_{i=1}^{n} N_{i,p}(\xi) w_i \mathbf{B}_i}{\sum_{k=1}^{n} N_{k,p}(\xi) w_k} = \frac{\sum_{i=1}^{n} N_{i,p}(\xi) w_i \mathbf{B}_i}{W(\xi)} = \sum_{i=1}^{n} R_{i,p}(\xi) \mathbf{B}_i \tag{6.5}$$

where $R_{i,p}$ are the rational NURBS basis functions. NURBS have the ability to represent any conical shapes such as a circle exactly. NURBS can represent both analytic shapes (cones, cubes, etc) and free form surfaces using the same method [74].

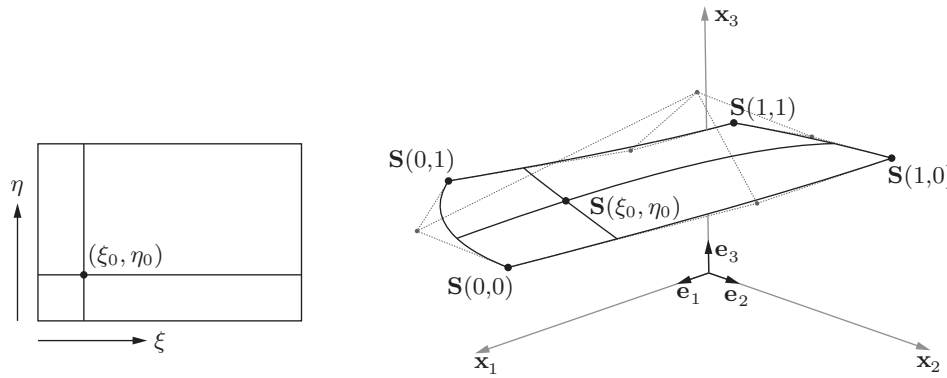


Figure 6.3: A bi-quadratic B-spline surface and its parametric space.

Similarly for surfaces each control point in the control point mesh is extended with a weight, $\mathbf{B}_{i,j} = (x_{i,j}, y_{i,j}, z_{i,j}, w_{i,j})$ and the NURBS surface is given by

$$\mathbf{S}(\xi,\eta) = \frac{\sum_{i=1}^{n}\sum_{j=1}^{m} N_{i,p}(\xi)M_{j,q}(\eta)w_{i,j}\mathbf{B}_{i,j}}{\sum_{k=1}^{n}\sum_{l=1}^{m} N_{k,p}(\xi)M_{l,q}(\eta)w_{k,l}}. \tag{6.6}$$

A geometrical interpretation of a NURBS is that a NURBS surface in $\mathbb{R}^3$ is obtained by a projective transformation of a B-Spline surface in $\mathbb{R}^4$. In practice the geometric interpretation is important in that algorithms developed for B-splines can be applied to NURBS by treating the NURBS as a B-spline in a higher dimension.

6.2.2 NURBS based isogeometric analysis

The term isogeometric analysis was coined by Hughes, [79], however, approaches for carrying out computation on design geometry were attempted before, by for instance Cirak et al. on thin-shell elements for subdivision surfaces [80]. There were other earlier precedents as well [81–83].

Finite element implementations using NURBS based IGA have much in common with classical FEA, though there are some points on which they differ. One important aspect is that *control points* in IGA are in general not interpolated like *nodal points* in classical FEA. Further, dofs in IGA are related to control points, and can not be directly interpreted in the same way as dofs are related to a node in classical FEA.

For more information on the topic of IGA, and the theory recited here, see [71] or [79].

The isogeometric concept

In FEA the use of the isoparametric concept is common. The basic idea is that the basis functions which are used to approximate the unknown field are also used to describe the geometry. Moreover the basis functions are described in some parent coordinates, $\tilde{\xi}, \tilde{\eta}, \tilde{\zeta} \in [-1, 1]$, [84], and a mapping from the parent domain to the global domain is employed, i.e. if the mapping describing the geometry is

$$\mathbf{x}(\tilde{\boldsymbol{\xi}}) = \sum N_i(\tilde{\boldsymbol{\xi}})\mathbf{x}_i^e \tag{6.7}$$

where $\mathbf{x}_i^e$ are the element global coordinates associated with element basis functions $N_i(\tilde{\boldsymbol{\xi}})$, then the element unknowns are

$$\mathbf{u}(\tilde{\boldsymbol{\xi}}) = \sum N_i(\tilde{\boldsymbol{\xi}})\mathbf{u}_i^e. \tag{6.8}$$

Depending on the basis functions used, the mapping may lead to approximate representations of the geometry.

Two general requirements on finite elements are that they must be compatible and complete. If both requirements are fulfilled monotonic convergence of the approximated field to the exact one when elements are made smaller is ensured, [84]. Isoparametric elements fulfil the completeness requirement if their basis functions are a partition of unity. For solid elements it is sufficient to require C^0 continuity between element borders and C^1 on the element interiors in order to fulfil the compatibility requirement, [71].

The isogeometric concept requires that the basis functions which are capable of representing the CAD geometry *exactly* are also used to approximate the unknown field. The basic convergence requirements stated in the earlier paragraphs are not restricted to classical Lagrangian finite elements with polynomial bases, but hold for any reasonably smooth isoparametric basis which is also a partition of unity, e.g. the NURBS basis functions used in this work, [71].

The strength of the isogeometric approach is that it builds upon the already well developed FEA and CAD theories without breaking backward compatibility.

NURBS elements

In here an element is defined as an interval in the knot vector. The divisions are marked in Fig. 6.2 for one-dimensional (line and curve) elements. In the figure it is apparent that the basis functions span over several elements, and that the basis functions allow for higher than C^0 continuity between elements.

The use of a parent element requires two separate mappings in NURBS based isogeometric analysis. A first mapping from the parent element coordinates $(\tilde{\xi}, \tilde{\eta})$ to the NURBS parametric coordinates (ξ, η), and a second mapping from the NURBS parametric coordinates to the

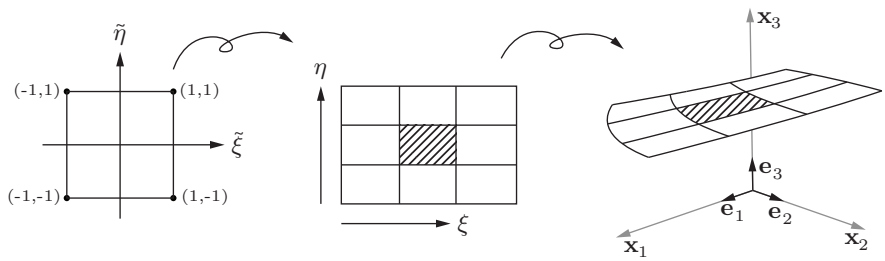


Figure 6.4: A B-spline surface patch consisting of 9 elements. The parent domain, parametric domain and physical surface are shown.

physical coordinates (x, y, z). Fig. 6.4 shows an example of the mappings for a surface consisting of 9 elements. Every element in the parametric and global domains is mapped from the same parent domain. The middle element of the surface is marked with diagonal lines.

Refinement

Geometry represented by B-splines is invariant during refinements and is represented exactly irrespective of the mesh being coarse or refined. There are three types of refinements possible for B-Splines/NURBS based IGA. The first is the same as for finite elements, namely making the elements smaller (h-refinement), which is done by performing so called knot insertion, whereby new knot values are inserted into the knot vector without affecting the geometry. The elements in NURBS based IGA are defined by the knot spans, and thus by introducing new knots one also introduces new elements. As for finite elements it is possible to increase the degree of the basis functions (p-refinement). Another type of refinement is possible with B-splines/NURBS where if the degree is first raised and the elements are made smaller (k-refinement) it is possible to obtain basis functions with continuous derivatives across element borders. The refinement possibilities make NURBS suitable for form finding where a coarse mesh can be used initially to explore shapes in near real time and a finer one can be used afterward to obtain a more accurate solution.

The tensor product nature of NURBS surfaces, as may be seen in Eq. (6.4), constrains standard isogeometric analysis with NURBS to 4-sided surfaces. However, by use of T-Splines [85], or trimmed NURBS [86] this can be avoided and other forms may be constructed.

6.2.3 Kirchhoff-Love shell and membrane theory

In Papers B and C geometrically non-linear isogeometric membrane elements are used for the form finding and linear elastic Kirchhoff-Love shell theory is used for analysis on the form

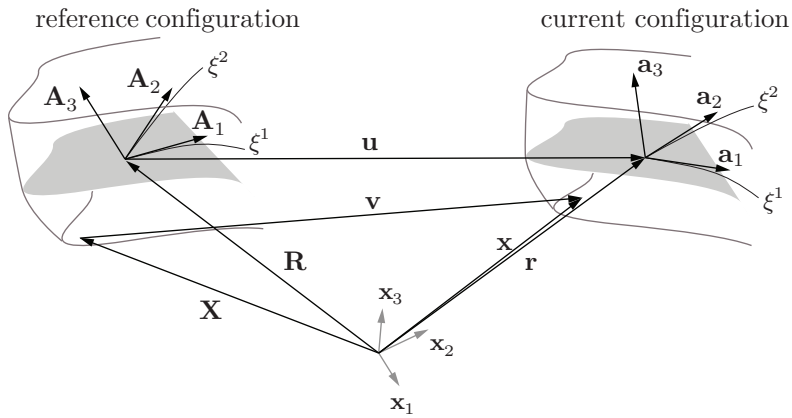


Figure 6.5: Shell geometry in reference and current configurations.

found geometry. The following sections contain the theory and the finite element discretization.

The Kirchhoff-Love shell theory requires C^1 continuity of the displacement field to fulfil the compatibility requirements, which is impossible to achieve with traditional Lagrange-type basis functions. NURBS allow for a higher order continuity and their use for Kirchhoff-Love shell elements fulfils the continuity requirement without the need for any rotational dofs. It was first presented in [87].

Geometry of curved surfaces and bodies

Shells and membranes are characterized by being much thinner in one of their dimensions than the other two, and are often curved. It is natural to describe them using a mid-surface description together with a thickness parameter t. Any point $\mathbf{r}(\xi^1, \xi^2)$ in three-dimensional physical space lying on the mid-surface can be described using only two parameters, (ξ^1, ξ^2). On each point on the mid-surface in the current configuration a set of covariant base vectors is defined

$$\mathbf{a}_\alpha = \mathbf{r}_{,\alpha} = \frac{\partial \mathbf{r}}{\partial \xi^\alpha}; \qquad \alpha = 1, 2. \tag{6.9}$$

Indices following a comma denote differentiation with respect to the parametric coordinates, unless otherwise stated. A third covariant base vector perpendicular to the surface is defined as

$$\mathbf{a}_3 = \frac{\mathbf{a}_1 \times \mathbf{a}_2}{|\mathbf{a}_1 \times \mathbf{a}_2|}. \tag{6.10}$$

Contravariant base vectors are related to the covariant [88] by

$$\mathbf{a}_i \cdot \mathbf{a}^j = \delta_i^j; \qquad i, j = 1, 2, 3 \tag{6.11}$$

where δ_i^j is 1 if $i = j$, 0 otherwise. Since $\mathbf{a}^\alpha$ lie in the tangent plane to the surface spanned by $\mathbf{a}_\alpha$, it follows that

$$\mathbf{a}_3 = \mathbf{a}^3. \tag{6.12}$$

The metric tensor on the tangent plane, also called the first fundamental form of the surface is

$$a_{\alpha\beta} = \mathbf{a}_\alpha \cdot \mathbf{a}_\beta \tag{6.13}$$

or in contravariant or mixed form

$$a^{\alpha\beta} = \mathbf{a}^\alpha \cdot \mathbf{a}^\beta; \qquad a^\alpha_{\cdot\beta} = a^{\cdot\alpha}_\beta = \delta^\beta_\alpha. \tag{6.14}$$

Equivalent equations can be formed in the reference configuration using the undeformed base vectors, $\mathbf{A}_i$.

Similarly, for points in the reference and current shell body the covariant base vectors are

$$\mathbf{g}_i = \mathbf{x}_{,i}; \qquad \mathbf{G}_i = \mathbf{X}_{,i} \tag{6.15}$$

and the metric components for the body are

$$g_{ij} = \mathbf{g}_i \cdot \mathbf{g}_j; \qquad G_{ij} = \mathbf{G}_i \cdot \mathbf{G}_j. \tag{6.16}$$

Mechanics

The Green-Lagrange strain components written in terms of the shell body metrics [89] are

$$E_{ij} = \frac{1}{2}(g_{ij} - G_{ij}). \tag{6.17}$$

The Kirchhoff-Love shell theory is due to the omission of transverse shear deformation applicable to thin and moderately thin shell structures where the thickness is assumed to be less than 1/20 of the shells radius of curvature. The theory assumes that lines normal to the middle surface before deformation remain straight, unstretched and normal to that surface after deformation. Cross-sections are assumed to remain straight, corresponding to a linear strain distribution in the thickness direction. For simplicity, the shell thickness is assumed to be constant with ξ^α [89]. The shell can be completely represented by its mid-surface. The assumptions imply that transverse normal and shear strains are neglected, reducing the strain components to

$$E_{\alpha\beta} = \frac{1}{2}(g_{\alpha\beta} - G_{\alpha\beta}). \tag{6.18}$$

The thin shell kinematic assumption describes the position vector $\mathbf{x}$ in the shell body by use of the shell mid-surface $\mathbf{r}$ and the shell director, which coincides with the normal, $\mathbf{a}_3$

$$\mathbf{x} = \mathbf{r} + \xi^3 \mathbf{a}_3; \qquad \xi^3 \in [-t/2, t/2] \tag{6.19}$$

and gives the body covariant base vectors in terms of the mid-surface base vectors

$$\mathbf{g}_\alpha = \mathbf{a}_\alpha + \xi^3 \mathbf{a}_{3,\alpha}. \tag{6.20}$$

Using Eq. (6.20) in Eq. (6.16)

$$g_{\alpha\beta} = (\mathbf{a}_\alpha + \xi^3 \mathbf{a}_{3,\alpha}) \cdot (\mathbf{a}_\beta + \xi^3 \mathbf{a}_{3,\beta}) = a_{\alpha\beta} - 2\xi^3 b_{\alpha\beta} + (\xi^3)^2 \mathbf{a}_{3,\alpha} \cdot \mathbf{a}_{3,\beta} \tag{6.21}$$

in which the quadratic term $(\xi^3)^2$ is neglected for very thin shells and

$$b_{\alpha\beta} = -\mathbf{a}_\alpha \cdot \mathbf{a}_{3,\beta} = \mathbf{a}_{\alpha,\beta} \cdot \mathbf{a}_3 \tag{6.22}$$

are the covariant components of the second fundamental form of the surface.

The results from Eq. (6.21) are used to split the strain components in membrane and bending parts

$$E_{\alpha\beta} = \epsilon_{\alpha\beta} + \xi^3 \kappa_{\alpha\beta} \tag{6.23}$$

where the membrane strains are

$$\epsilon_{\alpha\beta} = \frac{1}{2}(a_{\alpha\beta} - A_{\alpha\beta}) \tag{6.24}$$

and the bending strains, which represent the change in curvature are

$$\kappa_{\alpha\beta} = B_{\alpha\beta} - b_{\alpha\beta}. \tag{6.25}$$

Membrane part

For the form finding in this thesis we neglect the bending part, and focus on the membrane strains.

The components of the membrane strains are expressed in the base vectors of the reference configuration and displacements using $\mathbf{r} = \mathbf{R} + \mathbf{u}$, see Fig. 6.5,

$$\epsilon_{\alpha\beta} = \frac{1}{2}(\mathbf{A}_\alpha \cdot \mathbf{u}_{,\beta} + \mathbf{A}_\beta \cdot \mathbf{u}_{,\alpha} + \mathbf{u}_{,\alpha} \cdot \mathbf{u}_{,\beta}). \tag{6.26}$$

The components of the membrane stress resultant can be computed by integration of the 2nd Piola-Kirchhoff stress over the thickness, which for a homogeneous linear elastic material becomes

$$n^{\alpha\beta} = \int_{-t/2}^{t/2} S^{\alpha\beta} \mathrm{d}\xi^3 = tS^{\alpha\beta} = \frac{Et}{1-v^2} C^{\alpha\beta\gamma\delta} \epsilon_{\gamma\delta} \tag{6.27}$$

where

$$C^{\alpha\beta\gamma\delta} = \nu A^{\alpha\beta} A^{\gamma\delta} + \frac{1}{2}(1-\nu)(A^{\alpha\gamma} A^{\beta\delta} + A^{\alpha\delta} A^{\beta\gamma}) \tag{6.28}$$

and ν is Poisson's ratio, and E is Young's modulus.

The internal virtual work in Eq. (5.7) is used and by neglecting the bending part we obtain

$$\delta W_{\text{int}} = \int_V \mathbf{S} : \delta \mathbf{E} dV = \int_A \mathbf{n} : \delta \boldsymbol{\epsilon} dA = \int_A n^{\alpha\beta} \delta \epsilon_{\alpha\beta} \mathrm{d}A. \tag{6.29}$$

Finite element implementation

The following section explains the finite element discretization using NURBS based IGA of the internal and external virtual work for the membranes described in the previous section. For books on FEA see for instance Ottosen and Petersson [84] or Bathe [66], and on IGA, see Hughes et al. [79].

From the internal and external virtual work the internal and external forces can be derived

$$\delta W_{\text{int}} = \delta \mathbf{u}^T \mathbf{f}^{\text{int}}; \qquad \delta W_{\text{ext}} = \delta \mathbf{u}^T \mathbf{f} \tag{6.30}$$

where

$$\delta \mathbf{u} = \begin{bmatrix} \delta \hat{\mathbf{u}}_1 \\ \vdots \\ \delta \hat{\mathbf{u}}_A \\ \vdots \\ \delta \hat{\mathbf{u}}_{nm} \end{bmatrix}; \qquad \mathbf{f}^{\text{int}} = \begin{bmatrix} \mathbf{f}_1^{\text{int}} \\ \vdots \\ \mathbf{f}_A^{\text{int}} \\ \vdots \\ \mathbf{f}_{nm}^{\text{int}} \end{bmatrix}; \qquad \mathbf{f} = \begin{bmatrix} \mathbf{f}_1 \\ \vdots \\ \mathbf{f}_A \\ \vdots \\ \mathbf{f}_{nm} \end{bmatrix} \tag{6.31}$$

where $\delta \hat{\mathbf{u}}_A$ is the variation of the control point displacement vector for the A:th control point, $\mathbf{f}_A^{\text{int}}$ is the internal force vector for the A:th control point, and $\mathbf{f}_A$ is the external force vector for the A:th control point. The column matrices $\mathbf{f}$ and $\mathbf{f}^{\text{int}}$ contain the internal and external force vectors, respectively.

The equilibrium condition $\delta W_{\text{int}} - \delta W_{\text{ext}} = 0$ should hold for any virtual displacements and can thus be written as

$$\mathbf{f}^{\text{int}} - \mathbf{f} = 0. \tag{6.32}$$

To reach that expression the following FE discretizations are used for the displacements and virtual displacements, where the Galerkin method is adopted

$$\mathbf{u} = \sum_{A=1}^{nm} \tilde{N}_A \hat{\mathbf{u}}_A; \qquad \delta \mathbf{u} = \sum_{A=1}^{nm} \tilde{N}_A \delta \hat{\mathbf{u}}_A \tag{6.33}$$

where $\hat{\mathbf{u}}_A$ is the control point displacement vector for the A:th control point, $\delta \hat{\mathbf{u}}_A$ is the variation of the control point displacement vector for the A:th control point and $\tilde{N}_A$ is the A:th bi-variate NURBS basis function

$$\tilde{N}_A(\xi, \eta) = \frac{N_{i,p}(\xi) M_{j,q}(\eta) w_{i,j}}{\sum_{k=1}^{n} \sum_{l=1}^{m} N_{k,p}(\xi) M_{l,q}(\eta) w_{k,l}} = \frac{N_{i,p}(\xi) M_{j,q}(\eta) w_{i,j}}{W(\xi, \eta)} \tag{6.34}$$

where the tilde on the left hand side has been dropped for convenience in subsequent equations. No summations are implied on the right hand side in Eq. (6.34), and the commas do not denote differentiation with respect to the parametric coordinates. The global bi-variate basis number A is related to i, j through

$$A = n(j-1) + i \tag{6.35}$$

where n is the number of control points in the first direction of the control point net.

The internal virtual work from Eq. (6.29) is for convenience rewritten in matrix notation as

$$\delta W_{\text{int}} = \int_{\Omega_0} (\delta\boldsymbol{\epsilon})^T \mathbf{n} dA; \qquad \delta\boldsymbol{\epsilon} = \begin{bmatrix} \delta\epsilon_{11} \\ \delta\epsilon_{22} \\ 2\delta\epsilon_{12} \end{bmatrix}; \qquad \mathbf{n} = \begin{bmatrix} n^{11} \\ n^{22} \\ n^{12} \end{bmatrix}. \tag{6.36}$$

To introduce the discretization the virtual strains are written explicitly

$$\delta\boldsymbol{\epsilon} = \begin{bmatrix} \delta\epsilon_{11} \\ \delta\epsilon_{22} \\ 2\delta\epsilon_{12} \end{bmatrix} = \begin{bmatrix} \mathbf{A}_1 \cdot \delta\mathbf{u}_{,1} + \mathbf{u}_{,1} \cdot \delta\mathbf{u}_{,1} \\ \mathbf{A}_2 \cdot \delta\mathbf{u}_{,2} + \mathbf{u}_{,2} \cdot \delta\mathbf{u}_{,2} \\ \mathbf{A}_1 \cdot \delta\mathbf{u}_{,2} + \mathbf{A}_2 \cdot \delta\mathbf{u}_{,1} + \mathbf{u}_{,2} \cdot \delta\mathbf{u}_{,1} + \mathbf{u}_{,1} \cdot \delta\mathbf{u}_{,2} \end{bmatrix} \tag{6.37}$$

after the discretization the virtual strain is

$$\delta\boldsymbol{\epsilon} = \begin{bmatrix} \mathbf{A}_1 \cdot (N_{A,1}\delta\hat{\mathbf{u}}_A) + \mathbf{u}_{,1} \cdot (N_{A,1}\delta\hat{\mathbf{u}}_A) \\ \mathbf{A}_2 \cdot (N_{A,2}\delta\hat{\mathbf{u}}_A) + \mathbf{u}_{,2} \cdot (N_{A,2}\delta\hat{\mathbf{u}}_A) \\ \mathbf{A}_1 \cdot (N_{A,2}\delta\hat{\mathbf{u}}_A) + \mathbf{A}_2 \cdot (N_{A,1}\delta\hat{\mathbf{u}}_A) + \mathbf{u}_{,2} \cdot (N_{A,1}\delta\hat{\mathbf{u}}_A) + \mathbf{u}_{,1} \cdot (N_{A,2}\delta\hat{\mathbf{u}}_A) \end{bmatrix} \tag{6.38}$$

where summation over the repeated index A is implied, the equations are re-written as

$$\delta\boldsymbol{\epsilon} = \begin{bmatrix} N_{A,1}\mathbf{a}_1 \cdot \mathbf{e}_1 & N_{A,1}\mathbf{a}_1 \cdot \mathbf{e}_2 & N_{A,1}\mathbf{a}_1 \cdot \mathbf{e}_3 \\ N_{A,2}\mathbf{a}_2 \cdot \mathbf{e}_1 & N_{A,2}\mathbf{a}_2 \cdot \mathbf{e}_2 & N_{A,2}\mathbf{a}_2 \cdot \mathbf{e}_3 \\ \mathbf{b}_3 \cdot \mathbf{e}_1 & \mathbf{b}_3 \cdot \mathbf{e}_2 & \mathbf{b}_3 \cdot \mathbf{e}_3 \end{bmatrix} \delta\hat{\mathbf{u}}_A = \mathbf{B}_A \delta\hat{\mathbf{u}}_A \tag{6.39}$$

where

$$\begin{aligned} \mathbf{a}_1 &= \mathbf{A}_1 + \mathbf{u}_{,1} \\ \mathbf{a}_2 &= \mathbf{A}_2 + \mathbf{u}_{,2} \\ \mathbf{b}_3 &= N_{A,2}\mathbf{a}_1 + N_{A,1}\mathbf{a}_2 \end{aligned} \tag{6.40}$$

and the discrete forms of the covariant base vectors and displacement vector derivatives are

$$\mathbf{A}_\alpha = N_{A,\alpha}\mathbf{R}_A; \qquad \mathbf{u}_{,\alpha} = N_{A,\alpha}\hat{\mathbf{u}}_A. \tag{6.41}$$

For computer implementation the virtual strain is rewritten as

$$\delta\boldsymbol{\epsilon} = \begin{bmatrix} \mathbf{B}_1 & \cdots & \mathbf{B}_A & \cdots & \mathbf{B}_{nm} \end{bmatrix} \delta\mathbf{u} = \mathbf{B}\delta\mathbf{u} \tag{6.42}$$

from which we get the discretized internal forces

$$\delta W_{\text{int}} = \delta \mathbf{u}^T \mathbf{f}^{\text{int}} = \delta \mathbf{u}^T \int_A \mathbf{B}^T \mathbf{n} \mathrm{d}A \tag{6.43}$$

where $\mathbf{n}$ is from Eq. (6.36).

The components of the discrete membrane stress resultants in matrix notation are computed as

$$\mathbf{n} = \frac{Et}{1-\nu^2} \mathbf{C} \boldsymbol{\epsilon} \tag{6.44}$$

where the covariant strain components are

$$\boldsymbol{\epsilon} = \begin{bmatrix} \epsilon_{11} \\ \epsilon_{22} \\ 2\epsilon_{12} \end{bmatrix} = \begin{bmatrix} \mathbf{A}_1 \cdot \mathbf{u}_{,1} + \frac{1}{2}\mathbf{u}_{,1} \cdot \mathbf{u}_{,1} \\ \mathbf{A}_2 \cdot \mathbf{u}_{,2} + \frac{1}{2}\mathbf{u}_{,2} \cdot \mathbf{u}_{,2} \\ \mathbf{A}_1 \cdot \mathbf{u}_{,2} + \mathbf{A}_2 \cdot \mathbf{u}_{,1} + \mathbf{u}_{,2} \cdot \mathbf{u}_{,1} \end{bmatrix} \tag{6.45}$$

and the matrix $\mathbf{C}$ by use of Eq. (6.28) becomes

$$\mathbf{C} = \begin{bmatrix} (A^{11})^2 & \nu A^{11}A^{22} + (1-\nu)(A^{12})^2 & A^{11}A^{12} \\ & (A^{22})^2 & A^{22}A^{12} \\ \text{sym.} & & \frac{1}{2}[(1-\nu)A^{11}A^{22} + (1+\nu)(A^{12})^2] \end{bmatrix}. \tag{6.46}$$

The equations are implemented in an element form and integrated numerically using Gaussian quadrature over a parent element.

The linear elastic NURBS based Kirchhoff-Love shell

To perform verification studies after the form finding has been performed, a small displacements, linear elastic NURBS based Kirchhoff-Love shell is implemented. The verification studies are performed using the linear elastic Kirchhoff-Love shell in a static analysis with small deformations, after further refining the form found geometry into smaller elements. The same loading is used as during the form finding. The bending and strain energies are computed and used to check how fine resolution the mesh used in the form finding needs in order to find a geometry which works predominantly in membrane action. The studies are presented in Papers B and C.

To describe the strains up to first order in $\mathbf{u}$, the quadratic terms of the membrane strains are neglected, leading to

$$\epsilon_{\alpha\beta} = \frac{1}{2}(\mathbf{A}_\alpha \cdot \mathbf{u}_{,\beta} + \mathbf{A}_\beta \cdot \mathbf{u}_{,\alpha}) \tag{6.47}$$

which is supplemented with the linearized bending strains

$$\kappa_{\alpha\beta} = -\mathbf{A}_{\alpha,\beta} \cdot \Delta\mathbf{a}_3 - \mathbf{u}_{\alpha,\beta} \cdot \mathbf{A}_3 \tag{6.48}$$

with

$$\Delta \mathbf{a}_3 = \mathbf{a}_3 - \mathbf{A}_3 = -\frac{1}{|\mathbf{A}_1 \times \mathbf{A}_2|} \{\mathbf{A}_3 \times [\mathbf{A}_3 \times (\mathbf{u}_{,1} \times \mathbf{A}_2 + \mathbf{A}_1 \times \mathbf{u}_{,2})]\} \tag{6.49}$$

approximated to the first order in $\mathbf{u}$. For detailed derivations and the corresponding strain-displacement matrices for FE-implementation, see [90].

6.2.4 Dynamic relaxation

Dynamic relaxation was first suggested by Day [46] and further adopted to form finding of lightweight and large span tension structures by Barnes [47,91]. For a thorough discussion on dynamic relaxation, see [92] and [93]. There are several reasons for using dynamic relaxation for the form finding. It is a vectorized method, for which the cost of each iteration is cheap, resulting in that rapid results can be obtained. It is possible for the user to interact with the relaxation process, since the result from the last iteration can be used as an initial guess for a new problem, where for instance, the material properties or initial geometry is slightly modified. Since it is a dynamic method the presence of a mass matrix makes it possible to handle singularities of the stiffness matrix in the direction perpendicular to the surface of the membranes. The method is suitable for parallelization and has shown good performance on GPUs [94].

The dynamic relaxation method solves (non-linear) static problems by adding fictitious masses, fictitious damping and by using explicit time integration. The equation of motion (EOM) is given by

$$\mathbf{M}\ddot{\mathbf{u}} + \mathbf{C}\dot{\mathbf{u}} + \mathbf{f}^{\text{int}} = \mathbf{f} \tag{6.50}$$

where $\mathbf{f}^{\text{int}}$ is the column matrix of internal forces, $\mathbf{f}$ is the column matrix of external forces, $\mathbf{M}$ is the mass matrix, $\mathbf{C}$ is the damping matrix, and $\mathbf{u}$ contains the unknown displacements. Since only the static solution is of interest only $\mathbf{f}$ and $\mathbf{f}^{\text{int}}$ must represent the physical problem, all other parameters can be chosen freely. To obtain the motion in time the EOM is integrated using the central difference integration scheme

$$\dot{\mathbf{u}}^{t_n - h/2} = (\mathbf{u}^{t_n} - \mathbf{u}^{t_n - h})/h; \qquad \ddot{\mathbf{u}}^{t_n} = (\dot{\mathbf{u}}^{t_n + h/2} - \dot{\mathbf{u}}^{t_n - h/2})/h \tag{6.51}$$

$$\dot{\mathbf{u}}^{n} = \frac{1}{2}(\dot{\mathbf{u}}^{n - h/2} + \dot{\mathbf{u}}^{n + h/2}) \tag{6.52}$$

which applied to Eq. (6.50) gives a set of equations that update the velocities and displacements as

$$\dot{\mathbf{u}}^{t_n + h/2} = \frac{(2 - ch)}{(2 + ch)}\dot{\mathbf{u}}^{t_n - h/2} + 2h\mathbf{M}^{-1}\frac{(\mathbf{f} - \mathbf{f}^{\text{int}})}{(2 + ch)} \tag{6.53}$$

$$\mathbf{u}^{t_n + h} = \mathbf{u}^{t_n} + h\dot{\mathbf{u}}^{t_n + h/2} \tag{6.54}$$

where $\mathbf{M}$ must be diagonal to preserve the explicit form of the central difference integrator, [93]. $\mathbf{C}$ is chosen as being mass proportional, $\mathbf{C} = c\mathbf{M}$, where c is a damping coefficient for the structure, h is the time step. In the first iteration, $t = 0$ and $\mathbf{u}^0$ is known, then

$$\dot{\mathbf{u}}^{0+h/2} = h\mathbf{M}^{-1}(\mathbf{f} - \mathbf{f}^{\text{int}})/2. \tag{6.55}$$

An alternative to viscous damping (critical damping) is kinetic damping, where the total kinetic energy of the system is traced trough the motion in time and once a peak is detected the current velocities are set to zero. While kinetic damping typically requires more iterations to converge than the critically damped system, it is cheaper per iteration.

6.3 FORM FINDING EXAMPLES

In order to study the use of NURBS based isogeometric analysis for the form finding and early design phase of shell structures several objectives have been met. First, in Paper B, NURBS based elements are presented, implemented, numerically studied and compared to polynomial elements for use for form finding with dynamic relaxation. Second, Paper C presents a possible design method using IGA for form finding.

During the research some demonstrator plug-ins were developed to test the method in a CAD environment. This is presented in Paper C and in the following subsections.

6.3.1 Plug-ins

Conceptual design is an iterative procedure, and performing form finding often requires several iterations in order to get satisfactory results. To simplify this work-flow, it is favorable to be able to perform the form finding in design software. Using design software can simplify the modeling of the related parameters, such as the initial geometry, the boundary conditions, material parameters etc. Buildings are generally designed in CAD software, and it is of interest to include form finding into CAD. In order to study the possibilities of performing form finding directly in CAD software using NURBS which are well supported by the CAD software two demonstrator plug-ins for form finding with dynamic relaxation on NURBS elements were developed.

The results from Papers B and C was used for developing two demonstrator plug-ins for Rhinoceros 3D and for Grasshopper. Rhinoceros 3D is a popular NURBS modeler commonly used in practice by architects and engineers. Grasshopper is a plug-in for Rhinoceros 3D which provides users with a visual programming environment (VPE).

The plug-ins developed here have been written using RhinoCommon, which is a .NET plug-in Software Development Kit (SDK) available for Rhinoceros and Grasshopper.

A .NET library for FEA with support for IGA was implemented prior to the development of the plug-ins that acts as the back-end and runs the simulations independent of Rhino/Grasshopper. For the implemented library, the package Math.NET Numerics was used for the necessary linear algebra, together with Intel Math Kernel Library.

The plug-ins are limited in that they currently support form-finding with multiple patches, but there is no support for trimmed patches. There are, however, formulations of IGA with support for trimmed patches [86], but they have not been implemented here. The boundaries between adjoining patches need to be compatible, meaning that edges of bordering patches have to be compatible in their discretizations, i.e. exactly the same locations for control points, orders of interpolating functions, and the same knot vectors. The tools currently support uniformly applied loads to the initial geometry.

Rhinoceros 3D plug-in

The first plug-in interfaces directly with Rhinoceros 3D, and provides form finding capabilities trough a simple tabbed computer interface. By filling out the different tabs a form finding can be performed in Rhino, see Paper C.

The interface of the Rhinoceros 3D plug-in is developed using Windows Presentation Foundation (WPF). The interface consists of a tabbed docking panel where initial geometries, materials, and boundary conditions can be set up. The form finding can be performed by filling in the tabs and interactively running the application.

By first modeling the coarsest possible geometry the refinements to smaller elements can be handled by built in function in Rhinoceros. The limitations must be kept in mind while modeling the initial geometry, for instance, modeling a hole requires patch modeling techniques.

Using a CAD environment simplifies the modeling of the initial geometry compared to using a general finite element software. The form finding process typically requires several iterations to fulfill both architectural design and engineering criteria. This requires iterative modifications to the initial geometry which is simple to perform in a CAD software such as Rhinoceros, where unlike traditional FE-software an iterative work-flow is important.

Grasshopper 3D plug-in

The second plug-in provides form finding capabilities trough the Grasshopper VPE. The interface to the form finding is done trough the use of custom Grasshopper components. The inclusion of form finding into Grasshopper makes it possible to create parametric architectural models, where the form finding is a part of the parametric model. Since the form finding is performed using NURBS all of the existing components and functions in Grasshopper can be applied after the form finding process.

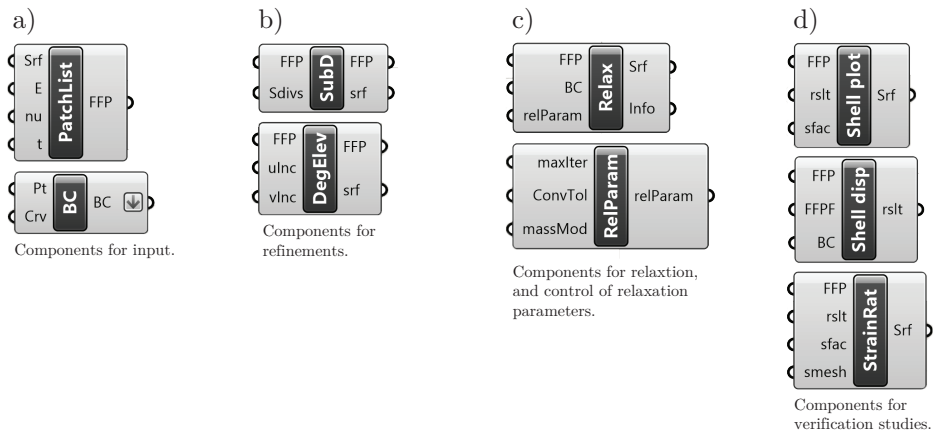


Figure 6.6: The developed grasshopper components, split into four categories: a) references to geometry, material, and boundary conditions. b) components for refinements. c) the dynamic relaxation and control. d) linear elastic small displacements Kirchhoff-Love shell components for studying the form found shape.

The custom components for the Grasshopper VPE were developed using the Grasshopper SDK, and RhinoCommon.

A Grasshopper component can be regarded as a black-box function with a set of custom inputs and outputs. Fig. 6.6 shows the developed Grasshopper components which are divided into four categories, components for input, components for refinements, components for the relaxation and finally components for verification studies.

6.3.2 Simple example

The capabilities of the two plug-ins are very similar, but since the UI of the second one, the Grasshopper plug-in, is not included in any of the appended papers its capability is shown in the following examples.

The ability to perform form finding with very few elements is favorable in design situations as it allows the designer to quickly explore alternative shapes. In the form finding exploration the first step is to define an initial shape, boundary conditions, material parameters and applied loads (typically the self-weight). Once this is done the form finding is run with a coarse mesh and the shape is computed. Some different shapes which were computed in real-time using coarse meshes are shown in Paper C.

The purpose of this example is to show of the advantages of using NURBS elements to integrate the form finding in CAD. The example is intended for showing the design process for a roof

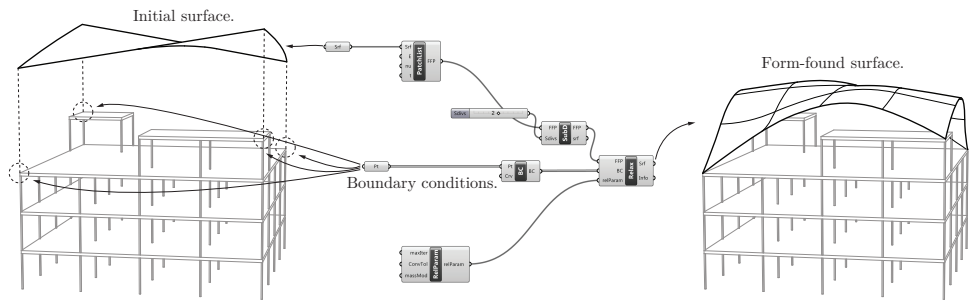


Figure 6.7: The combination of Grasshopper components for a simple form finding.

of a building. Fig. 6.7 shows the setup in Grasshopper for a simple form finding with an initial geometry with a single patch, consisting of one element which is subdivided twice into 4 X 4 NURBS elements with quadratic basis functions. The top left component in the figure (denoted Srf) refers to the initial geometry in Rhino. The bottom left component (denoted Pt) refers to constrained corner points in Rhino, it is also possible to constrain boundary edges. The output from the form finding component in the right in the figure is the form found surface. The building geometry is included in the design process, and the form finding results are viewed in this context.

After the first form finding iteration an evaluation of the shape follows. The shape is evaluated in terms of architectural and engineering criteria, such as structural performance, daylight, acoustics, limitations on the shape (height, span), asymmetric loads, buckling, and so on. The structural analysis is performed using shell elements. To fulfill the criteria it is often necessary to change initial parameters such as the initial geometry, boundary conditions, and loads before the form finding process is iterated. Fig. 6.8 shows a few design explorations of the simple geometry shown in Fig. 6.7 with a uniformly distributed load. Variations of the boundary conditions and geometry generates different shapes, all approximated with a coarse mesh. Since the resulting geometry is still represented by NURBS it can be used with a parametric model in Grasshopper, this is exemplified by the length of the vertical bars between the building and roof, which are automatically updated if the roof shape is altered.

Once the form found shape fulfills necessary design and engineering criteria, it can be further refined and ran through the form finding process once again, in order to obtain a more optimal shape. This is further discussed in Paper C.

Integrating the process into Rhinoceros simplifies several parts which are often included in the design process. The form finding can be performed within the architectural context, and thus simplifies considerations related to the surrounding buildings, such as e.g. shading and reflections.

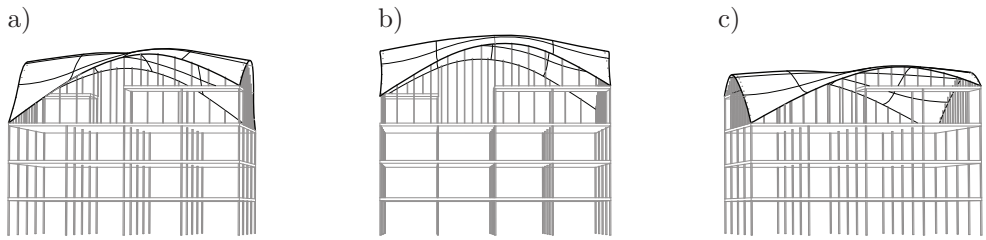


Figure 6.8: Different examples generated by changing the boundary conditions or initial geometry of the example shown in Fig. 6.7. a) added vertical bars. b) changed position of corner points. c) increased Young's modulus of the roof material.

Since the form found shape is already in the design software and being represented by the complete curved geometry description it is easy to do architectural renderings to present to clients. Further detailing operations in CAD be performed after the form finding since the geometry is still NURBS, and is well supported by the software. Another advantage of CAD tools is that they often include geometry diagnostics tools, such as curvature and edge analysis.

6.3.3 Multi-patch examples

For cases when more complex geometries than simple quadrilaterals are required, multiple patches can be studied. For the current example, if for instance an entrance would be designed at one of the corners of the building multiple patches are required for the geometry and the form finding, see Fig. 6.9.

If a rectangle is divided into multiple patches where the stiffness or boundary conditions are varied, various forms for the same initial surface can be explored, see Fig. 6.10.

6.4 SUMMARY

The research set out to develop and test numerical form finding using NURBS based membrane elements with dynamic relaxation. The contributions are:

- Demonstrator tools for form finding by use of the hanging model analogy with IGA are developed, see Paper C and Section 6.3
- The implementation of NURBS based IGA membrane elements with the dynamic relaxation solver is presented in Paper B. A study of how different choices of damping and mass affect the convergence of the dynamic relaxation method with NURBS based membrane elements is included.

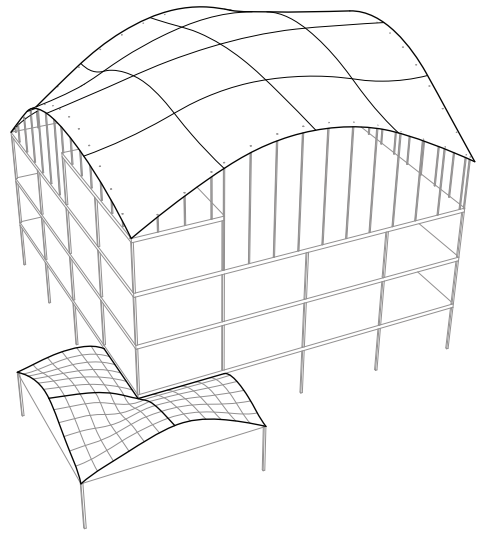


Figure 6.9: Building with added entrance, consisting of three patches.

- The advantages of using NURBS based IGA rather than classical finite elements for form finding are presented, see Papers B and C.

Advantages of using IGA:

- Straightforward to refine geometry for verification studies.
- Using NURBS makes it simple to use the form found shapes for other studies available in CAD (solar, etc..), and for further design.
- Thin shell theory is simpler to implement using IGA.

The convergence study with different choices of mass and damping in Paper B was made for a few different geometries. The study was made in order to ensure good performance in the later developed demonstrator tools. The choice of a mass matrix based on the initial stiffness and kinetic damping were implemented in the demonstrator tools for Rhino and Grasshopper.

Numerical form finding with the hanging model analogy is well developed, however, the use of NURBS elements brings some novel additions. It makes it possible to perform the form finding directly in a CAD software, with geometry that is fully supported by the CAD programs, in this case Rhino and Grasshopper. The NURBS elements are curved and C^1 continuity between elements can be achieved, which is favorable for form finding since the resulting shapes are often curved and continuous and the employed shell models for verification studies require C^1. It is possible to perform the form finding with very few elements, rapidly providing previews

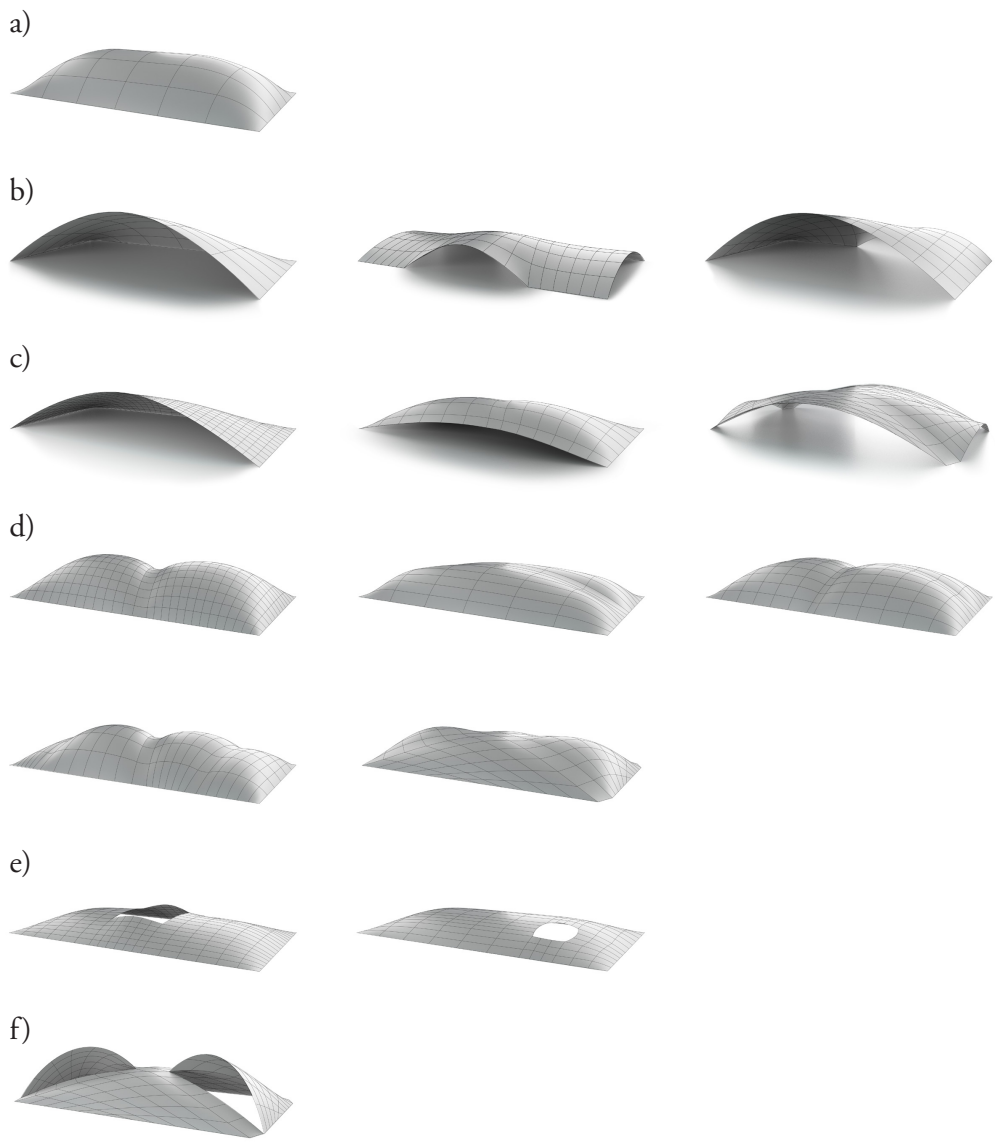


Figure 6.10: Examples with a rectangular initial shape, using multiple patches. a) single patch, fully constrained perimeter. b) multi-patch variants with perimeter openings. c) with stiffened bands and openings. d) with stiffened bands, fully constrained perimeter. e) with holes. f) with holes and stiffened bands.

of what a higher resolution mesh will result in, more or less in real-time. Wrinkling effects present in high resolution models are not observed for low resolution models. Supporting the form finding in Grasshopper means that it can be integrated into larger parametric models allowing for design explorations in context and simplifying the design process.

7 Design exploration using graphic statics

7.1 LITERATURE REVIEW

Graphic statics is a graphical method for determining the forces in an assembly of axially loaded members, such as trusses, cables, and arches. The first comprehensive presentation of graphical techniques was done by Culmann [95], who is considered the father of graphic statics. Other important contributors to graphic statics were Maxwell, Cremona, and Bow.

It is based on construction of two reciprocal diagrams: the form diagram representing the actual geometry of the structure, and the force diagram that represents the internal forces through vectors. Changes in the geometry are reflected in the force diagram, providing a visual relationship between the two. Because forces are graphically represented using vectors, no numerical analysis is required to calculate the forces. Fig. 7.1 shows an example solution for a cable using graphic statics.

Graphic statics can only provide unique solutions to statically determinate structures, for which the equations of equilibrium can be solved without the addition of further constraints

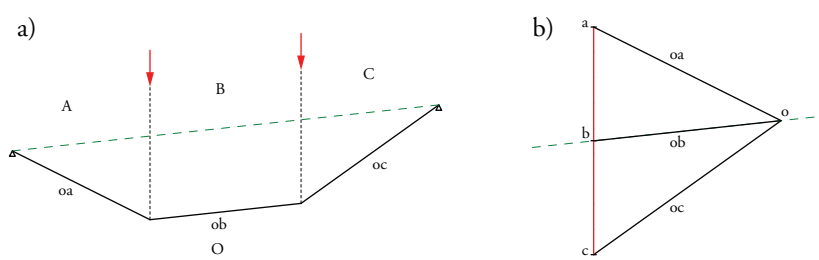


Figure 7.1: Graphic statics solution for a cable with two point loads. a) Form diagram. b) Force diagram.

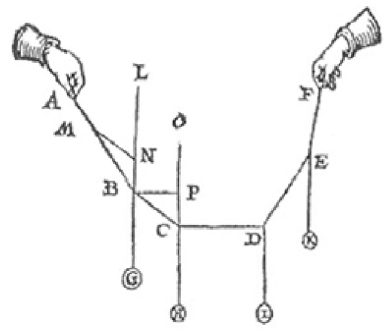


Figure 7.2: Stevin's drawing of force equilibrium [96].

(considering for instance elasticity or relative stiffness of members). A further requirement is that all the loads and members must be co-planar, limiting the use of graphic statics to two-dimensional problems. Graphic statics solutions to simple structures, such as the one in Fig. 7.1 are elegant and clear, however, for more complex structures the force diagrams can quickly become difficult to read.

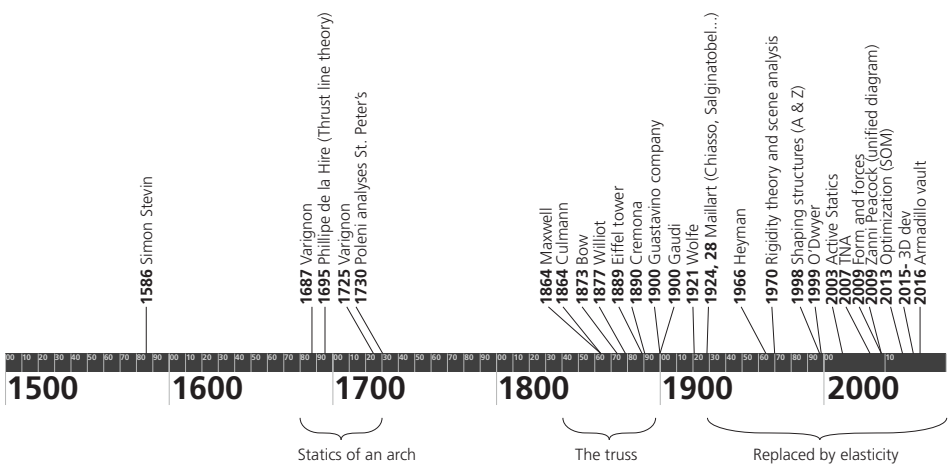


Figure 7.3: Scientific contributions related to graphic statics.

7.1.1 Background

Graphic statics were developed during the 19th century. Fig. 7.3 shows some of the scientific contributions and structural designs related to graphic statics. Philippe de la Hire published in 1695 the first application of statics to an arch. He represented forces in a diagram that were related to the arch of the geometry, which would later be developed into graphic statics. Another early trace was the parallelogram rule devised by Simon Stevin using force vectors to analyze forces, Fig. 7.2. Varignon introduced the funicular polygon [97, 98].

Various cracks in the dome at Saint Peter's Basilica along with further concerns following an earthquake in 1730 lead to an investigation concerning the structural safety of the dome [99]. Giovanni Poleni successfully applied the present theories at the time for assessing the safety of the dome. Poleni ignored the iron hoops that were already installed due to the cracks, and assumed that the masonry had large compressive strength and zero tensile strength. Poleni observed that the dome would be safe if the line of thrust lay entirely within the thickness of the masonry. Applying Hooke's principle of the hanging chain he demonstrated that the line of thrust was within the bounds, and was thus first to successfully assess the safety of a masonry structure using an equilibrium method by creating a physical model using weights proportional to the sections of the dome (two opposite wedges of the dome as arches). An image of his analysis is shown in Fig. 7.4. Using physical models can quickly become tedious when alterations are necessary and when the models become more complex than a single arch. Graphical statics would later become a simpler method of performing similar analysis as Poleni's.

Early graphical methods considered one joint at a time [99]. Graphic statics was formalized by Culmann [95, 98]. Maxwell combined the joint diagrams to a single force diagram using the state of the art mathematics - projective geometry. He devised the reciprocal diagrams of graphic statics. The diagrams were later widely adopted thanks to Robert Henry Bow's notation which made the creation of a reciprocal diagram straight forward. Bow's notation has been used to compute the reciprocal in Fig. 7.5b.

None of the books that were published during the intial development of graphic statics addressed issues related to shaping of structures [101], this has only been the topic for more recent books, such as [102].

Graphic statics have been used to design structures by amongst others Maurice Koechlin (co-designer of the Eiffel Tower) and Robert Maillart [102].

7.1.2 Graphic statics using Bow's notation

Allen and Zalewski [102] present how to step by step construct the diagrams of graphic statics by making use of Bow's notation [103].

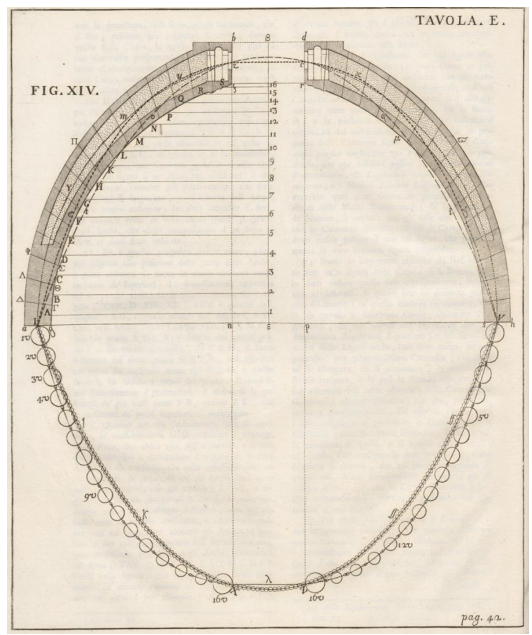


Figure 7.4: Poleni's analysis of St. Peter's [100].

Following Bow's notation, capital letters are placed in the spaces between the lines of action of the forces in the form diagram. Forces are named by the letters on both sides in lower case, for instance the force between the spaces A and O is ao (or oa). Nodes are named using a clockwise reading of all of the spaces surrounding a node, for instance the first node to the right of the left support in Fig. 7.5a is called ABO (or BOA, OAB). Points in the force diagram are designated

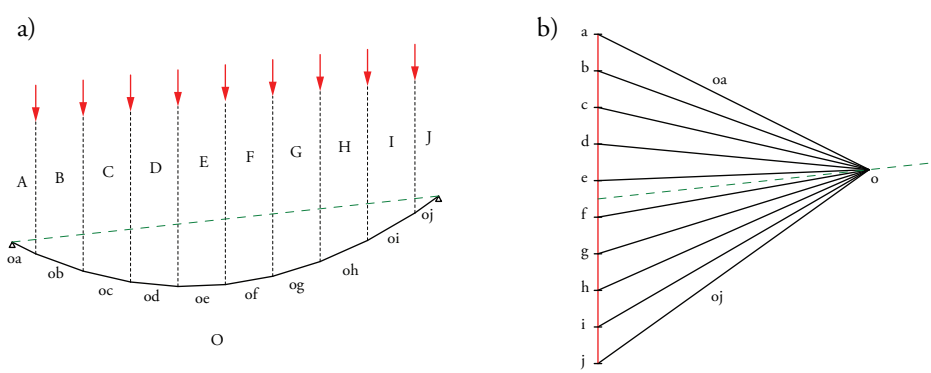


Figure 7.5: Graphic statics solution for a cable with a uniformly distributed load. a) Form diagram. b) Force diagram.

with lower case letters and correspond to the upper case letters that designate spaces in the form diagram. Bow's notation is thus a convenient way of establishing the reciprocal relationship between the diagrams.

The equilibrium of each point of the form diagram is represented by a closed polygon in the force diagram. For instance the equilibrium of point ABO in Fig. 7.5a is represented by the polygon abo in Fig. 7.5b. Using Bow's notation we can read the tension and compression, for instance, at node ABO in Fig. 7.5a, we move clockwise between B and O (where force bo is acting) and the direction from b to o in 7.5b is towards the lower right, the force bo at ABO is thus moving away from the point - corresponding to tension.

The drawing of graphic statics diagrams is easily performed using Bow's notation and appropriate drafting tools. There are procedures available for finding forms for different types of structures that fulfill desired criteria such as going through a set of points or having a certain height [102].

7.1.3 Renewed interest in graphic statics

The theory of elasticity and numerical methods lead to reduced interest in graphic statics. However, the reciprocal relationships would become rediscovered again. Some development related to graphic statics was seen in rigidity theory [104–106] where the diagrams were extended to three dimensions, and in scene analysis [107]. Heyman [108] investigated masonry structures using the principles of plastic design. He presented the assumptions necessary for limit state design of masonry.

For statically indeterminate cases graphic statics provides a simple way to explore different states of equilibrium. Based on Heyman's [108] demonstration of the assumtions necessary to apply plastic limit state analysis to masonry, O'Dwyer devised a method for funicular analysis of masonry vaults by modelling the principal stresses as a discrete network of forces [109]. Using optimisation, feasible solutions were found based on the safe theorem of plasticity. The method was later developed into thrust network analysis (TNA), where the reciprocal diagrams of graphic statics were used to explore the different possible lower bound solutions of the discrete network of forces [110]. The indeterminacy of graphic statics is exploited in the theory of TNA, which extends the method to three dimensions and generates compression only vaulted surfaces and networks under gravitational loading. Graphic statics and related methods are used for the assessment of the safety of historic masonry [110], and for the form finding and design of new vaulted structures.

In [111] the motivations for using geometric rather than analytic or numerical representations of the relationship between form and forces are presented. Graphic methods with reciprocals make it straightforward to control distribution of forces and explore the possible geometries, i.e. designing a truss with a constant force in a chord is performed by simply constraining the lengths of respective edges in the force diagram. Graphical methods are also able to display



Figure 7.6: Armadillo vault ©David Escobedo/Escobedo Group.

several stress-states for a statically indeterminate structure. Thrust-lines can be used to study the stability of masonry. Compression only solutions for shells can be connected to requiring a convex polyhedral airy stress function.

The doubly curved compression-only Armadillo vault shown in Fig. 7.6 was recently designed using graphical methods. The form was developed using RhinoVAULT, a TNA plug-in for Rhinoceros. The found form was used as the midsurface for the structure and after adding thickness it was discretized into stone voissours. At its thinnest the structure is five centimeters thick. The stresses from the self-weight do not exceed 0.1 MPa, the limestone used has a compressive strenght of 22 MPa. The stability of the discretized structure under different loading conditions was verified using discrete element modelling [112].

Recently, research on graphic statics has aimed been at developing a fully three-dimensional framework [113–116]. Further, general equilibria (not just axial forces) [115, 117], graphic kinematics, and approaches for including the principle of virtual work [118] have been studied, leading to a graphical approach to elasticity.

7.1.4 Computer based graphic statics

Some disadvantages of hand-drawn graphic statics are for example difficulties with drawing the parallel lines and solving by hand, and that the graphs can quickly become complex and difficult to read. The disadvantages disappear when implemented in a computer. The reciprocal relationships can be set-up in a parametric or constraint based environment [111]. Further, since the reciprocal relationships are encoded using graphs, it is simple to make interactive visualizations showing which vertex in the form diagram corresponds to which face in the force diagram. The variables between the diagrams - the nodal positions of the edges and the static indeterminacies - can through algebraic formulations be clearly presented to the end-user.

Several computer tools using graphic statics have been developed. One such tool is Active Statics, an on-line tool intended for educational use, where some predefined problems are solved with graphic statics. Users are able to manipulate structures and see how the internal

forces change. Another on-line tool is eQUILIBRIUM, containing some further examples. RhinoStatics is a plug-in which can be used for graphic statics in Rhinoceros 3D and is not limited to some pre-defined examples. Recently there has been a prototype tool developed for Grasshopper [119].

7.1.5 Present research

Until recently most of the tools and literature have only presented digital versions of graphic statics for some specific pre-defined structures. A general algebraic formulation of graphic statics using a graph theoretic approach is presented by Van Mele and Block [6], that given a form diagram, is able to generate a force diagram directly. The equilibrium of the structural systems [6] are investigated using the states of self-stress of an equivalent unloaded network, making use of the singular value decomposition of the equilibrium matrix [120]. A similar work, dealing with reciprocal diagrams for tensegrities is [121]. The algebraic approach of the graphic statics framework [6] is well suited for computer implementation as a back end for a CAD software. The work presented in this thesis is based on and extends [6].

The algebraic treatment of force-based form explorations is not present in the available scientific literature. Though the diagrams are reciprocal, and the algebraic formulation is similar to set-up, there are additional requirements necessary to enable force-based explorations. These range from being able to explore all forms related to a force diagram, down to including constraints in order to explore a sub-set of the available forms - techniques common when performing form finding or optimization. Papers D–F deal with different aspects of this theme.

7.2 THEORY

The computer based algebraic approach that is further developed in this thesis is based on [6]. The topics relevant to the implementation are related to planar and dual graphs, the force density method, the matrix methods for pin-jointed structures, and the lower bound theorem of plasticity.

7.2.1 Graph theory and reciprocal diagrams

A graph $G = (V, E)$ is an ordered pair consisting of a set V of vertices (or nodes or points) and a set E of edges (or arcs or lines). Each edge is associated with two vertices (not necessarily distinct) consisting of an unordered pair [122].

A graph is planar if it can be drawn in the plane such that edges only intersect at their ends, i.e. edges do not cross each other. Such a drawing is called a planar embedding. A planar embedding partitions the plane into a number of connected regions [122]. Each region enclosed

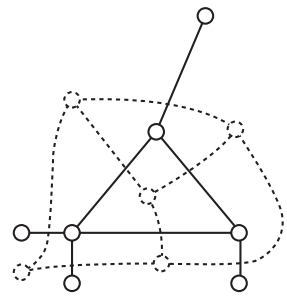


Figure 7.7: Planar graph as solid lines and dual as dashed lines.

by a polygon of edges in a planar embedding is called a face, including the unbounded region (called the exterior face). Due to the presence of external forces in the present approach, there are several unbounded regions, separated by external edges. The vertices that only connect to external edges in the present approach are referred to as leaf vertices (a leaf vertex is a vertex with degree one). Once a graph is drawn in the plane (i.e. embedded), a unique dual is defined. A dual graph G^* has a vertex for each face of the graph G, and an edge whenever two faces of G are separated by an edge. The dual is also planar. Fig. 7.7 shows a planar graph as solid lines and its dual as dashed lines.

The reciprocal relationships of the form and force diagram mean that the number of edges is the same in both diagrams. The number of vertices in one is equal to the number of faces in the other, and vice versa. Further in the Cremona convention adopted here, the reciprocal edges are parallel to each other, for instance edge oa in Fig. 7.5a is parallel to edge oa in Fig. 7.5b.

Micheletti [121] presents the relationships of reciprocal diagrams for self-stressed frameworks. By using graph theory the algebraic dualities between the edge lengths and forces in a self-stressed framework are formulated. The relationships are valid in any dimension provided that the underlying graphs are planar [121]. The reciprocal relationships can be formulated using dual polyhedra, however, here we have followed the graph formulation.

The construction of the incidence $\mathbf{C}$ and dual incidence $\mathbf{C}^*$ matrices (also referred to as connectivity matrices) is presented in Papers D and E.

Algebraic matrix formulations of 2D graphic statics are presented in [121] and [6]. The formulations presented in Papers D and E are an extension of [6].

7.2.2 The force density method

The force density method was developed to solve the equations of equilibrium for a cable-net without prescribing and initial nodal coordinates [48]. The nodal coordinates are solved for from a single linear system of equations. The equilibrium equations for a general network can be formulated as

$$\mathbf{CUL}^{-1}\mathbf{s} = \mathbf{f}_{\mathrm{x}} \tag{7.1}$$

$$\mathbf{CVL}^{-1}\mathbf{s} = \mathbf{f}_{\mathrm{y}} \tag{7.2}$$

$$\mathbf{CWL}^{-1}\mathbf{s} = \mathbf{f}_{\mathrm{z}} \tag{7.3}$$

where $\mathbf{C}$ is the incidence matrix of the graph G describing the network topology (the branch-node matrix in [48] is $\mathbf{C}^{\mathrm{T}}$). $\mathbf{U}$, $\mathbf{V}$ and $\mathbf{W}$ are diagonal matrices with the coordinate differences in x, y, and z respectively. $\mathbf{L}$ is a diagonal matrix containing the lengths of the cables, $\mathbf{s}$ are the internal forces in the cables and $\mathbf{f}_{\mathrm{x}}, \mathbf{f}_{\mathrm{y}}, \mathbf{f}_{\mathrm{z}}$ are the external force components. The equations are non-linear since $\mathbf{L}$ is a function of the coordinates, using

$$\mathbf{L}^{-1}\mathbf{s} = \mathbf{q} \tag{7.4}$$

where $\mathbf{q}$ are force densities (also known as force-length ratios), i.e. the force density of cable i is $q_i = s_i/L_i$. The introduction of the force densities linearises the equations of equilibrium [48], we have

$$\mathbf{CUq} = \mathbf{f}_{\mathrm{x}} \tag{7.5}$$

$$\mathbf{CVq} = \mathbf{f}_{\mathrm{y}} \tag{7.6}$$

$$\mathbf{CWq} = \mathbf{f}_{\mathrm{z}}. \tag{7.7}$$

The coordinate differences are given by $\mathbf{u} = \mathbf{C}^{\mathrm{T}}\mathbf{x}$, $\mathbf{v} = \mathbf{C}^{\mathrm{T}}\mathbf{y}$, $\mathbf{w} = \mathbf{C}^{\mathrm{T}}\mathbf{z}$. With the coordinate differences and using $\mathbf{Uq} = \mathbf{Qu}$, $\mathbf{Vq} = \mathbf{Qv}$, $\mathbf{Wq} = \mathbf{Qw}$, where $\mathbf{Q}$ is a diagonal matrix of force densities and $\mathbf{u}, \mathbf{v}, \mathbf{w}$ are vector versions of $\mathbf{U}, \mathbf{V}, \mathbf{W}$ respectively, we get

$$\mathbf{CQC}^{\mathrm{T}}\mathbf{x} = \mathbf{f}_{\mathrm{x}} \tag{7.8}$$

$$\mathbf{CQC}^{\mathrm{T}}\mathbf{y} = \mathbf{f}_{\mathrm{y}} \tag{7.9}$$

$$\mathbf{CQC}^{\mathrm{T}}\mathbf{z} = \mathbf{f}_{\mathrm{z}} \tag{7.10}$$

where only the coordinates are unknown. To solve the linear system of equations, it is first partitioned into prescribed and unknown parts, for details, see [48].

Using the force densities any state of equilibrium for a cable net can be obtained. Since only the force densities are prescribed the nets do not meet any other conditions, such as having equidistant meshes. This can, however, be included using a non-linear force density formulation [48].

7.2.3 Pin-jointed structures

Pin-jointed structures carry load using axial forces and do not transfer moments over joints. In the early design phases of pin-jointed structures it is important to determine if the structure contains mechanisms, is statically determinate or indeterminate. The number of members and their configuration are required to answer the questions. Maxwell showed that a 3D pin-jointed structure having j joints connected by b bars requires $3j - b$ to make it statically determinate, the result is referred to as Maxwell's rule [123]. However, Maxwell was aware of cases which satisfied the rule but were both statically and kinematically indeterminate. Maxwell's rule can be made more precise using linear algebra [124]. Introducing k kinematic constraints, the equilibrium equations are formulated as

$$\mathbf{Aq} = \mathbf{f} \tag{7.11}$$

where $\mathbf{A}$ is the equilibrium matrix of size $[3j - k \times b]$, for detailed construction of $\mathbf{A}$ see [124] or Papers D or E. We denote the force-density vector by $\mathbf{q} \in \mathbb{R}^b$ and the vector of external forces by $\mathbf{f} \in \mathbb{R}^{3j-k}$. The equilibrium matrix is formulated using the assumtions of small displacements, i.e. the equilibrium equations are set-up in the initial configuration. It is a linear map between the space of force densities and the space of external forces. We denote the rank of $\mathbf{A}$ as r_A, the dimension of the nullspace as s and the dimension of the left null space as m. The number of independent inexetensional mechanisms is now [124]

$$m = 3j - k - r_A \tag{7.12}$$

and the number of independent states of self-stress is

$$s = b - r_A \tag{7.13}$$

and combining the two equations gives the extended Maxwell rule

$$s - m = b - 3j + k. \tag{7.14}$$

The four fundamental subspaces of the equilibrium matrix are further discussed in [124]. The nullspace contains solutions to $\mathbf{Aq} = 0$, i.e. all states of self-stress (all states of stress which are in equilibrium with zero external load).

Note that in the formulation in Papers D, E, and F the external and reaction forces are considered part of the assembly and are not modeled as external loads, hence only nullspace solutions to the equilibrium equations are sought. As an example, in Fig. 7.8, vertices A, E, F, G in the form diagram are considered fixed and edges 0, 4, 5, 6 are considered structural components and not forces. Likewise, vertices 0, 1, 2, 3 in the force diagram are considered fixed when solving for the form diagram using the dual formulation.

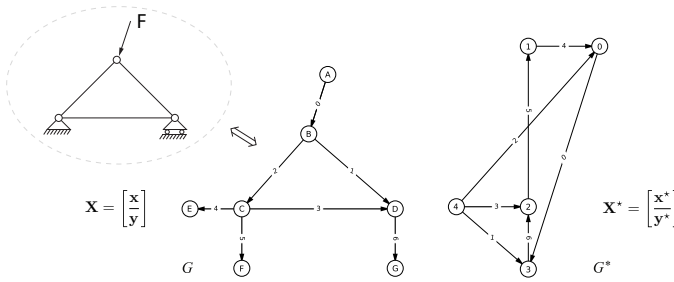


Figure 7.8: The form diagram G and the force diagram G^*. The figure in the top left shows the equivalent structural system represented by G.

7.2.4 Lower bound theorem of plasticity

The classical plastic collapse theorems have been used to determine the load capacities of structures like arches, concrete structures and soil foundations. The material is assumed to be elastic-ideal plastic which leads to the structure having a certain load capacity where the load can no longer be increased [125]. This means that a certain limit load exists that is referred to as the collapse load.

The lower bound theorem (safe theorem) states that the external loading corresponding to an allowable and statically admissible stress field is less than or equal to the collapse load [125]. Hence, for a given external load, if admissible internal stresses that are in equilibrium with the external load and do not violate the yield criterion can be found, then the structure will hold. An elastic solution (which nowhere violates the yield condition) is a lower bound solution.

7.3 DEVELOPED FRAMEWORK AND APPLICATIONS

The geometric relationship between form and forces offered by graphic statics provides means of exploring load carrying ideas. Fig. 7.8 presents a simple graphic statics example, with the structure, applied loads, and support forces to the left and the reciprocal force diagram to the right. The equivalent structural mechanics diagram of the form diagram is shown in the top left of the figure. The diagrams in Fig. 7.8 are represented as directed graphs. The form diagram G is shown to the left, and the force diagram G^* is to the right. In graph theory these are referred to as the primal, and dual graphs, respectively. The coordinates of the form and force diagrams are $\mathbf{X}$, $\mathbf{X}^*$ respectively. Equilibrium of forces in each internal point in the form diagram (points B, C, D in Fig. 7.8) is represented by closed polygons in the force diagram. The lengths of the edges in the force diagram are proportional to the magnitude of the forces in the corresponding edges in the form diagram. A vector of force densities, $\mathbf{q}$, contains the force to form edge length quotients. The force density vector also contains information regarding

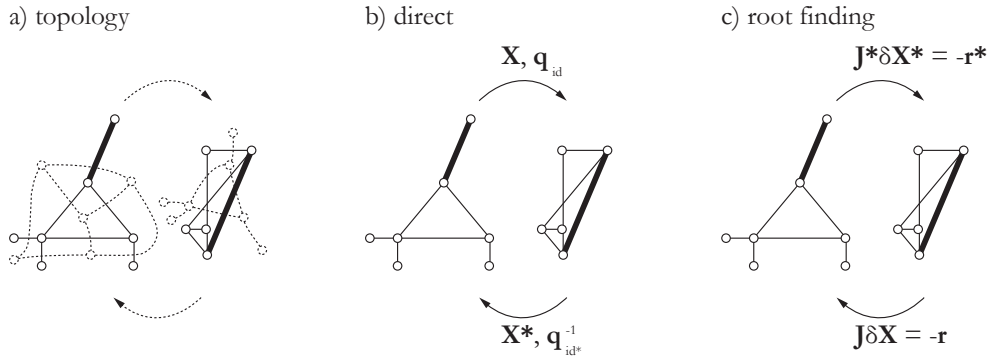


Figure 7.9: The different methods of manipulating the diagrams.

tension and compression, which can also be interpreted from the diagrams directly by making use of Bow's notation.

In the thesis two approaches for manipulating force diagrams are presented in Papers D and E. The appended papers present the framework required for both interactive manipulations and for parametric explorations. In the framework several types of manipulations of the form and force diagram are possible. Fig. 7.9 shows the different parts of the present computer based graphic statics implementation and the variables used in each computation. Fig. 7.9a shows the graph relationships, Fig. 7.9b shows the direct solutions and variables, Fig. 7.9c shows the root finding based approach.

The approach in Paper D uses the non-linear equations of computing the force diagram from the form. A root-finding formulation is used to compute the from diagram based on manipulations of the force diagram, the primary variables are then the form diagram coordinates $\mathbf{X}$ and a set of force densities $\mathbf{q}_{\mathrm{id}}$. Using the approach force diagram manipulations with general equality constraints are possible, however, since it is based on root-finding an initial guess close to the solution is required.

The approach in Paper E formulates a direct solution to compute the form diagram from the force diagram. The primary variables are the force diagram coordinates $\mathbf{X}^*$ and a set of reciprocal force densities $\mathbf{q}^{-1}_{\mathrm{id}^*}$, where $q^{-1}_{\mathrm{id}^*,i} = L_i/L^*_i$ and L_i and L^*_i are the lengths of edge i in the form and force diagrams respectively. Using this approach enables the force diagram to be the initial diagram used for design explorations, however, only linear equality constraints are included. The approach allows for topological refinements of the force diagram and can also be used to compute an initial guess for the root-finding approach in Paper D, improving convergence.

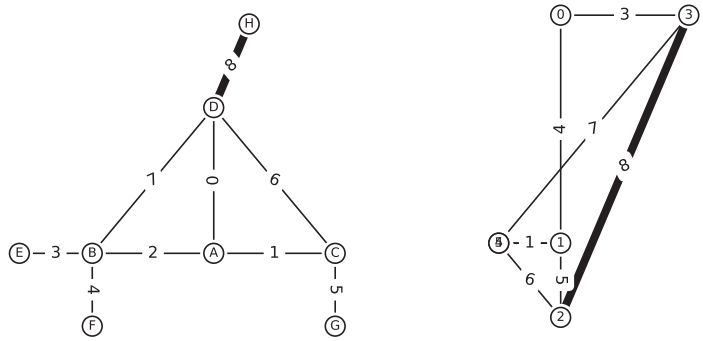


Figure 7.10: The structure in the form diagram to the left has an edge (edge zero) with zero force magnitude.

7.3.1 Need for both approaches

The example in Fig. 7.10 shows why both the direct and root finding approach are necessary. Edge 0 in the form diagram is perpendicular to edges 1 and 2, and leads to a force diagram with a corresponding edge 0 of length 0, hence $q_0 = 0$ and q_0^{-1} is undefined. This means that direct manipulation of the force diagram is not possible, however, the root finding approach is able to solve for the form diagram after force diagram manipulations since the primary variables are then $\mathbf{X}, \mathbf{q}_{\mathrm{id}}$, which are well defined. Using both approaches enables manipulations which are not possible when only one of the methods is available.

7.3.2 Developed graphic statics framework and Rhino plug-in

The framework presented in Papers D and E has been implemented using the programming language Python, together with Numpy, Scipy, and NetworkX. A Rhinoceros plug-in has been written using .NET in order to provide a graphical user interface. The Rhinoceros plug-in communicates with the Python back-end using JSON with the ZeroMQ messaging library [126].

The plug-in currently supports the definition of the form or force diagram and obtains a computed reciprocal diagram from the back-end. The user can add constraints to the form diagram, which are used when manipulating the force diagram. Topological refinements are also possible, constraints are kept after refinements when possible.

7.3.3 Automatic generation of strut-and-tie patterns

The strut-and-tie model (STM) was popularized by Jörg Schlaich and colleagues [127]. Before the STM truss analogies for modeling cracked reinforced concrete beams were considered appropriate whilst being limited to only parts of the structure where the beam hypothesis was valid. The STM generalized the truss analogy to every part of a concrete structure, even for points with statical or geometrical discontinuities.

A key step to the strut-and-tie method is the selection of an appropriate truss model, due to the static indeterminacy of reinforced concrete there are often several suitable models possible. An application using structural optimization of graphic statics for automatically generating strut-and-tie patterns is presented in Paper F. Optimal layouts are found by minimizing the total load path, which is formulated by measuring lengths in the form and force diagrams. Minimization of the total load path is equivalent to truss volume minimization under the assumption that all of the elements are equally stressed, a similar approach based on volume minimization is presented in [128], also for further references, see [129]. All of the examples presented in Paper F yield good results.

7.4 SUMMARY

Multiple techniques for manipulating force diagrams have been presented. The research builds upon an already existing framework and further extends it. The contributions are:

- A direct approach for computing the form based on the force diagram is presented in Paper E.
- A root finding approach for computing the form after manipulating the force diagram is presented in Paper D.
- Inclusion of linear and non-linear constraints is presented in Papers E and D respectively.
- Topological refinements of force diagrams is presented in Paper E.
- Different methods of design explorations based on force diagrams are presented in Paper E.
- Automatic generation of strut-and-tie patterns using graphic statics is presented in Paper F.
- Papers D, E, F contain several examples to illustrate the use of the methods.

The need and advantages of multiple techniques have been discussed. When one approach does not work, the other can be used. Combining the approaches allows for the inclusion of non-linear constraints together with large manipulations.

Using graphic statics for generating STM has been presented. This could be extended to finding optimal forms in arbitrarily shaped domains, and function as a general design tool rather than just be used for STM. However, better performing formulations of the constraints may be necessary.

8 Conclusions

Design is an iterative and often non-linear procedure. Different techniques and tools are used during design as they become necessary. In the thesis, research concerning methods and tools suitable for including structural considerations for some types of structures/phenomena in conceptual design are presented. The developed methods can be used in the conceptual design phase. This can potentially improve the communication and collaboration between engineers and architects, by providing rapid feedback, supporting use in design software, visualizing results and supporting some structural design spaces.

8.1 MAIN CONTRIBUTIONS

The main contributions include:

- A broadened scope of phenomena than can be part of the conceptual design. Specifically, by studying wave propagation in urban scales, which with increased population density resulting in increased vibration and noise levels will be an important tool for designing sustainable cities.
- Further the use of IGA for form finding by implementation and study of dynamic relaxation with NURBS based membrane elements. Implemented demonstrator tools and released a computational framework for IGA in MATLAB and .NET. It was shown how the form found geometry can be used after the form finding to for instance perform static verification studies.
- Development of computational graphical methods for structural design, by providing methods for bi-directional graphic statics, and the explicit computation of form diagrams based on changes in force diagrams. In the thesis, graphic statics has been applied to the automatic generation of strut-and-tie models.

During the course of the research, frameworks for making use of the methods have been implemented. The frameworks support different methods of design exploration. For the wave

propagation tool the focus was on the rapid feedback type of strategies, where it is simple to sketch designs, investigate their effects on the wave propagation, and iteratively discover strategies which might be feasible for urban designs. The IGA framework developed can be used directly in CAD software, both as an interactive tool where the designer can interact with the geometry during form finding, but also as a codification tool through a visual programming language which includes the form finding in a large parametric model. The developed graphic statics framework is perhaps the most general. It supports both interactive use where the parameters can be directly controlled and also provides means of displaying the entire design space for a force diagram. It can, moreover, be used in structural optimization as shown in the thesis trough examples with strut-and-tie pattern generation.

The methods provide limited and alternative views of a structural design for some different types of structures. They can be used as representations and quick models for exploration and decision making in the early design stages, where other aspects than structural performance should also be factored in.

8.2 FURTHER RESEARCH

Tools similar to the one presented in Paper A could be useful in urban planning, in order to reduce the noise and vibrations in the built environment. The ability for an engineer to provide feedback to others of the design team in minutes is important, since it means that it can support a creative and collaborative brain-storming session which often is a part of the earliest design phases. To make the computational tool more general, the model reduction process could be automated.

The reduction method used in Paper A is only valid for steady-state dynamics. If transient analyses are necessary to conduct, other methods for reducing the simulation time are required. This could be other model reduction methods, or the use of methods other than FEA.

Form finding can be seen as a first step in a design process. The research has so far primarily dealt with numerical methods, and perhaps the most important extension would be to apply the tools to design projects and real applications, in order to test and further develop the tools. To evaluate the usefulness of the tools, they should be tested further in case studies.

The dynamic relaxation method studied in Paper B converges fast for systems where elements are uniformly sized. It could be constructive to study other solution methods, both explicit and implicit, to find a method that converges fast for general element geometries. Another promising approach in explicit dynamics is the use of isogeometric collocation, which replaces all of the integration points in an element in a single collocation point with the potential to reduce computational costs. Recently, there have been developments of NURBS based IGA with trimmed patches. The methods are promising in that they simplify the application to complex geometries that are difficult to represent by non-trimmed patches.

The graphic statics framework is well developed. The use of graphic statics for generating initial strut-and-tie models shows a promising application. Further design applications of computational graphic statics should be studied. Paper E presents a framework suitable for topological explorations of force and form diagrams, the design possibilities of this approach should be further studied.

References

[1] Alexandersson, A. (2015), *Isogeometric analysis in form finding in architecture*, Master's thesis, Chalmers University of Technology.

[2] Alic, V. (2017), *Isogeometric Analysis toolbox for CALFEM*, `https://github.com/CALFEM/calfem-matlab-iga`.

[3] *Rhinoceros 3D*, `http://www.rhino3d.com/`, online; accessed 2015-10-05.

[4] *Grasshopper*, `http://www.grasshopper3d.com/`, online; accessed 2015-10-05.

[5] Alic, V. (2018), *compas_bi_ags*, `https://github.com/compas-dev/compas_ags/tree/rootfinding`.

[6] Mele, T.V., Block, P. (2014), *Algebraic graph statics*, Computer-Aided Design **53**, 104–116.

[7] Liew, A., Pagonakis, D., Van Mele, T., Block, P. (2018), *Load-path optimisation of funicular networks*, Meccanica **53**(1-2), 279–294.

[8] Landay, J., Myers, B., et al. (2001), *Sketching interfaces: Toward more human interface design*, Computer **34**(3), 56–64.

[9] Hsu, W., Liu, B. (2000), *Conceptual design: issues and challenges*, Computer-Aided Design **32**(14), 849–850.

[10] Wang, L., Shen, W., Xie, H., Neelamkavil, J., Pardasani, A. (2002), *Collaborative conceptual design—state of the art and future trends*, Computer-Aided Design **34**(13), 981–996.

[11] Akin, Ö. (2001), *Variants in design cognition*, in: *Design knowing and learning: Cognition in design education*, 105–124, Elsevier.

[12] Gero, J.S. (1994), *Computational models of creative design processes*, in: *Artificial intelligence and creativity*, 269–281, Springer.

[13] Luyten, L. (2012), *Structurally Informed Architectural Design*, Chalmers University of Technology.

[14] Schön, D.A. (1983), *The reflective practitioner: how professionals think in action* .

[15] Schlaich, M. (2006), *Challenges in Education–Conceptual and Structural Design*, in: *IABSE Symposium Report*, vol. 92, 20–26, International Association for Bridge and Structural Engineering.

[16] Ramm, E. (2011), *Baustatik I, Vorlesunsumdruck SS/SW 2005/2006*.

[17] Schlaich, J. (1996), *On the conceptual design of structures–an introduction*, in: *International symposium on'conceptual design of structures', Proceedings Volume 1. University of Stuttgart, October 7-11, 1996, Stuttgart, Germany*, 15–25.

[18] Holgate, A. (1997), *The art of structural engineering: the work of Jörg Schlaich and his team*, Edition Axel Menges.

[19] Salter, A., Gann, D. (2003), *Sources of ideas for innovation in engineering design*, Research Policy **32**(8), 1309–1324.

[20] Stromberg, L.L., Beghini, A., Baker, W.F., Paulino, G.H. (2012), *Topology optimization for braced frames: combining continuum and beam/column elements*, Engineering Structures **37**, 106–124.

[21] Balmond, C. (2002), *Informal*, Prestel London.

[22] Mueller, C.T. (2014), *Computational exploration of the structural design space*, Ph.D. thesis, Massachusetts Institute of Technology.

[23] Majowiecki, M. (2008), *The Free Form Design (FFD) in steel structural architecture–aesthetic values and reliability*, Steel Construction **1**(1), 3–15.

[24] WOODBURY, R.F., BURROW, A.L. (2006), *Whither design space?*, AI EDAM **20**(02).

[25] von Buelow, P. (2007), *Genetically Engineered Architecture*, in: *VDM*.

[26] Olsson, K.G. (2005), *Strukturmekanik & arkitektur Om strukturmekanisk förståelse i gestaltningsprocessen*, Chalmers University of Technology,.

[27] Rolvink, A., Coenders, J., Mueller, C. (2014), *State on the art of computational tools for conceptual structural design*, in: *Proceedings of the IASS-SLTE 2014 Symposium" Shells, Membranes and Spatial Structures: Footprints", Brasilia, Brazil, 15-19 September 2014*, International Association for Shell and Spatial Structures (IASS).

[28] Lindemann, J., Sandberg, G., Olsson, K.G. (2004), *An approach to teaching architectural and engineering students utilizing computational mechanics software ForcePAD*, ITcon **9**, 219–228.

[29] Lindemann, J., Dahlblom, O., Sandberg, G. (2001), *ObjectiveFrame-An educational tool for understanding the behaviour of structures*, in: *Applied Virtual Reality in Engineering & Construction Applicatins of Virtual Reality Current Initiatives and Future Challenges AVR II and CONVR*.

[30] Akesson, D., Lindemann, J. (2015), *A tablet computer application for conceptual design*, Proceedings of the ICE - Engineering and Computational Mechanics 1–8.

[31] *SAP2000*, `http://www.csiamerica.com/content/sap2000-24-model-alive-watch-learnl/`, online; accessed 2016-01-11.

[32] *Autodesk ForceEffect*, `https://forceeffect.autodesk.com/`, online; accessed 2016-01-11.

[33] Olsson, P. (2006), *Conceptual studies in structural design: pointSketch-a based approach for use in early stages of the architectural process*, Chalmers University of Technology.

[34] *Karamba*, `http://www.karamba3d.com/`, online; accessed 2015-10-05.

[35] *Kangaroo3d*, `http://www.kangaroo3d.com/`, online; accessed 2015-11-15.

[36] *Robot Structural Analysis*, `http://www.autodesk.com/products/robot-structural-analysis/overviewl`, online; accessed 2016-01-11.

[37] Sutherland, I.E. (1964), *Sketch pad a man-machine graphical communication system*, in: *Proceedings of the SHARE design automation workshop*, 6–329, ACM.

[38] Aish, R., Peters, B., Peters, T., *First Build Your Tools*, Inside Smartgeometry: Expanding the Architectural Possibilities of Computational Design 36–49.

[39] *Dynamo*, `http://www.autodesk.com/products/dynamo-studio/overview`, online; accessed 2016-01-11.

[40] Adriaenssens, S., Block, P., Veenendaal, D., Williams, C. (2014), *Shell structures for architecture: form finding and optimization*, Routledge.

[41] Coenders, J., Bosia, D. (2006), *Computational tools for design and engineering of complex geometrical structures: from a theoretical and a practical point of view.*, Rotterdam: Episode publishers.

[42] Veenendaal, D., Block, P. (2012), *An overview and comparison of structural form finding methods for general networks*, International Journal of Solids and Structures **49**(26), 3741–3753.

[43] Turrin, M., von Buelow, P., Stouffs, R. (2011), *Design explorations of performance driven geometry in architectural design using parametric modeling and genetic algorithms*, Advanced Engineering Informatics **25**(4), 656–675.

[44] Schanz, S., Otto, F., Rasch, B., Bayern, D.W., Stuck, K.V., anlässlich der Preisverleihung des Deutschen Werkbundes Bayern an Frei Otto und Bodo Rasch, A. (2006), *Frei Otto, Bodo Rasch: Finding form: towards on architecture of the minimal; the Werkbund shows Frei Otto, Frei Otto shows Bodo Rasch; exhibition in the Villa Stuck, Munich, on the occasion of the award of the 1992 Deutscher Werkbund Bayern Prize to Frei Otto und Bodo Rasch*, Ed. Menges.

[45] Ramm, E. (2011), *HEINZ ISLER SHELLS - THE PRIORITY OF FORM*, Journal of the International Association for Shell and Spatial Structures **52**(3), 143–154.

[46] Day, A. (1965), *An introduction to dynamic relaxation(Dynamic relaxation method for structural analysis, using computer to calculate internal forces following development from initially unloaded state)*, The engineer **219**, 218–221.

[47] Barnes, M. (1977), *Form-finding and analysis of tension space structures by dynamic relaxation.*, Ph.D. thesis, City University.

[48] Schek, H.J. (1974), *The force density method for form finding and computation of general networks*, Computer methods in applied mechanics and engineering **3**(1), 115–134.

[49] Haug, E., Powell, G. (1972), *Analytical shape finding for cable nets*, in: *Proceedings of the 1971 IASS Pacific Symposium Part II on Tension Structures and Space Frames*, 1–5.

[50] Argyris, J.H., Angelopoulos, T., Bichat, B. (1974), *A general method for the shape finding of lightweight tension structures*, Computer Methods in Applied Mechanics and Engineering **3**(1), 135–149.

[51] *CADenary tool v2*, `http://www.designexplorer.net/newscreens/cadenarytool/cadenarytool.html`, online; accessed 2016-01-11.

[52] *SmartForm*, `http://www.smart-solutions-network.com/page/introduction-to-smartform`, online; accessed 2015-11-15.

[53] *RhinoMembrane*, `http://www.ixforten.com/rhinomembrane.htm`, online; accessed 2015-11-15.

[54] *RhinoVault*, `http://block.arch.ethz.ch/brg/tools/rhinovault`, online; accessed 2016-01-11.

[55] Christensen, P.W., Klarbring, A. (2008), *An introduction to structural optimization*, vol. 153, Springer Science & Business Media.

[56] Bendsøe, M.P. (2001), *Topology optimization*, in: *Encyclopedia of Optimization*, 2636–2638, Springer.

[57] Bruggi, M. (2009), *Generating strut-and-tie patterns for reinforced concrete structures using topology optimization*, Computers & Structures **87**(23-24), 1483–1495.

[58] Biondini, F., Bontempi, F., Malerba, P.G. (2001), *Stress path adapting Strut-and-Tie models in cracked and uncracked R.C. elements*, Structural Engineering and Mechanics **12**(6), 685–698.

[59] Von Buelow, P. (2008), *Suitability of genetic based exploration in the creative design process*, Digital Creativity **19**(1), 51–61.

[60] Scott, S.D., Lesh, N., Klau, G.W. (2002), *Investigating human-computer optimization*, Proceedings of the SIGCHI conference on Human factors in computing systems Changing our world, changing ourselves - CHI '02 155.

[61] *structureFIT*, `http://www.caitlinmueller.com/structurefit/`, online; accessed 2016-01-11.

[62] Persson, P., Persson, K., Sandberg, G. (2014), *Reduction in ground vibrations by using shaped landscapes*, Soil Dynamics and Earthquake Engineering **60**, 31–43.

[63] Persson, P., Persson, K., Sandberg, G. (2016), *Numerical study on reducing building vibrations by foundation improvement*, Engineering Structures **124**, 361–375.

[64] Persson, P., Persson, K., Sandberg, G. (2016), *Numerical study of reduction in ground vibrations by using barriers*, Engineering Structures **115**, 18–27.

[65] Holzapfel, G.A. (2000), *Nonlinear solid mechanics*, vol. 24, Wiley Chichester.

[66] Bathe, K.J. (2006), *Finite element procedures*, Klaus-Jurgen Bathe.

[67] Craig, R., Kurdila, A. (2006), *Fundamentals of structural dynamics*, Wiley.

[68] Qu, Z. (2004), *Model order reduction techniques: with applications in finite element analysis*, Springer.

[69] Alic, V. (2012), *Good vibrations*, Master's thesis, Chalmers University of Technology.

[70] Lysmer, J., Kuhlemeyer, R.L. (1969), *Finite dynamic model for infinite media*, Journal of the Engineering Mechanics Division **95**(4), 859–878.

[71] Cottrell, J.A., Hughes, T.J., Bazilevs, Y. (2009), *Isogeometric analysis: toward integration of CAD and FEA*, John Wiley & Sons.

[72] Philipp, B., Breitenberger, M., Wüchner, R., Bletzinger, K.U. (2014), *Design of architectural membranes with isogeometric elements*, in: *11th World Congress on Computational Mechanics (WCCM XI)*.

[73] Miki, M., Igarashi, T., Block, P. (2015), *Parametric self-supporting surfaces via direct computation of airy stress functions*, ACM Transactions on Graphics (TOG) **34**(4), 89.

[74] Piegl, L. (1991), *On NURBS: a survey*, IEEE Computer Graphics and Applications (1), 55–71.

[75] Piegl, L., Tiller, W. (1997), *The NURBS book. 1997*, Monographs in Visual Communication .

[76] Rogers, D.F. (2000), *An introduction to NURBS: with historical perspective*, Elsevier.

[77] Cox, M.G. (1972), *The numerical evaluation of B-splines*, IMA Journal of Applied Mathematics **10**(2), 134–149.

[78] De Boor, C. (1972), *On calculating with B-splines*, Journal of Approximation Theory **6**(1), 50–62.

[79] Hughes, T.J., Cottrell, J.A., Bazilevs, Y. (2005), *Isogeometric analysis: CAD, finite elements, NURBS, exact geometry and mesh refinement*, Computer methods in applied mechanics and engineering **194**(39), 4135–4195.

[80] Cirak, F., Ortiz, M., Schroder, P. (2000), *Subdivision surfaces: a new paradigm for thin-shell finite-element analysis*, International Journal for Numerical Methods in Engineering **47**(12), 2039–2072.

[81] Celniker, G., Gossard, D. (1991), *Deformable curve and surface finite-elements for free-form shape design*, in: *ACM SIGGRAPH computer graphics*, vol. 25, 257–266, ACM.

[82] Terzopoulos, D., Qin, H. (1994), *Dynamic NURBS with geometric constraints for interactive sculpting*, ACM Transactions on Graphics (TOG) **13**(2), 103–136.

[83] Kagan, P., Fischer, A., Bar-Yoseph, P.Z. (2003), *Mechanically based models: Adaptive refinement for B-spline finite element*, International Journal for Numerical Methods in Engineering **57**(8), 1145–1175.

[84] Ottosen, N.S., Petersson, H., Saabye, N. (1992), *Introduction to the finite element method*, Prentice Hall Internationa,.

[85] Bazilevs, Y., Calo, V.M., Cottrell, J.A., Evans, J.A., Hughes, T., Lipton, S., Scott, M., Sederberg, T. (2010), *Isogeometric analysis using T-splines*, Computer Methods in Applied Mechanics and Engineering **199**(5), 229–263.

[86] Kim, H.J., Seo, Y.D., Youn, S.K. (2009), *Isogeometric analysis for trimmed CAD surfaces*, Computer Methods in Applied Mechanics and Engineering **198**(37), 2982–2995.

[87] Kiendl, J., Bletzinger, K.U., Linhard, J., Wüchner, R. (2009), *Isogeometric shell analysis with Kirchhoff–Love elements*, Computer Methods in Applied Mechanics and Engineering **198**(49), 3902–3914.

[88] Chapelle, D., Bathe, K.J. (2010), *The finite element analysis of shells-Fundamentals*, Springer Science & Business Media.

[89] Bischoff, M., Bletzinger, K.U., Wall, W., Ramm, E. (2004), *Models and Finite Elements for Thin-Walled Structures*, Encyclopedia of computational mechanics .

[90] Millán, D., Rosolen, A., Arroyo, M. (2011), *Thin shell analysis from scattered points with maximum-entropy approximants*, International Journal for Numerical Methods in Engineering **85**(6), 723–751.

[91] Barnes, M. (1988), *Form-finding and analysis of prestressed nets and membranes*, Computers & Structures **30**(3), 685–695.

[92] Papadrakakis, M. (1981), *A method for the automatic evaluation of the dynamic relaxation parameters*, Computer methods in applied mechanics and engineering **25**(1), 35–48.

[93] Underwood, P. (1983), *Dynamic relaxation(in structural transient analysis)*, Computational methods for transient analysis(A 84-29160 12-64). Amsterdam, North-Holland, 1983, 245–265.

[94] Joldes, G.R., Wittek, A., Miller, K. (2010), *Real-time nonlinear finite element computations on GPU–Application to neurosurgical simulation*, Computer methods in applied mechanics and engineering **199**(49), 3305–3314.

[95] Culmann, C. (1875), *Die graphische statik*, vol. 1, Meyer & Zeller.

[96] Stevin, S., *1586. De beghinselen der weeghconst*, The Principal Works of Simon Stevin **1**.

[97] Varignon, P. (1725), *Nouvelle Mecanique Ou Statique: Dont Le Projet Fut Donné En M. DC. LXXXVII*, vol. 2, Jombert.

[98] Kurrer, K.E. (2008), *The history of the theory of structures: from arch analysis to computational mechanics*, International Journal of Space Structures **23**(3), 193–197.

[99] Addis, W. (2007), *Building: 3000 years of design engineering and construction*, Phaidon New York.

[100] Poleni, G. (1748), *Memorie istoriche della gran cupola del tempio Vaticano e de'danni di essa e detristoramenti loro, divisi in libri 5*, Nella Stamperia del seminario.

[101] Mueller, C., Fivet, C., Ochsendorf, J. (2015), *Graphic Statics and Interactive Optimization for Engineering Education*, in: *Structures Congress 2015*, American Society of Civil Engineers.

[102] Allen, E., Zalewski, W. (2009), *Form and forces: designing efficient, expressive structures*, John Wiley & Sons.

[103] Bow, R.H. (2014), *Economics of construction in relation to framed structures*, Cambridge University Press.

[104] Crapo, H. (1979), *Structural Rigidity*, Structural Topology Vol.1 **1**, 26–45.

[105] Crapo, H., Whiteley, W. (1993), *Plane Self Stresses and projected Polyhedra I: The Basic Pattem*, Structural Topology 1993 núm 20 **20**, 55–78.

[106] Crapo, H., Whiteley, W. (1994), *Spaces of stresses, projections and parallel drawings for spherical polyhedra.*, Beitr. Algebra Geom. **35**, 259–281.

[107] Huffman, D. (1977), *A duality concept for the analysis of polyhedral scenes*, Machine Intelligence **8**, 475–492.

[108] Heyman, J. (1966), *The stone skeleton*, International Journal of solids and structures **2**(2), 249–279.

[109] O'Dwyer, D. (1999), *Funicular analysis of masonry vaults*, Computers & Structures **73**(1-5), 187–197.

[110] Block, P., Ochsendorf, J. (2007), *Thrust network analysis: A new methodology for three-dimensional equilibrium*, JOURNAL-INTERNATIONAL ASSOCIATION FOR SHELL AND SPATIAL STRUCTURES **155**, 167.

[111] Van Mele, T., Lachauer, L., Rippmann, M., Block, P. (2012), *Geometry-based understanding of structures*, Journal of the International Association of Shell and Spatial Structures **53**(4), 285–295.

[112] Block, P., Van Mele, T., Liew, A., DeJong, M., Escobedo, D., Ochsendorf, J., Van Mele, T., Méndez Echenagucia, T., Pigram, D., Liew, A., et al. (2018), *Structural design, fabrication and construction of the Armadillo Vault*, The Structural Engineer **96**, 10–20.

[113] Akbarzadeh, M., Van Mele, T., Block, P. (2015), *On the equilibrium of funicular polyhedral frames and convex polyhedral force diagrams*, CAD Computer Aided Design **63**, 118–128.

[114] Akbarzadeh, M., Van Mele, T., Block, P. (2016), *Three-dimensional graphic statics: Initial explorations with polyhedral form and force diagrams*, International Journal of Space Structures **31**(2-4), 217–226.

[115] McRobie, A. (2017), *The geometry of structural equilibrium*, Royal Society open science **4**(3), 160759.

[116] Lee, J., Mele, T.V., Block, P. (2018), *Disjointed force polyhedra*, Computer-Aided Design **99**, 11–28.

[117] Williams, C., McRobie, A. (2016), *Graphic statics using discontinuous Airy stress functions*, International Journal of Space Structures **31**(2-4), 121–134.

[118] McRobie, A., Konstantatou, M., Athanasopoulos, G., Hannigan, L. (2017), *Graphic kinematics, visual virtual work and elastographics*, Royal Society open science **4**(5), 170202.

[119] Lachauer, L., JUNGJOHANN, H., KOTNIK, T. (2011), *Interactive parametric tools for structural design*, in: *Proceedings of the International Association for Shell and Spatial Structures (IABSE-IASS) Symposium*.

[120] Pellegrino, S. (1993), *Structural computations with the singular value decomposition of the equilibrium matrix*, International Journal of Solids and Structures **30**(21), 3025–3035.

[121] Micheletti, A. (2008), *On Generalized Reciprocal Diagrams for Self-Stressed Frameworks*, International Journal of Space Structures **23**(3), 153–166.

[122] Bondy, J.A., Murty, U.S.R., et al. (1976), *Graph theory with applications*, vol. 290, Citeseer.

[123] Calladine, C. (1978), *Buckminster Fuller's "tensegrity" structures and Clerk Maxwell's rules for the construction of stiff frames*, International Journal of Solids and Structures **14**(2), 161–172.

[124] Pellegrino, S., Calladine, C.R. (1986), *Matrix analysis of statically and kinematically indeterminate frameworks*, International Journal of Solids and Structures **22**(4), 409–428.

[125] Ottosen, N.S., Ristinmaa, M. (2005), *The mechanics of constitutive modeling*, Elsevier.

[126] Alic, V., Åkesson, D., Persson, K. (2017), *Bi-directional Algebraic Graphic Statics: On Force Diagram Constraints*, in: *International Association for Shell and Spatial Structures IASS 2017*.

[127] Schlaich, J., Schafer, K., Jennewein, M. (1987), *Toward a Consistent Design of Structural Concrete*, PCI Journal **32**(3), 74–150.

[128] Kostic, N. (2009), *Topologie des champs de contraintes pour le dimensionnement des structures en beton arme* .

[129] Muttoni, A., Schwartz, J., Thürlimann, B. (1996), *Design of concrete structures with stress fields*, Springer Science & Business Media.

Part II

Appended publications

Paper A

Proceedings of the IASS-SLTE 2014 Symposium
"Shells, Membranes and Spatial Structures: Footprints"
15 to 19 September 2014, Brasilia, Brazil
Reyolando M.L.R.F. BRASIL and Ruy M.O. PAULETTI (eds.)

Form Finding for Ground Vibration Reduction in an Urban Scale

Vedad ALIC*,
Kent H. PERSSON[a]

*Division of Structural Mechanics, Lund University
Box 118, 221 00 Lund, Sweden
vedad.alic@construction.lth.se

[a] Division of Structural Mechanics, Lund University

Abstract

Form-finding is traditionally thought of in context of structures whose performance is dependent on their shape, such as grid-shells or cable nets, among others. This paper extends traditional form-finding by investigating the search of forms in an urban scale that are effective in reducing vibration propagation from external sources, such as highways, high-speed railroads and industrial plan. The aim is to lower their negative impact on the built environment. The scale of the urban forms can range from buildings, down to stones or concrete blocks, depending on site conditions (geometry, medium of propagating waves, targeted frequencies).

In this paper a state-of-the-art synchrotron facility, that is located both near a high-way and a city will serve as an example. The facility is located on clay which has resonant frequencies within the range that the facility is sensitive to. It is investigated if further urbanization of the area between the facility and the city can contribute in mitigating vibrations from the external sources, in order to ensure operational conditions for the facility. Forms are investigated numerically by placing out blocks of masses on top of the soil surface, in a tool developed for an iterative study. The vibration levels from external sources are evaluated, with the aim of finding optimal solutions in terms of vibration reduction and suitability as an urban plan.

Results indicate that masses on the ground can be used as a means to mitigate ground vibration, but in order for them to be effective they need to be very heavy. Locating masses in a careful manner can be effective for vibration mitigation, and by combining masses of different densities reduction in a wider frequency range can be reached. Some conclusions from the research were: Forms where masses are applied continuously over the whole area can lead to amplification due to lensing or acting as wave guides, however, all discrete organizations of masses show reductions in vibrations. Density variation for the different masses has greater effect than their position.

Keywords: Conceptual design, form finding, optimization, urban scale, vibration reduction, surface masses, soil dynamics.

1. Introduction

In the architectural design process, a given set of design requirements normally have to be fulfilled. In traditional architectural design the earlier phases of design, assessing the fulfillment of design requirements relies on the insight of the designer and focuses on a limited range of objectives (like functional and aesthetical). For other objectives (like engineering related aspects), the assessment is usually postponed to relatively advanced phases in the process, where a number of relevant aspects of the design may be unexplored, but already limited by decisions taken concerning other objectives. The opposite also holds, if only the engineering aspects are focused upon, functional and aesthetical design requirements may not be fulfilled.

Due to the nature of early stage design the amount of time is very limited. An engineering team cannot come up with a complete solution in this limited time, the focus should instead be on gaining an understanding of the overall behavior, catching interesting phenomena, and highlighting potential critical aspects of the design.

The lack of early stage, project-specific heuristic knowledge, such as experience, intuition, rules of thumb, and precedent examples that can be used as a base for new design needs to be compensated. The methods used should preferably require small investments of consultant time, in order to cope with the unpredictable and

Copyright © 2014 by the authors.
Published by the International Association for Shell and Spatial Structures (IASS) with permission.

rapidly changing nature of early stage design, excluding traditional time-consuming application of analysis techniques.

Modelling tools utilized in conceptual studies must be capable of interactively modifying the model once it has been created. This is a fundamental aspect in any design activity, where the designer is constantly going forward and backwards, re-elaborating over some particular aspect of the model, or its general layout, or even coming back to a previous solution that had been temporarily abandoned. Supporting an interactive and iterative design process, requires new interaction models and numerical approaches in the tools used.

This paper proposes a method/tool for the search of forms in an urban scale that are effective in reducing vibration propagation from external sources, such as highways, high-speed railroads and industrial plants, in that way lowering their negative impact on the built environment. The scale of the urban forms can range from buildings, down to stones or concrete blocks, depending on site conditions (geometry, medium of propagating waves, targeted frequencies), and in that way the method can be used in collaboration between Architect and Engineering disciplines (collaboration since both engineering and architecture related aspects are being decided upon simultaneously) in cases where vibration pollution in the built society is of concern, which with the continued increase in urban population will be a concern.

The tool is able to predict relative vibration levels at the positions of interest and trough an iterative study can lead to urban plans which are good at reducing soil wave propagation, and if care is taken with the design it can also enhance the aesthetic qualities of the site.

1.1. MAX-IV

To illustrate the method it is applied in a case study, at the site of MAX-IV, a new state-of-the-art synchrotron facility in Lund, Sweden. MAX-IV consists of an electron pre-accelerator, a 250 meter long linear accelerator, and two storage rings with 96 and 528 meters circumference respectively. The facility is located northeast of Lund, at the outskirt of a new area, Lund North-East roughly 100 meters southeast of the highway E-22. The instruments that are operating on nano-level scale at MAX-IV are sensitive to vibrations, where a vertical displacements limit of 20-30nm RMS during one second for frequencies above 5Hz and below 100Hz has been set in order to ensure good quality of the measurements. With the facility located closely to the highway and on top of very soft soil measures have been taken to ensure good operation of the facility. The measures include stabilization of the soil underneath the facility (stiffening), and the shaping of the ground topography around the facility in a way that will reduce vibrations, see for instance the study by Persson *et al* [8]. Other more conventional methods for vibration reduction have also been studied, such as open and in-filled trenches.

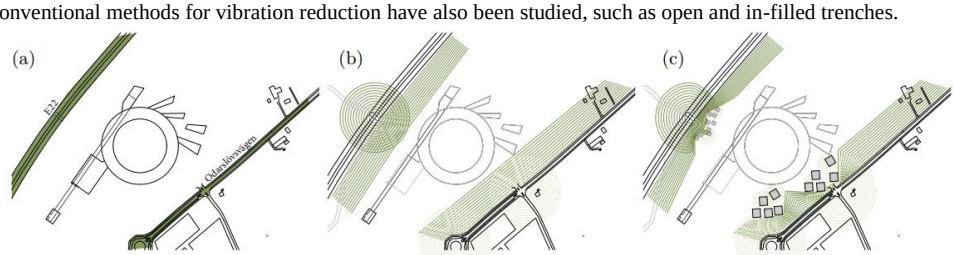


Figure 1: Research idea: (a) roads close to facility (b) vibrations from roads (c) reduced by masses?

Placing out heavy masses on the soil surface between the external sources and the facility, see Figure 1(c), could be seen as a cost effective and maintenance free solution, and as one that is more appropriate in an urban situation than more traditional methods such as trenches. As such, it is of interest to find out if it is a possible method of vibration mitigation, and which configurations are most effective.

Copyright © 2014 by the author(s).
Published by the International Association for Shell and Spatial Structures (IASS) with permission.

2. Heavy masses on the ground

Energy from traffic vibrations is usually concentrated in the frequency range of 5-50Hz, most of it is transmitted as Rayleigh waves close to the soil surface. The principle of operation for resonant mass scatterers (heavy masses on the ground) is based on the fact that any topographic irregularities on the surface cause scattering of incident Rayleigh waves, where some of the energy is reflected back, some is transmitted past the obstacle and some is scattered down into the soil. For masses on the ground the scattering is particularly strong around the natural frequencies of the masses resting on the ground, and as such they have been considered as a viable method of vibration mitigation both numerically, by Ford [2], Petyt and Jones [4], and theoretically by Krylov [5]. Petyt and Jones [4] consider an evaluation point 25 meters from the load, in between which they place different sets of heavy masses and come to the conclusion that in general a heavy mass close to the load works best for their situation. Krylov [5] shows in a 2D analytical model that only 10% of the incoming wave energy is transmitted past a lumped mass around its resonant frequency, the rest of it is either reflected back or propagated as body waves through the half-space medium. The solution should be taken as a very rough estimate as it does not take into account the mass moment of inertia, and models a mass - elastic half-space medium interaction. Recently, Mhanna *et al* [7] performed numerical studies, and verifications with full scale experiments, where they concluded that heavy masses on the ground can potentially lead to reductions of up to 70%. Even though the mentioned studies concerning the wave scattering properties of heavy masses on the ground have been done, the phenomena are not understood well enough to be accounted during design. Furthermore, soil in general, and at MAX-IV consists several sub-surface layers causing reflections and other phenomena which need to be accounted to the specific site. Previous parameter studies by Alic [1] investigated the effects of a heavy mass on the soil surface at the MAX-IV site. Figure 2 shows the geometry for the study.

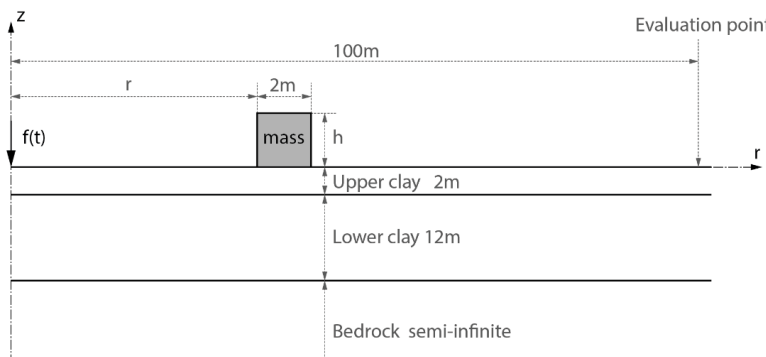


Figure 2: Axisymmetric model with a vertical unit load applied at rotation axis and masses on top of the surface, between the load and the evaluation point.

Figure 3 shows the general effect of a mass on the soil surface, part of the incoming surface wave is scattered down into the half-space which is seen as increased vertical displacements in Figure 3 (left) compared to Figure 3 (right). The scattering leads to smaller vertical displacements in the near-field behind the mass, however, as the bedrock has less damping than the soil, a secondary wave is observed close to the surface further away from the mass, at the far right in Figure 3 (left). This secondary wave was in this case of little concern due to the geometric attenuation of the surface wave.

The study concluded that the mass density showed largest reductions in vibration levels, and the position had some influence, while the height of the mass showed little influence as long as the density was modified to keep the same mass per surface area.

Figure 4 shows that a large reduction around the resonance frequencies can lead to slight amplifications for other frequencies, for example the response with the mass density $\rho = 16211 kg/m^3$ shows reductions around 10Hz compared to the reference model, but an increase around 13-14Hz. The unrealistically high densities can be achieved by using a taller mass with lower density, thereby getting the same mass per surface area. Heavier masses affect a lower frequency range.

Copyright © 2014 by the author(s).
Published by the International Association for Shell and Spatial Structures (IASS) with permission.

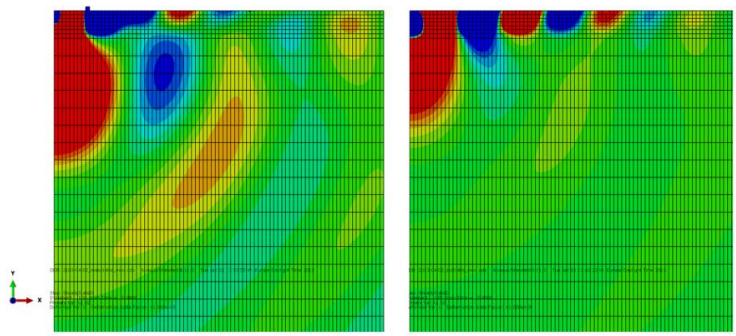


Figure 3: Vertical displacement amplitude of (left) soil model with mass $\rho = 8271 kg/m^3$ and (right) model with no mass, for a prescribed harmonic load with excitation frequency 14Hz and unit amplitude. Surface waves are reduced (left) due to the mass on top of the surface.

Masses with a density around from $\rho = 8271 kg/m^3$ were the most effective, as they showed large reductions in the range 13-15Hz, where the largest vertical displacements are in the reference model. With $\rho = 8271 kg/m^3$ a reduction of almost 30% is achieved, as seen in Figure 5 (left). In Figure 5 (right) amplification vs. mass distance from the load application point is shown. There is little change unless the mass gets close to the load, then negative effects (amplification) are observed, as the mass gets excited by the load.

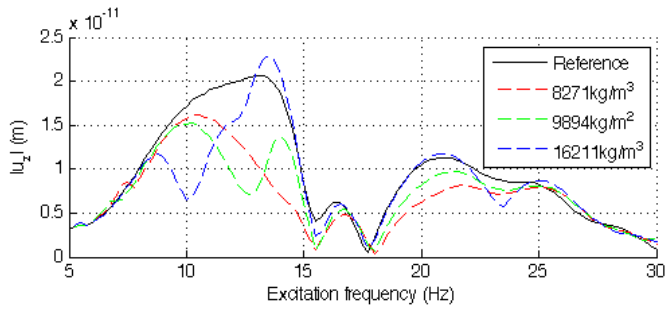


Figure 4: Vertical displacement magnitude response with 3 different densities.

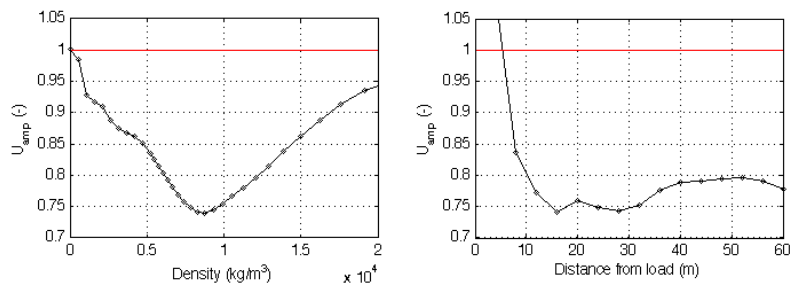


Figure 5: (left) Amplification vs. mass density, for a 2x2 meter mass. (right) Amplification vs. mass position in meters from the load application point, for a 2x2 meter mass with from $\rho = 8271 kg/m^3$.

Copyright © 2014 by the author(s).
Published by the International Association for Shell and Spatial Structures (IASS) with permission.

3. Form Finding Method

The work has been carried out using Finite Element Analysis (FEA) in two (axisymmetric), and three dimensions. Steady state models in the frequency range 5-30Hz have been established with main evaluation points along a line 100 meters from the load application point, which is about the distance from one of the roads to the facility. Unit loading was applied. Once an accurate model was set up masses were placed in between the load application point and the main evaluation points, see Figure 2. The results from the previous two-dimensional study were used to decide for the mass density range and possible mass positions on the soil surface. To aid in the form-finding of patterns a three-dimensional pattern exploration tool was developed, based on the findings from the two-dimensional studies and focused on finding effective and suitable urban patterns for the reduction of the vibration propagations.

3.1. Development of design tool for exploring different patterns

To get a sufficiently accurate model it is necessary to use small elements together with a large domain, leading to great computational costs, however, only a little part of the domain was of interest, namely the green parts on the soil surface in Figure 6. Because of this Guyan [3] reduction with frequency shift together with domain decomposition was applied and all degrees of freedom which were not part of the green parts were condensed away. The reduction method is exact at the angular frequency ω (apart from the approximation in the original dynamic matrices), performing the reduction for each frequency studied allowed for a reduced system with no loss of accuracy. The reduced system is no longer sparse and a large reduction in degrees of freedom is necessary in order for the method to be of benefit. In this case the model was reduced to 11 646 degrees of freedom, which allowed for simulations with a great number of configurations of masses, see Figure 8, where each pixel represents a mass with the size 2x2x2 m^3, and the gray-scale represents the density of each mass, where black is 8271kg/m^3 and white is no mass at all. Adjacent masses were assembled together to act as a larger geometric entity.

3.2. FE-model

The model used brick elements with quadratic approximation and reduced integration, and infinite elements along the boundary. In order for the 3D model to give accurate results for a steady state analysis in the frequency range of 5-30Hz, a fine mesh with 2x2x2m^3 elements for the soil (and 2x2x8.8m^3 for the bedrock) was necessary which resulted in about 2.6 million complex-number degrees of freedom, even though symmetry was used in the x-z plane to bring down the size of the model. The results were evaluated along the green line 100m away from the load application point, see Figure 6.

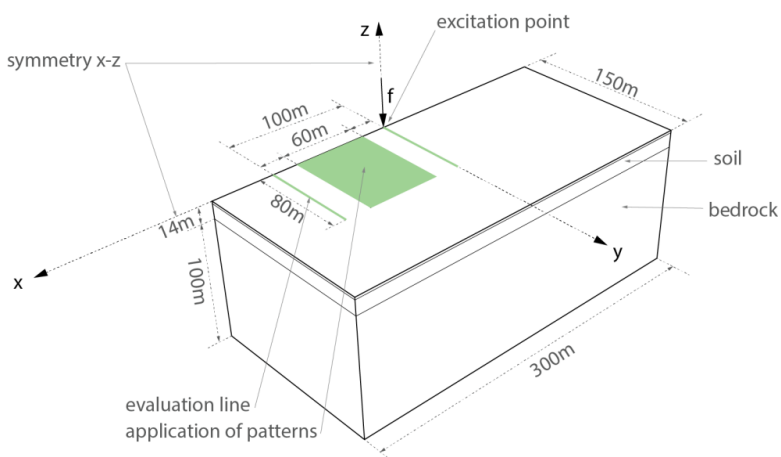


Figure 6: 3D model with the parts that were kept in the reduced model marked in green.

Copyright © 2014 by the author(s).
Published by the International Association for Shell and Spatial Structures (IASS) with permission.

3.3. Materials

Soil as a material is generally treated as highly non-linear and inhomogeneous, however, with the present low magnitude loading and large wavelengths in comparison to grain size it was possible to model the soil and bedrock using homogeneous linear elastic materials. Figure 7 lists the material properties of the upper and lower soil layers and of the bedrock layer. The loss factor includes all attenuation effects (e.g. varying topography of the soil and bedrock). The soil layers are considerably less stiff than the bedrock, and provide higher damping than the bedrock.

-	*Upper Clay*	*Lower Clay*	*Bedrock*
Depth (m)	2	12	-
E (MPa)	215	1136	8800
ν	0.48	0.48	0.4
ρ (Kg/m^3)	2125	2125	2600
Loss factor (%)	14	14	4
c_s (m/s)	185	425	1100
c_p (m/s)	943	2167	2694

Figure 7: Soil and bedrock properties

3.4. RMS evaluation

In order to simplify comparison the root mean square value (RMS) of the vertical displacement magnitudes is used

$$u_{RMS} = \frac{1}{n}\sqrt{(u_1^2 + u_2^2 + u_3^2 + \cdots + u_n^2)} \quad (1)$$

Where $u_i$is the vertical displacement magnitude at each angular frequency ω_i that is part of the steady state analysis, and u_{RMS} is the RMS value of u_i. This is further used to get the amplification as

$$U_{amp} = \frac{u_{RMS,tested}}{u_{RMS,reference}} \quad (2)$$

where $u_{RMS,tested}$ is the RMS value for a tested model with applied mass(es) on the soil surface, and $u_{RMS,reference}$ is for the reference model with no masses applied to it.

4. Results – Parameter study and effective/suitable patterns

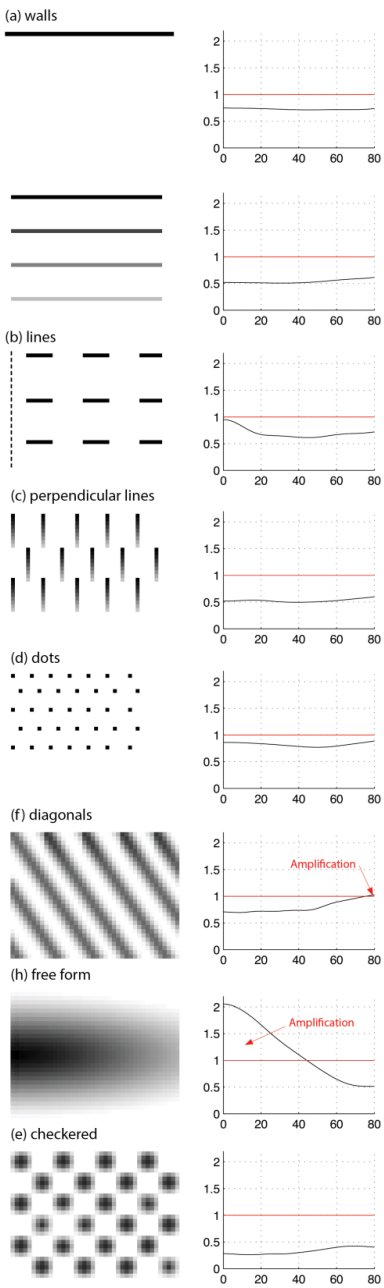
4.2. 3D – Tested patterns and results

As the previous 2D parameter studies showed that the mass density was the most important parameter it was the only one that was varied in the pattern studies. The design tool made it possible to digitally sketch different organizations of masses in any paint program, as the sketches were easily imported into the tool. With relatively quick feedback, 10-20 minutes compared to days for the large FE-Model, it was possible to try out many organizations and iteratively (a more interactive/real-time model would be preferred, but the method with current computing power does not allow it) find some patterns which worked better than others. Figure 8 shows some of the types of tested patterns and findings.

The tool made it possible to highlight critical aspects, like the shapes referred to as diagonals and free-form lenses in Figure 8, as well as openings in straight lines. It made it possible to study what type of density variation in terms of position was most effective.

The patterns in Figure 8 are oriented such that the x-axis points downward and y-axis points to the right. The amplification term, U_{amp}, was used to plot the results along a line 100m away from the load, see Figure 6.

Copyright © 2014 by the author(s).
Published by the International Association for Shell and Spatial Structures (IASS) with permission.



Wall like organizations were tried and showed similar reductions as the 2D analysis.

Models with variations in density showed greater vibration reduction than those that only involved a single density.

Lines with openings showed large reductions but showed less reduction at locations where there were no masses between the load and evaluation line.

Perpendicular lines with varying density showed good reduction.

Dotted patterns were too small and too far in-between to have any large effect on the vibration levels.

In cases where masses were connected in some direction, amplifications occurred at the point that the masses were pointing at.

It was found out that further amplifications could be gotten if the masses were organized n the form of a lens. However, the focusing effects were lost if the same patterns were made out of discrete masses (not shown).

Checkered patterns were very effective, and show some resemblance to the shaped landscape surrounding MAX-IV.

Figure 8: Examples of patterns used in 3D simulations applied on top of the green area in Figure 6, and the corresponding vibration levels in terms of U_{amp} evaluated along a line 100m from the load application point.

Copyright © 2014 by the author(s).
Published by the International Association for Shell and Spatial Structures (IASS) with permission.

5. Conclusions

Two-dimensional results indicate that masses on the ground can be used as a means to mitigate ground vibration, but in order for them to be effective they need to be very heavy. However, due to the nature of being effective around the mass-soil systems resonance frequency they can instead lead to larger vibrations in the soil, if they are excited at frequencies close to their resonant frequencies.

Different organizations of masses were assembled on top of the reduced ground model and steady state analysis was performed in the frequency range between 5-29Hz. Three-dimensional results show that locating masses in a careful manner can be effective for vibration mitigation, and by combining masses of different densities reduction in a wider frequency range can be reached. Some conclusions from the research were: Masses applied continuously over the whole area can lead to amplification due to lensing as seen in Figure 8 (h), or acting as wave guides, Figure 8 (f), however, all discrete masses show reductions in vibrations; Small masses applied with large spacing are ineffective, Figure 8 (d); Straight open paths from the load to the evaluation point lead to little reduction, Figure 8 (b); Density variation for the different masses has a larger effect on vibration reductions than their position.

5.1. Further development

In order for the tool to work in a productive environment the parameter study (2D) and creation of the 3D tool for the specific site (the assembly of the whole model, and the reduction method) could be automated so that the design team can spend time thinking about the urban planning and not the computational method.

References

[1] Alic, V., Vibration reduction in soil through the use of buildings at the synchrotron radiation facility MAX-IV. Master's Thesis, 2013.

[2] Ford. R., Inhibiting the transmission of ground-borne vibrations by placing masses on the surface of the ground. *Australian Vibration and Noise Conference 1990: Vibration and Noise measurement Prediction and Control;* Preprints of Papers. Institution of Engineers, Australia, 1990, p. 227.

[3] Guyan, R.J., Reduction of stiffness and mass matrices. *AIAA journal*, 1965; **3.2**; 380-380.

[4] Jones, D. and Petyt, M. Ground borne vibrations from passing trains: the effect of masses placed on the ground's surface. *ISVR Technical Memorandum*, 1986.

[5] Krylov, V. Control of traffic-induced ground vibrations by placing heavy masses on the ground surface, in *Low Frequency Noise, Vibration and Active Control*, 2007; **26(4)**; 311-320.

[6] Maxlab, 2013. *MAX-lab* [online] Available at:<https://www.maxlab.lu.se/> [Accessed March 2013]

[7] Mhanna, M., Shahrour, I., Sadek, M., and Dunez, P. Efficiency of heavy mass technology in traffic vibration reduction: Experimental and numerical investigation. *Computers and Geotechnics*, 2014; **55**; 141-149.

[8] Persson, P., Persson, K., & Sandberg, G., Reduction in ground vibrations by using shaped landscapes. *Soil Dynamics and Earthquake Engineering*, 2014; **60**; 31-43.

Copyright © 2014 by the author(s).
Published by the International Association for Shell and Spatial Structures (IASS) with permission.

Paper B

Available online at www.sciencedirect.com
ScienceDirect
Comput. Methods Appl. Mech. Engrg. 300 (2016) 734–747
Computer methods in applied mechanics and engineering
www.elsevier.com/locate/cma

Form finding with dynamic relaxation and isogeometric membrane elements

Vedad Alic*, Kent Persson

Division of Structural Mechanics, Lund Institute of Technology, Lund University, P.O. Box 118, SE-221 00 Lund, Sweden

Received 11 June 2015; received in revised form 4 December 2015; accepted 10 December 2015
Available online 17 December 2015

Abstract

A method for form finding with dynamic relaxation and Non-Uniform Rational B-Splines (NURBS) based isogeometric membrane elements has been implemented and studied regarding the influence of the discretization and element shape on the form finding. The procedure allows for rapid form finding since NURBS describe the curved geometry well and it is shown that the form-finding can be performed using a coarse mesh. However, to minimize the bending strain energy a fine mesh is needed. Using smaller elements is more advantageous than increasing the degree of the basis functions, keeping the number of integration points few and converging at a lesser number of iterations. Using isogeometric analysis (IGA) simplifies further studies since the form-found shape can be exactly represented with a shell element formulation. The method is suitable to be used in computer aided design environments such as Rhinoceros 3D during design stages, where the form finding can be evaluated together with other studies in a design context.
© 2015 Elsevier B.V. All rights reserved.

Keywords: Structural form finding; Dynamic relaxation; Isogeometric analysis; NURBS; Optimization

1. Introduction

1.1. Form finding

The load carrying capacity of shells and other form-active structures is provided by the shape of the structures, which for a certain load allows the shell to work in a membrane state, using the available material in an optimal way. When determining the shape of such a structure a form finding procedure is typically employed where the objective is to find a shape which minimizes bending, or more generally finds a shape which minimizes the strain energy in the structure [1].

Form finding methods are usually divided into two types. The first is related to pre-stressed structures, whose shapes are analogous to minimal surfaces. The second is the hanging chain and its inverse. As the chain cannot take any bending stresses the resultant shape will be in pure tension, which is generally a much more efficient use of

* Corresponding author.
E-mail address: vedad.alic@construction.lth.se (V. Alic).

http://dx.doi.org/10.1016/j.cma.2015.12.009
0045-7825/© 2015 Elsevier B.V. All rights reserved.

material than in bending. Inverting the shape creates an arch in pure compression. The method can be extended to membranes which are physically form-found using hanging cloths, which when inverted gives the shape of a vault in compression. Note that wrinkling of the surface may occur for a hanging model.

1.2. Numerical form finding

Several numerical methods for form finding exist, such as by use of dynamic relaxation [2], the force density method [3], or more recently by use of particle spring systems [4], or the updated reference strategy [5]. The methods were initially developed for the form finding of pre-stressed membrane structures. However, here the dynamic relaxation method will be used for the simulation of hanging cloths. All quantities in the method can be treated as vectors, leading to a low cost for each iteration and making it an efficient solution method [6] which is suitable for interactively exploring different designs in Computer Aided Design (CAD) software.

The hanging cloth may be simulated numerically by membrane finite elements with large displacements and a linear elastic material. By applying a form generating load, usually a uniformly distributed load, the initial geometry deforms into a shape which equilibrates the applied load. The resulting shape is optimal in the sense that forces are transferred mainly by membrane action.

The final shape achieved through form finding as a numerical process for simulating hanging cloth, depends on the initial geometry, the material properties (anisotropy, etc.), and the boundary condition. The relation between the initial and final shape is rather complex, requiring an iterative process of making changes to the initial geometry and evaluating the form-found shape until one which fulfills the specified design criteria is achieved [7]. Just as in the case of the physical hanging model, mesh dependent wrinkles may develop in the numerical model as well when membrane elements are used.

One drawback of many existing methods is that it is necessary to discretize the initial shape which often is described by Non-Uniform Rational B-Splines (NURBS), into structural elements in order to perform the form finding. During design stages this is sometimes unfavorable, since the discretized geometry is difficult to convert back to the initial geometry type. The design process may require many iterations of form finding, design evaluation and conversions between different geometry types before a desired shape is generated resulting in a time consuming process. The discretized geometry may be incompatible with available design software, making it hard to evaluate the form in the architectural context and to further detail it. By employing Isogeometric Analysis (IGA) the form finding and design evaluation can be integrated in design programs resulting in a simplified work flow where conversions between different geometry types are no longer necessary.

1.3. Isogeometric analysis

IGA [8] is an attempt at integrating CAD and Computer Aided Engineering (CAE) by using the same geometrical representation for both environments, typically NURBS, T-Splines or Subdivision Surfaces. Form finding with isogeometric membrane elements makes it possible to integrate the procedure in design software, and to avoid translations from one geometry type to another. NURBS based IGA is well suited since NURBS represent the smooth form found structures with very few control points, making them attractive numerically. A further advantage is that no re-meshing is required for the structural analysis as the form-found geometry can simply be reused with a shell element formulation.

The main part of this work relates to NURBS based IGA membrane elements. However, formulations of structural elements using IGA are plenty, and have been applied for shells [9–11], for beams and plates [12–14]. Recently isogeometric collocation techniques [15] have been used for beams and plates [16–18]. In [19] the Kirchhoff–Love shell model is discretized using polynomial splines over hierarchical T-meshes (PHT-splines). It shows superior performance per degree of freedom compared to cubic NURBS for the Scordelis-Lo roof, Hemispherical shell and Pinched cylinder with diaphragm. Although the method offers advantages in performance and a simple local refinement technique, it requires that the initial NURBS geometry must be able to be refined into bi-cubic NURBS with C^1 over knots in order for the PHT-splines refinement to be applicable, which somewhat limits their application to CAD programs. In [20] an extended isogeometric thin shell formulation based on Kirchhoff–Love theory is presented. Other spline approaches have been used for thin shells, such as those based on subdivision finite elements [21–23]. Subdivision surfaces provide an extension of NURBS to unstructured triangular or quadrilateral meshes [24].

1.4. Objective

Isogeometric analysis has been used together with the updated reference strategy for form finding [25], and isogeometric elements have been used together with dynamic relaxation for the steady-state solution of inflation of spherical shells and square airbags [26]. However, to the authors knowledge isogeometric elements have not been used with dynamic relaxation for form finding by simulation of hanging models. The objective of this paper is to investigate the use of large deformation isogeometric membrane elements with dynamic relaxation as a means of form finding. An overview of dynamic relaxation, isogeometric analysis and membrane kinematics is given in order to perform the investigation.

2. Dynamic relaxation

Dynamic relaxation was first suggested by Day [2] and further adopted to form finding of lightweight and large span structures by Barnes [27,28]. For a thorough discussion on dynamic relaxation see [29] and [30]. The method is suitable for parallelization and has shown good performance on graphics processing units (GPUs) [31]. The study will investigate dynamic relaxation with both critical damping and with kinetic damping. A description of both damping methods is also given.

2.1. Dynamic relaxation with critical damping

The dynamic relaxation method solves static problems by adding fictitious masses, fictitious damping and by using explicit time integration. The equation of motion (EOM) is given by

$$\boldsymbol{M}\ddot{\boldsymbol{u}} + \boldsymbol{C}\dot{\boldsymbol{u}} + \boldsymbol{f}^{\text{int}} = \boldsymbol{f} \tag{1}$$

where $\boldsymbol{f}^{\text{int}}$ is the column matrix of internal forces obtained from Eq. (24), $\boldsymbol{f}$ is the column matrix of external forces, $\boldsymbol{M}$ is the mass matrix, $\boldsymbol{C}$ is the damping matrix, and $\boldsymbol{u}$ contains the unknown displacements. Since only the static solution is of interest only $\boldsymbol{f}$ and $\boldsymbol{f}^{\text{int}}$ must represent the physical problem, all other parameters can be chosen freely. To obtain the motion in time the EOM is integrated using central differences giving a set of equations to update the velocities and displacements

$$\dot{\boldsymbol{u}}^{t_n+h/2} = \frac{(2-ch)}{(2+ch)}\dot{\boldsymbol{u}}^{t_n-h/2} + 2h\boldsymbol{M}^{-1}\frac{(\boldsymbol{f}-\boldsymbol{f}^{\text{int}})}{(2+ch)} \tag{2}$$

$$\boldsymbol{u}^{t_n+h} = \boldsymbol{u}^{t_n} + h\dot{\boldsymbol{u}}^{t_n+h/2} \tag{3}$$

where $\boldsymbol{M}$ must be diagonal to preserve the explicit form of the central difference integrator [30]. $\boldsymbol{C}$ has the form $\boldsymbol{C} = c\boldsymbol{M}$, where c is a damping coefficient for the structure, h is the time step. In the first iteration, $t = 0$ and $\boldsymbol{u}^0$ is given, then

$$\dot{\boldsymbol{u}}^{0+h/2} = h\boldsymbol{M}^{-1}(\boldsymbol{f}-\boldsymbol{f}^{\text{int}})/2. \tag{4}$$

To ensure numerical stability and optimal convergence rate the diagonal entries of $\boldsymbol{M}$ are chosen as suggested in [30] by

$$M_{ii} = \frac{1}{4}\hat{h}^2\sum_j |K_{ij}| \tag{5}$$

where $\hat{h} = 1.1h$ and the elements of the stiffness matrix K_{ij} are either computed by numerical differentiation of the internal force vector [30] or derived analytically. The damping coefficient c is set to critically damp the lowest eigenmode

$$c = 2\omega_{\text{min}} \tag{6}$$

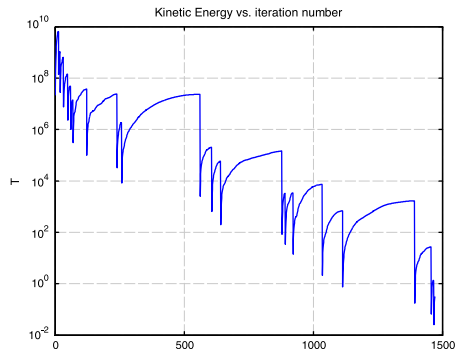


Fig. 1. Example of kinetic damping. The kinetic energy is reset each time a peak is detected.

which is estimated by use of Rayleigh's principle

$$\omega_{\min}^2 = \frac{\boldsymbol{u}^{\mathrm{T}}\boldsymbol{K}\boldsymbol{u}}{\boldsymbol{u}^{\mathrm{T}}\boldsymbol{M}\boldsymbol{u}}. \tag{7}$$

The dynamic relaxation process is stopped once the norm of the residual is smaller than $\|\boldsymbol{f} - \boldsymbol{f}^{\mathrm{int}}\|_2 < \epsilon_{\mathrm{err}}$, where $\| \bullet \|_2$ is the Euclidean norm. In this paper the error is set to $\epsilon_{\mathrm{err}} = \|\boldsymbol{f}\|_2/10^5$ for the benchmark studies.

2.2. Kinetic damping

An alternative to viscous damping is to use kinetic damping [27], where the total kinetic energy of the system is traced through the motion in time and once a peak is detected the current velocities are set to zero, see Fig. 1. The EOM for kinetic damping is

$$\boldsymbol{M}\ddot{\boldsymbol{u}} + \boldsymbol{f}^{\mathrm{int}} = \boldsymbol{f} \tag{8}$$

and the set of equations to update the velocities and displacements is simplified

$$\dot{\boldsymbol{u}}^{t_n+h/2} = \dot{\boldsymbol{u}}^{t_n-h/2} + h\boldsymbol{M}^{-1}(\boldsymbol{f} - \boldsymbol{f}^{\mathrm{int}}) \tag{9}$$

$$\boldsymbol{u}^{t_n+h} = \boldsymbol{u}^{t_n} + h\dot{\boldsymbol{u}}^{t_n+h/2}. \tag{10}$$

While kinetic damping typically requires more iterations to converge than the critically damped system, it is cheaper per iteration since it is not necessary to formulate $\boldsymbol{K}$ or update $\boldsymbol{M}$. On the other hand it requires a user selection of $\boldsymbol{M}$. In this paper two different choices of $\boldsymbol{M}$ have been tried, and are described in Section 4.1.

3. NURBS based isogeometric analysis

3.1. B-splines and NURBS

IGA was presented by Hughes et al. in an extensive report on NURBS based IGA [8]. NURBS are a further generalization of B-splines, non-interpolating, piecewise polynomial curves, but which unlike B-splines have the ability to represent any conical shape exactly.

Given a knot vector $\Xi = \{\xi_1, \xi_2, \ldots, \xi_{n+p+1}\}$, where $\xi_i \in \mathbb{R}$ is the ith knot (parametric coordinate), p is the polynomial order (or degree), and n is the number of basis functions. The B-spline basis functions are constructed recursively using the Cox–de Boor formula starting with piecewise constants (for $p = 0$)

$$N_{i,0}(\xi) = \begin{cases} 1 & \text{if } \xi_i \le \xi < \xi_{i+1} \\ 0 & \text{otherwise.} \end{cases} \tag{11}$$

For $p = 1, 2, 3, \ldots,$ recursively

$$N_{i,p}(\xi) = \frac{\xi - \xi_i}{\xi_{i+p} - \xi_i} N_{i,p-1}(\xi) + \frac{\xi_{i+p+1} - \xi}{\xi_{i+p+1} - \xi_i} N_{i+1,p-1}(\xi) \tag{12}$$

for which implementations can be found in [32]. A knot vector is open if its first and last knot values appear $p+1$ times. Basis functions are interpolatory at the ends of open knot vectors $\left[\xi_1, \xi_{n+p+1}\right]$ but are in general not interpolatory at interior knots, which distinguishes nodes in finite element analysis and control points in isogeometric analysis.

Using two one-dimensional B-spline basis functions $N_{i,p}(\xi)$, $M_{j,q}(\eta)$, from the knot vectors $\Xi = \left\{\xi_1, \xi_2, \ldots, \xi_{n+p+1}\right\}$ and $H = \left\{\eta_1, \eta_2, \ldots, \eta_{m+q+1}\right\}$, of orders p and q and a control point net $\boldsymbol{B}_{i,j}$ consisting of n x m points, a B-spline surface is constructed using the tensor product

$$\boldsymbol{S}(\xi, \eta) = \sum_{i=1}^{n} \sum_{j=1}^{m} N_{i,p}(\xi) M_{j,q}(\eta) \mathbf{B}_{i,j}. \tag{13}$$

A NURBS surface in $\mathbb{R}^3$ is constructed from the projection of a B-spline surface which is in $\mathbb{R}^4$. The NURBS surface is expressed using the tensor product

$$\boldsymbol{S}(\xi, \eta) = \frac{\sum_{i=1}^{n} \sum_{j=1}^{m} N_{i,p}(\xi) M_{j,q}(\eta) w_{i,j} \mathbf{B}_{i,j}}{\sum_{k=1}^{n} \sum_{l=1}^{m} N_{k,p}(\xi) M_{l,q}(\eta) w_{k,l}} \tag{14}$$

where the weights $w_{i,j}$ are stored as the fourth component in the control point net $\boldsymbol{B}_{i,j}(x_{i,j}, y_{i,j}, z_{i,j}, w_{i,j})$. Note that if all the weights are equal the NURBS surface reduces down to a B-spline surface. To get a notation which resembles finite element methodology closer the $i,\ j$ indices are, adhering to choices in [13], replaced by $A = n(j-1) + i$ leading to the bivariate NURBS basis

$$\tilde{N}_A(\xi, \eta) = \frac{N_{i,p}(\xi) M_{j,q}(\eta) w_{i,j}}{\sum_{k=1}^{n} \sum_{l=1}^{m} N_{k,p}(\xi) M_{l,q}(\eta) w_{k,l}} \tag{15}$$

and expressing the surface in Eq. (14) as

$$\boldsymbol{S} = \sum_{A=1}^{nm} \tilde{N}_A \mathbf{B}_A. \tag{16}$$

The tilde is henceforth dropped and the bivariate NURBS basis functions of order p and q are from now on simply referred to as N_A.

3.2. Refinement

The tensor product approach for creating NURBS surfaces or solids confines NURBS to structured meshes, deviation from the tensor product approach can be achieved using trimmed NURBS [33,34], or localized refinement (e.g. T-Splines [35–37]), none of which is considered in this paper. In [38] trimmed boundary representation (B-rep) CAD models are used for IGA and applied to Kirchhoff–Love shells. The approach seems promising and could be applied for form finding with complex initial geometries. However, there are many ways for enriching the NURBS basis without changing the geometry or its parametrization [8]. The mesh can be refined into smaller elements by insertion of new knots (h-refinement). Inserting a duplicate knot reduces the continuity for the bordering elements. Knot insertion thus allows both for control of element size and continuity. The degree of the basis can be increased through order elevation (p-refinement). During order elevation the multiplicity of each knot is raised by one, keeping the same continuity before and after the order elevation.

A third type of refinement (k-refinement) exists, where both the order and continuity are increased. This is done by first applying order elevation and afterwards inserting new knots. As previously stated the refinements do not change the geometry or parametrization.

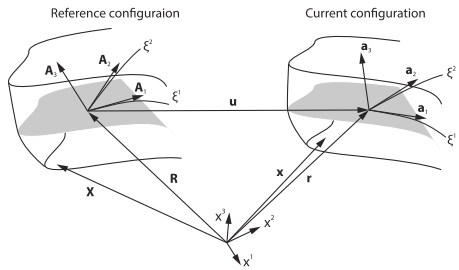


Fig. 2. Membrane kinematics.

3.3. NURBS based IGA membrane element

The dynamic relaxation method is here used with isogeometric membrane elements. If bending is neglected the form found shapes will be in equilibrium with the external loads using only membrane stresses. Hence the primary load carrying of the load applied for the form finding will be with membrane action only.

Membrane kinematics and virtual work. The membrane element is derived following standard procedure, assuming the membrane to be infinitely thin we get [39]

$$\boldsymbol{X} = \boldsymbol{R}, \qquad \boldsymbol{x} = \boldsymbol{r}, \qquad \boldsymbol{r} = \boldsymbol{R} + \boldsymbol{u} \tag{17}$$

where $\boldsymbol{X}$ is the position vector in a three dimensional body, $\boldsymbol{R}$ is the mid-surface vector, both in the reference configuration, and $\boldsymbol{x}, \boldsymbol{r}$ are the corresponding vectors in the current configuration, see Fig. 2. The displacement vector $\boldsymbol{u}$ relates the reference and current mid-surface vectors. The assumption results in that the Green–Lagrange strains $E_{\alpha\beta}$ are equal to the membrane strains $\epsilon_{\alpha\beta}$

$$E_{\alpha\beta} = \frac{1}{2}(a_{\alpha\beta} - A_{\alpha\beta}) = \epsilon_{\alpha\beta} \tag{18}$$

which are expressed in curvilinear coordinates where the Greek indices range from one to two and Latin from one to three throughout this article. Repeated follow the summation convention. $A_{\alpha\beta}$, and $a_{\alpha\beta}$ are the covariant components of first fundamental form of the surface in reference and current configurations. It is further implied that the transverse strains are zero

$$E_{3i} = E_{i3} = 0. \tag{19}$$

From the equations of virtual work [40] we get the part of the external forces as

$$\delta \Pi^{\text{ext}} = \int_{\Omega^0} t b^i \delta u_i d\Omega^0 \tag{20}$$

where t is the membrane thickness, b^i is the body load, δu_i are the virtual displacements and Ω^0 is the domain of the membrane mid surface in the reference configuration. The virtual work of the internal forces is expressed in terms of the stress resultant tensor and the membrane strains

$$\delta \Pi^{\text{int}} = -\int_{\Omega^0} \boldsymbol{n} : \delta\epsilon d\Omega^0 \tag{21}$$

where the stress resultant tensor using an isotropic linear elastic constitutive relation can be described as [21]

$$n^{\alpha\beta} = \frac{Et}{1-v^2} \tilde{C}_0^{\alpha\beta\gamma\delta} \epsilon_{\gamma\delta} \tag{22}$$

where

$$\tilde{C}_0^{\alpha\beta\gamma\delta} = \nu A^{\alpha\beta} A^{\gamma\delta} + \frac{1}{2}(1-\nu)(A^{\alpha\gamma} A^{\beta\delta} + A^{\alpha\delta} A^{\beta\gamma}) \tag{23}$$

in which E is Young's modulus and ν is Poisson's ratio.

For equilibrium we require that

$$\delta \Pi^{\text{ext}} + \delta \Pi^{\text{int}} = 0. \tag{24}$$

which in the paper is fulfilled using the dynamic relaxation method together with isogeometric membrane elements. A standard solution procedure by use of for instance Newton–Raphson iterations is difficult since stiffness matrices generated from membrane elements are not guaranteed to be invertible. The use of the dynamic relaxation method avoids this problem.

For further details see [9], where a Kirchhoff–Love shell element is formulated in NURBS based IGA. By neglecting the bending parts in that formulation one arrives at the equations given here.

Approximation. The approximation is performed using the isogeometric approach where the displacement field is approximated using the same basis functions as the geometry definition. Starting with the mid-surface

$$\boldsymbol{R}_h = \sum_{A=1}^{nm} N_A \mathbf{B}_A \tag{25}$$

where N_A is the Ath basis function associated with the Ath control point $\mathbf{B}_A$. The displacements are discretized using the same basis

$$\boldsymbol{u}_h = \sum_{A=1}^{nm} N_A \boldsymbol{u}_A \tag{26}$$

where $\boldsymbol{u}_A$ is the Ath displacement vector. The covariant basis vectors are found by differentiating the surface with respect to the curvilinear coordinates

$$\boldsymbol{A}_\alpha^h = R_{h,a} = \sum_{A=1}^{nm} N_{A,\alpha} \mathbf{B}_A \tag{27}$$

where $\bullet_{,\alpha}$ denotes differentiation with respect to the curvilinear coordinates, e.g.

$$N_{A,\alpha} = \frac{\partial N_A(\xi,\eta)}{\partial \xi^\alpha}, \quad \xi^1 = \xi,\ \xi^2 = \eta,\ \alpha = 1,2 \tag{28}$$

proceeding in a similar fashion we arrive at the membrane strains as well as the external and internal virtual work. In practice the local support of the NURBS basis is used and implementation is done on element level and necessary integrations are performed numerically.

4. Benchmarking and examples

4.1. Benchmark examples

In the benchmark studies isogeometric membrane elements are used together with the dynamic relaxation method for finding shapes which are in equilibrium with the external applied load, and as bending is omitted by definition the resulting shapes carry the loads using membrane action.

Three initial shapes are used for the benchmarks, one rectangular NURBS surface, and two triangular created by either placing two control points at the same location (collapsing edge), or by placing one control point in-line with each other (co-linear edges), see Fig. 3. K-refinement (by performing order elevation to a given degree p, and then inserting new knots with multiplicity one, getting C^{p-1} continuity) is applied and the number of iterations required to converge is studied with critical damping and with kinetic damping, see Fig. 4. The material properties are taken as $t = 0.05$ m, $E = 17$ GPa, $\nu = 0.3$, and a pressure load of $4.05 \cdot 10^7$ N/m^2 is applied to the initial configuration.

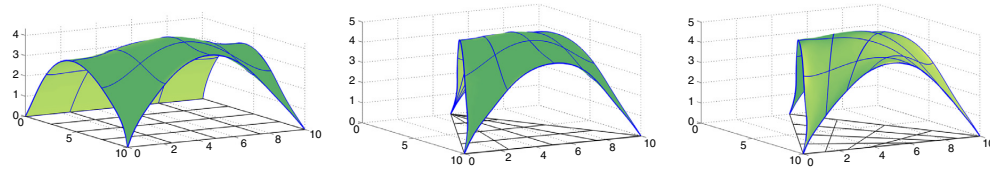


Fig. 3. Benchmarking examples, 4 elements per side with quintic basis and C^4 continuity, (left) rectangular shape, ten meters by ten meters (middle) triangular shape with collapsing edge (left) triangular shape with co-linear edges.

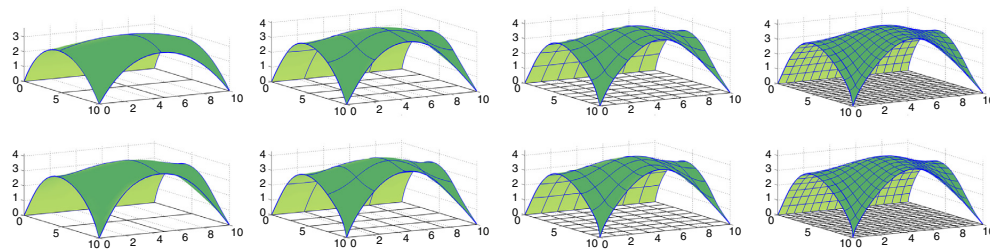


Fig. 4. Refinement, top shows quadratic basis ($p = q = 2$) and bottom shows quartic basis ($p = q = 4$), both with C^{p-1}. From left to right: 2×2 elements, 4×4 elements, 8×8 elements, 16×16 elements.

For the kinetic damping two different choices for the mass matrix have been applied. The first choice is by taking the mass matrix as $\mathbf{M} = \mathbf{I}\rho$, where $\mathbf{I}$ is the identity matrix (of right size) and ρ is either $2.1e9$ kg, $32 \cdot 2.1e9$ kg or $128 \cdot 2.1e9$ kg for the square, triangular (collapsed edge) and triangular (co-linear edges) respectively. The values were found through trial and error, being the smallest possible without causing any instability. The second choice of mass matrix for the kinetic damping was based on the initial stiffness matrix $\mathbf{K}_0$, where similarly to Eq. (5) we have

$$\tilde{M}_{ii} = \frac{1}{4}\hat{h}^2 \sum_j |K_{ij}| \tag{29}$$

where now K_{ij} are the elements of $\mathbf{K}_0$. The geometric stiffness was accounted for by summing the three degrees of freedom related to a control point and multiplying by four

$$M_{ii} = 4(\tilde{M}_{ii} + \tilde{M}_{ii+1} + \tilde{M}_{ii+2}); \quad M_{ii+1} = M_{ii};\ M_{ii+2} = M_{ii};\ i = 1, 4, 7, \ldots, n_{\text{dof}} - 2 \tag{30}$$

where n_{dof} is the number of degrees of freedom.

Since the membrane elements only provide in plane stiffness, Eq. (5) needs to be modified to avoid numerical issues due to diagonal entries being close to zero. In the paper any diagonal entry M_i which is smaller than $\max(\boldsymbol{M})/3$ is set to $\max(\boldsymbol{M})/3$.

The basis functions for the membrane elements need to be in the Hilbert space H^1, which is true for the rectangular shape, and the triangular shape created with the co-linear edges. This is, however, not the case for the triangular shape with control points that share the same physical coordinates (collapsed edge). This was remedied by taking the sum of the basis functions with a common control point [41].

4.2. Hausdorff distance

To determine the error in shape between different form found surfaces the Hausdorff distance is used [42]. The Hausdorff distance measures the maximum of the largest distance for any point on one surface to the closest point on a reference surface. The Hausdorff distance has to be calculated twice by letting each surface be the reference surface since the two distances are in general not equal. The Hausdorff distance $d_H(\boldsymbol{S}, \boldsymbol{S}')$ between two surfaces $\boldsymbol{S}$ and $\boldsymbol{S}'$ is

defined as

$$d_H(\boldsymbol{S}, \boldsymbol{S}') = \max \left\{ \max_{\boldsymbol{p}\in\boldsymbol{S}} \min_{\boldsymbol{p}'\in\boldsymbol{S}'} d(\boldsymbol{p}, \boldsymbol{p}'), \max_{\boldsymbol{p}'\in\boldsymbol{S}'} \min_{\boldsymbol{p}\in\boldsymbol{S}} d(\boldsymbol{p}, \boldsymbol{p}') \right\} \tag{31}$$

where $\boldsymbol{p}$ and $\boldsymbol{p}'$ are points on $\boldsymbol{S}$ and $\boldsymbol{S}'$, and $d(\boldsymbol{p}, \boldsymbol{p}') = \|\boldsymbol{p} - \boldsymbol{p}'\|_2$.

A mean distance d_m can be defined in a similar way

$$d_m(\boldsymbol{S}, \boldsymbol{S}') = \frac{1}{|\boldsymbol{S}|} \int_{p\in\boldsymbol{S}} \min_{p'\in\boldsymbol{S}'} \|\boldsymbol{p} - \boldsymbol{p}'\|_2 d\boldsymbol{S} \tag{32}$$

where $|\boldsymbol{S}|$ is the area of $\boldsymbol{S}$. The mean distance is not symmetric, i.e. $d_m(\boldsymbol{S}, \boldsymbol{S}') \neq d_m(\boldsymbol{S}', \boldsymbol{S})$. Whenever the mean distance is used $\boldsymbol{S}'$ represents the surface with the finest discretization (unless otherwise stated, i.e. p5h16, where p5 means that the degree is 5 and h16 means that there are 16 elements along one side of the geometry, that is 256 elements in total), and $\boldsymbol{S}$ being the surface that is compared.

4.3. Strain energy

The form finding procedure minimizes the bending part of the strain energy in the structure for the applied load. It is, however, not possible to reach zero bending strain energy since it depends on the discretization (and degree of the basis functions). The bending part of the strain energy is thus used as a metric to compare the results of the numerical studies. The strain energy is calculated as

$$U = \frac{1}{2} \boldsymbol{u}^T \boldsymbol{K} \boldsymbol{u} \tag{33}$$

where $\boldsymbol{u}$ is the displacement vector of the structure and the stiffness $\boldsymbol{K}$ is calculated using linear isogeometric Kirchhoff–Love elements [9]. The strain energy can be split into a bending U_b, and a membrane part U_m, where the bending part is calculated as [21]

$$U_b = \frac{1}{2} \int_\Omega \frac{Et^3}{12(1-\nu^2)} \kappa_{\alpha\beta} C_0^{\alpha\beta\gamma\delta} \kappa_{\gamma\delta} d\Omega \tag{34}$$

where $\kappa_{\alpha\beta}$ are the bending strains. The strain energy is calculated on a further refined structure by insertion of new knots. The refined models have 48×48 elements. The same load that was used for the form finding was applied to get the displacements of the refined discretization.

The strain energy was only calculated for triangular shape with co-linear edges since several basis functions for the triangular shape with the collapsed edge are not in H^2 [43].

4.4. Numerical studies

Rectangular initial shape. In Fig. 5 (Left column) the number of iterations required for the square shape to converge using either critical or kinetic damping is shown. For most cases the critically damped model converges on fewer iterations than the model with kinetic damping. For meshes with polynomial degree $p = 5$ there were convergence problems compared to the ones with lower degrees, and are excluded from Fig. 5. The bottom left subfigure (rectangular shape, constant mass) of Fig. 5 with $p = 5$ included is shown in Fig. 6. In Fig. 4 the results from models with quadratic and quartic basis functions, divided into 2, 4, 8, or 16 elements per side are shown. Visually it is only possible to notice differences between the most coarse meshes (to the left in the figures) and the ones with finer mesh.

In Fig. 7 (Left) the Hausdorff and mean distances from all the tested rectangular models to the finest rectangular model (p5h16) are shown. The coarsest model (p2h2) has a Hausdorff distance of over 1m, and is visually very different from the finer models, as shown in Fig. 4, top left image. The mean distances for all except the coarsest mesh (p2h2) are close to or less than 0.1m. In Fig. 8 (Left) the bending and strain energy for each model with the rectangular initial shape is shown. The bending part of the strain energy is small only for solutions with a fine mesh.

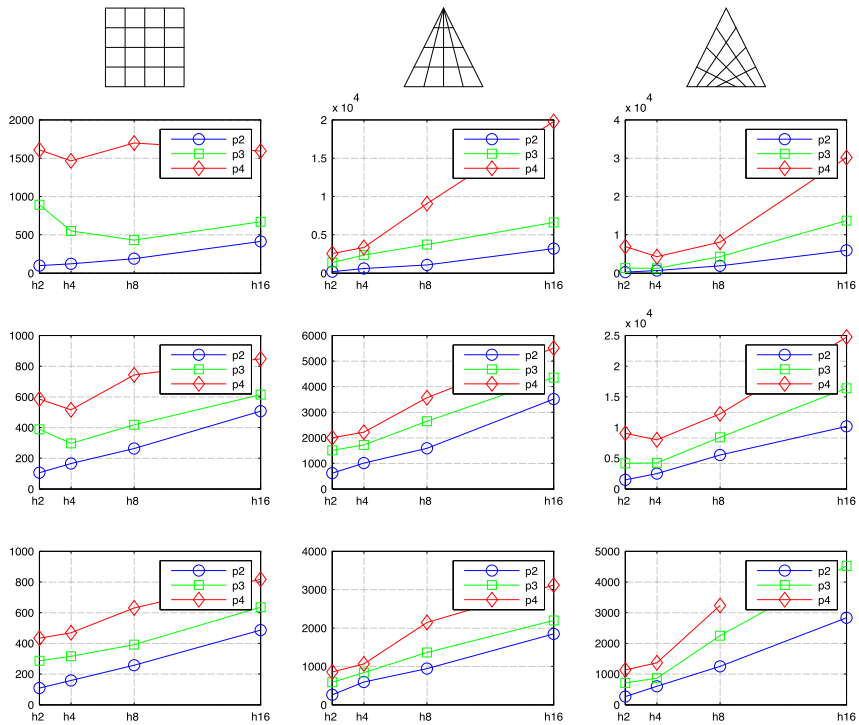


Fig. 5. Number of iterations to converge vs. number of elements per side. (Left column) Rectangular shape. (Middle column) Triangular shape with collapsed edge. (Right column) Triangular with co-linear edges. (Top to bottom) Critically damped, kinetic damping with constant mass matrix, kinetic damping with mass matrix from initial stiffness.

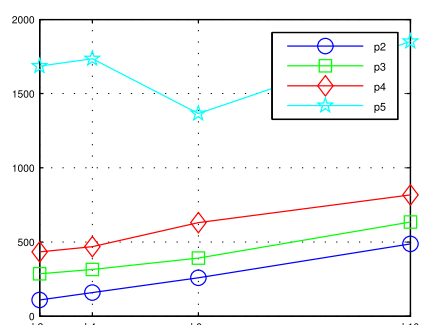


Fig. 6. Bottom left subplot of Fig. 5 with degree 5 mesh results included. The number of iterations required for convergence with degree 5 mesh is much larger.

Triangular initial shapes. Fig. 5 (Middle column) shows the number of iterations required for the initial form with collapsed edge to converge using critical or kinetic damping. Identical refinements have been applied as was made for the square shape. The model with quartic basis functions and 16 elements per side (p4h16) with kinetic damping and mass matrix from initial stiffness failed to converge, seen in the bottom right subfigure of Fig. 5. In Fig. 5 (Right column) the number of iterations to converge for the triangular shape with co-linear edges is found. Fig. 7 (Right)

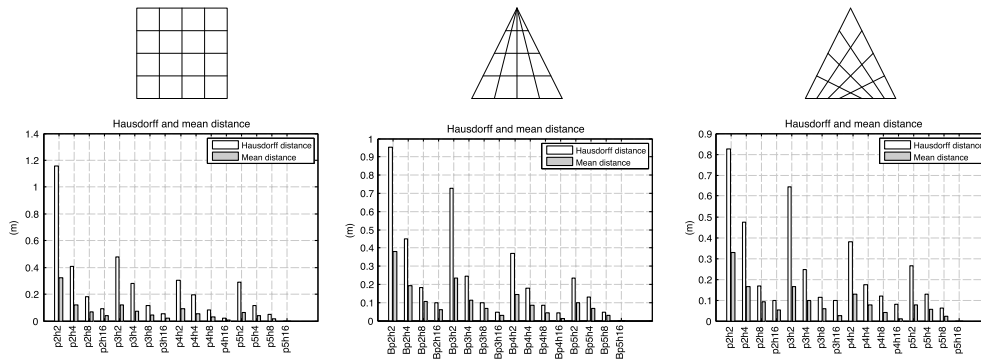


Fig. 7. Hausdorff and mean distances. (Left column) Rectangular shape. (Middle column) Triangular shape with collapsed edge. (Right column) Triangular with co-linear edges. All meshes are compared to the finest one (p5h24) with 24 × 24 elements and quintic basis.

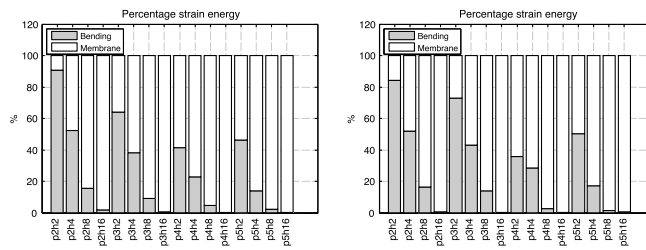


Fig. 8. Percentage of bending and membrane strain energy for (Left) Rectangular shape. (Right) Triangular with co-linear edges.

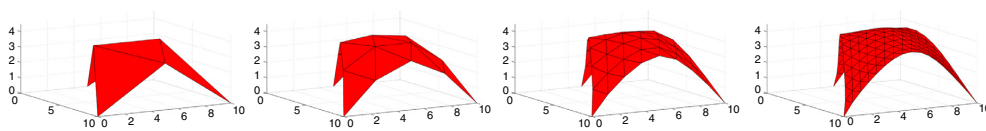


Fig. 9. Triangular shape with membrane finite elements, with 2, 4, 8, and 16 elements per side.

shows the Hausdorff and mean distances for the triangular shape (co-linear edges) compared to the finest model (p5h16). The Hausdorff distances are more than 0.5 m for some coarse discretizations. The mean distance is below 0.2 m for all except (p2h2). Fig. 8 (Right) shows the bending and strain energy for each model with the triangular (co-linear edges) initial shape. This is in agreement with the rectangular shape. The bending part of the strain energy is small only for solutions with many elements.

Fig. 7 (Middle) shows the Hausdorff and mean distances for the triangular shape (collapsed edges).

In order to compare the performance of the dynamic relaxation method with isogeometric elements, the form-finding was also performed on the triangular shape with triangular membrane finite elements [44]. The Hausdorff distance for the solutions with FE was calculated with the finest triangular IGA shape (p5h16) as reference. Discretizations of 2, 4, 8, 16, 32 and 64 elements per side were studied, see Fig. 9. The mean distance falls below 0.2 m only for discretizations with 32 side elements or more, see Fig. 11.

The number of iterations to converge for triangular shape with finite elements is shown in Fig. 10.

5. Conclusions and further work

The rectangular shape IGA elements with quadratic basis functions converge at about the same number of iterations to converge as the triangular shape with triangular finite elements. The number of iterations to converge is much larger

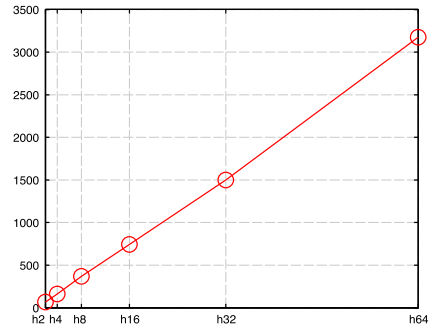


Fig. 10. Number of iterations required for the triangular membrane finite elements to converge using kinetic damping.

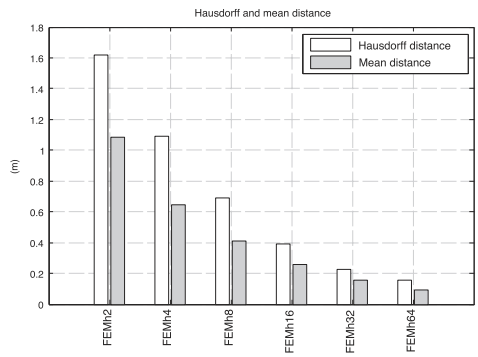


Fig. 11. Hausdorff and mean distance for the FEM triangular shape using 2, 4, 8, 16, 32, and 64 elements per side. All are compared to the finest isogeometric triangular shape with co-linear edges (p5h16) with 16×16 elements and quintic basis.

for the triangular shapes with isogeometric elements, where the mesh in the physical space no longer has a uniform size, the effect is greatest for the triangular discretizations with co-linear edges where the elements are the smallest. By applying some type of local refinement, e.g. T-Splines or trimmed NURBS, it would be possible to generate meshes of more uniform size for triangular, and other kinds of shapes.

Increasing the degree of the basis functions requires a larger number of iterations to converge. Since the numerical quadrature requires more integration points for a higher degree of the basis it requires longer computational time per iteration. Most of the time in the dynamic relaxation loop is spent evaluating stresses at integration points and as such it is good to keep the degree of the basis low. Increasing the degree of the basis to quintic leads to convergence difficulties.

The distance measures where the mean distance was below 0.2 m for all discretizations except the coarsest, which indicates that exploiting higher order NURBS basis functions allows for form-finding with very few elements, making the method attractive for form finding in the design stages. In such situations a coarse mesh can be used for design experiments and, then later can be refined to determine a form-found shape that is more optimal in terms of strain energy. Using the regular finite elements for design experiments would require a finer mesh, Fig. 7 shows that it is not until 32 by 32 finite elements are used that the mean distance falls below 0.2 m.

The use of NURBS based isogeometric elements simplifies verification studies, since it is straightforward to further discretize the form found shape into smaller elements and to evaluate the structure using IGA Kirchhoff–Love shells to check for a near membrane state of stress.

The use of membrane elements for form finding can lead to wrinkling of the surfaces when fine meshes are used due to compressive stresses and a lack of bending stiffness. Some of the benchmarking geometries used in the paper

show wrinkling for fine meshes of 64×64 elements or finer. This has not been further studied in the paper, since the problem is not specifically related to the use of isogeometric elements.

Mass matrix selection for dynamic relaxation with kinetic damping should be investigated further. In this study it was set through trial and error and selected in a way which allowed for the finest mesh to converge. For the coarser meshes smaller values in the mass matrix may result in fewer iterations for the procedure to converge. It is possible to use a critically damped structure as described here, but it is much more costly per iteration since it requires the evaluation of a tangent stiffness matrix, which in a sense loses the advantages of the explicit method, both in terms of efficiency and simplicity. A promising approach is to use kinetic damping and update the mass matrix after a stability criteria [30], or after every n iterations based on the tangent stiffness. It removed convergence difficulties seen in the bottom right subfigure of Fig. 5, where the mass matrix was updated every 100th iteration.

Further, the integration of CAE into CAD allows for continuous evaluation of the form found structures within a design context. It is possible to keep working with the geometry after the form finding and adding architectural details and to use the models for other types of studies, such as, daylight, energy, and evaluation within an architectural context, and to use the model for rendering/visualization. The integration also allows for the initial shapes to be much easier to model and modify in CAD than in most CAE software.

Acknowledgment

This work was supported by the Swedish strategic research programme eSSENCE. The support is gratefully acknowledged.

References

[1] K.-U. Bletzinger, R. Wüchner, F. Daoud, N. Camprubí, Computational methods for form finding and optimization of shells and membranes, Comput. Methods Appl. Mech. Engrg. 194 (30) (2005) 3438–3452.
[2] A. Day, An introduction to dynamic relaxation (dynamic relaxation method for structural analysis, using computer to calculate internal forces following development from initially unloaded state), Engineer 219 (1965) 218–221.
[3] H.-J. Schek, The force density method for form finding and computation of general networks, Comput. Methods Appl. Mech. Engrg. 3 (1) (1974) 115–134.
[4] A. Kilian, J. Ochsendorf, Particle-spring systems for structural form finding, J. Int. Assoc. Shell Spat. Struct. 148 (2005) 77.
[5] K.-U. Bletzinger, E. Ramm, A general finite element approach to the form finding of tensile structures by the updated reference strategy, Int. J. Space Struct. 14 (2) (1999) 131–145.
[6] G.R. Joldes, A. Wittek, K. Miller, An adaptive dynamic relaxation method for solving nonlinear finite element problems. application to brain shift estimation, Int. J. Numer. Methods Biomed. Eng. 27 (2) (2011) 173–185.
[7] E. Ramm, Shape finding of concrete shell roofs, J. Int. Assoc. Shell Spat. Struct. 45 (1) (2004) 29–39.
[8] T.J. Hughes, J.A. Cottrell, Y. Bazilevs, Isogeometric analysis: CAD, finite elements, NURBS, exact geometry and mesh refinement, Comput. Methods Appl. Mech. Engrg. 194 (39) (2005) 4135–4195.
[9] J. Kiendl, K.-U. Bletzinger, J. Linhard, R. Wüchner, Isogeometric shell analysis with Kirchhoff–Love elements, Comput. Methods Appl. Mech. Engrg. 198 (49) (2009) 3902–3914.
[10] J. Kiendl, Y. Bazilevs, M.-C. Hsu, R. Wüchner, K.-U. Bletzinger, The bending strip method for isogeometric analysis of Kirchhoff–Love shell structures comprised of multiple patches, Comput. Methods Appl. Mech. Engrg. 199 (37) (2010) 2403–2416.
[11] D. Benson, Y. Bazilevs, M.-C. Hsu, T. Hughes, A large deformation, rotation-free, isogeometric shell, Comput. Methods Appl. Mech. Engrg. 200 (13) (2011) 1367–1378.
[12] J. Cottrell, A. Reali, Y. Bazilevs, T. Hughes, Isogeometric analysis of structural vibrations, Comput. Methods Appl. Mech. Engrg. 195 (41) (2006) 5257–5296.
[13] J.A. Cottrell, T.J. Hughes, Y. Bazilevs, Isogeometric Analysis: Toward Integration of CAD and FEA, John Wiley & Sons, 2009.
[14] C.H. Thai, H. Nguyen-Xuan, N. Nguyen-Thanh, T.-H. Le, T. Nguyen-Thoi, T. Rabczuk, Static, free vibration, and buckling analysis of laminated composite Reissner–Mindlin plates using NURBS-based isogeometric approach, Internat. J. Numer. Methods Engrg. 91 (6) (2012) 571–603.
[15] F. Auricchio, L.B. Da Veiga, T. Hughes, A. Reali, G. Sangalli, Isogeometric collocation methods, Mathe. Models Methods Appl. Sci. 20 (11) (2010) 2075–2107.
[16] A. Reali, H. Gomez, An isogeometric collocation approach for Bernoulli–Euler beams and Kirchhoff plates, Comput. Methods Appl. Mech. Engrg. 284 (2015) 623–636.
[17] J. Kiendl, F. Auricchio, L.B. da Veiga, C. Lovadina, A. Reali, Isogeometric collocation methods for the Reissner–Mindlin plate problem, Comput. Methods Appl. Mech. Engrg. 284 (2015) 489–507.
[18] L.B. da Veiga, C. Lovadina, A. Reali, Avoiding shear locking for the Timoshenko beam problem via isogeometric collocation methods, Comput. Methods Appl. Mech. Engrg. 241 (2012) 38–51.
[19] N. Nguyen-Thanh, J. Kiendl, H. Nguyen-Xuan, R. Wüchner, K. Bletzinger, Y. Bazilevs, T. Rabczuk, Rotation free isogeometric thin shell analysis using pht-splines, Comput. Methods Appl. Mech. Engrg. 200 (47) (2011) 3410–3424.

[20] N. Nguyen-Thanh, N. Valizadeh, M. Nguyen, H. Nguyen-Xuan, X. Zhuang, P. Areias, G. Zi, Y. Bazilevs, L. De Lorenzis, T. Rabczuk, An extended isogeometric thin shell analysis based on Kirchhoff–Love theory, Comput. Methods Appl. Mech. Engrg. 284 (2015) 265–291.
[21] F. Cirak, M. Ortiz, P. Schroder, Subdivision surfaces: a new paradigm for thin-shell finite-element analysis, Internat. J. Numer. Methods Engrg. 47 (12) (2000) 2039–2072.
[22] F. Cirak, M. Ortiz, Fully c1-conforming subdivision elements for finite deformation thin-shell analysis, Internat. J. Numer. Methods Engrg. 51 (7) (2001) 813–833.
[23] F. Cirak, M.J. Scott, E.K. Antonsson, M. Ortiz, P. Schröder, Integrated modeling, finite-element analysis, and engineering design for thin-shell structures using subdivision, Comput.-Aided Des. 34 (2) (2002) 137–148.
[24] F. Cirak, Q. Long, Advances in Subdivision Finite Elements for Thin Shells, Springer, 2010.
[25] B. Philipp, M. Breitenberger, R. Wuchner, K.-U. Bletzinger, Design of architectural membranes with isogeometric elements, in: 11th World Congress on Computational Mechanics, WCCM XI, 2014.
[26] L. Chen, N. Nguyen-Thanh, H. Nguyen-Xuan, T. Rabczuk, S.P.A. Bordas, G. Limbert, Explicit finite deformation analysis of isogeometric membranes, Comput. Methods Appl. Mech. Engrg. 277 (2014) 104–130.
[27] M. Barnes, Form-finding and analysis of prestressed nets and membranes, Comput. Struct. 30 (3) (1988) 685–695.
[28] M. Barnes, Form-finding and analysis of tension space structures by dynamic relaxation (Ph.D. thesis), City University, 1977.
[29] M. Papadrakakis, A method for the automatic evaluation of the dynamic relaxation parameters, Comput. Methods Appl. Mech. Engrg. 25 (1) (1981) 35–48.
[30] P. Underwood, Dynamic relaxation (in structural transient analysis), in: Computational Methods for Transient Analysis (A 84-29160 12-64), North-Holland, Amsterdam, 1983, pp. 245–265.
[31] G.R. Joldes, A. Wittek, K. Miller, Real-time nonlinear finite element computations on GPU–application to neurosurgical simulation, Comput. Methods Appl. Mech. Engrg. 199 (49) (2010) 3305–3314.
[32] L. Piegl, W. Tiller, The NURBS Book, in: Monographs in Visual Communication, 1997.
[33] H.-J. Kim, Y.-D. Seo, S.-K. Youn, Isogeometric analysis for trimmed CAD surfaces, Comput. Methods Appl. Mech. Engrg. 198 (37) (2009) 2982–2995.
[34] R. Schmidt, R. Wüchner, K.-U. Bletzinger, Isogeometric analysis of trimmed NURBS geometries, Comput. Methods Appl. Mech. Engrg. 241 (2012) 93–111.
[35] Y. Bazilevs, V.M. Calo, J.A. Cottrell, J.A. Evans, T. Hughes, S. Lipton, M. Scott, T. Sederberg, Isogeometric analysis using t-splines, Comput. Methods Appl. Mech. Engrg. 199 (5) (2010) 229–263.
[36] M.A. Scott, M.J. Borden, C.V. Verhoosel, T.W. Sederberg, T.J. Hughes, Isogeometric finite element data structures based on Bézier extraction of t-splines, Internat. J. Numer. Methods Engrg. 88 (2) (2011) 126–156.
[37] M.R. Dörfel, B. Jüttler, B. Simeon, Adaptive isogeometric analysis by local h-refinement with t-splines, Comput. Methods Appl. Mech. Engrg. 199 (5) (2010) 264–275.
[38] M. Breitenberger, A. Apostolatos, B. Philipp, R. Wüchner, K.-U. Bletzinger, Analysis in computer aided design: Nonlinear isogeometric b-rep analysis of shell structures, Comput. Methods Appl. Mech. Engrg. 284 (2015) 401–457.
[39] M. Bischoff, K.-U. Bletzinger, W. Wall, E. Ramm, Models and finite elements for thin-walled structures, Encyclopedia Comput. Mech. (2004).
[40] K.-J. Bathe, Finite Element Procedures, Klaus-Jurgen Bathe, 2006.
[41] T. Takacs, B. Jüttler, Existence of stiffness matrix integrals for singularly parameterized domains in isogeometric analysis, Comput. Methods Appl. Mech. Engrg. 200 (49) (2011) 3568–3582.
[42] N. Aspert, D. Santa Cruz, T. Ebrahimi, Mesh: measuring errors between surfaces using the Hausdorff distance, in: ICME, vol. 1, 2002, pp. 705–708.
[43] T. Takacs, B. Jüttler, H2 regularity properties of singular parameterizations in isogeometric analysis, Graph. Models 74 (6) (2012) 361–372.
[44] B. Tabarrok, Z. Qin, Nonlinear analysis of tension structures, Comput. Struct. 45 (5) (1992) 973–984.

Paper C

Proceedings of the International Association for Shell and Spatial Structures (IASS)
Symposium 2015, Amsterdam
Future Visions
17 - 20 August 2015, Amsterdam, The Netherlands

Using isogoemetric elements and dynamic relaxation as a form finding technique

Vedad ALIC*, Kent PERSSON[a]

*Division of Structural Mechanics
Faculty of Engineering, Lund University
P.O. Box 118, SE-221 00 Lund, Sweden
vedad.acli@construction.lth.se

[a]Division of Structural Mechanics, Lund University

Abstract

In this paper, the use of NURBS based isogeometric analysis for form finding and further design of form found structures is presented. The form finding is performed with non-linear isogoemetric membrane elements together with dynamic relaxation [1]. The method has previously been tested on simple geometries in a computational environment, and is here further integrated in a Computer Aided Design program, Rhinoceros 3D where the method is evaluated for complex geometries in a design scenario. The form found shape is further studied and it is shown how the membrane and bending utilization can be plotted on the shape by making refinements to the mesh without affecting the geometry. Finally the form finding is employed on some complex geometries to show the possibilities of using coarse NURBS meshes for form finding.

Keywords: Form finding, isogeometric analysis, dynamic relaxation, design tool, NURBS, CAD.

1. Introduction

The load carrying capacity of shells and other form-active structures is provided by the shape of the structures. In order to find an efficient form of such structures several methods exist such as, dynamic relaxation [2], the force density method [11], or more recent ones such as thrust network analysis [4] and particle spring systems [7]. One drawback of many existing methods is that it is necessary to discretize the initial geometry into structural elements in order to perform the form finding. During design stages this is sometimes unfavourable, because after the discretization it is difficult to convert back to the initial geometry type, and the design process may require many iterations of form finding and evaluation (going between different geometry types) before a desired shape is generated. By employing isogeometric analysis using Non-Uniform Rational B-Splines (NURBS) the conversion between geometry types can be avoided and an integration of design and analysis can be achieved, where all computations are performed using the design geometry, or at the very least an analysis

model which is automatically created from the design geometry. A further advantage of form finding with isogeometric membrane elements is that no re-meshing is required for the structural analysis as the form found geometry can simply be reused with a shell element formulation for the subsequent analyses.

The paper describes a design process where isogeometric membrane elements with dynamic relaxation is used as a form finding method for shapes with minimal bending. Some advantages and drawbacks of the method are discussed. To test the integration of design and analysis the method is implemented in a Rhinoceros 5 plug-in.

2. Form finding with dynamic relaxation

A form finding process with isogeometric membrane elements has been implemented. It has been previously shown that the form finding can be performed with few elements [1], and makes the method suitable for design exploration. However, for the form finding to result in a good shape in terms of mechanical performance a discretization with smaller elements needs to be used. To find the static equilibrium of the membrane elements and the applied load dynamic relaxation is used [5]. The dynamic relaxation method solves static problems by simulating a dynamic problem with fictitious masses and fictitious damping. An advantage of the dynamic relaxation method is that it is an explicit method where only the internal forces need to be computed, there is no need to calculate the stiffness matrix, thus it is a vectorised method which is efficient and well suited for parallelization. For more information on the dynamic relaxation implementation with isogeometric membrane elements see [1], where different choices of mass matrix and damping were tried out in order to find appropriate choices.

3. NURBS based Isogeometric Analysis

To explain the advantages of NURBS based form finding and analysis of shell structures a brief introduction to NURBS and isogeometric analysis is given. NURBS are used by many practicing designers, for instance in the software Rhinoceros 5 [9]. The mathematical properties of NURBS surfaces make them suitable for representing curved geometries such as shells and membranes with very few control points.

NURBS are a generalization of B-splines, non-interpolating, piecewise polynomial curves, with the ability to represent any conical shapes such as circles exactly. A B-spline curve $C(\xi)$ is defined by its polynomial degree p, a knot vector $\Xi = \{\xi_1, \xi_2 \dots \xi_{n+p+1}\}$, and a set of n control points $\mathbf{B}_i = (x_i, y_i, z_i)$. The knot vector contains non decreasing values and divides the parametric space into intervals known as knot spans, the first and last values in the knot vector are repeated $p + 1$ times. If an internal knot is repeated r times it is said to have a multiplicity of r, and the continuity of the basis functions at a repeated knot is C^{p-r}. Each control point has an associated basis function which is non-zero in $p + 1$ knot spans, which is known as local support. The local support of the NURBS basis, where a change at some part of the geometry only has a local effect, makes them highly intuitive and predictable. The curve is computed by a summation of the basis functions multiplied by the control points

$$C(\xi) = \Sigma_{i=1}^{n} N_{i,p}(\xi)\mathbf{B}_i \quad (1)$$

where the i:th basis function $N_{i,p}$ is constructed recursively, for the formulas see *Piegl et al.* [10]. The basis functions are only interpolatory at the ends of the knot vector, and at knots with multiplicity $r = p$, leading to C^0 continuity. The number of knots does not coincide with the number of control points or basis functions.

A B-spline surface is defined using the tensor product approach, where another set of basis functions $M_{j,q}(\eta)$ of degree q, with the knot vector $H = \{\eta_1, \eta_2, \dots, \eta_{m+q+1}\}$, with m control points in the second direction and the control point net $\mathbf{B}_{i,j}$ is used

$$S(\xi, \eta) = \Sigma_{i=1}^{\mathrm{n}} \Sigma_{j=1}^{\mathrm{m}} N_{i,p}(\xi) M_{j,q}(\eta) \mathbf{B}_{i,j}. \tag{2}$$

To extend the B-spline surface to a NURBS surface each control point is extended with a weight, $\mathbf{B}_{i,j} = (x_{i,j}, y_{i,j}, z_{i,j}, w_{i,j})$ and we get the NURBS surface

$$S(\xi, \eta) = \frac{\Sigma_{i=1}^{\mathrm{n}} \Sigma_{j=1}^{\mathrm{m}} N_{i,p}(\xi) M_{j,q}(\eta) w_{i,j} \mathbf{B}_{i,j}}{\Sigma_{k=1}^{\mathrm{n}} \Sigma_{l=1}^{\mathrm{m}} N_{k,p}(\xi) M_{l,q}(\eta) w_{k,l}}. \tag{3}$$

Geometrically this can be explained that a NURBS surface in R^3 is a projection of B-Spline surface in R^4. If all weights are equal the NURBS surface is reduced to a B-Spline surface. In NURBS based isogeometric analysis (IGA) the basis functions chosen to represent the geometry are also used to approximate the unknown solution fields, for instance, the unknown displacements. For more information on IGA see the extensive report by *Hughes et al.* [5] on NURBS based IGA.

An attractive property of B-Splines for design and analysis is that the represented geometry is invariant during refinements and is represented exactly irrespective of the mesh being coarse or refined. There are three types of refinements possible for B-Splines/NURBS based IGA. The first is the same as for finite elements, namely making the elements smaller (h-refinement), which is done by performing so called knot insertion, whereby new knot values are inserted into the knot vector without affecting the geometry. The elements in NURBS based IGA are defined by the knot spans, and thus by introducing new knots one also introduces new elements. As for finite elements it is possible to increase the degree the basis functions (p-refinement). A new type of refinement is possible with B-splines/NURBS where if the degree is first raised and then the elements made smaller (k-refinement) it is possible to get basis functions with continuous derivatives across element borders. The refinement possibilities make NURBS suitable for form finding where a coarse mesh can be used initially to explore shapes in near real time and a finer one can be used afterward to get a better approximation.

The tensor product nature of NURBS surfaces, seen in Eq. (3), constrains standard isogeometric analysis with NURBS to 4-sided surfaces. Possible ways of getting around this is by use of T-Splines [3], or trimmed NURBS [8], but is out of the scope of this paper.

A NURBS based isogeometric Kirchhoff-Love shell element was first presented by *Kiendl et al.* [6]. It is used in this paper, and the membrane elements in the paper are formulated by neglecting the bending stiffness of the shell elements. A small deformations version of the shell element is used after the form finding in a static analysis to compute displacements, stresses and strain energies.

4. Design process

The ability to perform form finding with very few elements is favourable in design situations as it allows the designer to quickly explore alternative shapes. Figure 1 illustrates some of the advantages of a design process with isogeometric elements. It is split into three parts, an exploration of different form found shapes, followed by a final accurate form finding, and after that a verification part with further studies.

In the form finding exploration the first step is to define an initial shape, boundary conditions, material parameters and applied loads (typically the self-weight). Once this is done the form found shape is computed with a coarse mesh. An evaluation of the shape follows, where the shape is evaluated in terms of architectural and engineering criteria, such as structural performance, daylight, acoustics, limitations on the shape (height, span), and so on. To fulfil the criteria it is often necessary to change initial parameters such as the initial geometry, boundary conditions, loads before the form finding process is iterated. Using a coarse mesh allows for quick exploration of different shapes which geometrically are often similar to the same shapes that have been form found with a finer discretization [1]. Figure 1 a) shows a few design explorations of a simple geometry with a uniformly distributed load. Variations of the boundary conditions and geometry generates different shapes, all approximated with a coarse mesh.

Once the form found shape fulfils necessary design and engineering criteria, it can be further refined and ran through the form finding process once again, in order to obtain a more optimal shape. As shown in Figure 1 b) there is visually very little difference between the coarse and fine meshes used for the form finding, however, the difference can be large in terms of mechanical performance. This second form finding can be done using the same initial geometry, or from the results of the form finding with the coarse mesh can be used as the initial shape for the finer mesh in order to save computation time.

The form finding procedure reduces the bending part of the strain energy in the structure for the applied load. How well the bending strain energy is reduced depends on the discretization, i.e. how small the elements are and the degree of their basis functions. To compute the bending strain energy after the form finding it is necessary to first perform a further discretization to smaller elements, this is a straightforward procedure with NURBS based IGA since the geometry is always exactly represented. Doing the same refinement with finite elements which only approximate a geometry and often make use of flat elements would be very difficult and time consuming. Figure 1 c) shows the displacements (left) and percentage bending strain energy (right) in the chosen structure. A form finding with an even finer mesh would further reduce the bending strain energy.

A near optimal shape shows very little bending strain energy in a plot like the one shown in Figure 1 c). A shape that is modified from its optimal form may show high bending strain energy in the plot, this also provides information about the amount of material that is needed at different parts in the structure.

Implementing the form finding process with isogeometric elements in a Computer Aided Design software (CAD) can help with this design process and has several other benefits listed in the next section.

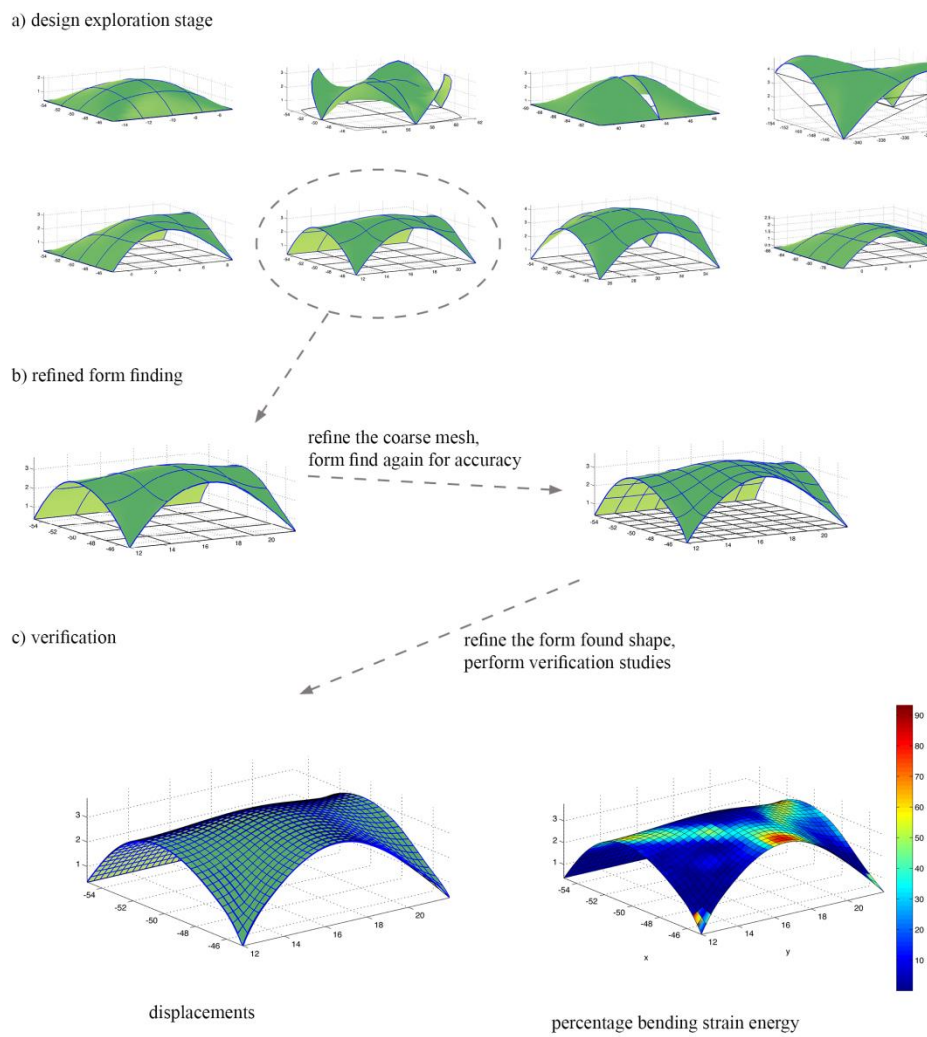


Figure 1: Design process with a) a form finding exploration step, b) a final form finding with a finer mesh, and c) further studies on a linear elastic model with a refined mesh after the form finding has been performed. The NURBS based geometry makes it straightforward to make further refinements without changing the geometry as necessary.

5. Integration of design and analysis, and modelling aspects

A Rhinoceros 3D V.5 [9] plugin by the authors and an ongoing master's thesis project is in development to integrate isogeometric form finding in a design software. The tool is currently at the very early stages. The interface consists of a tabbed docking panel where initial geometries, materials, and boundary conditions can be set up, and where the form finding can be performed.

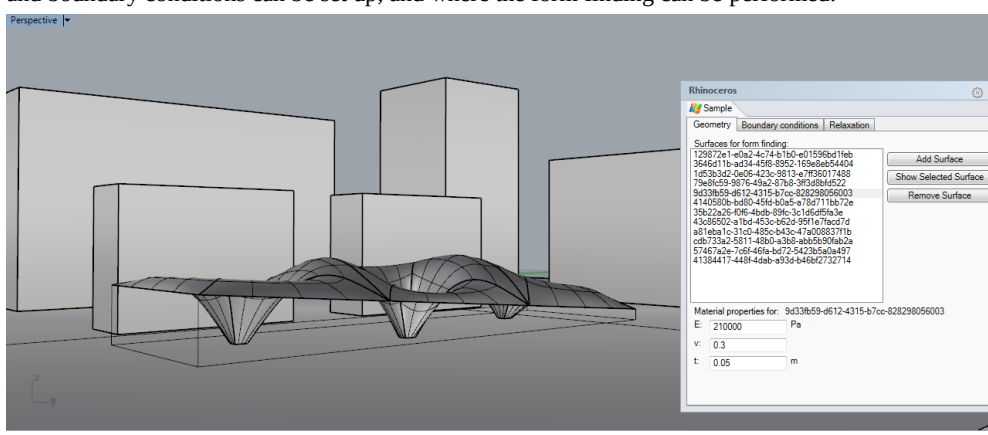


Figure 2: Displaying the user interface for the form finding tool in Rhinoceros 5.

The form finding can be performed with multiple patches which are connected. The limitations at the moment are that the edges of bordering patches have to have compatible discretizations, meaning that they need to have identical curves on the edges which border each other. In this way each patch is treated as a "super" element. By modelling the coarsest possible geometry the refinements to smaller elements can be handled by the plugin. The limitations must be kept in mind while modelling the initial geometry, if for instance modelling a hole it must be modelled following "patch" modelling techniques. Implementing T-Splines or trimmed NURBS for the form finding could simplify the creation of suitable models for the form finding. Using a CAD environment simplifies the modelling of the initial geometry compared finite element software. The form finding process typically requires several iterations to fulfil both architectural design and engineering criteria's, this requires modifications to the initial geometry and is simple to do in a CAD software, where unlike FE-software an iterative workflow is important.

Integrating the process into Rhinoceros simplifies several parts which are often included in the design process. The form finding can be performed within the architectural context, and thus simplifies considerations related to the surrounding buildings, such as shading and reflections, etc. Having the form found shapes in the design software and having them be the complete curved geometry description can make it easy to do architectural renderings to present to clients, further detailing can be performed after the form finding since the geometry is still NURBS. Another advantage of CAD tools is that they often include geometry diagnostics tools, such as curvature and edge analysis.

6. Design examples

In this section some examples are included to show the method applied to more complex geometries. Figure 3 shows the form finding of connected circular shapes, with the introduction of some openings. Figure 4 shows a free form shape with holes. The geometry consist of 9 patches where all the connecting boundaries are matching.

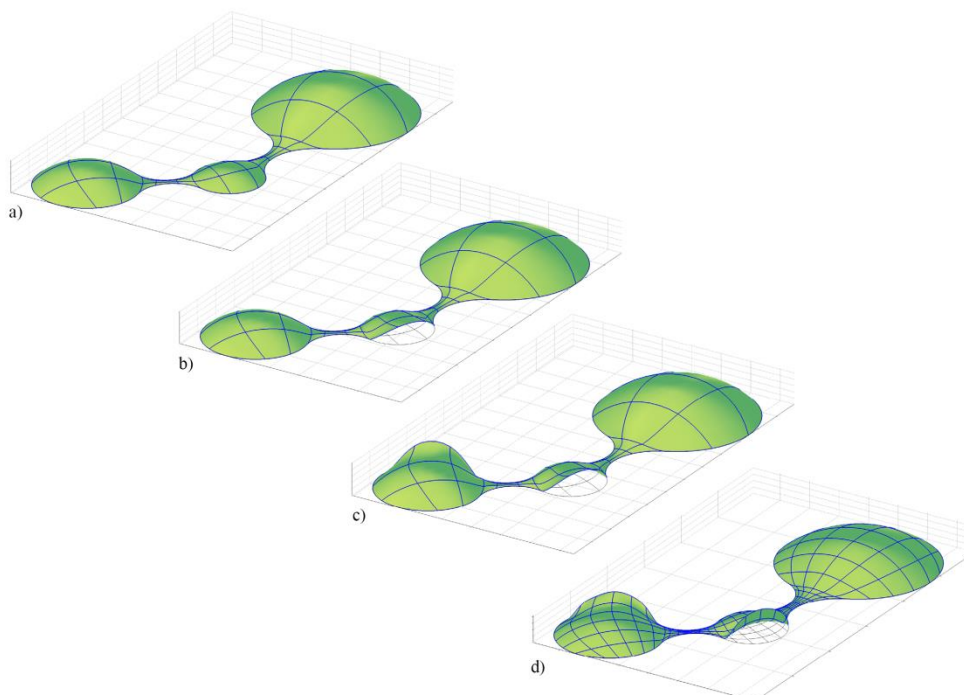


Figure 3: Connected circular forms with openings.

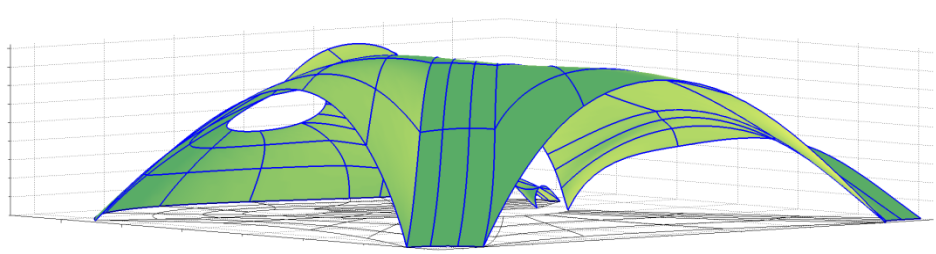


Figure 4: Free form shape with holes

7. Conclusions

The use of isogeometric membrane elements for form finding of structures with minimal bending has been presented. The form finding can be performed with few elements, and as such can be used in an interactive fashion. An advantage over other methods is that it is straightforward to do further discretisation after the form finding in order to perform other studies. A plugin for Rhinoceros 3D which is in the very early stages has been described. The tool allows for form finding within context and simplifies modelling of the initial geometries, however, using standard NURBS based IGA sets limitations on how to model the geometry in CAD software. Further work could include implementation of IGA with trimmed NURBS, or T-Splines.

References

[1] Alic V and Persson K., Isogeometric elements in the dynamic relaxation method. *Proceedings of 27th Nordic Seminar on Computational Mechanics* 2014, 256-259.

[2] Barnes M. R., Form finding and analysis of tension structures by dynamic relaxation. *International journal of space structures*, 1999, 14(2), 89-104.

[3] Bazilevs Y., Calo V. M., Cottrell J. A., Evans J. A., Hughes T. J. R., Lipton S., ... and Sederberg T. W., Isogeometric analysis using T-splines. *Computer Methods in Applied Mechanics and Engineering*, 2010, *199*(5), 229-263.

[4] Block P., and Ochsendorf J. Thrust network analysis: A new methodology for three-dimensional equilibrium. *JOURNAL-INTERNATIONAL ASSOCIATION FOR SHELL AND SPATIAL STRUCTURES*, 2007, *155*, 167.

[5] Hughes T. J., Cottrell J. and Bazilevs Y., Isogeometric analysis: Cad, finite elements, nurbs, exact geometry and mesh refinement. *Computer methods in applied mechanics and engineering 194* (39) 2005, 4135–4195.

[6] Kiendl J., Bletzinger K. U., Linhard J. and Wüchner R., Isogeometric shell analysis with Kirchhoff–Love elements. *Computer Methods in Applied Mechanics and Engineering*, 2009, *198*(49), 3902-3914.

[7] Kilian A., and Ochsendorf J. Particle-spring systems for structural form finding. *Journal-International Association for Shell and Spatial Structures*, 2005, *148*, 77.

[8] Kim H. J., Seo Y. D., and Youn, S. K., Isogeometric analysis for trimmed CAD surfaces. *Computer Methods in Applied Mechanics and Engineering*, 2009, *198*(37), 2982-2995.

[9] McNeel R., Rhinoceros 3D. http://www.rhino3d.com/ *Retrieved* 2009, *Jan*, *15*.

[10] Piegl L. A., and Tiller W., The NURBS book (Monographs in visual communication), 1996.

[11] Schek H. J., The force density method for form finding and computation of general networks. *Computer methods in applied mechanics and engineering*, 1974, *3*(1), 115-134.

Paper D

Computer-Aided Design 93 (2017) 26–37

Contents lists available at ScienceDirect

Computer-Aided Design

journal homepage: www.elsevier.com/locate/cad

Bi-directional algebraic graphic statics

Vedad Alic *, Daniel Åkesson

John Ericssons väg 1, 223 63 Lund, Sweden

ARTICLE INFO

Article history:
Received 22 December 2016
Accepted 15 August 2017

Keywords:
Interactive graphic statics
Matrix analysis of structures
Graph theory
Reciprocal figures
Force diagram manipulations
Conceptual design

ABSTRACT

A pre-existing algebraic graphic statics method is extended to allow for interactive manipulations of the force diagram, from which an updated form diagram is determined. Newton's method is used to solve a set of non-linear equations, and the required Jacobian matrix is derived. Additional geometric constraints on the form diagram are introduced, and methods for improving the robustness of the method are presented. We discuss the implementation of the method as a back-end to an interactive application, and demonstrate the usability of the method in several examples where the qualities of directly manipulating the force diagram are emphasized.

© 2017 Elsevier Ltd. All rights reserved.

1. Introduction

Graphic statics is a graphical method to compute the forces within a 2D axially loaded static structure. As forces are represented graphically by using vectors, no numerical analysis is required to calculate the magnitude of the forces. The use of graphic statics grew from the 19th and 20th centuries but lost popularity due to the emergence of computational analysis methods. However, being an intuitive method of visualizing form and forces, graphic statics has recently seen an increase in popularity.

Maxwell established that for axially loaded structures, the nodes and polygons in the form diagram have reciprocal polygons and nodes in the force diagram. The form diagram represents the structure, and the force diagram represents the static equilibrium [1] for that structure. Maxwell's reciprocal diagrams were extended by Cremona [2], which provided a base for graphic statics. However, the first comprehensive presentation of graphic statics was by Culmann [3]. The method has historically been used to design structures by, for instance, Maurice Koechlin (co-designer of the Eiffel Tower) and Robert Maillart [4]. The reciprocity between the form and force diagrams can provide the designer with insight into the force distribution within a structure, and aid the intuitive understanding of the relationship between form and forces.

In recent literature it has been applied to the design of structural masonry [5–7] and structural optimization [8]. Methods for using graphic statics for the design of post-tensioned funiculars has been presented in [9]. The relationship between graphic statics and the discrete Airy stress function have been the topic of [6,7,10]. The relationships are generalized to discontinuous Airy stress functions in [11], enabling the analysis of two-dimensional frames with bending moments. Extensions of graphic statics to three-dimensional structures are presented in [12–14]. Graphic statics has been combined with shape grammars in [15] for rapid generation of diverse structures in equilibrium. In [16,17] a constraints-based approach to graphic statics is presented, where geometric constraints are employed to enforce the conditions between the form and force diagrams.

Digital implementations of graphic statics have leveraged the graphical nature of the method into interactive applications that enable real-time feedback of the relationship between form and forces [18–20].

1.1. Problem statement

Several computer tools that make use of graphic statics have been developed [18–20]. However, until recently most of the tools and literature have only presented digital versions of graphic statics for some specific pre-defined structures. A general algebraic version of graphic statics using a graph theoretic approach is presented by Van Mele and Block in [21] that given a form diagram is able to generate a force diagram directly. A graph theoretic approach for self-stressed networks is also presented in [22]. The equilibrium of the structural systems in [21] are investigated using the states of self-stress of an equivalent unloaded network, making use of [23]. The algebraic approach of the graphic statics framework presented in [21] is well suited for computer implementation as a back end for a Computer Aided Design (CAD) software.

The ability to make changes in a general force diagram and subsequently compute a reciprocal form diagram has not been presented. The extension could be done in several different ways,

* Corresponding author.
E-mail address: vedad.alic@construction.lth.se (V. Alic).
URL: http://www.byggmek.lth.se/ (V. Alic).

http://dx.doi.org/10.1016/j.cad.2017.08.003
0010-4485/© 2017 Elsevier Ltd. All rights reserved.

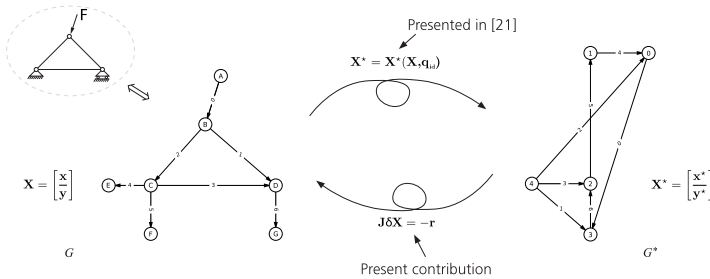


Fig. 1. Schematic illustration of the extension of the framework presented in [21] by also allowing for interactive manipulations of the force diagram.

and two of those are to formulate the extension as a constrained optimization problem (suggested in [21]), or to find the roots of a set of non-linear equations. The challenges with the former are constructing an objective function and avoiding local minima, and the risks of the latter are the method might fail to find solutions. In this paper we present an approach based on the root finding for a set of non-linear equations, which we solve using Newton's method.

1.2. Objective

The objective of this paper is to extend the framework presented in [21] to a bi-directional approach. Given a change in the force diagram, our objective is to compute and present the updated form diagram, see Fig. 1, and to present how this can be implemented as a computational tool to enable manipulations in both the form diagram and the force diagram, with continuous interactive updates of the reciprocal diagrams. Further, we present the benefits and applications of our approach using examples.

1.3. Outline

Section 2 reviews algebraic graphic statics and presents a method to compute the form diagram from a given force diagram. It is formulated as a root finding procedure for a set of non-linear equations, and the required derivatives for Newton's method are presented.

Section 3 presents implementation aspects of the method and presents how the implementation can be used as a back-end for a design application. A general overview of the implementation and the requirement of further geometric constraints are presented. An approach on how to identify appropriate constraints by making use of the null space is presented. Further, vertex perturbations and line searches are introduced to improve the robustness of the solver.

Section 4 demonstrates the method in a set of examples. The examples increase in complexity, and are presented in the following order: a simple truss, a practical arch example with constraints, a form finding arch example, a study of the null space of an arch, a truss with constant force in the chords, and finally an externally post-tensioned funicular geometry.

2. Theoretical framework

This section starts with a brief review of graphic statics and the algebraic method which is presented in [21]. The section then continues with the extension of the method to enable manipulation of the force diagram, and to compute the equivalent form diagram by solving a set of non-linear equations using Newton's method.

2.1. Graphic statics

Fig. 1 presents a simple graphic statics example, with the structure, applied loads, and support forces to the left and the reciprocal force diagram to the right. The equivalent structural mechanics diagram of the form diagram is shown in the top left of the figure. Equilibrium of forces in each internal point in the form diagram (points B, C, D in Fig. 1) is represented by closed polygons in the force diagram. The lengths of the edges in the force diagram are proportional to the magnitude of the forces in the corresponding edges in the form diagram. The interpretation of tension and compression can be done by making use of Bow's notation [24].

2.2. Reciprocal graphs

The diagrams in Fig. 1 are represented as directed graphs. The diagrams are projections of dual polyhedra, where the rules of 3D projective geometry apply [10]. Vertices in the form diagram map to faces in the force diagram and faces in the form diagram map to vertices in the force diagram. Edges map to edges, and in the convention adopted here, remain parallel (another option is for edges to map to perpendicular edges).

In Fig. 1 the form diagram G is shown to the left, and the force diagram $G^\star$ is to the right. In graph theory these are referred to as the primal, and dual graphs, respectively. The connectivity matrix $\mathbf{C}$ of graph G and incidence matrix $\mathbf{C}^\star$ of the reciprocal graph $G^\star$ are constructed as described in [21], and are also briefly presented here. The connectivity matrix is

$$C_{ij} = \begin{cases} +1, & \text{if vertex } i \text{ is the head of edge } j \\ -1, & \text{if vertex } i \text{ is the tail of edge } j \\ 0, & \text{otherwise} \end{cases} \tag{1}$$

and the rows of the incidence matrix are constructed from the form graph by cycling through its faces in a counter-clockwise direction. The ith row of $\mathbf{C}^\star$, corresponding to the ith face of G is

$$C^\star_{ij} = \begin{cases} +1, & \text{if edge } i \text{ is traversed in the same} \\ & \text{direction as its orientation } j \\ -1, & \text{if in the opposite direction} \\ 0, & \text{otherwise.} \end{cases} \tag{2}$$

The size of $\mathbf{C}$ is $[v \times e]$, and the size of $\mathbf{C}^\star$ is $[v^\star \times e]$. Here, e is the total number of edges, v is the number of vertices in the form diagram and $v^\star$ is the number of vertices in the force diagram. The number of faces f in the form diagram G is equal to the number of vertices $v^\star$ in the force diagram $G^\star$, and the opposite holds true since $v = f^\star$.

2.3. Computing the force diagram

This subsection describes the method for computing a force diagram from a form diagram, for further details, see [21]. The column matrices containing the respective coordinates of the dual and the primal graphs are

$$\mathbf{X}^\star = \begin{bmatrix} \mathbf{x}^\star \\ \hline \mathbf{y}^\star \end{bmatrix}; \qquad \mathbf{X} = \begin{bmatrix} \mathbf{x} \\ \hline \mathbf{y} \end{bmatrix}. \tag{3}$$

These are of size $[2v^\star \times 1]$ and $[2v \times 1]$, respectively.

Given a form graph, the related force graph can be computed from $\mathbf{X}^\star = \mathbf{X}^\star(\mathbf{X}, \mathbf{q}_{\text{id}})$, which is written explicitly

$$\mathbf{X}^\star = \begin{bmatrix} \mathbf{L}^{\star -1}\mathbf{C}^\star\mathbf{Q}\mathbf{u} \\ \hline \mathbf{L}^{\star -1}\mathbf{C}^\star\mathbf{Q}\mathbf{v} \end{bmatrix} \tag{4}$$

where $\mathbf{Q} = \mathbf{Q}(\mathbf{x}, \mathbf{y})$ is a diagonal matrix containing force densities [25], Q_{ii} is the force density of edge i. $\mathbf{L}^\star$ is the Laplacian matrix of the force graph, $\mathbf{L}^\star = \mathbf{C}^\star\mathbf{C}^{\star\mathrm{T}}$. The coordinate difference vectors of the form diagram are $\mathbf{u} = \mathbf{C}^\mathrm{T}\mathbf{x}$ and $\mathbf{v} = \mathbf{C}^\mathrm{T}\mathbf{y}$. The coordinates for one vertex in the force diagram in Eq. (4) must be chosen in order to obtain a unique solution, [21]. To obtain a unique solution it is further required to prescribe a set of force densities, $\mathbf{q}_{\text{id}}$, for details see [21]. It is evident that $\mathbf{X}^\star$ is a non-linear function of $\mathbf{X}$, since both $\mathbf{u}$, $\mathbf{v}$ and $\mathbf{Q}$ depend on $\mathbf{X}$.

2.4. Computing the reciprocal form diagram

Here we extend the method presented in [21], by solving for the form diagram, given changes in the force diagram. We formulate the problem as a root finding procedure by setting up a residual, which is zero at a root. To find the roots we employ Newton's method, for which the Jacobian matrix is required.

When the force diagram $\mathbf{X}^\star$ is manipulated due to a user input $\Delta\mathbf{X}^\star_{\text{user}}$ we need to find the coordinates of the form diagram $\mathbf{X}$ that give the updated $\mathbf{X}^\star$

$$\mathbf{X}^\star(\mathbf{X}, \mathbf{q}_{\text{id}}) = \mathbf{X}^\star_{\text{start}} + \Delta\mathbf{X}^\star_{\text{user}} \tag{5}$$

where $\mathbf{X}^\star_{\text{start}}$ are the coordinates of the force diagram prior to the user manipulation. To find a solution we seek to find a root $\mathbf{X}$ such that

$$\mathbf{r} = \mathbf{X}^\star - (\mathbf{X}^\star_{\text{start}} + \Delta\mathbf{X}^\star_{\text{user}}) = \mathbf{0} \tag{6}$$

where $\mathbf{r}$ is a residual. We proceed by linearizing the equation and using an iterative method

$$\mathbf{r}(\mathbf{X}^i) + \frac{\partial \mathbf{r}(\mathbf{X}^i)}{\partial \mathbf{X}}\delta X = \mathbf{0} \tag{7}$$

where i is the current iteration, not to be confused with exponentiation. $\mathbf{X}^\star_{\text{start}}$ and $\Delta\mathbf{X}^\star_{\text{user}}$ are constants, and $\mathbf{q}_{\text{id}}$ has been kept constant, giving

$$\mathbf{r}(\mathbf{X}^i) + \frac{\partial \mathbf{X}^\star(\mathbf{X}^i)}{\partial \mathbf{X}}\delta X = \mathbf{0} \tag{8}$$

where

$$\delta X = \mathbf{X}^{i+1} - \mathbf{X}^i. \tag{9}$$

The Jacobian matrix of $\mathbf{X}^\star$ with respect to $\mathbf{X}$ is

$$\mathbf{J} = \frac{\partial \mathbf{X}^\star}{\partial \mathbf{X}} \tag{10}$$

which is of size $[2v^\star \times 2v]$. The Jacobian matrix is used to solve for δX in Eq. (8).

2.5. Derivation of the Jacobian matrix

The kth column of the Jacobian is computed as

$$\frac{\partial \mathbf{X}^\star}{\partial X_k} = \begin{bmatrix} \mathbf{L}^{\star -1}\mathbf{C}^\star\left(\frac{\partial \mathbf{Q}}{\partial X_k}\mathbf{u} + \mathbf{Q}\mathbf{C}^\mathrm{T}\frac{\partial \mathbf{x}}{\partial X_k}\right) \\ \hline \mathbf{L}^{\star -1}\mathbf{C}^\star\left(\frac{\partial \mathbf{Q}}{\partial X_k}\mathbf{v} + \mathbf{Q}\mathbf{C}^\mathrm{T}\frac{\partial \mathbf{y}}{\partial X_k}\right) \end{bmatrix} \tag{11}$$

where the derivatives of $\mathbf{x}$ and $\mathbf{y}$ are trivial. In order to compute the derivatives of the force densities, $\mathbf{Q}$ [25] we introduce, $\mathbf{A}$, the equilibrium matrix [26]

$$\mathbf{A} = \begin{bmatrix} \mathbf{C}_\mathrm{i}\mathbf{U} \\ \hline \mathbf{C}_\mathrm{i}\mathbf{V} \end{bmatrix} \tag{12}$$

where $\mathbf{U}$ and $\mathbf{V}$ are the diagonal matrices of $\mathbf{u}$ and $\mathbf{v}$, respectively, and $\mathbf{C}_\mathrm{i}$ contains the rows of $\mathbf{C}$ corresponding to the inner vertices of G.

For the force densities, we first write them in their vector form $\mathbf{q}$ and partition them into an independent part, $\mathbf{q}_{\text{id}}$, and a rest part, $\mathbf{q}_{\text{d}}$. The equilibrium matrix is similarly partitioned in an independent, $\mathbf{A}_{\text{id}}$, and a dependent part, $\mathbf{A}_{\text{d}}$, together satisfying the following equation [21]:

$$\begin{bmatrix} \mathbf{A}_{\text{id}} \mid \mathbf{A}_{\text{d}} \end{bmatrix}\begin{bmatrix} \mathbf{q}_{\text{id}} \\ \hline \mathbf{q}_{\text{d}} \end{bmatrix} = \mathbf{0}. \tag{13}$$

The independent edges can be identified by transforming $\mathbf{A}$ into a row reduced echelon form [21]. The number of independent edges amounts to the number of associated force densities that must be prescribed.

From Eq. (13) we solve for the force densities:

$$\mathbf{q} = \begin{bmatrix} \mathbf{q}_{\text{id}} \\ \hline \mathbf{A}_{\text{d}}^{-1}(-\mathbf{A}_{\text{id}}\mathbf{q}_{\text{id}}) \end{bmatrix}. \tag{14}$$

The derivative of $\mathbf{q}$, after partitioning, is

$$\frac{\partial \mathbf{q}}{\partial X_k} = \begin{bmatrix} \mathbf{0} \\ \hline \frac{\partial \mathbf{A}_{\text{d}}^{-1}}{\partial X_k}(-\mathbf{A}_{\text{id}}\mathbf{q}_{\text{id}}) + \mathbf{A}_{\text{d}}^{-1}(-\frac{\partial \mathbf{A}_{\text{id}}}{\partial X_k}\mathbf{q}_{\text{id}}) \end{bmatrix}. \tag{15}$$

From Eq. (15) it is evident that the derivative of the independent part, $\mathbf{q}_{\text{id}}$ is zero, since the independent force densities remain unchanged during manipulations of the force diagram. To compute the derivatives $\mathbf{A}$, Eq. (12) is differentiated with respect to $\mathbf{X}$.

$$\frac{\partial \mathbf{A}}{\partial X_k} = \begin{bmatrix} \mathbf{C}_\mathrm{i}\frac{\partial \mathbf{U}}{\partial X_k} \\ \hline \mathbf{C}_\mathrm{i}\frac{\partial \mathbf{V}}{\partial X_k} \end{bmatrix}. \tag{16}$$

From $\mathbf{u} = \mathbf{C}^\mathrm{T}\mathbf{x}$ it follows that

$$\frac{\partial \mathbf{U}}{\partial X_k} = \begin{cases} \operatorname{diag}(\mathbf{c}_k), & \text{if } X_k \in \mathbf{x} \\ \mathbf{0}, & \text{if } X_k \in \mathbf{y} \end{cases} \tag{17}$$

and similarly

$$\frac{\partial \mathbf{V}}{\partial X_k} = \begin{cases} \mathbf{0}, & \text{if } X_k \in \mathbf{x} \\ \operatorname{diag}(\mathbf{c}_k), & \text{if } X_k \in \mathbf{y} \end{cases} \tag{18}$$

where $\mathbf{c}_k$ is the kth row in $\mathbf{C}$

$$\mathbf{C} = \begin{bmatrix} \mathbf{c}_1^\mathrm{T} \cdots \mathbf{c}_k^\mathrm{T} \cdots \mathbf{c}_v^\mathrm{T} \end{bmatrix}^\mathrm{T}. \tag{19}$$

To complete this section $\partial\mathbf{A}/\partial X_k$ is partitioned into a dependent, $\partial\mathbf{A}_{\text{d}}/\partial X_k$ and an independent part $\partial\mathbf{A}_{\text{id}}/\partial X_k$, and finally the derivative of the inverse of the dependent part required in Eq. (15) is

$$\frac{\partial \mathbf{A}_{\text{d}}^{-1}}{\partial X_k} = -\mathbf{A}_{\text{d}}^{-1}\frac{\partial \mathbf{A}_{\text{d}}}{\partial X_k}\mathbf{A}_{\text{d}}^{-1} \tag{20}$$

which is the last part required to compute the Jacobian matrix.

2.6. Jacobian matrix with respect to force densities

In this section we present the derivatives $\partial \mathbf{X}^\star / \partial \mathbf{q}_{\text{id}}$ for completeness. The following derivatives could be used to relax the conditions on edges with prescribed force densities. In the implementation and the examples we keep these fixed in order to simplify the presentation.

The derivatives of $\mathbf{X}^\star$ with respect to the jth prescribed force density are [25]

$$\frac{\partial \mathbf{X}^\star}{\partial q_{\text{id},j}} = \begin{bmatrix} \mathbf{L}^{\star -1}\mathbf{C}^\star \frac{\partial \mathbf{Q}}{\partial q_{\text{id},j}} \mathbf{u} \\ \mathbf{L}^{\star -1}\mathbf{C}^\star \frac{\partial \mathbf{Q}}{\partial q_{\text{id},j}} \mathbf{v} \end{bmatrix} \tag{21}$$

where the column matrix version of $\frac{\partial \mathbf{Q}}{\partial q_{\text{id},j}}$ is

$$\frac{\partial \mathbf{q}}{\partial q_{\text{id},j}} = \begin{bmatrix} \frac{\partial \mathbf{q}_{\text{id}}}{\partial q_{\text{id},j}} \\ \mathbf{A}_{\text{d}}^{-1}(-\mathbf{A}_{\text{id}} \frac{\partial \mathbf{q}_{\text{id}}}{\partial q_{\text{id},j}}) \end{bmatrix}. \tag{22}$$

Finally, $\frac{\partial \mathbf{q}_{\text{id}}}{\partial q_{\text{id},j}}$ has a one at the jth element, and zeros elsewhere

$$\frac{\partial \mathbf{q}_{\text{id}}}{\partial q_{\text{id},j}} = \begin{bmatrix} \frac{\partial q_{\text{id},1}}{\partial q_{\text{id},j}} \\ \vdots \\ \frac{\partial q_{\text{id},j-1}}{\partial q_{\text{id},j}} \\ \frac{\partial q_{\text{id},j}}{\partial q_{\text{id},j}} \\ \frac{\partial q_{\text{id},j+1}}{\partial q_{\text{id},j}} \\ \vdots \\ \frac{\partial q_{\text{id},n}}{\partial q_{\text{id},j}} \end{bmatrix} = \begin{bmatrix} 0 \\ \vdots \\ 0 \\ 1 \\ 0 \\ \vdots \\ 0 \end{bmatrix}. \tag{23}$$

2.7. Inextensible mechanisms

The number of static and kinematic indeterminacies in a pin-jointed structure can be determined from Maxwell's rule. The extended Maxwell rule for a form graph is

$$k - m = e - 2v_i \tag{24}$$

where k is the number of independent states of self-stress, m is the number of inextensible mechanisms, and v_i is the number of internal vertices of G. By using a singular value decomposition (SVD) of the equilibrium matrix $\mathbf{A}$, the values of k and m can be determined [26,21].

Eq. (20) can only be determined if the number of inextensible mechanisms, m, is zero. When $m = 0$, Eq. (13) can be rewritten as [21]

$$\mathbf{q}_{\text{d}} = -\mathbf{A}_{\text{d}}^{-1}\mathbf{A}_{\text{id}}\mathbf{q}_{\text{id}}. \tag{25}$$

However, in the case when $m > 0$, then $\mathbf{A}_{\text{d}}$ is not square and the remaining force densities are solved from the equivalent equation

$$\mathbf{A}_{\text{d}}^{\text{t}}\mathbf{A}_{\text{d}}\mathbf{q}_{\text{d}} = -\mathbf{A}_{\text{d}}^{\text{t}}\mathbf{A}_{\text{id}}\mathbf{q}_{\text{id}} \tag{26}$$

as described in [21].

In our method, when $m > 0$ for the equivalent of Eq. (15) we must compute the derivatives of the Moore–Penrose pseudoinverse $(\mathbf{A}_{\text{d}}^{\text{t}}\mathbf{A}_{\text{d}})^{-1}\mathbf{A}_{\text{d}}^{\text{T}}$, since $\mathbf{A}_{\text{d}}$ is not square. It is possible to calculate the derivatives if the rank is unchanged, however, very small perturbations of the shape will in general lead to a reduction of the number of inextensible mechanisms (m), and thus to a change of rank. Manipulations which keep the rank constant can be explored by selecting different states of self-stress, by selecting a new $\mathbf{q}_{\text{id}}$, and thus generating a new force diagram.

Algorithm 1 Iterative solution loop

Get initial solution and store it:
$\mathbf{X}^0 = \mathbf{X}_{\text{start}}$
$\mathbf{X}^\star_{\text{start}} = \mathbf{X}^\star(\mathbf{X}^0)$

Get user change in force diagram, $\Delta \mathbf{X}^\star_{\text{user}}$

while $||\mathbf{r}||_2 > \epsilon$ **do**
  Update:
  $\mathbf{J}(\mathbf{X}^i)$
  $\mathbf{r}(\mathbf{X}^i) = \mathbf{X}^\star(\mathbf{X}^i) - (\mathbf{X}^\star_{\text{start}} + \Delta \mathbf{X}^\star_{\text{user}})$

  Remove rows in $\mathbf{J}$ and $\mathbf{r}$ due to the constrained vertex in the force diagram.

  Solve for $\delta \mathbf{X}$ from:
  $\mathbf{J}(\mathbf{X}^i)\delta \mathbf{X} = -\mathbf{r}(\mathbf{X}^i)$

  Update $\mathbf{X}$:
  $\mathbf{X}^{i+1} = \mathbf{X}^i + \delta \mathbf{X}$

  update $\mathbf{X}^\star(\mathbf{X}^{i+1})$

  update $||\mathbf{r}||_2$
  increment i
end while

2.8. The solution loop

To find the coordinates of a form diagram that is reciprocal to the force diagram, the Jacobian matrix is used. The solution is implemented in an iterative scheme, employing Newton's method, as shown in Algorithm 1.

Generally, the Jacobian matrix is not a square and represents an underdetermined system. To ensure that at least one solution exists, the rank of the Jacobian matrix should be equal to the rank of the augmented matrix

$$rank(\mathbf{J}) \geq rank(\mathbf{J} \mid \mathbf{r}). \tag{27}$$

Further, if the rank of the Jacobian is less then the number of variables, then $2v - rank(\mathbf{J})$ linearly independent solutions exist. If this occurs, we choose a single solution by making use of the least squares principle [25].

The effects of prescribing a vertex's coordinates in the force diagram in Eq. (4) to zero means that two rows in the Jacobian will be zero. These rows, along with the corresponding rows of $\mathbf{r}$ can be reduced, resulting in a Jacobian of size $[(2v^\star - 2) \times 2v]$, and $\mathbf{r}$ of size $[(2v^\star - 2) \times 1]$. Applying manipulations to the position of the prescribed vertex in the force diagram can be achieved by applying the opposite manipulation to all other vertices.

2.9. Additional requirements

A requirement of the form graph is that it must be a planar graph [27,21]. A further requirement of the method is that edges that have a prescribed force density cannot have zero length in either of the reciprocal diagrams as this leads to division by zero.

3. Computer implementation

In this section a general overview of the implementation of the presented method is provided. It also indicates that the presented method can be used as a back-end in an interactive graphic statics application where the user can manipulate both form and

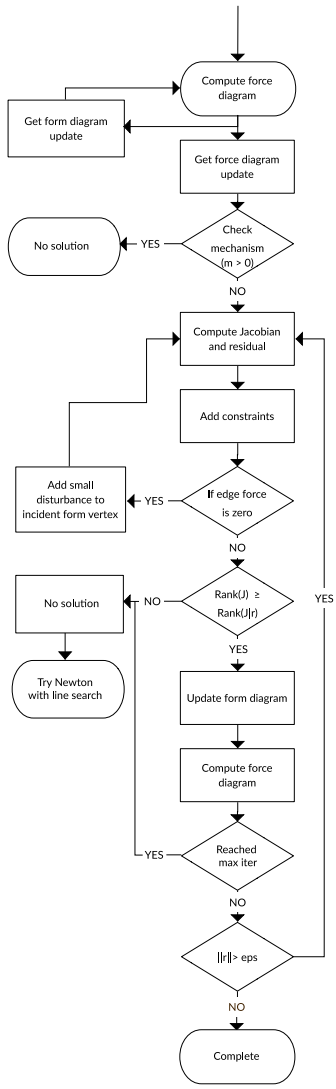


Fig. 2. Flow chart of implementation.

force diagrams with continuous bi-directional updates. A general overview of how the method is implemented is shown in Fig. 2, and various checks are performed to ensure that the user's manipulations to the force diagram are valid and that the problem has one or multiple solutions. The implementation of the method is described in more detail in Algorithm 1.

Our implementation has been made by using the programming language Python [28], together with Numpy [29] and Scipy [30] for performing matrix operations. The Python package NetworkX [31] has been used for graph operations and visualizations.

3.1. Adding geometric constraints to form diagrams

It is necessary to add additional geometric constraints for certain types of structures, e.g. to keep the span of a truss constant. This can be achieved through adding derivatives of constraint equations to the Jacobian matrix and changes to the constraint equation to the residual, i.e.

$$\begin{bmatrix} \mathbf{J} \\ \mathbf{J}_c \end{bmatrix} \delta\mathbf{X} = \begin{bmatrix} \mathbf{r} \\ r_c \end{bmatrix} \tag{28}$$

where

$$J_{c,k} = \frac{\partial f(\mathbf{X})}{\partial X_k}; \; r_c = \delta f(\mathbf{X}) \tag{29}$$

where $f(\mathbf{X})$ is the added constraint equation to the cth row of the Jacobian matrix and X_k is the kth coordinate, corresponding to the kth column of the Jacobian matrix.

In the present work the following constraints have been implemented:

- Horizontal length between two vertices
- Vertical length between two vertices
- Length between two vertices
- Direction between two vertices
- Horizontal position of a vertex
- Vertical position of a vertex

In general, there are a few constraints that always should be applied. Rigid body motions of the form diagram will produce the same force diagram, and as such are of no interest. These can be removed by constraining the position of a vertex in the form diagram. An example is shown in Fig. 3a. It is possible to find solutions, i.e. form diagrams, that results in the same force diagram by scaling of the form diagram, as illustrated in Fig. 3b. In order to remove solutions that only scale the form diagram constraints can be introduced. It is often sufficient to constrain the horizontal length between the supports. Finally, there is a third type of constraint which in our implementation is automatically introduced. It is related to edges which connect to leaf vertices in the form diagram. A leaf vertex is a vertex that only has one edge connected to it. If one such edge does not have a prescribed force-density, it will result in the same force diagram regardless of its length in the form diagram. An example is presented in Fig. 3c. The change in lengths of these edges is of no interest and as such we constrain the lengths of all free edges.

3.2. Null space of the Jacobian matrix

If $2v > rank(\mathbf{J})$, then $2v - rank(\mathbf{J})$ linearly independent solutions, of form diagrams, exist. After a form diagram is found from a specific force diagram, the null space of the Jacobian is a vector space with dimension $2v - rank(\mathbf{J})$, which shows how the form diagram can be changed without affecting the force diagram. This allows the user to explore alternative form diagrams for a specific force diagram. The null space can also be studied to find suitable constraints in order to obtain more desirable solutions.

The null space of the Jacobian can be found by computing the SVD [23] or by using a rank-revealing QR factorization [32].

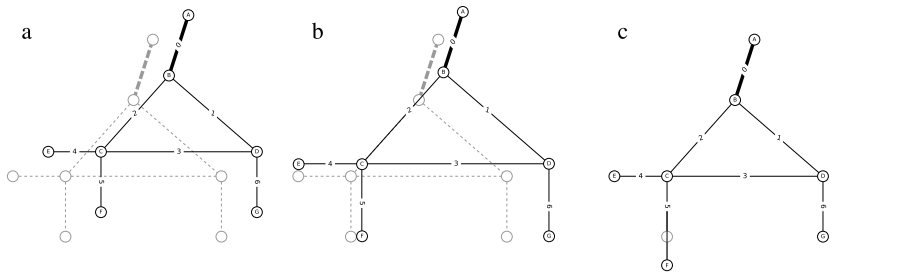


Fig. 3. Examples of changes in the form diagram that result in the same force diagram. (a) Rigid body motion. (b) Scaling motion, note that edge zero does not scale because of the prescribed force density. (c) Extension of an edge connected to a leaf vertex without prescribed force density.

3.3. Vertex perturbation

If the length of an edge in the force diagram is zero the reciprocal structural member obviously carries no force. If this is the case, that edge will not have any contribution to the Jacobian matrix, i.e. the corresponding derivatives are zeros. To solve this numerical problem, zero length edges in the force diagram are identified in each iteration. Zero length edges can easily be identified since their corresponding force densities in the vector **q** are zero. If such edges exist, a very small random value is added to the length of that zero edge by moving the incident vertices in the form diagram. For the movement we successfully use a pair of (for x- and y-coordinate) random numbers from a normal distribution, with zero mean and a standard deviation of 10^{-6}, $\mathcal{N}(0, 10^{-12})$. The implementation of the Newton method with the vertex perturbation is presented in Fig. 2.

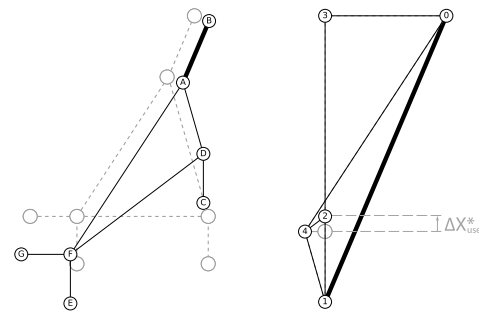


Fig. 4. A small manipulation of the force diagram leads to a large change in form.

3.4. Large manipulations

In order for the proposed method to work, an initial form diagram is required. The initial form is used as an initial guess for Newton's method. As Newton's method is a gradient based method it converges towards local extreme points. This is an advantageous property in case multiple solutions exists, as solutions close to the initial form are often preferred. When the initial guess is too far from the root Newton's method may not converge. For this case the method is modified to include a line search. For details on how to implement the line search, see [33]. The line search is used on iterations where the norm of the residual has increased compared to the previous iteration. The Jacobian matrix is modified with vertex perturbations even for the Newton method with line search, the modification is performed in the same way as presented in Fig. 2. In Section 4.2 we show why we try the method without line search first.

The non-linearity of the problem can sometimes lead to unexpected results, for instance, some small manipulations in the force diagram can result in large changes of the form diagram. This problem can be observed when a vertex that is connected to a short edge in the force diagram is manipulated. A small manipulation in distance can then result in a large change in direction of the adjacent edge. An example is provided in Fig. 4, where vertex 2 is moved in the vertical direction. Even though the method manages to find solutions, these solutions might sometimes become too distorted. In such cases it is, in a computer implementation, possible to revert to a previous state and continue exploring the design from that state.

4. Examples

In this section we present the method with a few practical examples. These emphasize the strengths of the possibility of manipulating the force diagram. The examples also show the importance of selecting proper constraints to obtain the desired solutions, for instance, a common design criteria can be used to span a certain length, this can be achieved by adding constraints that keep the positions of where the structure meets the supports fixed. The initial form and force diagrams in the following examples are visualized with gray dashed lines.

4.1. Simple example

A simple example is shown in Fig. 5. Vertex four in the force diagram is moved to the left, and the corresponding change in the form diagram is visualized. Only the edges that are connected to vertex four in the force diagram are affected.

In the following paragraphs we constrain the positions of vertices C and D of Fig. 5. These constraints keep the position, length, and direction of edge 3 in the form diagram fixed, thereby imposing limitations on the allowable manipulations of the force diagram. The manipulations of the force diagram must be such that the direction of edge 3 in the force diagram is unchanged. For instance, moving vertex 4, or vertex 2 in the vertical direction would change the direction of edge 3 and is thus not possible. However, moving both vertex 4 and 2 vertically by the same amount is allowed, since the direction of edge 3 is then constant during the manipulation.

In the implementation, information regarding inadmissible manipulations of parameters in the force diagram can be found by

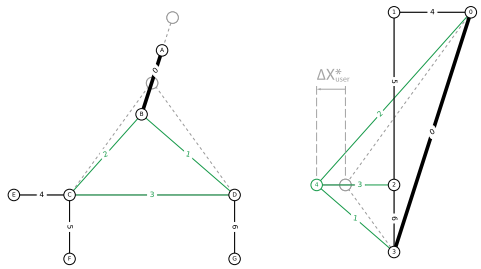


Fig. 5. Simple example where vertex 4 in the force diagram has been moved to the left, the corresponding change is visible in the form diagram.

computing the left null space of the Jacobian matrix. The left null space complements the column space of the Jacobian matrix, and any force manipulations, i.e. any **r**, that is not perpendicular to the left null space is invalid. To further clarify, we compute a basis for the left null space (consisting of one base vector) for the structure in Fig. 5 with vertices C, D constrained. The vector is of size $[2v^\star - 2 + n_{\text{constraints}} \times 1]$ and after normalization with respect to $y^\star_{r2}$ is

$$\mathbf{n}^{\mathrm{T}} = \begin{matrix} x^\star_{r0} & \cdots & y^\star_{r1} & y^\star_{r2} & y^\star_{r3} & c \end{matrix} \\ \begin{bmatrix} 0 & \cdots & 0 & 1 & 0 & \cdots \end{bmatrix} \tag{30}$$

where the parts related to the constraints have been omitted. Manipulations of the force diagram will lead to residual vectors with non-zero elements only on the parts related to x and y, and will thus always be perpendicular to the constraints part. The residual vector associated with moving vertex 2 a unit displacement vertically is

$$\mathbf{r}_1^{\mathrm{T}} = \begin{matrix} & x^\star_{r3} & y^\star_{r0} & y^\star_{r1} & y^\star_{r2} & y^\star_{r3} & c_1 & \end{matrix} \\ \begin{bmatrix} \cdots & 0 & 0 & 0 & -1 & 0 & 0 & \cdots \end{bmatrix} \tag{31}$$

and the residual vector associated with moving vertex 4 a unit displacement vertically is

$$\mathbf{r}_2^{\mathrm{T}} = \begin{matrix} & x^\star_{r3} & y^\star_{r0} & y^\star_{r1} & y^\star_{r2} & y^\star_{r3} & c_1 & \end{matrix} \\ \begin{bmatrix} \cdots & 0 & 1 & 1 & 1 & 1 & 0 & \cdots \end{bmatrix} \tag{32}$$

where vertices 0–3 are moved in the opposite direction, since vertex 4 is constrained in the implementation and not part of the vector. This leads to

$$\mathbf{n} \cdot \mathbf{r}_1 \neq 0, \ \mathbf{n} \cdot \mathbf{r}_2 \neq 0, \ \mathbf{n} \cdot (\mathbf{r}_1 + \mathbf{r}_2) = 0 \tag{33}$$

where the dot is the scalar product. It is seen that only the application of both movements is perpendicular to the left null space, and thus the only admissible manipulation of the three.

In general, the left null space can consist of more than one vector, in such cases it is not always possible to, in a simple way, identify the parameters that can be changed in the force diagram. For solutions to exist, the requirement is that **r** must be perpendicular to the left null space.

4.2. Arch—Practical example with constraints

In Fig. 6 an example is presented of how the form diagram is changed when manipulating the force diagram.

In this example, constraints are added to obtain a desired solution. The Jacobian matrix has the dimension $[2v^\star - 2 \times 2v]$, in this example $[18 \times 36]$. Before constraints are added, the Jacobian matrix has *rank* $=$ 18. Three constraints are added to remove rigid body motions (horizontal, vertical and scaling, applied by fixing A_x, A_y, and H_x). Three additional constraints are added to constrain the size of the boundary forces. Note that the length of edge zero cannot be constrained since the force density for this edge has already been prescribed. The size of the external forces and their horizontal positions are also constrained, adding 12 more constraints. In total 18 constraints are added. After these constraints have been added, the Jacobian has the dimension $[18 + 18, \times 36]$ and as the added constraints are linearly independent *rank* $= 36$, a unique solution now exists.

After these constraints have been added, the force diagram is manipulated. In this example, vertices 0–2 are moved to the right, making the internal forces (edge 1–7) and the boundary forces (edge 0 and 8) smaller. As seen in the figure, the resulting form diagram shows an increased height of the arch, as expected. Moving vertices 0–2 further to the right past the externally applied loads (edges 11–16) flip the arch upside-down into a cable in tension. This solution is found when using the approach presented in Algorithm 1. Trying to solve for the manipulation by using the globally convergent Newton method with line search fails as the arch tends towards infinite height as vertices 0–2 get closer to the externally applied loads (edges 11–16) from the left, which is why we in Fig. 2 try the Newton method without line search first. Fig. 7 presents the convergence of the two methods, where the Newton method with line search fails to converge, and is aborted on iteration 32 due to the Jacobian matrix becoming rank deficient.

Adding another constraint to the example, by fixing the vertical position of vertex H, leads to a left null space of dimension 1. The basis vector for the left null space is not as simple as in the

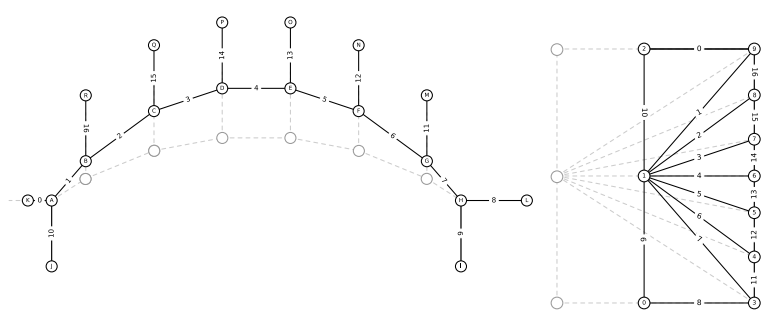


Fig. 6. Form finding for an arch, the dashed lines in the form diagram indicate the constrained horizontal positions.

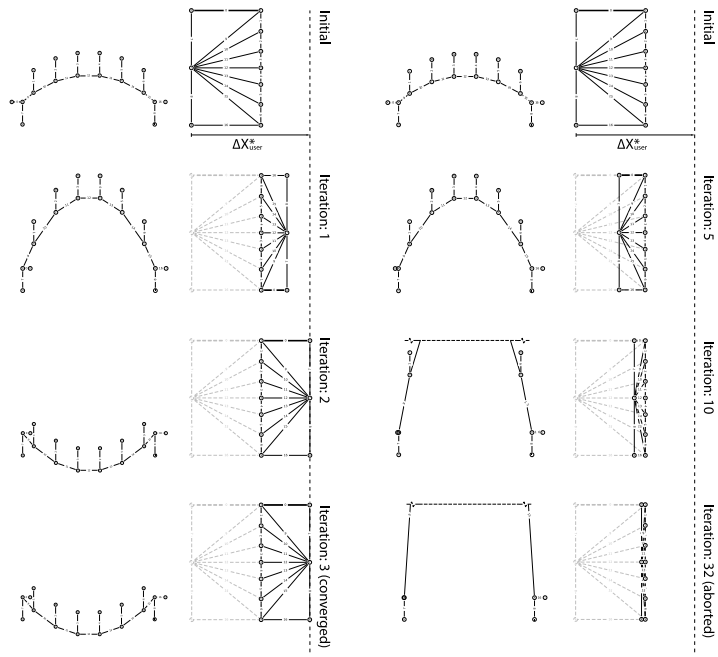


Fig. 7. Left side shows the convergence of Newton's method. Right side shows the convergence of Newton's method with line search, which fails to converge in this case. The form diagrams are all in the same scale, however, the force diagrams are not.

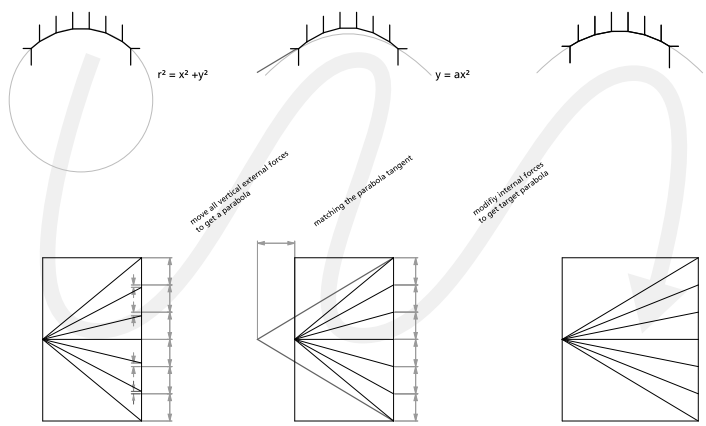


Fig. 8. Form finding of an arch where the forces are manipulated to become uniformly distributed.

previous example, and restricts the possible manipulations of the force diagram parameters since they must be perpendicular to the basis vector. From studying the basis vector for the left null space, it can be seen that, for instance, vertices 4 and 8 have to be moved by the same amount horizontally, and by opposite amounts vertically. Introducing further constraints will increase the rank and number of basis vectors for the left null space. Finding an intuitive method for presenting possible manipulations of the force diagram would be good in such cases.

4.3. Arch—Form finding

An extension of the previous example is shown in Fig. 8, which indicates how this method can be used in the design process of

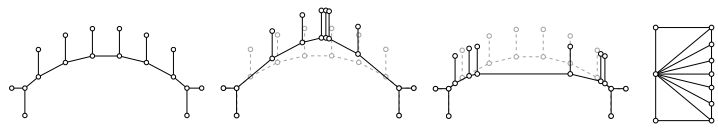


Fig. 9. All the forms in this figure result in the same force diagram that can be seen to the right.

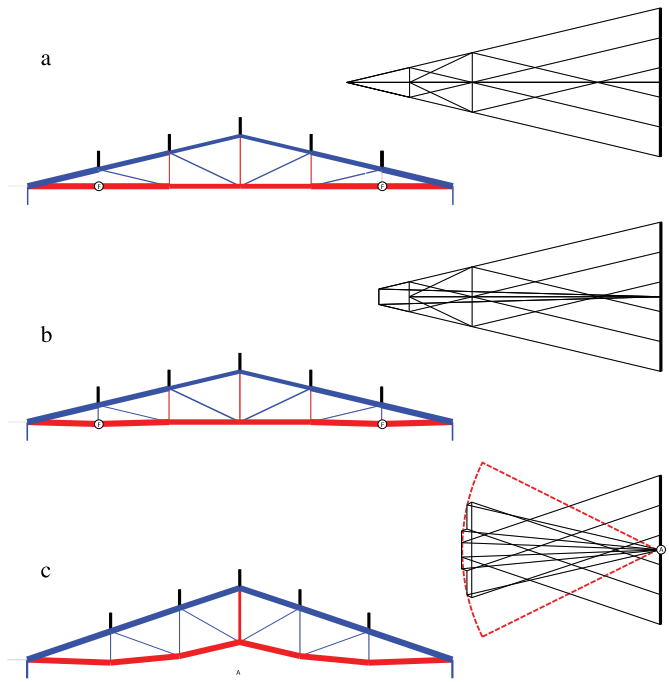


Fig. 10. (a) Gable truss with varying force magnitude in chords. (b) Vertices marked with F in the form diagram are translated slightly downwards, the forces in the connecting vertical edges are no longer zero. (c) Design of a constant-force gable truss.

a structure. The initial form in this example can be described as an arc of a circle. The external forces need to have different magnitudes in order for the structure to be in equilibrium. Using the same constraints for this example as in the previous example, the external forces are manipulated so that their magnitudes are equal. The resulting form after employing our method can, as expected, be described using a parabola, since the configuration of forces is a discrete representation of a uniformly distributed load, see Fig. 8b. A retained quality from the method of graphic statics is that edges in the force and form diagram have the same direction. Thus, to get a specific direction of an edge in the form diagram, the reciprocal edge in the force diagram can be manipulated. In the figure a sought tangent is drawn in the form diagram, then transferred and matched to the reciprocal edge in the force diagram, see Fig. 8c. The resulting form diagram now has the sought form.

4.4. Arch—Null space

In Fig. 9 multiple form diagrams that have the same force diagram is shown. The original form is the same as in the previous two examples, however, the horizontal constraints on the external force positions have been removed. By computing the null space of the Jacobian a vector space is obtained. Linear combinations of null space basis vectors can be used to explore different forms, all of which have the same force diagram. An example is shown in Fig. 9. In a potential application the free variables could be connected to a parametric modeler which would allow the user to easily explore different solutions.

In all of the form variations in Fig. 9 the reaction forces at the supports remain unchanged. The position of the externally applied forces varies with the form variations, however, the position of the line of action for the resultant of the applied forces remains unchanged, which is a requirement for the resulting force diagrams to be the same.

4.5. Chord force truss

Fig. 10 shows an example where the developed method is applied to the design of a truss with constant force in the top and bottom chords. All of the external loads are applied vertically. In

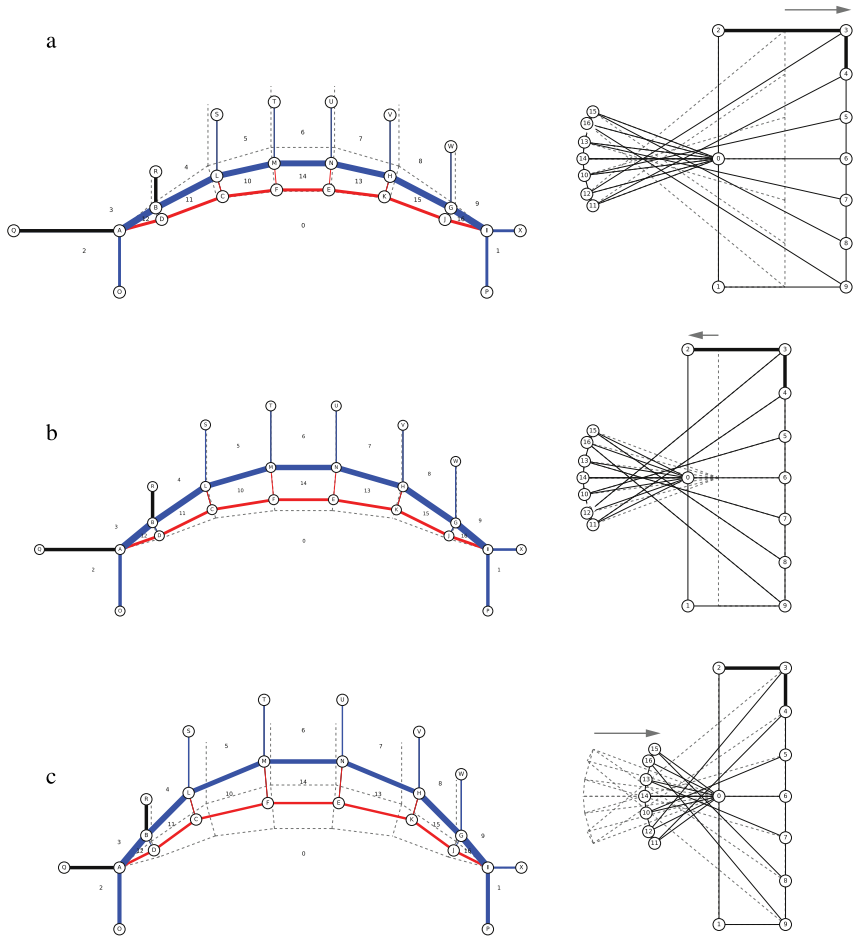


Fig. 11. Manipulations of the force diagram for a post-tensioned funicular structure. The gray dashed lines represent the starting geometry.

this example we have constrained rigid body motions, scaling, and lengths of free leaf edges.

Fig. 10a shows the starting position where the top and bottom chord edges do not carry the same amount of force in all edges. Edges in compression are shown in blue, edges in tension are shown in red in the form diagrams, and the thickness of the edge is proportional to the force.

Two edges in the initial form in Fig. 10a in the form diagram do not carry any load, and their bottom vertices are marked with (F). A small manipulation of adjacent vertices can lead to large changes in the force diagram, as shown in Fig. 10b. If the null space of the initial form is studied (Fig. 10a), it is seen that it contains null-modes where the zero force edges can rotate around their top vertices without affecting the force diagram. However, this is not present in the shape in Fig. 10b.

To obtain the form of a constant-force gable truss is fairly straight-forward. By manipulations in the force diagram of Fig. 10a we arrive at the example shown in Fig. 10c, where all the edges of the bottom chord carry the same amount of force. Since the bottom chord edges connect to the same vertex in the force diagram (marked with A in Fig. 10c), their opposite vertices are constrained to lie on a circle, shown in Fig. 10c. The diagonal elements inside of the truss carry a small amount of force compared to the other members of the structure. These could be made smaller in another iteration, but have been kept in the figure for clarity.

An example of such a truss is seen in the Magazzini Generali warehouse at Chiasso, Switzerland, designed by Robert Maillart [4]. The principle of restraining chord forces to the same length can be used to find other similar forms as well, see for instance [34].

4.6. Post tensioned funicular structure

Fig. 11 shows our method applied to the design of an externally post-tensioned funicular geometry. For further examples of such

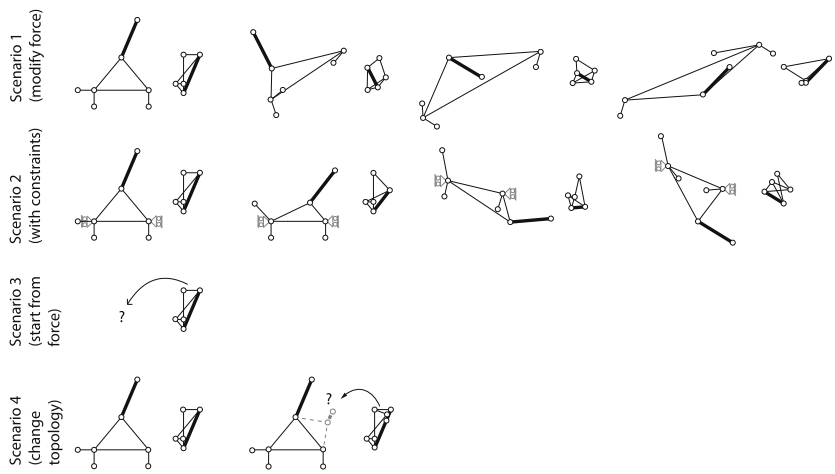


Fig. 12. Force diagram manipulation exploration scenarios.

structures, see for instance [9]. Two force densities must be selected by the user to get a unique solution. In this case we have selected the force density for one of the horizontal supports (edge 0) and for one of the applied loads (edge 1). Vertex order 1, 0, 2–9, 1 in the force diagram represents the global equilibrium of the structure. The positions of vertices A and I in the form diagram are fully constrained.

Fig. 11a shows the horizontal translation of vertices 3–9 in the force diagram, resulting in the lowering of the upper chord of the form. Fig. 11b shows the horizontal translation of vertices 0–2 in the force diagram, resulting in the raising of the lower chord in the form diagram. By these manipulations the relationship between the form and the force diagram can easily be understood, for instance by lowering the effective structural height (the distance between the lower and upper chords) an increase in the magnitude of the forces in the horizontal supports (edges 0 and 29) is obtained.

Fig. 11c shows the horizontal translation of vertices 10–16 in the force diagram, resulting in smaller force magnitudes in the upper and lower chords. This is achieved by increasing the overall height of the post tensioned structure, and a slight decrease in the distance between the upper and lower chords.

In the example, the lines of action of the externally applied loads have not been fixed, and the corresponding Jacobian matrix is under-determined. Accordingly the truss has a non-trivial null space, and alternative forms for the same force diagram, similar to the example in Fig. 9.

5. Conclusions

In this paper, we propose a new method for finding a reciprocal form diagram after manipulations have been carried out on the force diagram. This has previously only been possible through using the geometrical relationship between form diagram and force diagram, either by drawing or in predefined examples that follow graphic statics procedures for specific geometries. The method employs a gradient-based solver for solving the non-linear problem of finding the reciprocal form diagram to a force diagram. Further, the derivation of the Jacobian matrix, which is needed for Newton's method, is presented. We show how constraints can be added as additional equations to the Jacobian matrix in order to control solutions from the non-linear solver. In the examples of Sections 4.1 and 4.2 we show that the left null space of the Jacobian can be used to get information on which parameters cannot be changed in the force diagram. In Section 4.4 it is also shown how a vector space of possible solutions of form diagrams for the same force diagram can be computed by computing the null space of the Jacobian matrix.

When the problem becomes over constrained (has a non-trivial left null space) the parameters that can be changed in the force diagram become restricted, and the manipulations need to be perpendicular to the left null space of the Jacobian matrix. It might be worthwhile to investigate if there are graphical methods of presenting this information to the end user. The geometric constraints in the paper have been introduced to steer the solver towards solutions that meet certain design criteria, for instance, keeping the position of a support fixed, or keeping the line of action of an external force fixed. It could be of further interest to study if the constraints can be used to drive the design of 2D axially loaded structures.

The presented method can be used as a back-end for an interactive application, however, in order to enable full interactivity in computer aided graphic statics based on force diagram manipulations, some further work is required. Fig. 12 illustrates different scenarios based on manipulations of the force diagram. Scenario one shows explorations of a simple form using manipulations of the force diagram. Scenario two shows explorations with included constraints on the form diagram. In both scenarios a couple of manipulation steps are shown, in order to show that the resulting form and force diagrams can be far from the initial state. Both scenarios are supported by the presented framework, however, when there are multiple solutions the framework converges to one form out of many possible, and provides alternative forms through the use of the null space of the Jacobian matrix. These alternative forms are local to the current state, since they depend on the linearization. In an unbiased exploration the user should be able to get feedback from all possible manipulations and variations of solutions.

Scenarios three and four in Fig. 12 rely on starting from, or modifying the topology of, a force diagram. The topology matrices in Eqs. (1) and (2) are constructed from the form diagram. These

can also be constructed from the force diagram, however, this has not been covered in the paper. To further adopt the methodology presented in this paper to scenarios three and four requires some additional methods to get suitable initial guesses (for instance, taking advantage of corresponding form and force edges being parallel, and that some vertices in one diagram correspond to closed polygons in the other), and a discussion on valid changes and valid starting topologies of the force diagram.

In order to improve robustness of the solver suitable methods are introduced. The global convergence is improved by including a line search, and the vertex perturbations help with difficult cases when some edges in the force diagram are of zero length. The least squares approach to solving the equation system could be used to get solutions in over-determined cases, however, this has not been done in this paper or discussed. A tangent to this for future work could be the introduction of softer constraints, which allow for some changes in the geometry. The strength and application of being able to manipulate the force diagrams have been shown through a number of examples.

Acknowledgment

This work was supported by the Swedish strategic research program eSSENCE.

References

[1] Maxwell, XLV JC. On reciprocal figures and diagrams of forces. London Edinburgh Dublin Philos Mag J Sci 1864;27(182):250–61.
[2] Cremona L, Beare TH. Graphical statics: Two treatises on the graphical calculus and reciprocal figures in graphical statics. Clarendon Press; 1890.
[3] Culmann K. Die graphische statik, vol. 2. Meyer & Zeller (A. Reimann); 1875.
[4] Allen E, Zalewski W. Form and forces: Designing efficient, expressive structures. John Wiley & Sons; 2009.
[5] Block P, Ochsendorf J. Thrust network analysis: A new methodology for three-dimensional equilibrium. Int Assoc Shell Spat Struct 2007;155:167.
[6] Fraternali F. A thrust network approach to the equilibrium problem of unreinforced masonry vaults via polyhedral stress functions. Mech. Res. Commun. 2010;37(2):198–204.
[7] Fraternali F, Carpentieri G. On the correspondence between 2d force networks and polyhedral stress functions. Int J Space Struct 2014;29(3):145–59.
[8] Beghini LL, Carrion J, Beghini A, Mazurek A, Baker WF. Structural optimization using graphic statics. Struct Multidiscip Optim 2014;49(3):351–66.
[9] Todisco L, Fivet C, Peiretti HC, Mueller C. Design and exploration of externally post-tensioned structures using graphic statics. J Int Assoc Shell Spat Struct 2015;56(4):249–58.
[10] McRobie A, Baker W, Mitchell T, Konstantatou M. Mechanisms and states of self-stress of planar trusses using graphic statics, part II: Applications and extensions. Int J Space Struct 2016;31(2–4):102–11.
[11] Williams C, McRobie A. Graphic statics using discontinuous airy stress functions. Int J Space Struct 2016;31(2–4):121–34.
[12] Akbarzadeh M, Van Mele T, Block P. On the equilibrium of funicular polyhedral frames and convex polyhedral force diagrams. Comput. Aided Des. 2015;63:118–28. http://dx.doi.org/10.1016/j.cad.2015.01.006.
[13] Akbarzadeh M, Van Mele T, Block P. Three-dimensional graphic statics: initial explorations with polyhedral form and force diagrams. Int J Space Struct 2016;31(2–4):226.
[14] Dacunto P, Ohlbrock PO, Jasienski J-P, Fivet C, 2016. Vector-based 3d graphic statics (part I): Evaluation of global equilibrium. In: Proceedings of the IASS annual symposium 2016 "Spatial Structures in the 21st Century".
[15] Lee J, Mueller C, Fivet C. Automatic generation of diverse equilibrium structures through shape grammars and graphic statics. Int J Space Struct 2016;31(2–4):147–64.
[16] Fivet C, Zastavni D. Constraint-based graphic statics: new paradigms of computer-aided structural equilibrium design. J Int Assoc Shell Spat Struct 2013;54(4):271–80.
[17] Fivet C, Zastavni D. A fully geometric approach for interactive constraint-based structural equilibrium design. Comput. Aided Des. 2015;61:42–57.
[18] Greenwold S, Allen E, Active statics. URL http://acg.media.mit.edu/people/simong/statics/data/index.html.
[19] Block P, Equilibrium. URL http://block.arch.ethz.ch/equilibrium/.
[20] Lachauer L, Jungjohann H, Kotnik T, Interactive parametric tools for structural design, in: Proceedings of the International Association for Shell and Spatial Structures (IABSE-IASS) Symposium, 2011.
[21] Van Mele T, Block P. Algebraic graph statics. Comput. Aided Des. 2014;53:104–16.
[22] Micheletti A. On generalized reciprocal diagrams for self-stressed frameworks. Int J Space Struct 2008;23(3):153–66.
[23] Pellegrino S. Structural computations with the singular value decomposition of the equilibrium matrix. Int. J. Solids Struct. 1993;30(21):3025–35.
[24] Bow RH. Economics of construction in relation to framed structures. Cambridge University Press; 2014.
[25] Schek H-J. The force density method for form finding and computation of general networks. Comput. Methods Appl. Mech. Engrg. 1974;3(1):115–34.
[26] Pellegrino S, Calladine CR. Matrix analysis of statically and kinematically indeterminate frameworks. Int. J. Solids Struct. 1986;22(4):409–28.
[27] Crapo H, Whiteley W. Plane self stresses and projected polyhedra I: The basic pattern. Struct. Topol 1993;20.
[28] Python Software Foundation, Python 3.5. URL http://www.python.org.
[29] NumPy. URL http://www.numpy.org/.
[30] SciPy. URL https://www.scipy.org/.
[31] Networkx. URL http://networkx.github.io/.
[32] Gu M, Eisenstat SC. Efficient algorithms for computing a strong rank-revealing QR factorization. SIAM J. Sci. Comput. 1996;17(4):848–69.
[33] Press WH, Flannery BP, Teukolsky SA, Vetterling WT, Kramer PB. Numerical recipes: The art of scientific computing. AIP; 1987.
[34] Van Mele T, Lachauer L, Rippmann M, Block P. Geometry-based understanding of structures. J Int Assoc Shell Spat Struct 2012;53(4):285–95.

Paper E

Paper F

IASS 2018 BOSTON, JULY 16-20
CREATIVITY IN STRUCTURAL DESIGN

Proceedings of the IASS Symposium 2018
Creativity in Structural Design
July 16-20, 2018, MIT, Boston, USA
Caitlin Mueller, Sigrid Adriaenssens (eds.)

Generating initial reinforcement layouts using graphic statics

Vedad ALIC*, Kent PERSSON[a]

* Division of Structural Mechanics, Faculty of Engineering, Lund University,
P.O. Box 118, SE-221 00 Lund, Sweden,
vedad.alic@construction.lth.se
[a] Division of Structural Mechanics, Faculty of Engineering, Lund University

Abstract

A key step to the strut-and-tie method is the selection of an appropriate truss model, due to the static indeterminacy of reinforced concrete there are often several suitable models possible. A method for automatically generating a suitable truss model by using graphic statics is presented. Optimal layouts are found by minimizing the total load path. A formulation of constraints suitable for generating an initial strut-and-tie model confined to an arbitrary polygon with holes is also presented. The performance by using derivative based and derivative free solvers is compared. The method is applied to several examples and the results are compared to existing methods from literature as well as to the principal stress patterns based on finite element analysis. All of the presented examples yield good results and the optimal layouts found can be used as a starting point for further design with the strut-and-tie method.

Keywords: graphic statics, strut-and-tie, reinforcement layout, optimization

1. Introduction

The design and detailing of cracked reinforced concrete members can be performed by reducing the concrete member into a truss-like structure, where some members act in compression (struts) and some in tension (ties). The strut-and-tie model (STM) is a general approach for the design of reinforcement layout for parts a concrete structure where the beam hypothesis is invalid, i.e. at static or geometric discontinuities. Since the regular truss model holds for the beam-like parts of the structure, the STM generalizes the design approach for structural concrete for all parts [1]. A key step to the strut-and-tie method is the selection of an appropriate truss model, due to the static indeterminacy of reinforced concrete there are often several suitable models possible. In this paper, we present a method for automatically generating a suitable truss model by using graphic statics.

Research of graphic statics has increased recently and several research directions are being explored, such as constraint based graphic statics, 3D graphic statics, generalizations that include bending, etc. Of particular interest for this research is the algebraic formulation of graphic statics [2, 3] and structural optimization with graphic statics [4].

There have been several research papers on generating strut-and-tie models, both using topology optimization and the ground structure approach, see [5, 6] and the references therein respectively.

The following motivate research on the use of graphic statics for STM:

- In complex strain fields it may be difficult for a novice designer to select an appropriate truss model, automatic STM generation been researched in [5, 6]. Graphic statics provides an alternative to this.
- STM design tends to lead to solutions containing mechanisms, when searching for alternative solutions this is simple to handle with graphic statics [4].

Copyright © 2018 by Vedad ALIC, Kent PERSSON
Published by the International Association for Shell and Spatial Structures (IASS) with permission.

- The STM network is a pin-jointed structure; graphic statics is a natural approach for modeling such structures.
- The STM is based on the lower bound theorem of plasticity and algebraic graphic statics provides simple and direct means of exploring all possible equilibria. A unique force diagram (equilibrium state) is computed by selection [2], and not indirectly by for instance selecting a set of stiffness parameters.

2. A method for automatic generation of initial truss layouts

The first step in the STM is to identify Bernoulli regions (B-regions) and discontinuity regions (D-regions). B-regions are designed according to beam truss models while D-regions display more complex strain fields. The STM extends the truss model analogy to the D-regions and provides a consistent design approach to the whole structure. In order to apply the STM to a D-region the first step is to identify the section stresses on the region, for instance by a linear elastic finite element analysis (FEA) using a homogeneous isotropic material or by appropriate hand computations, see Fig. 1a. In the case that the whole region is a D-region one only needs to determine the reaction forces at the supports before the method can be applied.

The stresses on the boundary of the D-region are translated to discrete forces which along with external forces serve as the initial points for generating a form diagram, see Fig. 1b, which is where the method deviates from the common approaches used in STM (load-paths or stress trajectories). The initial form diagram generated is a structured/uniform mesh and does not take into account internal stresses, only the position of the external and section forces and the solid structure geometry. Once an initial form diagram has been generated an optimization procedure is run in order to find a form diagram suitable as an initial strut-and-tie model, Fig. 1c. The form diagram in Fig. 1c still has the same topology as in Fig. 1b, however, visualization techniques are used to make only the members with significant force magnitudes visible, thereby illustrating a potential strut-and-tie model. The present work investigates the optimization step of from Fig. 1b to Fig. 1c, using a graphic statics based optimization.

After the optimization, it is necessary to check that the network follows the principal stress field, due to the limited ductility of the concrete [1]. The computed network might require further rationalizations and all of the other requirements and detailing need to be checked, Fig. 1d.

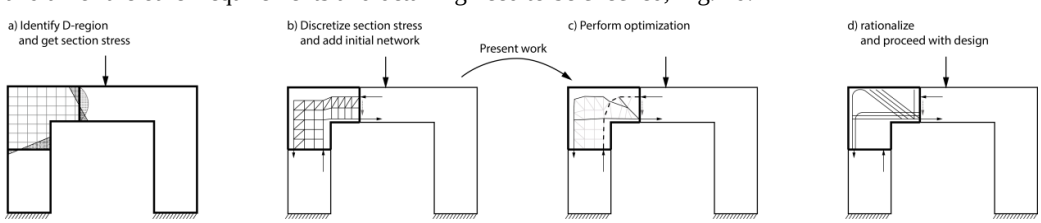


Figure 1: Schematic of the present work.

3. The optimization problem

In [4] graphic statics is used to minimize the total volume of a structure, which is shown to be equivalent to minimizing the total load path in trusses where all members are equally stressed. In this work, we use the total volume as the objective function and formulate the optimization problem as

$$\min_{\boldsymbol{x}} f(\boldsymbol{x}) = \frac{1}{\sigma}\sum L_i L_i^* \qquad \text{s.t.} \quad \begin{cases} 1 - g(\boldsymbol{x}, \boldsymbol{p}) \leq 0 \\ g(\boldsymbol{x}, \boldsymbol{q}) \leq 0 \\ \boldsymbol{x} \in [\boldsymbol{x}_{\min}, \boldsymbol{x}_{\max}] \end{cases} \tag{1}$$

where $\boldsymbol{x}$ are the design variables, which have upper and lower bounds. σ is the normal stress magnitude, assumed to be equal in all edges. Under these conditions minimization of the total volume is equivalent

to minimization of the total load path, $\sum L_i L_i^*$ [4]. L_i and L_i^* are the length and force magnitude of the i:th edge. $g(\boldsymbol{x}, \boldsymbol{p})$ is a binary function returning one if all of the edges of the form diagram are inside of the polygon defined by the matrix $\boldsymbol{p}$ and zero otherwise. Hence the first constraint requires all of the edges to be inside $\boldsymbol{p}$ while the second constraint requires all the edges to be outside a hole $\boldsymbol{q}$. Additional holes are defined similarly. The implementation of the polygonal constraints is such that the constraints are checked on y user-selected points per edge. Edges that correspond to external forces, section forces, or supports, are not included in the constraints.

The design variables $\boldsymbol{x}$ are the form diagram coordinates along with a set of force densities used to define the magnitude of external loads and section forces (and can be used to determine unique force diagrams in the case of statically indeterminate form diagrams). Using the form diagram coordinates as the design variables makes it simple to formulate the geometric constraints. The bounds for the design variables that are related to the form diagram coordinates are set to the bounding box of $\boldsymbol{p}$ for the coordinates, and for the force densities are set to [-1,1]. The form diagram edges which correspond to external forces or boundary stresses are kept fixed during the optimization, and so are their force magnitudes (keeping the external equilibrium constant) by fixing the respective force densities. In order to compute the force diagram, and to run the optimization, an algebraic formulation of graphic statics as described in [2, 3] is used.

The two constraints are discrete and do not have any derivatives. To solve the optimization problem derivative free solvers from the global optimization toolbox for MATLAB are used.

In order to use gradient based solvers, the two constraints need to be re-formulated. The distance for each point on an edge that is outside the polygon to the nearest point on the polygon is computed and these are summed for each edge. This results in $g_i \leq 0$ new constraints, where g_i is the summed distance for the points of edge i, see Fig. 2. A significant speedup is obtained by subdividing the polygon into a set of convex polygons since any line whose endpoints lie in the same convex polygon will then, by definition, be inside the original polygon.

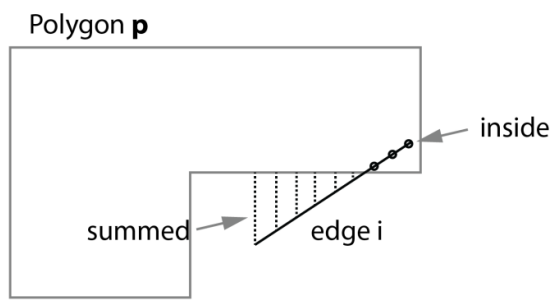


Figure 2: Illustration of constraint.

The same type of constraint is used for holes, except with the summed distance of the points that are inside of the polygon $\boldsymbol{q}$ rather than outside.

Another approach for constraining edges to be inside the polygon $\boldsymbol{p}$ is to consider the closed faces of the form diagram as polygons and perform a Boolean subtraction of the of the form diagram polygons by the polygon $\boldsymbol{p}$ and subsequently require that the area of what is left should be zero. This approach, however, cannot include holes.

To summarize, the geometric constraints have been implemented in three different ways, first as binary constraints, second as shown in Fig. 2, and finally by using the Boolean subtraction approach.

3.1 Multiple load cases

The minimization of a weighted sum of the individual load case objective functions [5] is performed in order to account for multiple load cases. The objective function becomes

$$f(\boldsymbol{x}) = \psi_1 f_1(\boldsymbol{x}) + \psi_2 f_2(\boldsymbol{x}) + \psi_3 f_3(\boldsymbol{x}) + \cdots \quad (2)$$

where ψ_i is a weight factor and all $f_i(\boldsymbol{x})$ have the same initial form diagram but different magnitudes on external and section forces. This is controlled trough the force densities of the external and section forces. The total load path for the i:th load case is $f_i(\boldsymbol{x})$.

4. Examples and results

In this section, the results of applying the method to some examples are presented. First, some simple models with the purpose to test the method are shown. A convergence study using the presented models is performed, where different optimization algorithms and versions of the constraints are compared. Results for some models with multiple discontinuities and deep beams are shown. Finally, an example with multiple load cases is presented. The section and reaction forces in the examples were computed either by hand or by FEA when required. The initial form diagrams were manually drawn, however, there are meshing techniques available which could be used for this step, but it is out of the scope of the present study.

4.1 Models

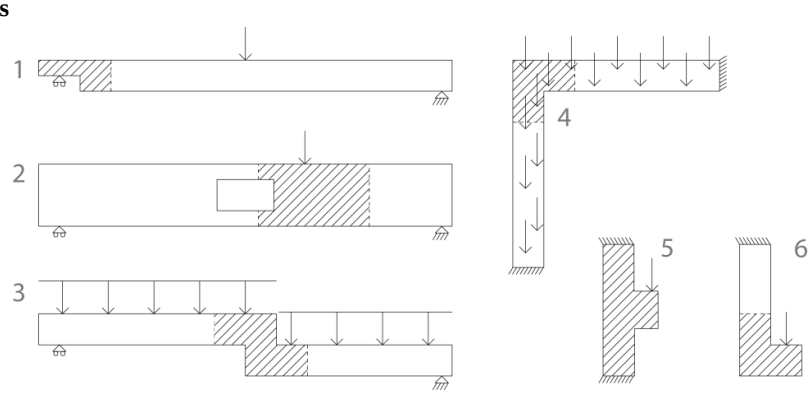


Figure 3: The structures used for the convergence study.

Here six models used for the convergence study and their solutions are discussed. The models are based on the structures shown in Fig. 3, which also show the D-regions as hatched areas.

4.1.1. Results

The left most column with sub-figures in Fig. 4 are the initial form diagrams. The last column shows the principal stress components from an FEA, the second and third columns show are the form and force diagrams of the solved GD_1 solution (which has shown best performance, see section 4.2). Note that only the D-regions for each model are shown. Red is tension, blue is compression. After the optimization the form diagram still has the same topology as the initial form diagram. Highly stressed edges are emphasized by modifying the line weights according to the force magnitudes. Edges with a force magnitude less than 1% of the largest force magnitude are dashed, further emphasizing the load-carrying network. The result of model 6 in Fig. 4 is similar to Fig. 40b in [1], and the result of model 5 is similar to Fig. 11 in [5].

In many cases the solved forms tend to extend to the limits of the constraint-polygon, because of this, the polygon has been reduced in size in models 2-4, i.e. the polygons are not the actual dimensions of the beam, but are offset inward to almost near the positions of the section resultants.

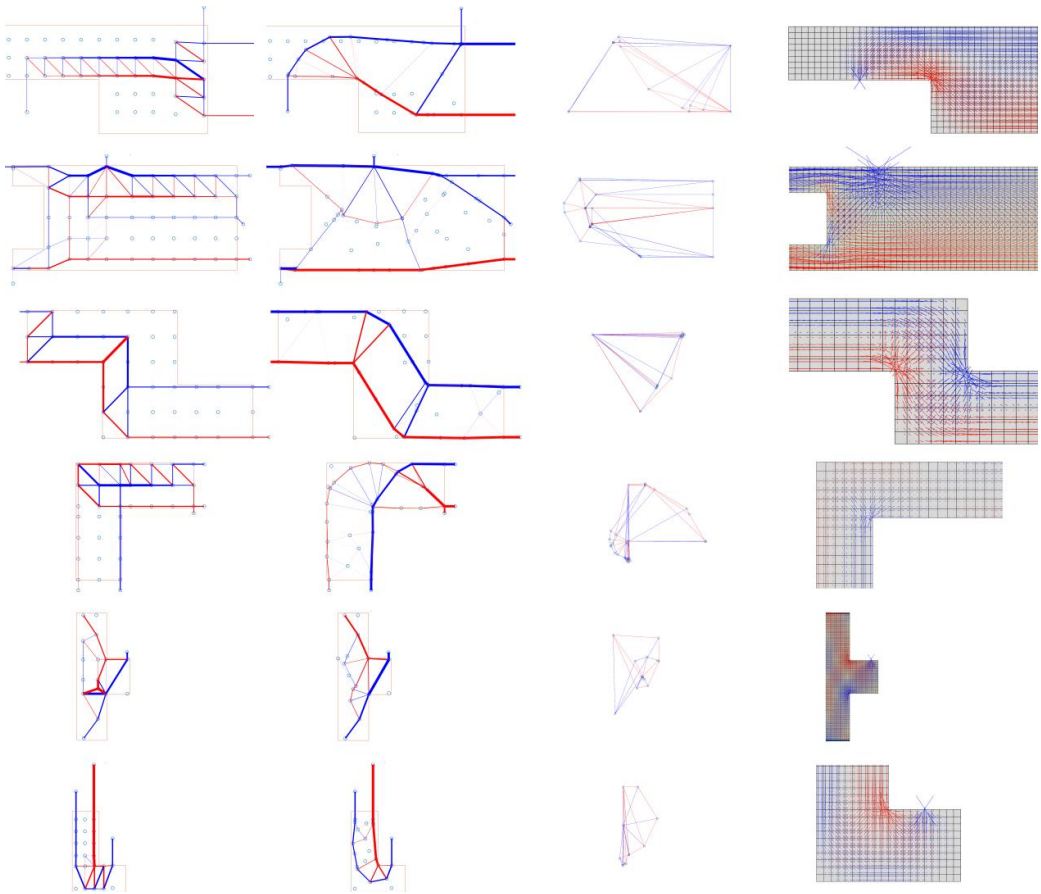


Figure 4: Columns from left to right: Initial form diagram, form diagram after optimization, force diagram after optimization, and finally the principal stresses from FEA. Rows 1-6 are models 1-6 respectively.

4.2 Convergence study

Table 1 presents the total load paths for the presented models and solution methods used. PS is pattern search with the binary polygon constraints. GD_1 and GD_2 use the MATLAB routine fmincon (using the interior point algorithm), where GD_1 uses the constraint formulated as in Fig. 2, and GD_2 is with the constraint following the Boolean subtraction approach. The genetic algorithm solver was also tested, however, no solutions were found.

Table 1: Total load paths for the different models and solution methods (normalized to initial). Color: Yellow = failed to satisfy constraints. White = Satisfied constraints to within accuracy limits, Red = Exceeds iteration limit

-	Model 1	Model 2	Model 3	Model 4	Model 5	Model 6
Initial	1.0	1.0	1.0	1.0	1.0	1.0
PS	0.4120	0.5610	0.2647	0.3572	0.5855	0.7203
GD_1	0.2916	0.4268	0.5174	0.3462	0.5811	0.6758
GD_2	N/A	0.4736	0.5071	0.3243	0.3419	0.7146

4.3 Models with multiple discontinuities and deep beams

Here some examples with more complex stress fields are discussed. Fig. 5a shows an example of a frame corner with a corbel exposed to a point load. A FEA solution reveals bending and compression in the wall and bending in the floor, see Fig. 5d. The section stresses in the wall have been discretized into three loads for the truss-network, two that balance the moment, and a third due to the normal force. The method generates a solution where it is seen that reinforcement is required in the top of the floor, and some additional reinforcement on the inside of the wall. Fig. 5c shows a simplified model based on the one from Fig 9b to be used for reinforcement layout computations.

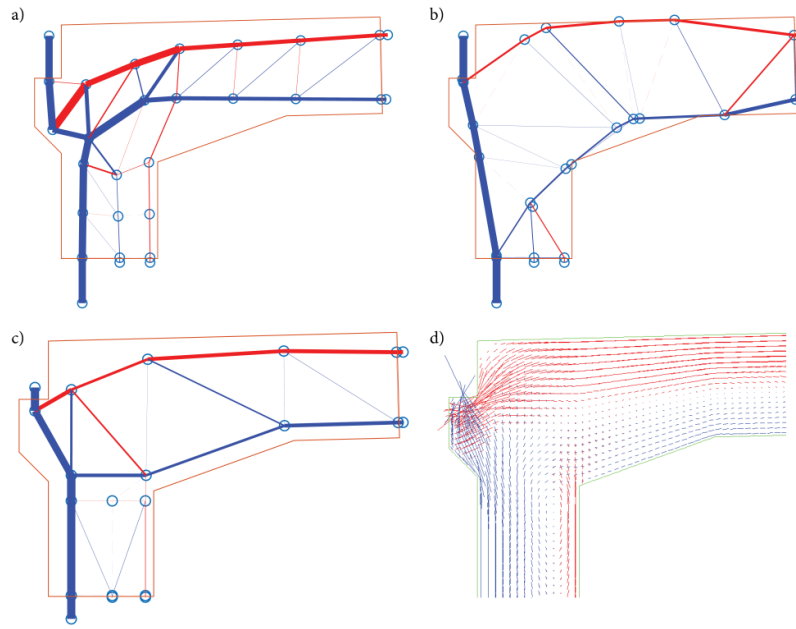


Figure 5: Frame corner with corbel. d) is reproduced from [7].

In Fig. 6a, the method is applied to a D-region with a hole. The result in Fig. 6b is similar to one of the two STM models used in [1] on the same geometry. The model is in accordance with the principal stress pattern. The polygon constraints are checked on 10 points per edge, leading to edges that slightly go through the hole in the bottom left of the geometry in Fig. 6b. This can be improved by increasing the number of points per edge used.

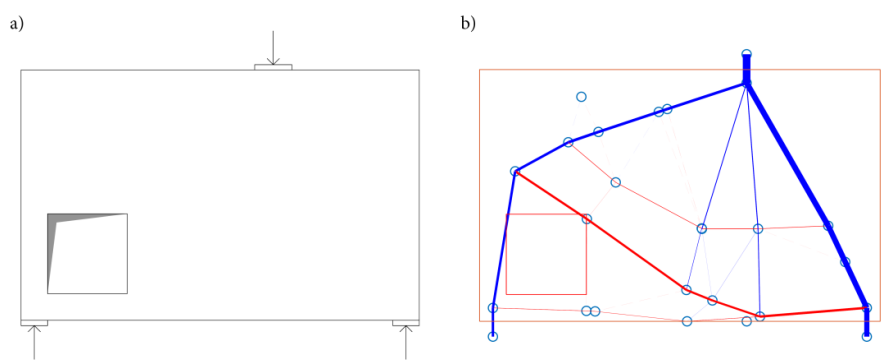


Figure 6: a) method applied to deep beam with a hole. b) the result after optimization.

4.4 Multiple loads

Fig. 7 shows a double corbel with multiple load cases. Fig. 7a shows the initial form and force diagrams a load on the right, Fig. 7b shows the initial solution for loads on both sides and Fig. 7c shows for a load to the left. The form and force diagrams after applying the optimization method for multiple loads is shown in Figs. 11d-11f respectively. Note that it is the same solution that is shown in Figs. 11d-11f, it is only the external loads that are different, i.e. the form diagrams in Figs. 11d-11f are the same while the force diagrams are different. The result is similar to [5].

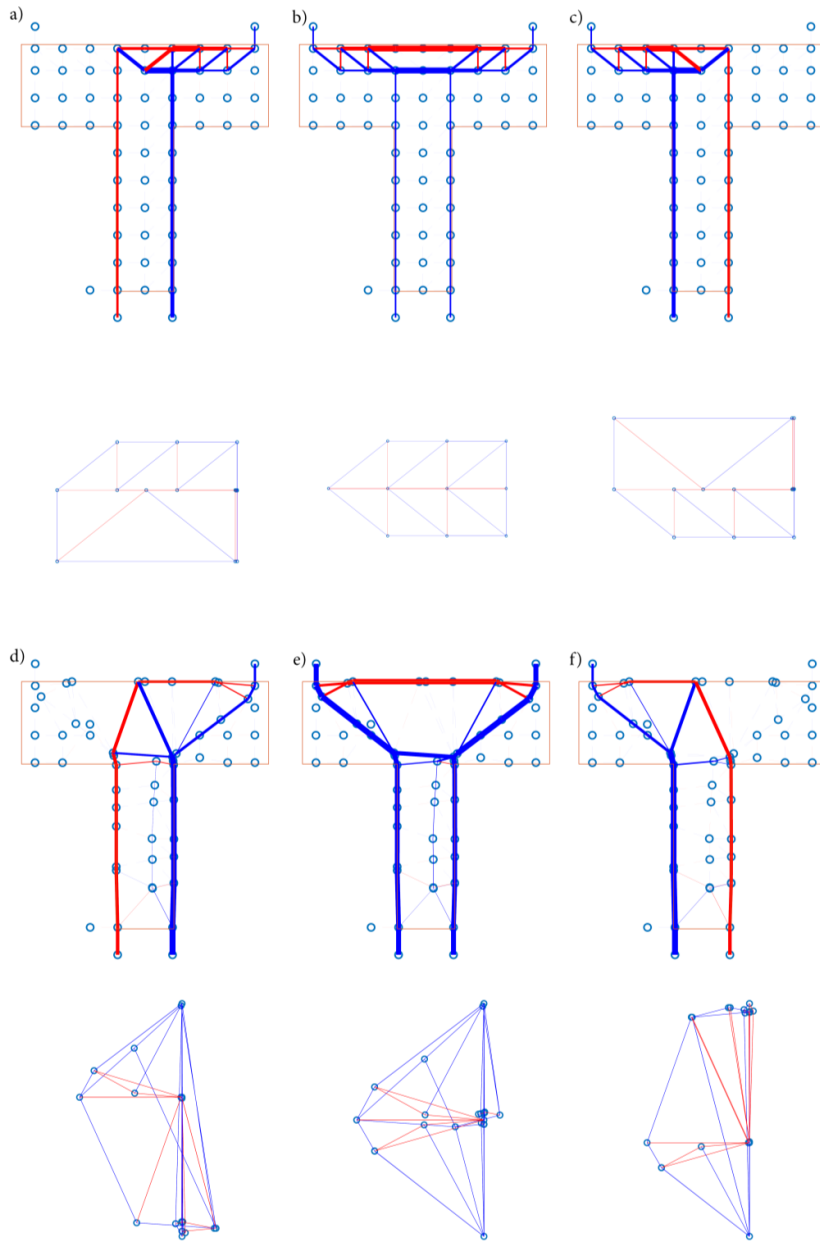


Figure 7: Double corbel with multiple load cases. Sub-figures a) b) and c) are the initial form and force diagrams with right, both, and left external loads respectively. Sub-figures d) e) and f) show the corresponding form and force diagrams after optimization.

5. Discussion

In the strut-and-tie method it is common to spread out a strut with a large force over a larger area, in order to approximate the spread of stress in the concrete better. The objective function used in this paper will minimize the total load path. Maxwell showed that the difference of the compression load path and tension load path is constant, thus, in order to minimize the total load path in the structure in Fig. 8a one only needs to remove the ties, resulting in Fig. 8b. When using the method this should be kept in mind, and large struts should be replaced accordingly, as for instance, the strut in the right part of the example in Fig. 6.

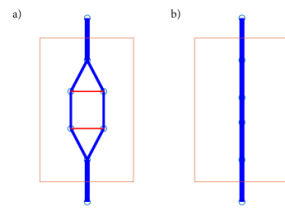


Figure 8: a) compression strut with ties. b) result after optimization using GD_1.

A method for generating initial reinforcement layouts using graphic statics was presented. In many cases, the solutions resemble the principal stress patterns and the method manages to capture appropriate load paths, however, it is still necessary to refine and rationalize the models in subsequent design stages. When there are uncertainties on how to select a good truss geometry for the STM our approach may be used to generate a starting point.
This work was supported by the Swedish Research Council Formas.

5.1 Further work

There are several aspects requiring further study and automation. The initial form diagram generation needs to be automated. For this, the influence of the initial form diagram needs to be studied further. Most strut-and-tie models are for parts of a structure, and consist of relatively few members, however, in order to support much larger assemblies than the ones presented in the paper the constraints need to be reformulated. Additional work on multiple load cases is required. Finally, the automatic generation of a simplified form diagram after the optimization procedure would be beneficial.

References

[1] J. Schlaich, K. Schafer, and M. Jennewein, “Toward a Consistent Design of Structural Concrete,” *PCI Journal*, vol. 32, no. 3, pp. 74–150, May 1987.

[2] T. Van Mele and P. Block, “Algebraic graph statics,” *Computer-Aided Design*, vol. 53, pp. 104–116, Aug. 2014.

[3] V. Alic and D. Åkesson, “Bi-directional algebraic graphic statics,” *Computer-Aided Design*, vol. 93, pp. 26–37, Dec. 2017.

[4] L. L. Beghini, J. Carrion, A. Beghini, A. Mazurek, and W. F. Baker, “Structural optimization using graphic statics,” *Structural and Multidisciplinary Optimization*, vol. 49, no. 3, pp. 351–366, Nov. 2013.

[5] M. Bruggi, “Generating strut-and-tie patterns for reinforced concrete structures using topology optimization,” *Computers & Structures*, vol. 87, no. 23–24, pp. 1483–1495, Dec. 2009.

[6] F. Biondini, F. Bontempi, and P. G. Malerba, “Stress path adapting Strut-and-Tie models in cracked and uncracked R.C. elements,” *Structural Engineering and Mechanics*, vol. 12, no. 6, pp. 685–698, Dec. 2001.

[7] T. Dahl, “Optimering av böjarmering genom fem-analys och strut-and-tie modellering - En effektivisering av armeringsprocessen,” Master’s dissertation, Div. Struct. Mech., Lund Univ., Lund, 2018.